UAB
Universitat Autònoma de Barcelona

Brassinosteroid-mediated drought tolerance in Arabidopsis thaliana and translation to Sorghum bicolor

Juan Bautista Fontanet-Manzaneque

ADVERTIMENT. L'accés als continguts d'aquesta tesi doctoral i la seva utilització ha de respectar els drets de la persona autora. Pot ser utilitzada per a consulta o estudi personal, així com en activitats o materials d'investigació i docència en els termes establerts a l'art. 32 del Text Refós de la Llei de Propietat Intel·lectual (RDL 1/1996). Per altres utilitzacions es requereix l'autorització prèvia i expressa de la persona autora. En qualsevol cas, en la utilització dels seus continguts caldrà indicar de forma clara el nom i cognoms de la persona autora i el títol de la tesi doctoral. No s'autoritza la seva reproducció o altres formes d'explotació efectuades amb finalitats de lucre ni la seva comunicació pública des d'un lloc aliè al servei TDX. Tampoc s'autoritza la presentació del seu contingut en una finestra o marc aliè a TDX (framing). Aquesta reserva de drets afecta tant als continguts de la tesi com als seus resums i índexs.

ADVERTENCIA. El acceso a los contenidos de esta tesis doctoral y su utilización debe respetar los derechos de la persona autora. Puede ser utilizada para consulta o estudio personal, así como en actividades o materiales de investigación y docencia en los términos establecidos en el art. 32 del Texto Refundido de la Ley de Propiedad Intelectual (RDL 1/1996). Para otros usos se requiere la autorización previa y expresa de la persona autora. En cualquier caso, en la utilización de sus contenidos se deberá indicar de forma clara el nombre y apellidos de la persona autora y el título de la tesis doctoral. No se autoriza su reproducción u otras formas de explotación efectuadas con fines lucrativos ni su comunicación pública desde un sitio ajeno al servicio TDR. Tampoco se autoriza la presentación de su contenido en una ventana o marco ajeno a TDR (framing). Esta reserva de derechos afecta tanto al contenido de la tesis como a sus resúmenes e índices.

WARNING. The access to the contents of this doctoral thesis and its use must respect the rights of the author. It can be used for reference or private study, as well as research and learning activities or materials in the terms established by the 32nd article of the Spanish Consolidated Copyright Act (RDL 1/1996). Express and previous authorization of the author is required for any other uses. In any case, when using its content, full name of the author and title of the thesis must be clearly indicated. Reproduction or other forms of for profit use or public communication from outside TDX service is not allowed. Presentation of its content in a window or frame external to TDX (framing) is not authorized either. These rights affect both the content of the thesis and its abstracts and indexes.

UNIVERSITAT AUTÒNOMA DE BARCELONA

CENTRE FOR RESEARCH IN AGRICULTURAL GENOMICS (CRAG)

Brassinosteroid-mediated drought tolerance in *Arabidopsis thaliana* and translation to *Sorghum bicolor*

Author

Juan Bautista Fontanet-Manzaneque

Supervisor

Dr. Ana I. Caño-Delgado

Date

12th July 2024





UNIVERSITAT AUTÒNOMA DE BARCELONA

Animal Biology, Plant Biology, and Ecology Department

Plant Biology and Biotechnology Ph.D. Program

CENTRE FOR RESEARCH IN AGRICULTURAL GENOMICS (CRAG)

Molecular Genetics Department

Brassinosteroid-mediated drought tolerance in *Arabidopsis thaliana* and translation to *Sorghum bicolor*

Dissertation submitted in partial fullfillment of the requirement for obtaining the degree of Doctor (Ph.D.) by Univeristat Autònoma de Barcelona (UAB) (Barcelona, Spain)

Author

Juan Bautista Fontanet-Manzaneque

Supervisor

Dr. Ana I. Caño-Delgado

Date

12th July 2024





ABSTRACT

The present PhD thesis dissertation unveils novel mechanisms of the brassinosteroid receptor BRI1-LIKE 3 (BRL3) and its downstream molecular players in coping with abiotic stresses in *Arabidopsis thaliana*. Additionally, it reports a significant advancement in *Sorghum bicolor* genetic transformation, leading to the development of cultivars better adapted to drought stress.

Brassinosteroids, essential plant steroid hormones, are perceived by plasma membrane leucine-rich repeat receptor-like kinases, with BRASSINOSTEROID INSENSITIVE 1 (BRI1) driving cell elongation and growth from the outer cell layers and BRL3 regulating drought and temperature stress adaptation from the vascular tissues. Through an interdisciplinary approach encompassing molecular biology, genetics, biotechnology, biochemistry, physiology, and bioinformatics, this thesis deciphers *BRL3* transcriptional regulation under abiotic stress and its downstream transcription factors that modulate drought stress tolerance in *Arabidopsis thaliana*.

Key findings include the characterization of CLASS III HOMEODOMAIN-LEUCINE ZIPPER (HD-Zip III) transcription factors in regulating *BRL3* vascular expression and the uncovering novel roles for MYB transcription factors MYB96 (AT5G62470), MYB305 (AT3G24310), and HD-Zip II transcription factor HAT9 (AT2G22800) as critical players in vascular BRL3-mediated signaling through BRASSINAZOLE RESISTANT 1 (BZR1) to control plant abiotic stress adaptation.

In this PhD thesis, translational work of these findings to *Sorghum bicolor*, a cereal of great agronomical importance, demonstrates that modulation of brassinosteroid signaling can enhance abiotic stress tolerance in crops. By employing transcriptomics, metabolomics, and physiological assays of untargeted mutagenesis of the Sorghum *BRI1* receptor, the study reveals BRI1 as a negative regulator of drought stress, primarily affecting the phenylpropanoid pathway involved in lignin and flavonoid synthesis. Additionally, the thesis establishes a highly efficient *Agrobacterium*-mediated transformation protocol for *Sorghum bicolor*, leveraging morphogenic regulators and a ternary vector system and overcoming the difficulty of genetic transformation in Sorghum for the first time in European academic laboratories. This breakthrough enabled the generation of transgenic plants that enhance Sorghum bicolor BRL3 receptor levels, resulting in plants better adapted to drought stress by altering leaf epinasty.

Overall, this dissertation not only deciphers novel components of the BRL3-mediated signaling in drought stress tolerance, but also paves the way for creating smart crops better adapted to climate change, underscoring the potential of brassinosteroid signaling modulation and advanced genetic transformation techniques in crop improvement.

TABLE OF CONTENTS

GENERAL INTRODUCTION 1
1.1 Brassinosteroid hormones perception in plants 3
1.1.1 The BRI1 receptor 4
1.1.2 The brassinosteroid vascular receptors BRL1 and BRL3 6
1.2 Brassinoteroid signal transduction 7
1.2.1 Brassinoteroid signal transduction when it is attenuated 7
1.2.2 Brassinosteroid signal transduction when it is activated 8
1.3 Activity and regulation of BES1 and BZR1 9
1.4 Brassinosteroid transcriptional network 12
1.5 Brassinosteroids in plant development and adaptation to abiotic stress 15
1.5.1 Brassinosteroids in plant development 15
1.5.2 Brassinosteroids in plant adaptation to abiotic stress 20
1.6 Brassinosteroids in crops 28
1.7 Current context of climate emergency and its impact on crop yield 30
1.8 Engineering brassinosteroid signaling in crops to improve drought resistance. 33
1.9 Sorghum as a monocot model for drought research 36
1.9.1 Sorghum drought tolerance mechanisms 38
1.9.2 Effects of drought stress on Sorghum 40
1.9.3 Sorghum gene identification and manipulation 41
1.10 Sorghum transformation 47
1.10.1 Sorghum transformation limitations 47
1.10.2 Sorghum transformation progress 50
OBJECTIVES 55
STUDYING AND ENGINEERING BRL3 PROMOTER TO ENHANCE ABIOTIC STRESS ADAPTATION IN *ARABIDOPSIS THALIANA* 57
2.1 Introduction 59

2.2 Results 61

2.2.1 In-silico analysis of *BRL3* promoter identifies four *cis*-regulatory enriched regions 61

2.2.2 Promoter deletion analysis of *BRL3* reveals its expression in stomata and pinpoints a specific 100 bp region crucial for vascular expression 68

2.2.3 *BRL3* promoter deletion analysis reveals *cis*-regulatory regions governing quiescent center and vascular initials *BRL3* expression . 72

2.2.4 *BRL3* expression is induced in the hypocotyl upon elevated temperatures: implication of KUA1 as putative mediator 74

2.2.5 *BRL3* expression is induced in the root meristem following DNA damage: implication of SOG1 and ERF115 as putative mediators .. 78

2.2.6 HB15 is repressing *BRL3* transcriptionally through direct binding to its promoter 81

2.2.7 Several homeobox transcription factors are repressing *BRL3* transcriptionally 84

2.2.8 Engineering *BRL3* promoter to enhance its vascular expression 87

BRL3 DOWNSTREAM TRANSCRIPTION FACTORS MODULATE DROUGHT TOLERANCE IN *ARABIDOPSIS THALIANA* 89

3.1 Introduction 91

3.2 Results 94

3.2.1 Screening of genes transcriptionally regulated by BRL3 identifies three transcription factors involved in thermomorphogenesis and drought adaptation 94

3.2.2 MYB96 is a BRL3-dowsntream transcription factor modulating abiotic stress adaptation 103

3.2.3 MYB305 is a BRL3-dowsntream transcription factor modulating abiotic stress adaptation 116

3.2.4 HAT9 is a BRL3-dowsntream transcription factor modulating abiotic stress adaptation 127

UNTARGETED MUTAGENESIS OF BRASSINOSTEROID RECEPTOR SBBRI1 CONFERS DROUGHT TOLERANCE BY ALTERING PHENYLPROPANOID METABOLISM IN *SORGHUM BICOLOR* 139

4.1 Introduction 141
4.2 Results 145
4.2.1 Sorghum BRI1 receptor is restoring Arabidopsis *bri1-301* insensitivity to osmotic stress 145
4.2.2 Overexpression of *BRI1* results in drought susceptibility in *Arabidopsis thaliana* 148
4.2.3 Sorghum *bri1* mutants are less sensitive to osmotic stress . 150
4.2.4 Sorghum *bri1* mutants show increased tolerance to drought stress without penalizing growth 152
4.2.5 The cistrome of Sorghum BES1 shows functional conservation and transcription factor binding to the G-box element, regulating brassinosteroid biosynthesis 155
4.2.6 Sorghum *bri1* mutants exhibit distinctive transcriptional regulation of photosynthesis and lignification 163
4.2.7 Sorghum *bri1* lines are defective in the phenylpropanoid pathway, leading to reduced levels of lignin precursors and accumulation of flavone 168
ENHANCING EXPRESSION OF SORGHUM BRL RECEPTOR VIA EFFICIENT SORGHUM TRANSFORMATION USING A TERNARY VECTOR SYSTEM COMBINED WITH MORPHOGENIC REGULATORS 173
5.1 Introduction 175
5.2 Material and Methods 178
5.2.1 Sorghum transformation 178
5.2.2 RNA *in situ* hybridization in Sorghum shoots 190
5.3 Results 196
5.3.1 Sorghum BRL receptor is enriched in vascular tissues 196
5.3.2 Optimizing conditions of Optical Density (OD) of Agrobacterium, co-cultivation time and temperature 201
5.3.3 Excision-based transformation system 203
5.3.4 Overexpression of *SbBRL* promotes leaf epinasty 206
GENERAL DISCUSSION 211
6.1 Studying and engineering *BRL3* promoter to enhance abiotic stress adaptation in *Arabidopsis thaliana* 213

6.2 BRL3 downstream transcription factors modulate drought stress tolerance in *Arabidopsis thaliana* 219

6.3 Untargeted mutagenesis of brassinosteroid receptor SbBRI1 confers drought tolerance by altering phenylpropanoid metabolism in Sorghum bicolor 226

6.4 Enhancing expression of Sorghum BRL receptor via efficient Sorghum transformation using a ternary vector system combined with morphogenic regulators 232

CONCLUSIONS 239

MATERIAL AND METHODS 247

Chapter 2: Studying and engineering BRL3 promoter to enhance abiotic stress adaptation in *Arabidopsis thaliana* 249

Plant material 249

Engineering BRL3 promoter by CRISPR-Cas9 system 249

BRL3 promoter *in silico* analysis and phylogenetic shadowing. 250

GUS staining 251

Luciferase reporter assay 252

Chromatin immunoprecipitation assay 253

Chapter 3: BRL3 downstream transcription factors modulate drought stress tolerance in *Arabidopsis thaliana* 254

Plant material 254

Thermomorphogenesis 254

Drought stress in adult plants 255

Hydrotropism 255

GUS staining 256

Western blot 257

Co-immunoprecipitation 258

Bimolecular fluorescence complementation 259

Gene ontology enrichment analysis and Venn diagrams 259

Chapter 4: Untargeted mutagenesis of brassinosteroid receptor SbBRI1 confers drought tolerance by altering phenylpropanoid metabolism in *Sorghum bicolor* 260

Plant material 260
Sorbitol sensitivity in root Arabidopsis seedlings 261
Drought stress in Arabidopsis adult plants 261
Sorbitol sensitivity in Sorghum seedlings 262
Drought stress in Sorghum seedlings 263
DNA affinity purification sequencing (DAP-seq) 263
Transcriptomic profiling analysis 266
Metabolite profiling analysis 267
Chapter 5: Enhancing expression of Sorghum BRL receptor via efficient Sorghum transformation using a ternary vector system combined with morphogenic regulators 269
BIBLIOGRAPHY 271
LIST OF FIGURES 335
LIST OF TABLES 339
ACKNOWLEDGMENTS 341

ABBREVIATIONS

ABA: Abscisic acid
ABI: ABA INSENSITIVE
ACE: ACTIVATOR FOR CELL ELONGATION
AIF: ATBS1 INTERACTING FACTORS
ARF6: AUXIN RESPONSE FACTOR 6
ATG8: AUTOPHAGY-RELATED 8
ATM: ATAXIA TELANGIECTASIA MUTATED
BAK1: BRI1 ASSOCIATED RECEPTOR KINASE 1
BES1: BRI1-EMS-SUPRESSOR 1
BiFC: Bimolecular fluorescence complementation
BIM1: BES1-INTERACTING MYC-LIKE1
BIN2: BRASSINOSTEROID-INSENSITIVE 2
BIR3: BAK1 INTERACTING RECEPTOR 3
BKI1: BRI1 KINASE INHIBITOR 1
BL: Brassinolide
BR: Brassinosteroid
BRAVO: BRASSINOSTEROIDS AT VASCULAR AND ORGANIZING CENTER
BRI1: BRASSINOSTEROID INSENSITIVE 1
BRL1: BRI1-LIKE 1
BRL2: BRI1-LIKE 2
BRL3: BRI1-LIKE 3
BBM: BABY BOOM
BRRE: BR responsive elements
BSA: Bovine serum albumin
BSK: BRASSINOSTEROID SIGNALING KINASES
BSU1: BRI1 SUPPRESSOR 1
BZR1: BRASSINAZOLE RESISTANT 1
CDG1: CONSTITUTIVE DIFFERENTIAL GROWTH 1
Col-0: Columbia ecotype
CPD: CONSTITUTIVE PHOTOMORPHOGENIC DWARF
CRER: *cis*-regulatory enriched regions
CRISPR: Clustered regularly interspaced short palindromic repeats
DAI: Days after infection
DAP-seq: DNA affinity purification sequencing
DSK2: DOMINANT SUPPRESSOR OF KAR 2
DET2: DE-ETIOLATED 2

DLT: DWARF LOW TILLERING
DMSO: Dimethyl sulfoxide
DNA: Deoxyribonucleic acid
DREB: DEHYDRATION-RESPONSIVE ELEMENT-BINDING
DWF4: DWARF4
EDTA: Ethylenediamine tetraacetic acid
ELF6: EARLY FLOWERING 6
EMS: Ethyl methanesulfonate
ERF115: ETHYLENE RESPONSE FACTOR 115
FAST: Fluorescence-accumulating seed technology
FC: Field capacity
FDR: False discovery rate
GFP: Green fluorescence protein
GO: Gene ontology
GOE: Gene ontology enrichment
GOI: Gene of interest
GSK: Glycogen synthase kinase
GUS: Beta-glucuronidase
HAT1: HOMEODOMAIN-LEUCINE ZIPPER PROTEIN 1
HBI1: HOMOLOG OF BEE2 INTERACTING WITH IBH1
HBP1b: HISTONE-BINDING PROTEIN-1B
HLH: Helix-loop-helix
HSP: HEAT SHOCK PROTEINS
IWS1: INTERACT-WITH-SPT6
KUA1: KUODA1
LEA: LATE EMBRYOGENESIS ABUNDANT
LRR: Leucine-rich repeat
MAX2: MORE AXILLARY SHOOT 2
MEME: Multiple EM for motif elicitation
mRNA: Messenger ribonucleic acid
MYBL2: MYELOBLASTOSIS FAMILY TRANSCRIPTION FACTOR-LIKE 2
NAC: NAM, ATAF1/2, and CUC2 TF
OD: Optical density
OFP: OVATE FAMILY PROTEIN
PIF: PHYTOCHROME-INTERACTING FACTOR
PKL: PICKLE
PP2A: PROTEIN PHOSPHATASE 2A
PPT: Phosphinothricin

PRE1: PACLOBUTRAZOL RESISTANCE 1
PUB40: PLAN-U-BOX 40
QC : Quiescent center
qPCR: Quantitative polymerase chain reaction
QTL: Quantitative trait loci
RBOHD: RESPIRATORY BURST OXIDASE HOMOLOG D
RD26: RESPONSIVE TO DESICCATION 26
REF6: RELATIVE OF ELF6
ROS: Reactive oxygen species
RSAT: Regulatory sequence analysis tool
RWC: Relative water content
SDG8: SET DOMAIN GROUP 8
SERK: SOMATIC EMBRYOGENESIS RECEPTOR KINASE
SNP: Single nucleotide polymorphism
SnRK2: SNF1-RELATED PROTEIN KINASE
SOG1: SUPPRESSOR OF GAMMA RESPONSE 1
Stg: Stay-green
TOTEM: Tissue-enrichment web tool
TPL: TOPLESS
TF: Transcription factor
UBC32: E2 UBIQUITIN-CONJUGATIN ENZYME 32
YFPC: YELLOW FLUORESCENT PROTEIN C-terminal
YFPN: YELLOW FLUORESCENT PROTEIN N-terminal
WOX5: WUSCHEL-RELATED HOMEOBOX 5
WT: Wild-type
WUS: WUSCHEL 2

Chapter 1

GENERAL INTRODUCTION

1.1 Brassinosteroid hormones perception in plants

Brassinosteroids (BRs) are plant steroid hormones. The first discovered BR biologically active hormone was brassinolide (BL), present in the pollen extracts of *Brassica napus* and having a growth promoting effect when applied to pinto bean plants (Grove et al., 1979). Since then, approximately 70 naturally occurring BRs have been reported in their free form or conjugated, and the most frequently distributed are BL, castasterone and typhasterol (Bajguz et al., 2020; Kanwar et al., 2017). All BRs contain a steroid nucleus with a side chain at C17 (D ring), similar to cholesterol, and are typically hydroxylated at C-3, C-22, and C-23, and generally differ in functional groups at C-24 present in the steroid side chain (Mandava et al., 1988).

The initial discovery of BR biosynthesis enzymes, DE-ETIOLATED 2 (DET2) and CONSTITUTIVE PHOTOMORPHOGENIC DWARF (CPD), came from genetic screening of dwarf and de-etiolated in dark *Arabidopsis thaliana* (Arabidopsis) mutants, which reverted to a wild-type (WT) phenotype upon exogenous BL application (Li et al., 1996; Szekeres et al., 1996). Subsequent investigations identified additional BR biosynthesis enzymes, such as DWARF4 (DWF4), a cytochrome P450 that mediates hydroxylation steps in the biosynthesis pathway (Choe et al., 1998). These discoveries underscored the critical role of BRs in growth promotion, cell elongation, and proliferation (Clouse et al., 1996).

Interestingly, in the same context, Clouse et al., 1993, discovered the root growth inhibitory effect at low BRs concentrations. By screening an ethyl methanesulfonate (EMS)-mutagenized population, they identified

a BR-insensitive mutant in Arabidopsis, *brassinosteroid insensitive 1* (*bri1)*, firstly pointing out the presence of a gene important in BR perception or signal transduction. *bri1* mutants exhibited multiple developmental defects that could not be rescued by BR treatment, including dwarf stature, dark green, thickened leaves, male sterility, and de-etiolation of dark-grown seedlings. These phenotypes were alike to those observed in the BR biosynthesis mutants but could not be rescued by BRs (Clouse et al., 1996). Characterization of dwarfed mutants isolated by transposon mutagenesis identified the *cabbage2* mutant as also insensitive to the hormone, with the mutation mapped to the same loci as the *bri1* mutant, further reinforcing the importance of that specific gene in BR perception (Kauschmann et al., 1996).

1.1.1 The BRI1 receptor

One year later, a total of 18 EMS-mutagenized Arabidopsis mutants were identified as *det2*-like mutants showing impaired response to BL (Li et al., 1997). All 18 mutants were alleles of a single previously described gene, *BRI1*. BRI1 was initially characterized as a leucine-rich repeat (LRR) receptor-like kinase, with ubiquitous expression throughout Arabidopsis plants (Li et al., 1997). Functionally, BRI1 is a plasma membrane-localized receptor that harbors a serine/threonine kinase domain responsible for mediating BR signaling through serine/threonine phosphorylation events (Friedrichsen et al., 2000). Its extracellular region is composed of 25 tandem LRRs, facilitating the perception of BRs (He et al., 2000). Notably, BR perception, particularly BL perception, occurs at the cell surface, contrasting with animal steroid perception mechanisms mediated by nuclear proteins (Wang et al.,

2001). BL specifically binds to a 70-amino acid island domain situated between LRR21 and LRR22 (Kinoshita et al., 2005; Caño-Delgado et al., 2004). BRI1 undergoes ligand-independent homo-oligomerization and transphosphorylation within its C-terminal domain. Upon ligand binding inhibits the C-terminal kinase activity, thereby activating BRI1 (Wang et al., 2005). Homodimerization of BRI1 primarily occurs at the plasma membrane, although upon hormone perception, it heterodimerizes with BRI1 ASSOCIATED RECEPTOR KINASE 1 (BAK1) to initiate plant steroid signaling (Nam et al., 2002; Russinova et al., 2004). Analogous to animal systems, ligand-dependent oligomerization followed by autophosphorylation leads to intracellular kinase activation. This mechanism is mirrored in BRI1/BAK1 heterodimerization, where transphosphorylation of their kinase domains propagates the signal downstream by phosphorylating cytoplasmic substrates (Wang et al., 2005). BRI1 KINASE INHIBITOR 1 (BKI1) negatively modulates BR signaling by directly interacting with the BRI1 kinase. BKI1 binds to the BRI1 C-lobe domain, essential for BRI1 binding to BAK1, thereby preventing BRI1/BAK1 interaction (Jaillais et al., 2011). Upon BL binding, the BRI1-BKI1 interaction is disrupted, leading to BKI1 dissociation from the plasma membrane (Wang et al., 2006). Lastly, another negative regulator involved in avoiding hormone perception is BAK1 INTERACTING RECEPTOR 3 (BIR3). BIR3 interacts directly with BRI1 and negatively regulates BR signaling. Upon ligand exposure, BIR3 is released from BAK1 and BRI1, enabling the formation of the BAK1/BRI1 complex (Imkampe et al., 2017).

1.1.2 The brassinosteroid vascular receptors BRL1 and BRL3

Based on sequence similarity, three members of the BRI1 family were identified: BRI1-LIKE 1, 2, and 3 (BRL1, BRL2, and BRL3). BRL1 and BRL3, but not BRL2, demonstrated high-affinity binding to BL (Caño-Delgado et al., 2004). Expression of *BRL1* and *BRL3* under the control of the *BRI1* promoter or the constitutive *Cauliflower Mosaic Virus 35S* promoter successfully rescued the phenotypes of *bri1* mutant, confirming their functionality in perceiving BRs (Caño-Delgado et al., 2004; Zhou et al., 2004).

One notable distinction among these BR receptors is their expression patterns. While *BRI1* is ubiquitously expressed, *BRL1* and *BRL3* are primarily enriched in vascular tissues (Caño-Delgado et al., 2004; Fàbregas et al., 2013). Specifically, *BRL1* and *BRL3* are localized in the differentiation zone of the root, particularly within the vasculature, and in the root meristem, specifically within the quiescent center (QC), columella stem cells, and provascular cells, including vascular initials (Nawy et al., 2005; Fàbregas et al., 2013; Salazar-Henao et al., 2016). Further characterization of *BRL3* expression revealed its presence in the phloem pole pericycle of the differentiated zone and the protophloem cell files of the root meristem (Fàbregas et al., 2013; Salazar-Henao et al., 2016). Additionally, BRL3 was found to interact with the BAK1 coreceptor, underscoring the conservation of BR sensing mechanisms (Fàbregas et al., 2013).

1.2 Brassinoteroid signal transduction

Upon hormone perception, BRI1/BAK1 heterodimerization and posterior transphosphorylation propagates the signal downstream. The final signal transduction is mediated by BR-related transcription factors (TFs) BRI1-EMS-SUPRESSOR 1 (BES1) and BRASSINAZOLE RESISTANT 1 (BZR1) (Figure 1.1).

1.2.1 Brassinoteroid signal transduction when it is attenuated

When BRs are present at low levels, BR signaling is suppressed by the action of the glycogen synthase kinase 3 (GSK3)/SHAGGY-like kinase BRASSINOSTEROID-INSENSITIVE 2 (BIN2). BIN2 functions downstream of the BRI1 receptor to negatively modulate BR signaling (Li et al., 2001; Li et al., 2002). TFs BES1 and BZR1, which serve as the final effectors of BR signaling, possess conserved GSK3 phosphorylation sites and are susceptible to phosphorylation by BIN2 (Zhao et al., 2002). Although BES1 and BZR1 are primarily localized in the nucleus, their phosphorylation by BIN2, in the absence of BRs, leads to their destabilization and compromises protein accumulation (Zhao et al., 2002; Yin et al., 2002; He et al., 2002). Following BIN2-mediated phosphorylation, BES1 and BZR1 are sequestered in the cytoplasm by 14-3-3 proteins, resulting in increased proteasome-mediated degradation and inhibition of their Deoxyribonucleic acid (DNA) binding activity (Gampala et al., 2007; He et al., 2002; Vert et al., 2006).

1.2.2 Brassinosteroid signal transduction when it is activated

When BR are perceived, the BRI1/BAK1 receptor complex initiates signal transduction by phosphorylating cytoplasmic substrates. This cascade culminates in the dephosphorylation and subsequent nuclear accumulation of the TFs BES1 and BZR1, which orchestrate downstream BR responses and provide feedback regulation of BR biosynthesis (Yin et al., 2002; Wang et al., 2002; He et al., 2002).

To facilitate the dephosphorylation and nuclear activation of BES1 and BZR1 TFs, several phosphorylation events occur. BRI1-SUPPRESSOR 1 (BSU1), a nuclear-localized serine-threonine phosphatase, modulates the phosphorylation status of BES1, counteracting the action of BIN2 and thereby increasing the steady-state levels of dephosphorylated BES1 (Mora-García et al., 2004). Additionally, PROTEIN PHOSPHATASE 2A (PP2A) interacts with BZR1, dephosphorylating and activating it (Tang et al., 2011). Concurrently, BRs induce the proteasome-mediated degradation of BIN2, facilitating the dephosphorylation of BES1 and BZR1 (Peng et al., 2008).

The connection between the plasma membrane receptor complex BRI1/BAK1 and the subsequent dephosphorylation of BES1 and BZR1 or degradation of BIN2 is mediated by several intermediate kinases. BRASSINOSTEROID SIGNALING KINASES 1 and 3 (BSK1 and BSK3) interact with the inactive form of BRI1. Phosphorylation of BSKs by the BRI1/BAK1 complex results in BSKs dissociation (Tang et al., 2008). BRI1-mediated phosphorylation of BSK1 promotes its interaction

with BRI1 SUPPRESSOR 1 **(**BSU1), which then inactivates BIN2 by dephosphorylating a conserved phosphor-tyrosine residue, consequently inhibiting BZR1 phosphorylation mediated by BIN2 (Kim et al., 2009). Although BSKs exhibit redundant biological functions in BR signaling, suggesting a regulatory interplay between BSKs and GSK3-like kinases (Sreeramulu et al., 2013). Additionally, BRI1 phosphorylates and activates CONSTITUTIVE DIFFERENTIAL GROWTH 1 (CDG1) receptor-like cytoplasmic kinase, which in turn phosphorylates and activates BSU1, leading to BIN2 inactivation by dephosphorylation (Kim et al., 2011).

1.3 Activity and regulation of BES1 and BZR1

BES1 and BZR1 are highly specific TFs in plants, characterized by a nuclear localization signal, a conserved N-terminal domain shared across the family, a BIN2 phosphorylation domain, a PEST motif involved in protein degradation in the absence of BRs, and a carboxyl-terminal domain. These TFs exhibit an 88% homology and bind DNA primarily through their N-terminal domains, known as BZR domains due to their high conservation among BZR1-related proteins (He et al., 2005). A diverse range of BRs-regulated gene expression studies have revealed that BRs regulate more than 5000 genes, with about half induced and half repressed by the hormone (Guo et al., 2013).

BZR1 acts as a transcriptional regulator, displaying both activator and repressor functions on various promoters. BES1 and BZR1 share similar binding sequences, with a high affinity for BR responsive elements

(BRRE) (CGTG T/C G) and a lower affinity for E-boxes (CANNTG). The determination of whether BZR1 activates or represses a target gene depends on the promoter structure. In addition to BRRE and E-boxes, other BZR1 enriched cis-elements include the G-box (CACGTG, containing two inverted repeats of the BRRE core sequence CGTG, also a type of E-box), CATGTG (another type of E-box), and a GGTCC motif. BRRE and G-box elements are more enriched in BR-repressed genes, while the CATGTG motif is more enriched in BR-induced genes. These findings suggest a possible mechanism in which BZR1 homodimers repress gene expression through BRRE and heterodimers with other TFs mediate activation through other motifs (Sun et al., 2010).

BES1 primarily binds to and regulates BR target gene promoters. It synergistically binds to E-boxes (CANNTG) in conjunction with BES1-INTERACTING MYC-LIKE1 (BIM1) (Yin et al., 2005). BES1 binding to E-boxes is observed in both BR-repressed and BR-induced genes, while BRRE is more prevalent in BR-repressed genes. BES1 can bind to both BRRE and E-boxes (CACGTG and CACTTG). The stronger binding of BES1 to BRRE elements compared to E-boxes likely stems from its requirement for a heterodimer partner to efficiently bind E-boxes (Yu et al., 2011).

As previously noted, BIN2-mediated phosphorylation of BES1 and BZR1 sequesters them in the cytoplasm, leading to proteasome-mediated degradation and inhibition of their DNA binding activity (Gampala et al., 2007; He et al., 2002; Vert et al., 2006). However, the regulation of BES1 and BZR1 involves a more intricate post-translational process.

BRI1 signaling not only suppresses BIN2 kinase activity to facilitate BZR1 dephosphorylation but also elevates cellular H_2O_2 levels, inducing

the oxidation of BZR1 and enhancing its transcriptional activity. This effect is achieved through the promotion of interaction between BZR1 and AUXIN RESPONSE FACTOR 6 (ARF6) or PHYTOCHROME-INTERACTING FACTOR 4 (PIF4) (Tian et al., 2018).

While phosphorylation of BES1 and BZR1 contributes to proteasome-mediated degradation, ubiquitination is the primary mechanism driving degradation through the 26S proteasome system, rather than phosphorylation (Sharma et al., 2016). The ubiquitin E3 ligase PLAN-U-BOX 40 (PUB40) coordinates phosphorylation and ubiquitination to facilitate the proteasomal degradation of BZR1. BIN2-induced phosphorylation of PUB40 enhances the interaction between PUB40 and BZR1, leading to BZR1 degradation and stabilizing PUB40 (Kim et al., 2019). Furthermore, BES1 degradation is mediated by MORE AXILLARY SHOOT 2 (MAX2)-mediated polyubiquitination triggered by strigolactone signaling (Wang et al., 2013).

Additionally, a proteasome-independent ubiquitination-dependent regulatory mechanism for BES1 has been elucidated. BES1 interacts with the ubiquitin-binding receptor protein DOMINANT SUPPRESSOR OF KAR 2 (DSK2), leading to its targeting to the autophagy pathway through interaction with AUTOPHAGY-RELATED 8 (ATG8). BIN2-mediated phosphorylation of DSK2 promotes the interaction between DSK2 and ATG8, facilitating BES1 autophagy-mediated degradation (Nolan et al., 2017).

1.4 Brassinosteroid transcriptional network

BES1 and BZR1 play a crucial role in orchestrating the expression of numerous genes involved in BR signaling. However, the intricate regulation of BR signaling often involves a transcriptional network where BES1 and BZR1 interact antagonistically or synergistically with other TFs to finely tune gene expression. Notably, BES1 and BZR1 exhibit both activating and repressive effects on gene expression, highlighting the complexity of their regulatory roles.

Numerous co-regulators have been recognized as positive regulators of gene expression, synergistically acting with BES1 and BZR1. BES1 collaborates with BIM1 to synergistically bind E-boxes and activate gene expression (Yin et al., 2005). Additionally, MYB30 interacts with BES1 to promote BR target gene expression, binding simultaneously to MYB-binding sites and E-boxes (Li et al., 2009). Furthermore, BES1 directly interacts with INTERACT-WITH-SPT6 (IWS1), a protein involved in RNA polymerase II recruitment and transcriptional elongation, essential for BR-induced gene expression (Li et al., 2010). BES1 and BZR1 interaction also contribute to the epigenetic regulation of histone modifications. SET DOMAIN GROUP 8 (SDG8) interacts with both BES1 and IWS1, facilitating H3K36 methylations crucial for gene expression regulation (Wang et al., 2014). Moreover, histone demethylases EARLY FLOWERING 6 (ELF6) and RELATIVE OF ELF6 (REF6) interact with BES1 to remove H3K27me3, enabling gene expression (Yu et al., 2008). Additionally, BZR1 interacts with chromatin-remodeling factor PICKLE (PKL) and PHYTOCHROME-

INTERACTING FACTOR3 (PIF3) to coregulate skotomorphogenesis by removing H3K27me3 on target promoters (Zhang et al., 2014).

Conversely, BES1 and BZR1 also have co-regulators to downregulate BR-repressed genes. HOMEODOMAIN-LEUCINE ZIPPER PROTEIN 1 (HAT1) directly interacts with BES1 to inhibit BR-repressed genes cooperatively, and HAT1 stabilization is mediated by BIN2-mediated phosphorylation (Zhang et al., 2013). BES1 interacts with MYELOBLASTOSIS FAMILY TRANSCRIPTION FACTOR-LIKE 2 (MYBL2) to downregulate BR-repressed gene expression, with BIN2-mediated phosphorylation further stabilizing MYBL2 (Ye et al., 2012). Additionally, the EAR motif in BZR1 mediates interaction with the Groucho/TUP1-like corepressor TOPLESS (TPL), recruiting TPL to the promoters of BZR1-repressed genes (Oh et al., 2014). Moreover, BES1 forms a transcriptional repressor complex with TPL and HDA1 to suppress abscisic acid (ABA) signaling during early seedling development (Ryu et al., 2014).

Furthermore, BR signaling promotes growth while antagonizing drought stress responses, and various complexes have been identified to balance these responses. PIF4, directly interacts with BZR1 to coordinate the regulation of nearly 2000 common target genes, promoting cell elongation and integrating BR signaling with environmental cues such as light and temperature (Oh et al., 2012). BES1 can also interact with PIF4. BES1 homodimers bind to conserved BRRE and G-box elements in BR biosynthesis promoters to inhibit their expression during light conditions. However, elevated levels of PIF4 in the dark compete for BES1 dimer formation, resulting in the activation of BR biosynthesis

genes and subsequent promotion of hypocotyl growth at dawn or under elevated temperatures (Martinez et al., 2018).

Moreover, WRKY46, WRKY54, and WRKY70 have been identified as positive regulators of BR-mediated plant growth. WRKY54 interacts with BES1 to negatively regulate dehydration-induced genes synergistically, and its activity is modulated by phosphorylation and destabilization by BIN2 kinase (Chen et al., 2017).

In contrast, BES1 and BZR1 interaction can act antagonistically to balance growth and drought responses. For example, TINY, an AP2/ERF TF, inhibits BR-regulated plant growth while promoting drought responses by antagonizing BES1-mediated transcriptional regulation. BIN2 phosphorylates and stabilizes TINY, thereby positively regulating its activity (Xie et al., 2019). RESPONSIVE TO DESICCATION 26 (RD26) interacts with BES1 to antagonize its transcriptional activity on BR-regulated genes. BR signaling represses *RD26* expression and its homologues to inhibit drought responses (Ye et al., 2017).

Furthermore, protein phosphatase ABA INSENSITIVE 1 (ABI1), a negative regulator in ABA signaling, dephosphorylates and destabilizes BIN2 to inhibit its activity. RD26 is stabilized by ABA in a BIN2-dependent manner. BIN2 interacts with and phosphorylates RD26, activating this TF to regulate drought-responsive genes. In summary, drought induces ABA signaling, relieving ABI1 inhibition of BIN2 and allowing BIN2 activation. Subsequently, BIN2 phosphorylates and activates RD26, promoting drought stress responses (Jiang et al., 2019).

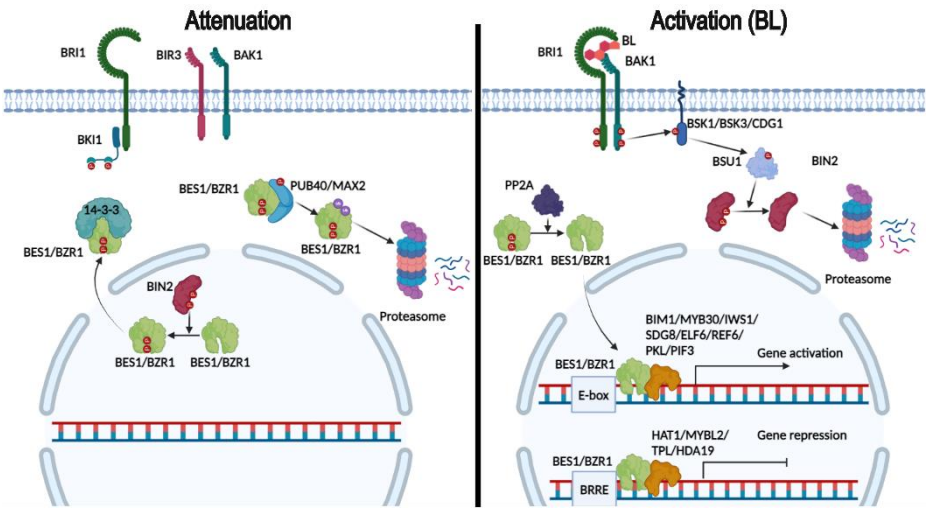


Figure 1.1 Working model of the brassinosteroid signal transduction. In the absence of BRs, BRI1 and BAK1 heterodimerization is inhibited by BKI1 binding to the BRI1 kinase. This inhibition prevents signal transduction, resulting in the cytoplasmic retention and degradation of BES1 and BZR1, as well as reduced DNA binding due to the direct action of BIN2, 14-3-3 proteins, PUB40, and MAX2. Upon BR perception, BRI1 and BAK1 undergo heterodimerization and transphosphorylation, leading to the dephosphorylation and activation of BES1 and BZR1. The heterodimerization triggers multiple phosphorylation events, including BIN2 dephosphorylation and degradation by BSU1, and dephosphorylation of BES1/BZR1 by PP2A. Once dephosphorylated and activated, BES1 and BZR1 interact with various TFs to modulate BR-mediated gene expression, either activating or repressing target genes.

1.5 Brassinosteroids in plant development and adaptation to abiotic stress

1.5.1 Brassinosteroids in plant development

BRs promote overall plant growth, playing essential roles in cell expansion, vascular differentiation, etiolation, and reproductive development (Clouse et al., 1998). Postembryonic growth involves cell proliferation, elongation, and differentiation. Although BRs regulate each of these processes, research has focused on cell elongation, primarily inferred from changes in hypocotyl length (Fridman et al.,

2013). Light, temperature, BRs, auxins, and gibberellins, among other signals, regulate cell elongation. Both auxins and BRs promote cell expansion interdependently, showing synergistic interactions at the downstream level but not at the biosynthetic level (Nemhauser et al., 2004). BR promotion of cell elongation occurs from the epidermis tissue (Savaldi-Goldstein et al., 2007).

Molecular mechanisms have been described to characterize BR-mediated hypocotyl elongation. PIF4, which integrates light signals, and BZR1, which integrates BR signaling, heterodimerize and regulate gene expression to promote cell elongation (Oh et al., 2012). Light and BRs, along with temperature, regulate cell elongation by influencing the expression of the helix-loop-helix (HLH) TF *PACLOBUTRAZOL RESISTANCE 1* (*PRE1*). This cell elongation promotion is mediated by an antagonistic HLH/basic HLH module, regulated by the BZR1/PIF4 heterodimer, which increases RNA levels of the HLH TF *PRE1* and represses the basic HLH TF *ILI1 BINDING PROTEIN 1* (*IBH1*). PRE1, through heterodimerization, also represses the activity of IBH1 (Zhang et al., 2009).

IBH1 is a negative regulator of cell elongation, interacts with and inhibits the TFs HOMOLOG OF BEE2 INTERACTING WITH IBH1 (HBI1) and ACTIVATOR FOR CELL ELONGATION (ACEs), which are positive regulators of cell elongation. These regulators directly bind to promoters and activate *EXPANSIN* genes encoding cell-wall-loosening enzymes. Thus, the BZR1/PIF4 promotion of *PRE1* expression induces the activation of HBI1 and ACEs by sequestering IBH1 (Bai et al., 2012; Ikeda et al., 2013). Additional ATBS1 INTERACTING FACTORS (AIFs) AIF2, AIF3, and AIF4 can also interact with PRE1, similarly to

IBH1, negatively regulating cell elongation. However, these *AIFs* are induced by light, contrasting with the BR dependence of *IBH1* expression (Wang et al., 2009; Ikeda et al., 2012). In summary, BZR1 and PIF4 TFs integrate light, temperature, and BR signaling to regulate cell elongation through the HLH module.

Additional signaling pathways, specifically driven by gibberellins and auxins, are integrated into the molecular mechanisms regulating cell expansion. Under low gibberellin levels, DELLA proteins accumulate and bind BZR1 and PIF4, inhibiting their activity (De Lucas et al., 2008; Li et al., 2012). Additionally, the ARF6, TF, regulated by auxins, is interconnected with the HLH module and the DELLA proteins, regulated by gibberellins. BZR1, PIF4, and ARF6 interact and cooperatively regulate shared target genes and hypocotyl cell elongation. In the absence of gibberellins, DELLA proteins also interact with ARF6, inhibiting its DNA-binding domain. Moreover, ARF6 modulates the HLH module via a positive feedback loop with HBI1 (Oh et al., 2014).

In conclusion, BR signaling, in conjunction with other environmental signals, primarily regulates cell elongation through the HLH module, ARF6, and DELLA proteins, in a coordinated manner.

BRs also tightly regulate root development, promoting root growth in a dose-dependent manner (Müssig et al., 2003; Chaiwanon et al., 2015; González-García et al., 2011). Despite some physiological similarities between BRs and auxins, their functional interaction in root development remains unclear. However, BRs are required for lateral root development and act synergistically with auxins to promote lateral root formation. BR signaling facilitates auxin transport, specifically promoting the acropetal auxin transport necessary for lateral root formation (Bao et al., 2004).

Another study demonstrated that BR signaling is spatially patterned and interacts antagonistically with auxins to control the spatiotemporal balance of stem cell dynamics required for optimal root growth. BZR1 primarily activates target genes in the elongation zone while repressing its targets in the QC and surrounding stem cells, with auxin generally having opposite effects. Furthermore, low levels of BR-activated nuclear BZR1 are found in the root stem cell niche, while high levels are present in the root elongation zone, with this BZR1 pattern requiring auxin synthesis (Chaiwanon et al., 2015).

A balance of BRs is essential for proper root meristem development. BR-insensitive mutants, such as *bri1-116*, exhibit reduced meristem size due to lower mitotic activity. Conversely, exogenous BL treatment or BR signaling-enhanced mutants, such as *bes1-D*, show premature cell cycle exit, leading to early differentiation of meristematic cells and negatively impacting meristem size and overall growth (González-García et al., 2011). Additionally, BRs are necessary to maintain a gradient of cells in the meristem, positively affecting cell cycle activity and cell expansion rate. Notably, BRI1 can control root meristem size from the epidermis, confirming that BR signaling mediated by BRI1 is required for proper root meristem development and root growth regulation (Hacham et al., 2011). The Sizer model was subsequently proposed to better define BR-mediated cell cycle control in the root meristem. This model suggests that cells sense their length and stop elongating upon reaching a threshold value, with BRI1 being crucial for regulating this mechanism (Pavelescu et al., 2018).

The *bri1brl1brl3* triple mutants exhibit protophloem and root growth defects. Later studies revealed that the reduced meristem size in

bri1brl1brl3 mutants could be entirely attributed to reduced cell elongation, contrasting with previous studies that emphasized cell cycle progression regulation (Kang et al., 2017). Further research showed that expressing *BRI1* in developing phloem was sufficient to systematically correct the cellular growth and patterning defects underlying the triple mutant phenotype. Although this reversion was BR-dependent, it did not rely on BRI1 downstream effectors, possibly involving non-canonical signaling. This phloem-specific rescue was attributed to CLAVATA3/EMBRYO SURROUNDING REGION-RELATED 45 (CLE45) peptide signaling in roots, as mutation in *CLE45* in *bri1brl1brl3* mutants rescued the abnormal phloem development (Kang et al., 2017; Graeff et al., 2021). However, later studies suggested that a threshold level of BR perception across multiple tissues, if not all, is necessary for a comprehensive rescue of *bri1brl1brl3* mutants, indicating that BR receptors largely act in a cell-autonomous manner (Blanco-Touriñan et al., 2024).

Digital 3D single-cell shape analysis and single-cell messenger ribonucleic acid **(**mRNA) sequencing demonstrated that BR signaling does not affect cell volume or cell proliferation but is essential for the precise orientation of cell division planes and cell expansion (Graeff et al., 2022). Another study found that BR biosynthesis is restricted to the elongation zone and low in the meristem, suggesting that both BR signaling, and biosynthesis are important for regulating root development, given the absence of long-distance hormone transport in plants (Vukasinovic et al., 2021).

In conclusion, BRs control root meristem development and root growth through combinatorial effects on cell cycle progression and cell expansion, maintaining a precise balance in a cell-autonomous manner.

1.5.2 Brassinosteroids in plant adaptation to abiotic stress

In addition to their explicit roles in plant growth and development, integrating environmental signals such as light, temperature and other hormonal pathways, BRs also regulate plant adaptation to abiotic stresses such as drought, osmotic and genotoxic stress (Figure 1.2). The ability of plants to cope with abiotic stresses relies on a finetuned balance between growth and adaptation to stress (Planas-Riverola et al., 2019).

1.5.2.1 Brassinosteroids in plant adaptation to drought stress

BRs have been described to act antagonistically to ABA, the main hormone accumulated and positively regulating plant adaptation to drought and osmotic stress and with an inhibitory effect on plant growth (Cutler et al., 2010). There is a high number of co-regulated genes by ABA and BRs, reinforcing the interplay between these two hormone types. A study of the conserved motifs found in the genes that are behaving differently upon ABA vs BR treatment, found that BRRE motif was enriched in promoters from genes upregulated by ABA and downregulated by BR, conversely, they found an enrichment in GAGA motif in promoters from genes downregulated by ABA and upregulated by BR (Chung et al., 2014). BR-insensitive mutants, as *bin2* mutants, are

showing a hypersensitivity to ABA hormone, highlighting the antagonistic role of these two hormones (Li et al., 2001). Posterior studies established a molecular relation between BIN2 and ABA signaling. Whereas BIN2 represses the BR signaling pathway through phosphorylation of BES1/BZR1, it instead activates the ABA-mediated stress response by directly interacting and phosphorylating SNF1-RELATED PROTEIN KINASE 2 (SnRK2) (Cai et al., 2014) and ABSCISIC ACID INSENSITIVE5 (ABI5) (Hu and Yu, 2014).

Apart from BIN2 involvement in ABA signaling activation, it seems that BES1 is one of the main players promoting growth and antagonistically acting in drought responses. BES1 directly interacts with DSK2, a ubiquitin-binding receptor involved in protein degradation pathway. During abiotic stress conditions, drought or fixed-carbon starvation, BES1-DSK2 interaction leads to BES1 ATG8-mediated autophagy, reducing plant growth under drought stress conditions (Nolan et al., 2017). This study highlights the importance of BES1 posttranslational regulation upon stress conditions to avoid growth and prioritize the drought stress responses.

In addition to regulating BES1 protein levels upon drought stress, we can find direct interaction of BES1 with other TFs modulating the transcriptional control to balance BR-driven growth and ABA-driven drought stress responses. RD26 and BES1 act antagonistically in the regulation of gene expression. RD26 protein is accumulated upon high salt, drought and ABA treatment and function as a transcriptional activator of ABA-responsive genes (Fujita et al., 2004). BES1 inhibits the transcription of *RD26* upon BR signaling, while RD26 is directly interacting and inhibiting BES1 transcriptional regulation of BR-

responsive genes. BES1 binding to BRRE elements drives to target transcriptional repression and BES1 binding to E-boxes to activation, but RD26 neutralizes BES1 transcriptional regulation by forming an inactive heterodimer. This complex regulation at transcriptional and protein level is stablishing a balance between growth and drought survival. Whereas constitutively active *BES1* in *bes1-D* plants is resulting in drought susceptibility, low transcriptional regulation activity of BES1 through *RD26* overexpression is resulting in drought tolerance and a growth penalization (Ye et al., 2017). RD26 is also phosphorylated and activated by BIN2 kinase, a negative regulator of BR signaling, promoting drought stress responses (Jiang et al., 2019). TINY, an AP2/ERF family TF, acts in a similar manner to RD26. TINY can interact with BES1 to inhibit the transcriptional regulation of BR-responsive genes, therefore promoting the drought-responsive genes and inhibiting growth. BIN2 is also phosphorylating and stabilizing TINY (Xie et al., 2019). Finally, WRKY46, WRKY54 and WRKY70, act synergistically with BES1, by direct protein interaction, in order to promote BR signaling and growth and inhibit drought responses. These WRKY TFs are induced transcriptionally by BES1 and negatively regulated by BIN2 phosphorylation in a similar manner than BES1/BZR1 TFs, reinforcing the idea that they are involved in the BR signaling pathway (Chen, et al., 2017).

Altogether, these findings suggest that BR signaling negatively regulates drought stress-responsive genes in an ABA-dependent or independent manner, promoting the overall growth of the plant. Recent studies perform in our lab, further suggest the role of BR signaling in growth promotion and their antagonistic function in drought stress. BR loss-of-function mutants (such as *bri1* and *bak1*) were showing drought

resistance phenotypes caused by a reduction in the overall growth therefore having a reduced exposure to the effect of drought, a known process called drought avoidance (Fàbregas et al., 2018).

Interestingly and in contrast with the previously mentioned results, BL application have resulted in increased tolerance to diverse abiotic stress, in *Zea mays* (maize) (Anjum et al., 2011), Arabidopsis and *Brassica napus* (Kagale et al., 2007). BR increase concentration in *DWF4* overexpressor plants also enhanced plant survival upon drought stress in *Brassica napus* (Shani et al., 2016). Overexpression of the vascular-specific BR receptor BRL3, enriched in the vasculature, also conferred drought resistance without affecting growth arrest. The drought tolerance driven by BRL3 was provided through an increase water stress-induced program cell death, enhanced hydrotropic response and the accumulation of osmoprotectants as raffinose, trehalose and proline (Fàbregas et al., 2018), leading to a higher survival rate after severe water deprivation. A study in *Solanum lycopersicum* (tomato) determined that exogenous application of BL was enhancing drought tolerance and drought-related gene expression, while overexpressing *SlBRI1* resulted in increased H_2O_2 levels and drought susceptibility (Nie et al., 2019). Finally, BRs were found to modulate the ABA-induced stomatal closure in Arabidopsis. BL treatment promoted stomatal closure in an ABA-independent manner, however also inhibited the ABA-induced stomatal closure. In addition, the ABA-mediated induction of expression of several genes involved in reactive oxygen species (ROS) production, important for stomatal closure, such as *RESPIRATORY BURST OXIDASE HOMOLOG D* (*RBOHD*), were repressed by BL (Ha et al., 2016). These findings are suggesting that probably some of the drought tolerant phenotypes obtained by exogenous application of BL or

overexpression of biosynthetic enzymes are not driven by BRI1 signaling cascade including BES1 activation but by BRL3 signaling in a cell-specific manner. Further work needs to be done to decipher the mechanisms downstream BR application that are conferring drought tolerance.

1.5.2.2 Brassinosteroids in plant adaptation to osmotic stress

Exogenous applications of BRs have been shown to alleviate the effects of salt stress in various plant species, including *Robinia pseudoacacia* (black locust), *Cucumis sativus* (cucumber), *Vigna radiata* (mung bean), *Brassica juncea* (brown mustard), *Linum usitatissimum* (flax), and Arabidopsis (Yue et al., 2019; Yuan et al., 2012; Hayat et al., 2010; Hayat et al., 2012; Ali et al., 2008; Amraee et al., 2019; Divi et al., 2010).

BR treatment induces ethylene production by activating 1-aminocyclopropane-1-carboxylate synthase, an enzyme involved in ethylene synthesis. Ethylene signaling is also induced by BRs. When ethylene production or signaling is silenced, BR-mediated salt tolerance is inhibited, and the BR-induced expression of several antioxidant enzymes is blocked. Pretreatment with ROS scavengers inhibits BR-induced ethylene production. This suggests that BRs induce ethylene production to cope with salt stress by enhancing the expression of ethylene biosynthesis enzymes and antioxidant enzymes, triggered by ROS accumulation, such as H_2O_2 (Zhu et al., 2016). Additionally, BR application can rescue the hypersensitivity to salt stress in *ethylene insensitive 2* mutants, further reinforcing the interconnection of these hormonal pathways under osmotic stress conditions (Divi et al., 2010).

BR-mediated salt stress tolerance may involve BRI1. Inhibiting BRI1 ubiquitination, which is mediated by the UBC32, reverses the salt hypersensitivity of *bri1-9* mutants, which have a single amino acid substitution causing BRI1 retention and endoplasmic reticulum-mediated degradation (Cui et al., 2012). Moreover, overexpressing *BSK1* from maize, which interacts with BRI1 and transduces the BR signal downstream, results in improved salt tolerance (Tang et al., 2008; Liu et al., 2022). Fàbregas et al. (2018) also showed that the *bri1* mutation leads to sorbitol insensitivity in root meristems, while Zeng et al. (2010) found that *bin2* mutants are hypersensitive to salt stress, further supporting the role of BRI1 in sensing salt/osmotic stress.

In summary, BRs enhance salt stress tolerance in plants through a complex interplay involving ethylene production and signaling, ROS management, and specific BR signaling components such as BRI1 and BSK1.

1.5.2.3 Brassinosteroids in plant adaptation to genotoxic stress

BR signaling has been previously described to control the maintenance of QC cells in plants. In the absence of BRs, the TF BRASSINOSTEROIDS AT VASCULAR AND ORGANIZING CENTER (BRAVO) maintains the quiescence of QC cells (Vilarrasa-Blasi et al., 2014). When BR signaling is activated, such as through the exogenous application of BL, BRAVO is degraded, leading to QC cell division (Vilarrasa-Blasi et al., 2014; González-García et al., 2011). This regulation of quiescence is further modulated by WUSCHEL-RELATED HOMEOBOX 5 (WOX5), which forms a complex with

BRAVO to repress QC cell divisions in the absence of BR signaling (Betegón-Putze et al., 2021). Additionally, BRs activate the expression of the TF ETHYLENE RESPONSE FACTOR 115 (ERF115), which also promotes QC cell divisions (Heyman et al., 2013).

Genotoxic stress, such as DNA double-strand breaks caused by DNA damage, activates the ATAXIA TELANGIECTASIA MUTATED (ATM) kinase. ATM kinase phosphorylates and activates the TF SUPPRESSOR OF GAMMA RESPONSE 1 (SOG1) (Yoshiyama et al., 2013). SOG1 activation leads to various responses, including programmed cell death, endoreduplication, cell cycle regulation, and DNA repair mechanisms through the direct regulation of several genes, including *BREAST CANCER SUSCEPTIBILITY 1* (*BRCA1*) (Ogita et al., 2018). To maintain a functional stem cell niche, dead cells are replenished by inducing QC cell divisions (Heyman et al., 2013). Recently, it has been shown that SOG1 directly induces *BRL3*, which is required for ERF115-mediated QC cell divisions upon DNA damage (Takahashi et al., 2024).

In summary, BR signaling plays a crucial role in regulating QC cell maintenance and division, particularly under stress conditions. The interplay between BRAVO, WOX5, ERF115, and SOG1 ensures the dynamic control of QC cell activity, allowing plants to respond effectively to both developmental cues and environmental stresses.

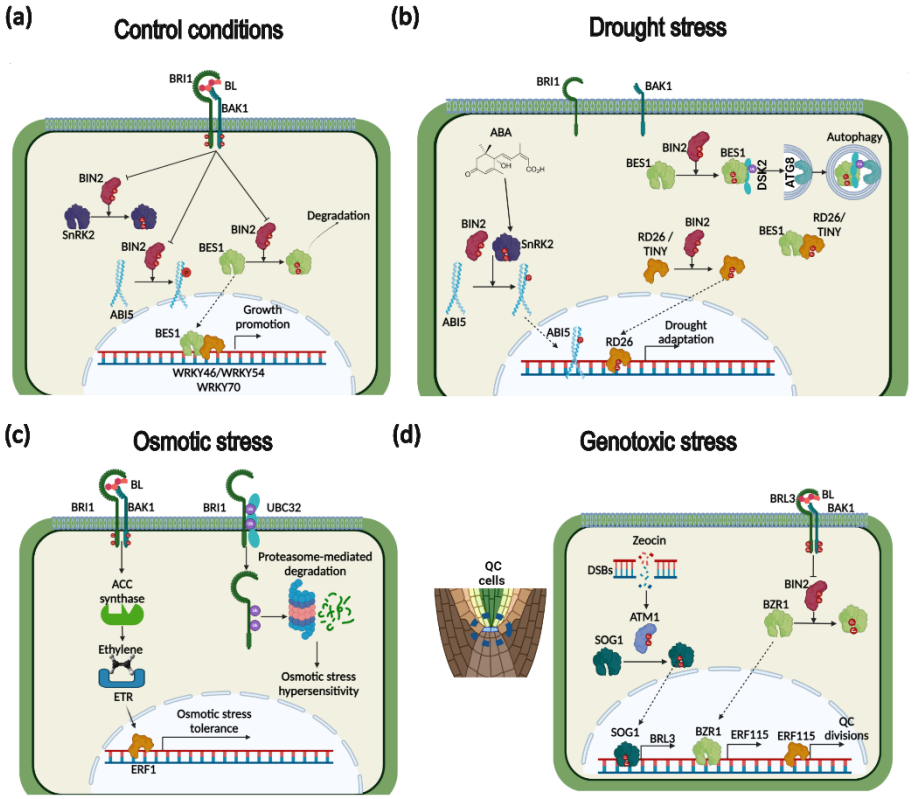


Figure 1.2 Brassinosteroids in plant adaptation to abiotic stress. (a) Under control conditions, BRs promote growth while inhibiting ABA signaling. At the TF level, BES1, in cooperation with WRKYs, antagonizes drought mechanisms and promotes growth transcriptionally. (b) During drought stress conditions, BR signaling is attenuated. This attenuation occurs through mechanisms such as ATG8-mediated autophagy of BES1 or RD26-mediated BES1 inhibition, allowing BIN2 to positively regulate ABA signaling by phosphorylating SnRK2 and ABI5. (c) Under osmotic stress conditions, BR signaling, through BRI1, positively regulates osmotic stress tolerance by promoting ethylene biosynthesis and signaling. This tolerance can be hindered by UBC32, a ubiquitin receptor induced upon salt stress, which ubiquitinates BRI1, leading to subsequent proteasome-mediated degradation. (d) In response to genotoxic stress, specifically double-strand breaks (DSBs), ATM1 activation leads to SOG1-mediated BRL3 transcriptional induction. Subsequent BRL3-mediated signaling induces ERF115 expression, leading to QC divisions.

1.6 Brassinosteroids in crops

BRI1, the primary BR receptor, has been extensively investigated in various crops, with molecular and physiological studies implicating this receptor in the regulation of growth and development. In *Oryza sativa* (rice), phenotypic and molecular characterization of the rice dwarf mutant *d61* revealed the involvement of OsBRI1 in diverse developmental processes, including overall growth, internode elongation, lamina joint bending, skotomorphogenesis, and panicle development (Yamamuro et al., 2000). Homologs of OsBRI1, such as OsBRL1 and OsBRL3, were also found to contribute, at least partially, to BR perception in roots, where they exhibited high expression levels (Nakamura et al., 2006). Additionally, OsBAK1, a co-receptor of OsBRI1, has been explored as a potential molecular breeding tool, with mutations leading to erect-leaf varieties and overexpression resulting in a dwarf phenotype, suggesting functional conservation with Arabidopsis BAK1 as a BRI1 co-receptor (Li et al., 2009).

In tomato, the *curl3* mutant displays extreme dwarfism, altered leaf morphology, de-etiolation, reduced fertility, and insensitivity to BR application, with subsequent studies identifying a missense mutation in the *SlBRI1* gene as the cause (Koka et al., 2000; Montoya et al., 2002). Similarly, the *Hordeum vulgare* (barley) *"uzu"* dwarf variety, known for its lodge resistance, was found to result from a single nucleotide polymorphism (SNP) mutation in the *HvBRI1* gene, leading to reduced hormone sensitivity and altered BR concentration (Chono et al., 2003). In maize, an RNA interference knockdown mutant targeting maize *BRI1* homologs exhibited BR insensitivity and a dwarf phenotype, indicating the significance of these receptors in growth regulation (Kir et al., 2015).

Recent work has shown that the SbBRI1 receptor in *Sorghum bicolor* (Sorghum) shares structurally and functionally conserved roles, playing an important role in root meristem and panicle development (Rico-Medina et al., 2024).

Additionally, several molecular components of BR signaling have been elucidated, with conservation observed across species. In rice, 14-3-3 proteins were found to interact with OsBZR1, modulating its nuclear localization and inhibiting OsBZR1 function (Bai et al., 2007). TaBZR2, a wheat homolog, acts as a positive regulator of drought responses by mediating the crosstalk between BR and drought pathways (Cui et al., 2019).

New components of the BR signaling pathway have also been identified in rice, such as the *dwarf and low tillering* rice mutant (*dlt*), which revealed a new member of the plant GRAS TFs, further elucidating the BR signaling pathway (Tong et al., 2009). GLYCOGEN SYNTHASE KINASE 2 (OsGSK2), a BIN2 rice ortholog, was identified and found to negatively regulate BR responses by phosphorylating DLT (Tong et al., 2012).

Furthermore, *GW5*, a major Quantitative Trait Loci (QTL) associated with rice grain width and weight, was found to be expressed in the plasma membrane and physically interact with and repress the kinase activity of BIN2 rice homolog OsGSK2. This interaction resulted in the accumulation of unphosphorylated OsBZR1 and OsDLT proteins in the nucleus, facilitating BR-responsive gene expression and growth responses, ultimately enhancing grain width and weight (Liu et al., 2017). Additionally, OVATE FAMILY PROTEIN 1 (OFP1) was found to directly interact with DLT. Overexpression of *OFP1* led to BR-

induced phenotypes such as enlarged leaf angles, reduced plant height, and altered grain shape, resembling *DLT* overexpressing plants. BR signaling through OsBZR1 was found to enhance OFP1 levels. Moreover, OFP1 directly interacts with OsGSK2 kinase, and inhibition of the kinase activity leads to OFP1 protein accumulation (Xiao et al., 2017).

Rice HOMEOBOX1 (OsH1) was identified as a repressor of the BR phytohormone pathway. OsH1 activates BR catabolism genes, including *CYP734A2*, *CYP734A4*, and *CYP734A6*, thereby suppressing BR signaling (Tsuda et al., 2014). These newly identified components contribute to the intricate regulation of BR signaling in rice, shedding light on the molecular mechanisms underlying growth and development in this important crop species.

Interestingly, differences between Arabidopsis and rice BR signaling pathways have been uncovered. In rice, PUTATIVE PROTEIN PHOSPHATASE KELCH-LIKE REPEAT DOMAIN 2 (OsPPKL2), a putative homolog of BSU1, was found to regulate grain length by suppressing BR signaling through interaction, dephosphorylation and stabilization of BIN2 ortholog OsGSK3, indicating species-specific regulatory mechanisms (Zhang et al., 2012; Gao et al., 2019).

1.7 Current context of climate emergency and its impact on crop yield

Human activities, principally through the emissions of greenhouse gases, have significantly raised global surface temperatures, reaching 1.1ºC

above 1850-1900 levels in the period 2011-2020. This increase has been particularly rapid since 1970, faster than in any other 50-year period over the last 2000 years. By 2019, atmospheric CO_2 concentrations (410 ppm) were the highest in at least 2 million years, while methane (1866 ppb) and nitrous oxide (332 ppb) levels were the highest in 800,000 years. These changes, driven by human influence, have heightened the frequency of extreme events, such as heatwaves and droughts, since the 1950s, exposing millions to acute food and water insecurity, especially in Africa, Asia, and Central and South America. Moderate future climate change scenarios predict global warming of 1.5ºC in the near term (2021-2040), exacerbating extreme events, flooding, biodiversity loss, and food production insecurity (IPCC, 2023). Therefore, in our current climate change scenario and its respective predictions, we observe a continuous increase in CO_2 levels resulting from human activities, alongside the consequences of reduced water security, increasing frequency of extreme drought and heatwaves, and a global rise in temperature. The increase in CO_2 concentrations and temperature, combined with reduced water availability and more frequent drought periods, are the main contributors to yield changes under climate change (Rezaei et al., 2023).

Elevated CO_2 levels can increase the assimilation and photosynthetic rates in C3 plants, such as wheat and rice, but have minimal or negative effects on C4 plants like Sorghum and maize, due to limitations in Rubisco carboxylation and CO_2 concentrating mechanisms (Xu et al., 2015). Heat stress and elevated CO_2 can enhance net photosynthesis in C3 plants but reduce the thermotolerance of C4 and Crassulacean acid metabolism (CAM) species (Wang et al., 2008). While elevated CO_2 reduces stomatal conductance and transpiration, this may not translate to better water use due to increased leaf area and canopy effects (Ainsworth

et al., 2007; Torngern et al., 2014). Furthermore, elevated CO_2 levels, although promoting grain yield, adversely affect grain quality, including protein and nutrient content (Mcgrath et al., 2013; Högy et al., 2009).

Heat stress around flowering can severely impact cereal grain yields, affecting ovule and pollen sterility, pollen abortion, resource translocation, and grain development (Rezaei et al., 2015; Ullah et al., 2021). Sorghum, which optimizes flowering during cooler hours, still suffers from heat stress impacts on pistils (Jagadish et al., 2020). Drought combined with heat stress can drastically reduce yield by affecting the harvest index, life cycle, and seed quality, independent of C3 or C4 metabolism (Cohen et al., 2020).

Drought alone is a major limitation to food production, causing more annual crop yield loss than all pathogens combined, with an estimated $30 billion loss in the past decade (Gupta et al., 2020). The timing of drought within the plant cycle is critical, with significant impacts during germination, seedling establishment, flower induction, and grain development (Dietz et al., 2021; Barnabás et al., 2007).

In addition to climate change, demographic changes contribute to food security challenges. The global population is projected to increase from the current 8 billion to between 9.7 and 10.9 billion by the end of the century, raising global food demand by 35-62% by 2050 (United Nations, 2022; Van Dijk et al., 2021).

In conclusion, the combined pressures of climate change and a growing global population underscore the urgent need for crops better adapted to changing environments to meet the increasing food demand and ensure food security.

1.8 Engineering brassinosteroid signaling in crops to improve drought resistance.

The engineering of BR signaling pathways and biosynthesis has yielded crop varieties better adapted to prevailing climate change conditions, underscoring the significance of BR signaling modulation in agriculture.

Manipulating BR biosynthesis enzymes to elevate endogenous BR levels has proven effective in improving drought and salt tolerance in crops. Elevated BR levels through *DWF4* overexpression enhanced drought survival in *Brassica napus* (Sahni et al., 2016). Similarly, overexpression of spinach cytochrome P450 involved in BR biosynthesis, *SoCTP85A1*, in *Nicotiana tabacum* (tobacco), enhanced drought tolerance by reducing ROS accumulation and increasing proline content (Duan et al., 2017), whereas overexpression of *Populus euphratica* BR biosynthesis enzyme *CPD* (*PeCPD*) in *Populus tomentosa* improved plant height, biomass, and salt tolerance (Feng et al., 2020). Furthermore, mutation in the BR cytochrome P450 C-6 oxidase *LILIPUTIAN1* enhanced maize seedling adaptation to water scarcity (Castorina et al., 2018). Conversely, overexpressing Arabidopsis BR-inactivating enzyme *BR-RELATED ACYLTRANSFERASE 1* (*AtBAT1*) in creeping grass enhanced drought tolerance (Han et al., 2017).

Engineering BR signaling components in crops has also proven fruitful in fortifying plants against drought and salt stress. Altering the expression levels of key BR receptors like BRI1 and its downstream components has been a commonly employed strategy. Overexpression of *SlBRI1* in tomatoes increased drought susceptibility (Nie et al., 2019), as did overexpression of ZmBRI1-downstream TF ZmBES1/BZR1-1 in

transgenic Arabidopsis and rice (Feng et al., 2023). Conversely, overexpressing *SlBRI1* in tomatoes improved tolerance to salt stress by enhancing cell membrane integrity, osmoprotectant accumulation, photosynthetic capacity, antioxidant activity, and stress-related gene upregulation, thereby enhancing yield and biomass accumulation under high salt concentrations (Wang et al., 2023). In concordance, SOMATIC EMBRYOGENESIS RECEPTOR KINASE 2 (SERK2) was identified as a new BR signaling component in rice as an interactor of OsBRI1. *SERK2* overexpressing rice plants showed enhanced grain size and salt stress resistant, without affecting plant architecture (Dong et al., 2020). In summary, we conclude that the overexpression of *BRI1* was conferring drought susceptibility while obtaining crops more tolerant to salt stress. However, overexpression of another BR-related kinase *BRASSINOSTEROID-SIGNALING KINASE 1 (ZmBSK1)* resulted in drought and salt tolerant maize plants (Liu et al., 2021; Liu et al., 2022).

Furthermore, inducing mutations to downregulate BRI1 receptors has emerged as an effective approach for enhancing drought tolerance in crops. RNA interference knockdown mutants for *BdBRI1* in *Brachypodium distachyon*, a model for cereals, exhibited reduced plant height and enhanced drought tolerance accompanied by elevated expression of drought-responsive genes (Feng et al., 2015). In addition, knockdown mutants for *BdBRI1* in *Brachypodium distachyon* exhibited reduced height and enhanced drought tolerance, accompanied by elevated expression of drought-responsive genes (Feng et al., 2015).

Beyond receptor-level interventions, targeting downstream BR molecular components has shown promise in fortifying crops against drought. Overexpression of *Glycine max* (soybean) *BIN2* homolog *GmBIN2* in Arabidopsis and soybean hairy roots resulted in heightened resistance to both salt and drought stress (Ling-Shuang et al., 2018). Additionally, *OsNAC016* TF emerged as a novel member of the BR signaling pathway in rice. OsNAC016 governs plant architecture by modulating BR signaling, being phosphorylated and destabilized by OsGSK2, and its degradation mediated by E3 ubiquitin ligase OsPUB43, akin to BES1 and BZR1 regulation in Arabidopsis. Moreover, Clustered Regularly Interspaced Short Palindromic Repeats (CRISPR)-mediated mutation in *OsNAC016* led to enhanced drought adaptation by conferring a negative role in ABA-mediated drought response. *Osnac016* mutants exhibited reduced water loss and enhanced stomatal closure (Wu et al., 2022).

Soybean MYB14 TF (GmMYB14) was identified as a participant in BR signaling. Its overexpression resulted in decreased endogenous BR levels, while exogenous application could alleviate BR-related phenotypes such as semi-dwarfism and reduced cell size. *GmMYB14*-overexpressing soybean plants exhibited improved drought tolerance. Furthermore, overexpression of *TaBZR2* significantly enhanced drought tolerance in transgenic wheat (Cui et al., 2019). *Setaria italica* BZR1 regulation by BRs, particularly its dephosphorylation status and nuclear localization, influenced drought stress sensitivity. Overexpression of *SiBZR1* in transgenic plants heightened sensitivity to drought stress by suppressing the expression of *PLETHORA-LIKE 1* (*SiPLT-L1*). Conversely, overexpression of *SiPLT-L1* conferred enhanced drought resistance in *Setaria italica* plants (Zhao et al., 2021).

In cotton, the bHLH TF BEE3-LIKE (GhBEE3-LIKE) is a BR-regulated protein directly modulated by the cotton homolog BZR1. Knockdown mutants of *Ghbee3-like* via virus-induced gene silencing exhibited heightened tolerance to drought stress (Chen et al., 2022).

In conclusion, engineering BR signaling pathways and components presents a multifaceted approach for enhancing drought and salt tolerance in crops, with potential applications across diverse agricultural contexts.

1.9 Sorghum as a monocot model for drought research

Sorghum, a C4 monocot grass that diverged from maize 15 million years ago, is the fifth most important cereal grown worldwide in terms of production, yielding around 57 million tons per year (Mullet et al., 2002; FAOSTAT, 2022). While serving as a significant food source for millions in Africa and Asia, Sorghum remains underutilized in developed countries, where Sorghum is primarily used for animal feed. Nonetheless, Sorghum exhibits considerable potential for human consumption, notably as a gluten-free alternative. Sorghum-based food products, including bread, pasta, porridges, and parboiled rice-like products, present viable options for people with celiac disease (Taylor et al., 2006). In the context of feeding a growing population at the same time as climate change conditions, Sorghum's high protein content and its low irrigation requirements make it a promising alternative to replace other cereal crops like rice. By substituting rice production with Sorghum, water demand can be reduced by 33% while improving protein

production by 1% (Davis et al., 2018). Furthermore, Sorghum offers a climate-resilient alternative to wheat, as it exhibits higher adaptation to elevated temperatures (DeFries et al., 2023).

The demand for renewable energy has driven increased research into alternative biomass conversion methods for fuel production, notably bioethanol. Sweet Sorghum has emerged as a particularly promising energy source for bioethanol due to its high biomass yield on marginal lands unsuitable for food or feed production. Recent studies on sweet Sorghum have identified the *Dry* gene, which encodes a NAM, ATAF1/2, and CUC2 TF (NAC) crucial for stem juiciness traits. This discovery enables the breeding of Sorghum varieties to modulate secondary cell wall biosynthesis and sugar accumulation, crucial factors for biofuel production (Guigou et al., 2011; Zhang et al., 2018).

In addition to its multiple uses, one of the primary benefits of Sorghum cultivation is its drought tolerance mechanisms (Figure 1.3). Sorghum is predominantly grown in semi-arid and arid tropics of Africa and South Asia, with significant production also in China, Southeast Asia, and the Americas (Venkateswaran et al., 2019). Consequently, drought stress is considered the most common abiotic stressor that Sorghum encounters in its major production regions. As a result, significant attention has been devoted to understanding the effects of drought stress on Sorghum and its stress tolerance mechanisms. This research is crucial for the future development of tolerant cultivars and the implementation of efficient mitigation strategies in Sorghum production. Those will be essential to preserve food security globally.

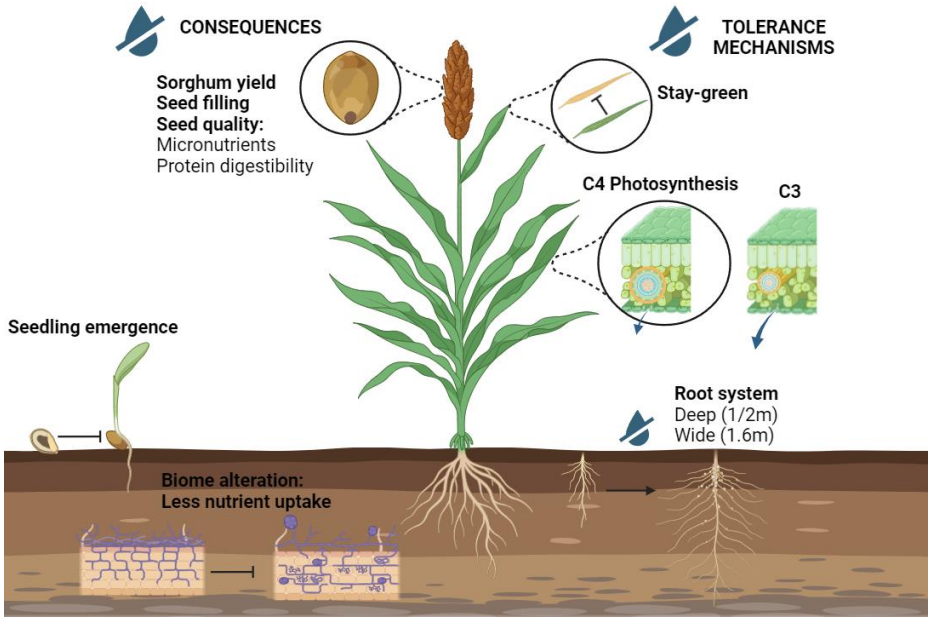


Figure 1.3 The impact of drought on Sorghum and its tolerance mechanisms. Drought stress affects Sorghum development at various stages, including seedling emergence, root establishment, and seed filling. However, Sorghum possesses several mechanisms to cope with this abiotic stress, such as deep and extensive root system, C4 photosynthesis to minimize water loss, and stay-green traits.

1.9.1 Sorghum drought tolerance mechanisms

The "stay-green" (Stg) trait is a crucial characteristic of Sorghum that enables the retention of photosynthetically active leaves during periods of post-flowering drought, thereby extending the grain-filling period (Borrell et al., 2000). This complex trait has been linked to four major QTLs known as *Stg1-4* (Sanchez et al., 2002). Subsequent studies aimed at identifying specific genes contributing to this trait in various Sorghum cultivars have revealed that each QTL individually reduces post-flowering drought-induced leaf senescence. Among these, *Stg2* has been

identified as the most significant QTL for maintaining green leaf area at maturity under terminal drought conditions (Harris et al., 2006).

The presence of each individual QTL (*Stg1-4*) in Sorghum cultivars is characterized by a reduction in canopy and tillering at the anthesis stage, leading to a decrease in transpirational leaf area and conservation of soil water before anthesis for subsequent use during grain filling (Borrell et al., 2014).

It is noteworthy that the relationship between stay-green traits and yield, although influenced by both environmental conditions and genetic background, exhibits a positive association in environments where yield is below 6 tonnes/ha. Consequently, the adoption of Sorghum hybrids with stay-green QTLs could prove beneficial in enhancing yields across a wide range of environments, particularly since average yields worldwide are below 2.5 tonnes/ha (Jordan et al., 2012).

Another morphological feature of Sorghum that contributes to its drought tolerance is its root system. Sorghum roots can penetrate depths of 1 to 2 meters and efficiently extract water up to a lateral distance of 1.6 meters from the plant. This deep root system allows Sorghum plants to access moisture from deeper soil layers (Krupa et al., 2017). Experimental studies have demonstrated that Sorghum plants with deeper root systems exhibit higher yields and greater dry matter weight, which also influences the photosynthetic machinery (Chen et al., 2020). Moreover, genetic studies have shown that QTLs for nodal root angle, which affects root distribution in the soil and is important for drought adaptation, are co-located with QTLs for stay-green traits associated with drought adaptation (Mace et al., 2012). This indicates that root angle and architecture play a role in influencing yield under drought stress

conditions, even though there may not be a direct relationship with plant size (Singh et al., 2011).

Additionally, Sorghum possesses the C4 photosynthetic pathway, which is crucial for its drought tolerance. Unlike many other plants that utilize the C3 photosynthesis pathway, in which CO_2 is initially converted to a C3 compound, Sorghum utilizes the C4 pathway. This specialized pathway allows Sorghum to rapidly produce C4 compounds using a specialized enzyme, thereby reducing water loss through CO_2 absorption pores (Pennisi et al., 2009). Consequently, Sorghum maintains a high photosynthetic rate and low transpiration rates, thanks to its efficient C4 photosynthetic pathway.

1.9.2 Effects of drought stress on Sorghum

Although Sorghum is renowned as a drought-tolerant crop and can thrive under low-input conditions, drought stress remains the most prevalent abiotic stressor faced by Sorghum in its primary production regions (Figure 1.3; Abreha et al., 2022). Drought stress begins to impact Sorghum development from the early stages, with seedling death during emergence and establishment being a common occurrence in drylands. Drought significantly influences the germination rate in Sorghum (Smith et al., 1989). Subsequent studies have identified that the primary losses due to drought occur at various stages of early seedling development, including germination, emergence, seedling growth, and the lengths of coleoptiles, mesocotyls, radicles, shoots, and roots, as well as root area (Bayu et al., 2005). Further investigations have examined the effects on

germination rate and time, root and shoot length, dry matter, and seedling vigor (Queiroz et al., 2019).

Additionally, drought stress impacts Sorghum's ability to uptake soil nutrients and mobilize and transport nutrients by altering root biome, ultimately affecting its primary production trait, yield (Symanczik et al., 2018; Sarshad et al., 2021). Furthermore, drought not only adversely affects Sorghum yield but also seed filling and grain quality (Sehgal et al., 2018). Water deficit decreases protein digestibility and alters the micronutrient composition in Sorghum grain nutrition (Impa et al., 2019).

Given the significant impact of drought stress on Sorghum, considerable attention must be directed towards developing tolerant cultivars and implementing efficient mitigation strategies in Sorghum production.

1.9.3 Sorghum gene identification and manipulation

Sorghum, with its relatively small genome of around 730 Mb, contains approximately 27,640 bona fide protein-coding genes, with 24% being grass-specific and 7% Sorghum-specific (Paterson et al., 2009). Since the sequencing of the Sorghum genome, numerous genetic and transcriptional studies have aimed to uncover the specific genes involved in its drought adaptation mechanisms (Table 1.1).

Table 1.1 Summary of currently available genetic tools in Sorghum. Feature included in the table from elf to right. The protein name, functional characterization, the identification methodology, gene IDs and bibliographic references. **(PAGE 41)**

Protein name	Functional characterization	Identification	Gene Ids	Reference
LATE EMBRYOGENESIS ABUNDANT	Protecting cells from abiotic stress	Transcriptomics	*Sb01g046490*, *Sb09g027110*, *Sb07g015410*, *Sb04g017790*, *Sb03g032380*, *Sb01g021320*, *Sb03g001170*	Johnson et al. (2014); Abdel-Ghany et al. (2020); Zhang et al. (2019)
DELTA 1-PYRROLINE-5-CARBOXYLATE SYNTHASE 2	Proline metabolism	Transcriptomics	*Sb03g039820*	Johnson et al. (2014,2015); Varoquax et al. (2019)
HIGH-AFFINITY K+ TRANSPORTER 1	Sodium ion transmembrane transporter	Transcriptomics	*Sb06g027900*	Johnson et al. (2014)
EXPANSINS	Cell wall loosening	Transcriptomics	*Sb06g026480*, *Sb10g024380*, *Sb03g038290*, *Sb04g009990*, *Sb07g001540*, *Sb03g005140*, *Sb04g032830*	Johnson et al. (2014); Fracasso et al. (2016); Zhang et al. (2019)
GLUTATHIONE TRANSFERASES	Antioxidant	Transcriptomics	*Sb03g031780*	Abdel-Ghany et al. (2020); Varoquax et al. (2019)
DEHYDRATION-RESPONSIVE ELEMENT-BINDING	Enhancing abiotic stress tolerance	Transcriptomics	*Sb02g030310*, *Sb02g030300*	Abdel-Ghany et al. (2020)
HEAT SHOCK PROTEINS	Proteostasis and buffer stresses	Transcriptomics	*Sb10g027230*, *Sb06g000660*, *Sb03g003530*, *Sb03g034390*, *Sb03g006920*, *Sb01g041180*, *Sb01g025610*	Abdel-Ghany et al. (2020); Zhang et al. (2019)
PHOSPHORUS TRANSPORTERS	Exchange phosphorus and carbon in mycorrhizal symbiosis	Transcriptomics	*Sb03g029970*, *Sb06g002540*, *Sb01g046890*, *Sb06g002560*	Varoquax et al. (2019)
DEHYDRATION-RESPONSIVE ELEMENT-BINDING 2	Enhancing abiotic stress tolerance	Heterologous expression	*Sb03g004980*	Bihani et al. (2011); Izadi-Darbandi et al. (2023)
NAC1	Enhancing drought tolerance	Heterologous expression	*Sb01g003710*	Lu et al. (2013)
WRKY30	Influence root architecture, proline content, and ROS scavenging	Heterologous expression	*Sb10g004000*	Yang et al. (2020)
WIN1 LIKE 1	Wax and cutin accumulation	Heterologous expression	*Sb04g006970*	Bao et al. (2017)
ERECTA2	Increased drought tolerance	Heterologous expression	*Sb04g034820*	Li et al. (2019)
STRESS-ASSOCIATED PROTEIN 14	Enhance tolerance to salt stress and oxidative damage	Heterologous expression	*Sb01g005640*	Wang et al. (2013)
ALKALINE TOLERANCE 1	Regulate flux of hydrogen peroxide by regulating aquaporins	Genetic modification of Sorghum	*Sb01g032830*	Zhang et al. (2023)
NAC19	Enhanced drought tolerance and increased ROS scavenging	Genetic modification of Sorghum	*Sb05g005450*	Jin et al. (2023)
MYC2	Enhanced drought tolerance and increased ROS scavenging	Genetic modification of Sorghum	*Sb01g028230*	Wang et al. (2024)
PIN FORMED 1, 2 and 4	Stay-green; Auxin efflux carrier	Genetic modification of Sorghum	*Sb02g029210*, *Sb03g029320*, *Sb03g037350*	Borrell et al. (2022)

Transcriptomic profiling of Sorghum responding to combined heat and drought stress has unveiled several stress-specific genes and key players crucial for adaptation to the current climate context. Notably, LATE EMBRYOGENESIS ABUNDANT (LEA) proteins were found to be the most highly elevated transcripts under drought conditions. Additionally, the *DELTA 1-PYRROLINE-5-CARBOXYLATE SYNTHASE 2 (P5CS2)* gene, involved in proline metabolism, and *HIGH-AFFINITY K+ TRANSPORTER 1 (HKT1)*, a sodium ion transmembrane transporter, were highly upregulated. Under combined stress conditions, several heat shock proteins, senescence-associated genes, and glutathione transferases were identified. Expansins, LEAs, and non-specific lipid transfer proteins (nsLPTs) were exclusively upregulated in response to drought (Johnson et al., 2014). Later studies comparing stay-green Sorghum with senescent Sorghum found a significant upregulation of the proline metabolism enzyme *P5CS2* in the stay-green variety, which lies within the *Stg1* QTL (Johnson et al., 2015). Additionally, a study by Abdel-Ghany et al. (2020) revealed that deregulation of glutathione transferases is a common mechanism across all Sorghum varieties in response to drought stress, suggesting a conserved regulatory mechanism to cope with abiotic stress in Sorghum. However, specific changes observed in drought-resistant varieties include upregulation of TFs such as *DEHYDRATION-RESPONSIVE ELEMENT-BINDING PROTEINS* (*DREBs*) and *HISTONE-BINDING PROTEIN-1b* (*HBP1b*), as well as *LEA*s, *HEAT SHOCK PROTEINS* (*HSPs*), and osmoprotectant production enzymes.

Furthermore, Fracasso et al. (2016) suggested that the lower constitutive expression of secondary metabolic process and glutathione transferase genes could explain the sensitivity upon water stress of a drought-

sensitive variety. Even in the seedling stage, a conserved mechanism was observed in which HSPs, LEAs, chaperones, aquaporins, and expansins may play an important role in drought stress adaptation (Zhang et al., 2019).

Large-scale field trials, imposing pre- and post-flowering drought, resulted in a dataset of nearly 400 transcriptomes, revealing genotypic differences involving deregulation of photosynthesis and the ROS scavenging pathway, highlighting the main characteristic of Sorghum stay-green phenotypes. Additionally, the large-scale depletion in the expression of genes critical for arbuscular mycorrhizal symbiosis was accompanied by a reduction in mycorrhizal fungal mass in Sorghum roots. Roots exhibited greater transcriptional disruption than leaves under drought stress, underscoring their specific importance in coping with abiotic stresses. Genes associated with stay-green phenotypes included *PHOTOSYSTEM II SUBUNITS D1* and *CP47*, the rate-limiting enzyme *P5CS2*, and glutathione transferases such as *GST29*. Genes involved in mycorrhizal symbiosis included inorganic phosphate transporters and homologs to *SENESCENCE-ASSOCIATED GENE 12 (SAG12)* (Varoquaux et al., 2019).

In conclusion, Sorghum plants have highly conserved mechanisms to cope with drought stress, involving the deregulation of *LEAs*, *HSPs*, the proline metabolism rate-limiting enzyme *P5CS2*, and glutathione transferases such as *GST29*. However, specific resistant mechanisms are observed in Sorghum drought-tolerant varieties, such as *DREBs* and *HBP1b*.

Genetic engineering studies have pinpointed specific genes crucial for drought adaptation in Sorghum. Given the challenges of Sorghum

transformation, researchers often resort to manipulating genes in close relatives or the model plant Arabidopsis to explore the functional characterization of these stress-related genes.

One such gene, Sorghum DREB TF *SbDREB2*, when constitutively expressed in rice, resulted in pleiotropic effects. However, inducible expression under drought conditions led to the development of drought-tolerant rice plants, exhibiting increased yield during drought stress (Bihani et al., 2011). Similarly, introduction of the DREB TF into maize conferred salt and drought tolerance, with higher K^+/Na^+ ratio and proline content observed (Izadi-Darbandi et al., 2023).

Another noteworthy example is the overexpression of Sorghum NAC TF *SbNAC1* in Arabidopsis, a stress-induced TF with transactivation activity in the C-terminal region. This manipulation resulted in improved drought stress tolerance without developmental retardation (Lu et al., 2013).

Sorghum WRKY TF, *SbWRKY30*, induced upon drought stress, exhibited transactivation activity in the nucleus. Heterologous expression in Arabidopsis and rice enhanced drought tolerance by influencing root architecture, proline content, and ROS scavenging activity (Yang et al., 2020).

The overexpression of wax inducer TF *SbWINL1* in Arabidopsis resulted in enhanced drought tolerance by promoting wax and cutin accumulation (Bao et al., 2017).

Expression of a LRR receptor-like kinase *ERECTA2* from Sorghum *SbER2* in maize and Arabidopsis increased drought tolerance, particularly in terms of water-use efficiency and net photosynthetic rate (Li et al., 2019).

Finally, overexpression of Sorghum *STRESS-ASSOCIATED PROTEIN 14 SbSAP14* TF in rice prevented leaf tip yellowing and withering under salt stress. This manipulation also enhanced tolerance to oxidative damage caused by salt stress (Wang et al., 2013).

However, in a more reliable approach, only a few laboratories have succeeded in manipulating Sorghum plants to identify specific genes involved in its drought stress-tolerant mechanisms.

A genome-wide association study in Sorghum revealed a significant locus, *ALKALINE TOLERANCE 1* (*AT1*), associated with alkaline tolerance. Overexpression of *SbAT1* led to reduced alkaline tolerance in both Sorghum and rice, whereas knockout of *AT1* in Sorghum, millet, rice, and maize increased tolerance by regulating the efflux of hydrogen peroxide under environmental stresses. This study demonstrated that *SbAT1* encodes an atypical G protein γ subunit and inhibits the phosphorylation of aquaporins, which may function as H_2O_2 exporters under alkaline stress conditions (Zhang et al., 2023).

Furthermore, another study identified a Sorghum NAC TF, *SbNAC9*, which, when overexpressed, exhibited enhanced drought tolerance with increased ROS scavenging capacity (Jin et al., 2023). Overexpression of *SbMYC2*, a bHLH TF, conferred drought tolerance by reducing ROS accumulation, while mutation via virus-induced gene silencing compromised drought tolerance in Sorghum seedlings (Wang et al., 2024). Together, these studies underscore the effectiveness of generating drought-tolerant Sorghum genotypes and emphasize the importance of ROS scavenging in mitigating abiotic stresses, including salt and water stress.

Additionally, another investigation identified three members of the PIN FORMED family of auxin efflux carriers as causative factors for the stay-green phenotypes conferred by the *Stg1*, *Stg2*, and *Stg3* QTLs. Expression of these PIN genes, *SbPIN1*, *SbPIN2*, and *SbPIN4*, along with their native promoters, in a non-stay-green senescent Sorghum cultivar promoted canopy development, root architecture, and panicle growth to levels resembling those of a stay-green cultivar under drought conditions (Borrell et al., 2022).

1.10 Sorghum transformation

Given the significant impact of drought on Sorghum and the identification of specific genes involved in drought-tolerant mechanisms, it is crucial to enhance Sorghum genetic transformation methods. This would speed up the genetic manipulation process, enabling the development of Sorghum cultivars better adapted to the current climate change context.

1.10.1 Sorghum transformation limitations

Sorghum is considered the most recalcitrant crop among cereals for tissue culture due to the accumulation of phenolic compounds and a high degree of genotype dependence (Azhakanandam et al., 2015).

Several factors induce the accumulation of phenolic pigments in Sorghum in vitro cultures. *Agrobacterium tumefaciens* infection increases phenolic pigment production, and the high concentration of

phenolics hampers efficient callus propagation (Zhao et al., 2000). The presence of the selecting agent, specifically phosphinothricin, stresses Sorghum cells, causing them to release phenolic substances that accumulate to toxic levels for transformed cells (Tadesse et al., 2003).

Various strategies have been adopted to minimize phenolic compound accumulation. The first and simplest strategy involves performing short subculture intervals and adding 1% polyvinylpolypyrrolidone (Cai et al., 1987; Zhao et al., 2000). While this can reduce the negative effects of phenolic compounds, it also adds labor, and the addition of polyvinylpolypyrrolidone can impact the effective concentration of growth regulators, thereby influencing the in vitro response (Gao et al., 2005).

Additional approaches have also been effective in reducing phenolic compound accumulation. The toxic effect of phenolic substances secreted during phosphinothricin selection was avoided by using the selection agent geneticin (Tadesse et al., 2003). Although activated charcoal in the induction medium reduced black pigment production, it also inhibited callus formation. Cold pre-treatment of immature seeds positively affected both explant survival and callus formation while reducing phenolic compounds, likely due to the inhibition of key enzymes involved in phenolic compound synthesis (Nguyen et al., 2007; Dicko et al., 2006).

Supplementing the media with L-asparagine (6.7 mM), L-proline (17.4 mM), and different concentrations of NO_3^-, NH_4^+, and PO_4^- resulted in increased induction and growth of Sorghum friable embryogenic callus without medium pigmentation (Elkonin et al., 2000). Combining this

supplemented media with geneticin selection further mitigated the compounding effect of phenolic secretion (Howe et al., 2006).

These strategies collectively avoid the toxic effects of phenolic accumulation and are the basis of current Sorghum transformation methodologies.

Sorghum callus induction and regeneration have also been quite limited by genotype. The genotype dependence of Sorghum transformation poses a significant limitation for the field, as even with established transformation methods, many elite varieties are not amenable to transformation (Botella et al., 2019). Evaluation of 41 elite and exotic inbred Sorghum genotypes showed just 12 genotypes amenable for high-quality Sorghum callus production, including “Tx430,” the most used variety for transformation (Kaeppler et al., 1997). Another experiment testing genotypes for their response in callus induction and regeneration identified only three genotypes with a relatively good response to culture conditions, including “Tx430,” “C.Kafir,” and “PE932 025” (Hagio et al., 2002).

Although these experiments validate the difficulties encountered with genotype-dependent callus formation and regeneration, the implementation of new methodologies to ameliorate phenolic toxicity and increase regeneration frequencies has allowed for the transformation of previously un-transformable varieties (Raghuwanshi et al., 2010; Liu et al., 2015; Omer et al., 2018; Nelson-Vasilchik et al., 2018; Flinn et al., 2020).

1.10.2 Sorghum transformation progress

The first successful genetic transformation of Sorghum was achieved using microprojectile bombardment with immature embryos as explants (Casas et al., 1993). Although various explants such as immature inflorescences, shoot tips, mature embryos, embryogenic calli, and leaf whorls have been used for Sorghum transformation, immature embryos remain the predominant target (Bretell et al., 1980; Tadesse et al., 2003; Silva et al., 2020).

Initially, direct DNA delivery via microprojectile bombardment was the primary method for Sorghum transformation. The first report using this technique achieved a transformation efficiency of 0.3% (Casas et al., 1993). Optimization of bombardment parameters, including acceleration pressure, distance to the target, aperture of the helium inlet valve, gap width, and microprojectile travel distance, improved efficiency to 1.08% (Able et al., 2001; Tadesse et al., 2003). Further refinements, such as the addition of $CuSO_4$, KH_2PO_4, L-proline, and L-asparagine to the culture medium, along with optimized DNA delivery conditions (0.6 μm gold particles, 18.5 cm flying distance, and 1000 psi helium pressure), increased efficiency to 20.7% (Liu et al., 2012).

Simultaneously, Agrobacterium-mediated Sorghum transformation was optimized through adjustments in infection, co-cultivation, and selection conditions. This included using different selecting agents like kanamycin and mannose, applying various treatments like cold or heat pretreatment to promote callus induction, and reduce phenolic compounds (Gao et al., 2005; Nguyen et al., 2007; Gurel et al., 2009). Despite these efforts,

Agrobacterium-mediated transformation efficiency remained lower than particle bombardment until Wu et al. (2013) achieved a 33% efficiency. This study incorporated elevated copper sulfate and 6-benzylaminopurine in the resting and selection media and used super binary vectors. Super binary vectors, which enhance the virulence of *Agrobacterium tumefaciens*, were first utilized in plant transformation with *Chenopodium quinoa* (Komari et al., 1990) and are binary vectors (small T-DNA carrying plasmid) including additional virulence genes (virB, virC, and virG) (Komari et al., 2006).

A significant breakthrough in monocot transformation substantially increased the transformation efficiencies of cereals, including Sorghum, maize, rice, and sugarcane (Lowe et al., 2016). This approach leveraged morphogenic TFs like maize *BABY BOOM* (*BBM*) and *WUSCHEL2* (*WUS*), which promote the transition from vegetative to embryonic growth (Boutilier et al., 2002; Zuo et al., 2002). Although this work preceded Wu et al. (2013), it increased Sorghum transformation frequencies from 1.9% to 18.3% with morphogenic genes present in the T-DNA of a super binary vector. However, to regenerate plants, it was necessary to remove *BBM* and *WUS2* expression cassettes due to their pleiotropic effects. This was achieved using a drought-inducible maize promoter (p*RAB17*) to drive *CRE* recombinase gene expression, which excised the sequences flanked by loxP sites upon desiccation (Lowe et al., 2016).

The development of a ternary vector system further improved transformation efficiencies. Traditional super binary vectors (e.g., pSB1) have limitations due to their large size and the need for a co-integration step. To address this, new "pVIR" vectors were created, featuring small

size, enhanced stability, improved bacterial selectable markers, and an optimal set of amended *vir* genes (operons virC, virD, and virE) (Anand et al., 2018; Lowe et al., 2018). These genes were assembled into the called ternary vector, also known as cohabitating vector, in which a T-DNA-less accessory pVIR plasmid and a T-DNA transfer competent binary plasmid are cotransformed into Agrobacterium cells. This introduction of the pVIR plasmid *in trans* with T-DNA binary vector in the same Agrobacterium strain enabled the development of a rapid maize transformation system (Lowe et al., 2018).

Che et al. (2018) combined the ternary vector system with media optimization techniques described by Wu et al. (2014), achieving high transformation efficiencies in recalcitrant African varieties, including Macia, Malisor 84-7, and Tegemeo. The combination of the ternary vector system, media optimization, and morphogenic regulators (*ZmWUS2* and *ZmBBM*) led to the highest reported Sorghum transformation efficiency of 69.7% (Che et al., 2022). Additionally, the use of alternative morphogenic regulators like GRF4-GIF1 achieved transformation efficiencies of 39.68% (Li et al., 2024), demonstrating the versatility and effectiveness of these advanced transformation methodologies. The advancements in Sorghum genetic transformation have significantly progressed from the initial use of microprojectile bombardment to more sophisticated techniques involving Agrobacterium-mediated methods and the incorporation of morphogenic regulators. Early efforts yielded modest transformation efficiencies, but through continuous optimization of culture conditions, DNA delivery parameters, and the introduction of advanced vector systems, these efficiencies have dramatically improved.

The development and utilization of ternary vector systems, alongside media optimization and innovative morphogenic regulators, have culminated in unprecedented transformation efficiencies, even in previously recalcitrant Sorghum varieties. These methodological advancements not only enhance the feasibility of genetic transformation in Sorghum but also open new avenues for developing drought-resistant and climate-resilient Sorghum cultivars. The integration of these cutting-edge molecular techniques holds great promise for addressing global food security challenges and adapting crop production to the changing climate.

OBJECTIVES

The general objective of this PhD thesis is to decipher the transcriptional regulation of brassinosteroid receptors under abiotic stress conditions and translate these findings into *Sorghum bicolor* to develop stress-resistant crops.

In particular, the following specific objectives have been accomplished:

1. Investigate the transcriptional regulation of *BRL3* receptor under control and abiotic stress conditions. Identify TFs that directly bind the *BRL3* promoter and regulate *BRL3* expression. Engineer the *BRL3* promoter to enhance its expression.

2. Investigate the downstream signaling components involved in BRL3-mediated drought stress tolerance.

3. Translate the modulation of brassinosteroid receptors into *Sorghum bicolor* to develop abiotic stress-resistant crops.

4. Establish an efficient transformation protocol for *Sorghum bicolor* and modulate brassinosteroid receptor expression through stable genetic transformation.

Chapter 2

Results

STUDYING AND ENGINEERING BRL3 PROMOTER TO ENHANCE ABIOTIC STRESS ADAPTATION IN *ARABIDOPSIS THALIANA*

Part of this chapter is published in:

Gupta, A., Rico-Medina, A., Lozano-Elena, F., Marquès-Bueno, M., Fontanet-Manzaneque, J.B., Fàbregas, N., Alseekh, S., Fernie, A.R., & Caño-Delgado, A. I. (2023). Brassinosteroid receptor BRL3 triggers systemic plant adaptation to elevated temperature from the phloem cells. *bioRxiv*, 2023-03.

2.1 Introduction

Plants, as sessile organisms, have developed intricate mechanisms to adapt to changes in their environment. These changes are perceived by sensors or receptors located in their membranes or cell walls. Subsequently, these external signals are translated into internal changes involving secondary messengers such as ROS, nitric oxide, and calcium ions (Tuteja et al., 2007; Besson-Bad et al., 2008; Mittler et al., 2011). This process, known as signal transduction, involves the phosphorylation and dephosphorylation of proteins by kinases and phosphatases, ultimately regulating gene expression through TFs proteins (Xiong et al., 2001). The transcriptional regulation of each gene depends on the combinatorial effect of different TFs. There are more than 1500 genes encoding TFs, around a 5% of the Arabidopsis genes, grouped into 50 families. This large number of TFs in plant implies a high degree of complexity in the regulation of gene expression (Riechmann et al., 2000).

The transcription of genes into mRNA is carried out by RNA polymerase II, facilitated by the formation of a transcription preinitiation complex. This complex comprises RNA polymerase II, general TFs, and a coactivator called Mediator. The general TFII D is a multiprotein complex itself and is key for the formation of the transcription preinitiation complex, as one of its components, the TATA box binding protein, is the responsible for binding to TATA box and trigger the transcription preinitiation complex formation (Schilbach et al., 2017). Specific TFs, distinguished by their ability to activate, repress, or perform both functions, play a crucial role in gene regulation. These TFs

possess distinct domains, including a DNA binding domain and a transactivation domain (Buchanan et al., 2015).

The coordinated action of specific TFs results in the formation of nucleoprotein complexes known as enhanceosomes. These complexes modulate gene activity in response to environmental signals (Singh et al., 1998). Understanding the regulation of transcription requires knowledge of promoter structure and its elements. Promoters consist of basal elements, responsible for RNA polymerase II binding, and *cis*-elements, which vary between genes and regulate gene expression. *Cis*-elements are bound by trans acting factors, which in turn interact with the basal transcriptional machinery. The *cis*-elements are generally short sequences of less than 10 bp and often cluster together to form *cis*-regulatory modules or *cis*-regulatory enriched regions (CRERs). These modules likely allow cooperative action of several TFs in the regulation of gene expression by bringing them in proximity. These modules are called enhancers or silencers depending on its function enhancing or silencing the gene expression. Modules can also act as inhibitors, blocking the signal from enhancers or silencers (Buchanan et al., 2015).

BRL3, a vascular-specific BR receptor, plays a crucial role in plant responses to various stresses. Mutations in *BRL3* affect the plant's ability to respond to elevated temperatures and DNA damage (Gupta et al.,2023; Takahashi et al., 2023). Enhancing *BRL3* expression resulted in a better drought stress tolerance and higher hydrotropic response, both essential mechanisms to cope with water-related abiotic stress conditions (Fàbregas et al., 2018). This study investigates the specific TFs modulating *BRL3* expression in different tissues, particularly in the vascular and root meristem, under both normal and stress conditions. The

aim is to identify *cis*-regulatory elements and CRERs within the *BRL3* promoter to understand how specific TFs regulate *BRL3* expression in response to environmental stresses.

Cis-regulatory mutations play a significant role in crop domestication, and manipulating promoters has been suggested as an effective approach to introduce diversity in gene expression (Swinnen et al.,2016; Rodriguez-Leal et al., 2017; Wang et al., 2021). Hence, our study focuses on modifying the *BRL3* promoter to boost its expression while maintaining its responsiveness to environmental cues. By doing so, we aim to enhance traits like drought tolerance and hydrotropic responses without compromising the plant's ability to regulate *BRL3* expression under specific conditions.

2.2 Results

2.2.1 In-silico analysis of *BRL3* promoter identifies four *cis*-regulatory enriched regions

To determine *cis*-regulatory elements important for the regulation of *BRL3* expression, we conducted an in-silico analysis of the 2Kb *BRL3* promoter region using Regulatory Sequence Analysis Tool (RSAT) (Turatsinze et al., 2008). RSAT employs statistical inference to identify putative binding sites for TFs within the query sequence, also identifying CRERs. The 2Kb 5´ upstream non-coding region of *BRL3*, and a series of TF position-based matrices, which were retrieved from different databases, such as Cis-BP, JASPAR, and DNA Affinity Purification

sequencing DAP (DAP-seq) (O´Malley et al., 2016), were used as a query. As an output we obtained precise TF binding site locations within the input sequence and highlighted genome segments enriched in these matches. These identified binding sites and CRERs were validated using a Markov-chain background model of a high-order degree (Thijs et al., 2001), with a stringent significance threshold (p-value<1e-5).

The findings are categorized based on the dataset from which the position-based matrices were obtained. Employing the Cis-BP dataset, we deduced 23 TF binding sites attributed to 16 distinct TFs (Figure 2.1a). These sites were situated within two separate CRERs, spanning the -892 to -751 and the -1204 to -1130 regions of the BRL3 promoter (Figure 2.1b). Utilizing the JASPAR dataset, we uncovered 42 TF binding sites linked to 30 TFs (Figure 2.2a). These sites were dispersed across four separate CRERs, spanning from -1821 to -1456, -1165 to -1087, -795 to -671, and -417 to -262 regions (Figure 2.2b).

Combining the outcomes from both datasets, a total of 44 TFs were predicted to bind *cis* elements within the *BRL3* promoter (Table 2.1). These TFs come from 13 distinct families, with notable representation from MYB, WRKY, and Dof families. Additionally, four distinct CRERs were delineated, spanning the regions from -1821 to -1456, -1204 to -1087, -892 to -671, and -417 to -262. These CRERs are visually depicted in Figure 2.3.

Table 2.1 Transcription factors putatively binding to *BRL3* promoter. In the table is included: The transcription factor family, Gene ID, Gene symbol and Gene name.

TF family	Gene ID	Gene symbol	Gene name
MYB	AT2G32460	MYB101	myb domain protein 101
	AT1G69560	MYB105	myb domain protein 105
	AT1G17950	MYB52	myb domain protein 52
	AT5G17800	MYB56	myb domain protein 56
	AT2G23290	MYB70	myb domain protein 70
	AT4G37260	MYB73	myb domain protein 73
	AT3G50060	MYB77	myb domain protein 77
	AT4G32730	PC-MYB1	
	AT5G17300	RVE1	REVEILLE 1
WRKY	AT4G31550	WRKY11	WRKY DNA-binding protein 11
	AT1G30650	WRKY14	WRKY DNA-binding protein 14
	AT2G23320	WRKY15	WRKY DNA-binding protein 15
	AT2G24570	WRKY17	WRKY DNA-binding protein 17
	AT2G30590	WRKY21	WRKY DNA-binding protein 21
	AT4G01250	WRKY22	WRKY DNA-binding protein 22
	AT4G23550	WRKY29	WRKY DNA-binding protein 29
	AT2G38470	WRKY33	WRKY DNA-binding protein 33
	AT5G49520	WRKY48	WRKY DNA-binding protein 48
	AT5G64810	WRKY51	WRKY DNA-binding protein 51
	AT1G69310	WRKY57	WRKY DNA-binding protein 57
Dof	AT2G28810	AT2G28810	
	AT1G51700	DOF1	DOF zinc finger protein 1
	AT3G50410	OBP1	OBF binding protein 1
	AT3G55370	OBP3	OBF-binding protein 3
	AT5G66940	AT5G66940	
	AT5G02460	PEAR2	
DREBS	AT1G75490	AT1G75490	
	AT3G57600	AT3G57600	
	AT1G21910	DREB26	dehydration response element-binding protein 26
GATAS	AT4G36620	GATA19	GATA transcription factor 19
	AT2G18380	GATA20	GATA transcription factor 20
	AT3G54810	BME3	BLUE MICROPYLAR END 3
HD-Zip III	AT1G52150	ATHB-15	
	AT1G30490	PHV	PHAVOLUTA
ERF	AT1G03800	ERF10	ERF domain protein 10
	AT5G07310	ERF115	ERF domain protein 115
MADS-box	AT2G45660	AGL20	AGAMOUS-like 20
	AT5G15800	SEP1	SEPALLATA1
BZR	AT1G19350	BES1	BRASSINAZOLE-RESISTANT 2
	AT1G75080	BZR1	BRASSINAZOLE-RESISTANT 1
B3	AT3G18990	VRN1	REDUCED VERNALIZATION RESPONSE 1
bHLH	AT4G21330	DYT1	DYSFUNCTIONAL TAPETUM 1
bZIP	AT5G10030	TGA4	TGACG motif-binding factor 4
NAC	AT1G25580	SOG1	SUPRESSOR OF GAMMA RADIATION 1

Within the -417 to -262 region CRER1, binding *cis*-elements for SEP1, GATA8, PEAR2, OBP1, and SOG1 were identified. Notably, Dof TFs such as PEAR2 and OBP1 play crucial roles in root procambial development and cell cycle regulation, pivotal processes for root growth and development (Miyashima et al., 2019; Skirycz et al., 2008).

In the -892 to -671 region CRER2, binding *cis*-elements for TGA4, DOF1, as well as various HD-Zip III and WRKY TFs were detected. WRKY TFs in CRER2 are primarily associated with stress adaptation mechanisms, including pathogen resistance by WRKY11, WRKY17, WRKY48, and WRKY51 (Journot-Catalino 2006; Xing et al., 2008; Gao et al., 2011), and drought/salt tolerance by WRKY11, WRKY17

(a)

seq_id	ft_type	ft_name	strand	start	end	sequence	weight	Pval	ln_Pval	sig	rank	rank_pm
2kb	limit	START_END	D	-2000	-1	.	0	0	0	0		
2kb	site	M2347_1.02	D	-1160	-1140	AAAAAAAGAAAAAAAAAAAA	8.4	5.0e-07	-14.508	6.301	1	1
2kb	site	M2347_1.02	D	-1154	-1134	AGAAAAAAAAAAAAAAAAAA	8.3	7.1e-07	-14.160	6.149	2	2
2kb	site	M1680_1.02	R	-891	-882	TACGTCAACT	6.5	1.4e-06	-13.496	5.861	3	1
2kb	site	M1686_1.02	R	-891	-882	TACGTCAACT	6.5	1.4e-06	-13.496	5.861	4	1
2kb	site	M2347_1.02	D	-1153	-1133	GAAAAAAAAAAAAAAAAAAA	8.1	1.4e-06	-13.457	5.844	5	3
2kb	site	M2347_1.02	D	-1152	-1132	AAAAAAAAAAAAAAAAAAAA	7.9	2.3e-06	-12.964	5.630	6	4
2kb	site	M2347_1.02	D	-1151	-1131	AAAAAAAAAAAAAAAAAAAA	7.9	2.3e-06	-12.964	5.630	7	5
2kb	site	M2347_1.02	D	-1150	-1130	AAAAAAAAAAAAAAAAAAAA	7.9	2.3e-06	-12.964	5.630	8	6
2kb	site	M2347_1.02	D	-1169	-1149	CTAAAAAAAAAAAAAAGAAAA	7.8	3.3e-06	-12.629	5.485	9	7
2kb	site	M2377_1.02	R	-493	-476	GATTCCACATAAAGGAAG	8.3	4.1e-06	-12.395	5.383	10	1
2kb	site	M0271_1.02	D	-890	-881	GTTGACGTAG	7.7	4.4e-06	-12.323	5.352	11	1
2kb	site	M2347_1.02	D	-1168	-1148	TAAAAAAAAAAAAAGAAAAA	7.6	5.4e-06	-12.125	5.266	12	8
2kb	site	M2366_1.02	D	-769	-751	TCACGTAAAGATTAGTCTC	8.8	5.9e-06	-12.047	5.232	13	1
2kb	site	M1678_1.02	R	-892	-883	ACGTCAACTG	6.4	7.4e-06	-11.812	5.130	14	1
2kb	site	M1682_1.02	R	-892	-883	ACGTCAACTG	6.4	7.4e-06	-11.812	5.130	15	1
2kb	site	M1693_1.02	R	-892	-883	ACGTCAACTG	6.4	7.4e-06	-11.812	5.130	16	1
2kb	site	M1683_1.02	R	-891	-882	TACGTCAACT	5.2	8.5e-06	-11.677	5.071	17	1
2kb	site	M1687_1.02	R	-891	-882	TACGTCAACT	5.2	8.5e-06	-11.677	5.071	18	1
2kb	site	M1690_1.02	R	-891	-882	TACGTCAACT	5.2	8.5e-06	-11.677	5.071	19	1
2kb	site	M1692_1.02	R	-891	-882	TACGTCAACT	5.2	8.5e-06	-11.677	5.071	20	1
2kb	site	M1699_1.02	R	-891	-882	TACGTCAACT	5.2	8.5e-06	-11.677	5.071	21	1
2kb	site	M1702_1.02	R	-891	-882	TACGTCAACT	5.2	8.5e-06	-11.677	5.071	22	1
2kb	site	M0591_1.02	D	-1204	-1195	TATTTGAATA	6.1	9.5e-06	-11.562	5.021	23	1

(b)

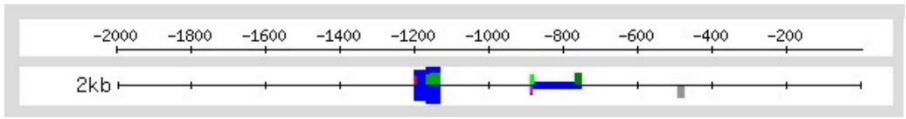


Figure 2.1 Regulatory sequence analysis output for *BRL3* promoter using Cis-BP dataset. (a) *BRL3* promoter TF binding sites including information about the *cis*-element position, DNA strand, and sequence. TF IDs: M2347 (SOC1); M1680 (WRKY57); M1686 (WRKY21); M2377 (SEP1); M0271 (TGA4); M2366 (ATHB9); M1678 (WRKY14); M1682 (WRKY15); M1693(WRKY11) M1683 (WRKY17); M1678 (WRKY33); M1690 (WRKY22); M1692 (WRKY29); M1699 (WRKY48); M1702 (WRKY51). (b) Schematic representation of BRL3 promoter (2 Kb) including the identified *cis*-regulatory enriched regions, in blue, and TF binding sites, in other colors.

(a)

seq_id	ft_type	ft_name	strand	start	end	sequence	weight	Pval	ln_Pval	sig	rank	rank_
2kb	limit	START_END	D	-2000	-1	.	0	0	0	0		
2kb	site	MYB105	D	-1546	-1534	GTAGTTACCGTTA	11.7	4.6e-07	-14.598	6.340	1	1
2kb	site	AT1G69570	D	-317	-291	TCTGTACTTTCTCCCTTCTCTTTTTCC	11.1	9.7e-07	-13.844	6.012	2	1
2kb	site	AdoF1	R	-740	-720	GAGGAGAAAAAGCTAAAGAAG	10.1	1.0e-06	-13.784	5.986	3	1
2kb	site	OBP3	D	-735	-715	TTAGCTTTTTCTCCCTCTTTTT	10.5	1.2e-06	-13.634	5.921	4	1
2kb	site	RAMOSA1	R	-334	-321	GAGACAGAGAGAGT	11.3	1.2e-06	-13.621	5.915	5	1
2kb	site	AT1G69570	R	-1149	-1123	TTGTAACTTTTTTTTTTTTTTTTTTT	10.8	1.6e-06	-13.358	5.801	6	2
2kb	site	GATA8	R	-417	-409	CGGATCCGG	8.6	1.6e-06	-13.349	5.797	7	1
2kb	site	MYB56	R	-1543	-1529	TTAATTAACGGTAAC	10.4	1.7e-06	-13.289	5.771	8	1
2kb	site	MYB52	D	-1544	-1534	AGTTACCGTTA	10.7	1.8e-06	-13.243	5.752	9	1
2kb	site	MYB70	R	-1547	-1534	TAACGGTAACTACG	10.5	1.9e-06	-13.175	5.722	10	1
2kb	site	AT2G28810	D	-697	-677	TTTCTTCTCTTTCGCTTTTAC	10.0	2.0e-06	-13.122	5.699	11	1
2kb	site	MYB77	D	-1548	-1534	TCGTAGTTACCGTTA	10.3	2.2e-06	-13.038	5.662	12	1
2kb	site	AT1G69570	D	-737	-711	CTTTAGCTTTTTCTCCTCTTTTTTTCT	10.5	2.5e-06	-12.911	5.607	13	3
2kb	site	OBP3	R	-1145	-1125	GTAACTTTTTTTTTTTTTTT	10.1	2.7e-06	-12.814	5.565	14	2
2kb	site	PHYPADRAFT_153324	D	-1744	-1736	GGTAAAGCG	6.9	2.9e-06	-12.760	5.541	15	1
2kb	site	AT2G28810	D	-745	-725	TTTGTCTTCTTTAGCTTTTTC	9.8	3.2e-06	-12.653	5.495	16	2
2kb	site	AT5G66940	D	-747	-719	GTTTTGTCTTCTTTAGCTTTTTCTCCTCT	10.1	3.6e-06	-12.527	5.440	17	1
2kb	site	AT5G02460	D	-1159	-1139	AAAAAAGAAAAAAAAAAAAA	9.9	4.2e-06	-12.376	5.375	18	1
2kb	site	MYB73	R	-1544	-1534	TAACGGTAACT	9.5	4.3e-06	-12.357	5.367	19	1
2kb	site	OBP3	D	-724	-704	TCCTCTTTTTTTCTTCTCTTT	9.8	4.7e-06	-12.270	5.329	20	3
2kb	site	AT5G66940	D	-699	-671	AATTTCTTCTCTTTCGCTTTTACATTTTC	9.9	4.9e-06	-12.225	5.309	21	2
2kb	site	GATA19	D	-1821	-1811	TGGATCCGATT	10.3	5.5e-06	-12.104	5.257	22	1
2kb	site	ATHB-9	D	-769	-751	TCACGTAAAGATTAGTCTC	9.1	5.6e-06	-12.088	5.250	23	1
2kb	site	RVE1	R	-1469	-1456	CCATAAATATCTGC	9.7	5.7e-06	-12.083	5.248	24	1
2kb	site	RAMOSA1	R	-332	-319	AAGAGACAGAGAGA	8.8	5.9e-06	-12.034	5.226	25	2
2kb	site	AT5G02460	R	-312	-292	GAAAAAGAGAAGGGAGAAAGT	9.7	6.1e-06	-11.999	5.211	26	2
2kb	site	GATA20	R	-1819	-1812	ATCGGATC	10.9	6.2e-06	-11.992	5.208	27	1
2kb	site	ATHB15	D	-795	-781	TAATATAATGATTAT	10.2	6.6e-06	-11.926	5.179	28	1
2kb	site	AT1G75490	R	-1575	-1561	TCCCCACCACCGTTC	9.4	6.7e-06	-11.920	5.177	29	1
2kb	site	AT3G57600	R	-1574	-1564	CCACCACCGTT	9.2	7.0e-06	-11.871	5.156	30	1
2kb	site	BZR1	R	-1605	-1586	CCACGCGTGTATGTAACTTT	9.2	7.0e-06	-11.865	5.153	31	1
2kb	site	AT5G02460	R	-745	-725	GAAAAAGCTAAAGAAGACAAA	9.6	7.3e-06	-11.827	5.136	32	3
2kb	site	AT5G66940	R	-1165	-1137	TTTTTTTTTTTTTTTTCTTTTTTTTTTT	9.6	7.8e-06	-11.758	5.106	33	3
2kb	site	GATA8	D	-1122	-1114	CAGATCCGA	8.3	7.9e-06	-11.753	5.104	34	2
2kb	site	MYB101	D	-1101	-1087	TACGGAAACCGAACT	9.5	8.0e-06	-11.735	5.097	35	1
2kb	site	DYT1	D	-1696	-1683	AATAAGTCACGAGA	9.4	8.1e-06	-11.724	5.092	36	1
2kb	site	MYB3R1	D	-1547	-1533	CGTAGTTACCGTTAA	10.1	8.5e-06	-11.670	5.068	37	1
2kb	site	OBP1	D	-282	-262	CAGCCTTTGATTCCGCTTTTT	9.1	8.6e-06	-11.667	5.067	38	1
2kb	site	DREB26	R	-1574	-1555	CCTAATTCCCCACCACCGTT	8.9	9.1e-06	-11.612	5.043	39	1
2kb	site	OsRR22	R	-293	-284	CAGATACGGA	9.9	9.2e-06	-11.592	5.035	40	1
2kb	site	GATA19	D	-1122	-1112	CAGATCCGAAT	9.9	9.3e-06	-11.581	5.030	41	2
2kb	site	ERF10	R	-1574	-1554	ACCTAATTCCCCACCACCGTT	7.9	9.7e-06	-11.539	5.011	42	1

(b)

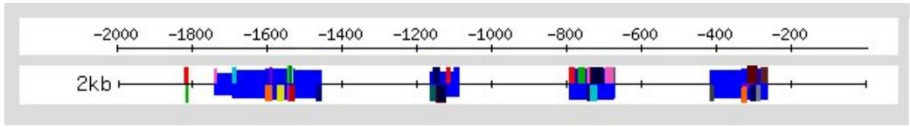


Figure 2.2 Regulatory sequence analysis output for *BRL3* promoter using JASPAR dataset. (a) *BRL3* promoter TF binding sites including information about the *cis*-element position, DNA strand, and sequence. (b) Schematic representation of *BRL3* promoter (2 Kb) including the identified *cis*-regulatory enriched regions, in blue, and TF binding sites, in other colors.

WRKY33, WRKY57 (Ali et al., 2018; Jiang et al., 2009, Jiang et al., 2012). HD-Zip III TFs, such as HB15, are implicated in vascular development (Kim et al., 2005; Du et al., 2015).

Within the -1204 to -1087 region CRER3, binding *cis*-elements for SOC1, OBP3, PEAR2, and GATA8/19 were found. Noteworthy are the Dof TFs OBP3 and PEAR2, which are linked to root development, along

with SOC1, a pivotal regulator of flowering (Miyashima et al., 2019; Kang et al., 2000; Lee et al., 2010).

Lastly, the -1456 to -1821 region CRER4 contains binding *cis*-elements for DYT1, GATA19/20, and various ERF, MYB, DREB, and BZR TFs. CRER4 is implicated in diverse brassinosteroid-related molecular mechanisms, including BR homeostasis by BZR TFs (Salazar-Henao et al., 2016), and BR-mediated QC cell division by MYB56 and ERF115 (Heyman et al., 2013; Vilarrasa-Blasi et al., 2014). Furthermore, TFs associated with salt and osmotic stress tolerance, such as DREB26, are present within CRER4 (Kazama et al., 2013).

Following the identification and functional characterization of four distinct CRERs within the *BRL3* promoter, we employed a phylogenetic shadowing strategy to discover conserved regions essential for BRL3 expression regulation across various species and within different Arabidopsis BR receptors of the same family (Castrillo et al., 2011). To achieve this, we compared the 2Kb promoter regions of *BRL3* orthologs across six species within the *Brassicaceae* family: *Arabidopsis thaliana, Arabidopsis lyrata, Boechera stricta, Eutrema salsugineum, Capsella rubella, and Capsella grandiflora*. CRER1 and CRER2 exhibited significant conservation, with a maximum homology of 64.4% (Figure 2.3a), indicating their crucial role in fundamental *BRL3* regulatory functions.

Moreover, when comparing Arabidopsis BR receptors, we distinguished notable homology only between the vascular-specific receptors BRL1 and BRL3. This homology peaked at 72.8% within CRER2, particularly at the HD-Zip III TF binding site (Figure 2.3b). These findings suggest that CRER2, conserved among vascular-specific receptors and across species, likely harbors regulatory *cis*-elements pivotal for *BRL3* vascular expression regulation.

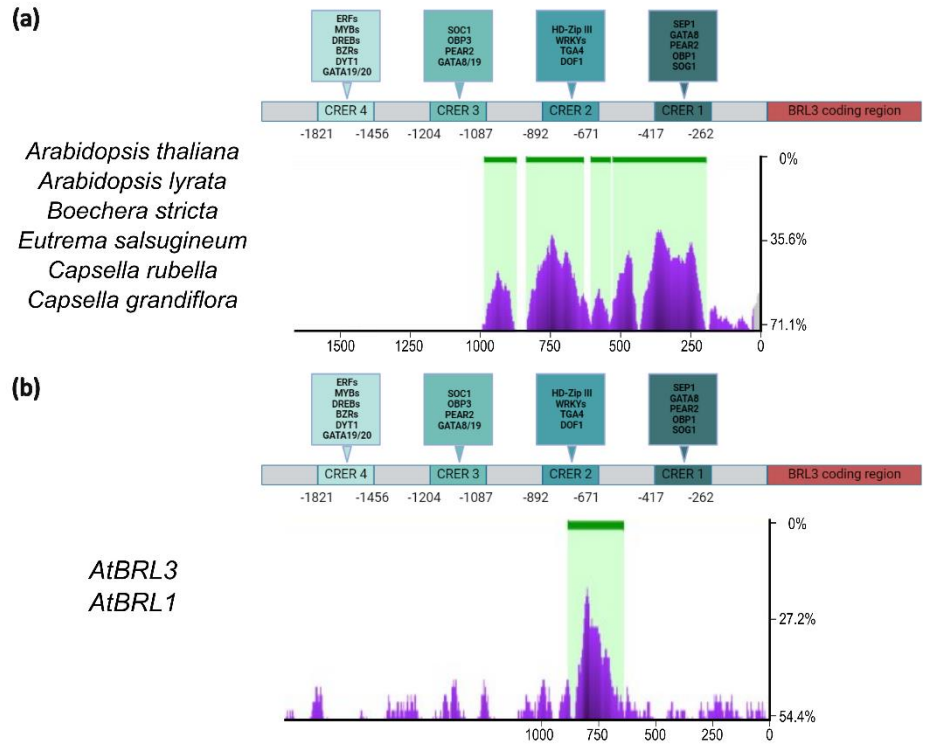


Figure 2.3 Phylogenetic shadowing in *BRL3* promoter. (a) Schematic representation of *BRL3* promoter including the identified *cis*-regulatory enriched regions and the main TF families binding sites. The graph shows the result of the phylogenetic shadowing, showing the conservation in the *BRL3* promoters from different species. X axis represents the distance from the transcription starting site and the Y axis represents the percentage of analogy (%) (b) Schematic representation of *BRL3* promoter including the identified *cis*-regulatory enriched regions and the main TF families binding sites. The graph shows the result of the phylogenetic shadowing, showing the conservation in the *BRL3* and *BRL1* promoters in Arabidopsis. X axis represents the distance from the transcription starting site and the Y axis represents the percentage of analogy (%)

2.2.2 Promoter deletion analysis of *BRL3* reveals its expression in stomata and pinpoints a specific 100 bp region crucial for vascular expression

Promoter deletion analysis has proven to be a valuable tool for discerning *cis*-regulatory regions governing spatiotemporal expression patterns and responsiveness to abiotic stress (Karthikeyan et al., 2009; Podia et al., 2023). In a study by Salazar-Henao et al., 2016, the *BRL3* promoter deletion analysis was conducted. Through this investigation, six different transgenic lines were generated, each carrying varying lengths of the *BRL3* promoter fused to the *BETA-GLUCURONIDASE (GUS)* and *GREEN FLUORESCENCE PROTEIN (GFP)* coding sequence (CDS). This strategy enabled the confinement of *BRL3* expression to the root vasculature, two protophloem cell files, and in the QC. Moreover, several regions crucial for *BRL3*'s spatiotemporal expression were identified: the -1719 to -1098 region for QC expression, the -1098 to -755 region for root vasculature expression, and the -755 to -498 region for protophloem expression. Additionally, *BRL3* expression was detected in the veins and tip of cotyledons, as well as in the shoot apical meristem. Notably, the -1098 to -755 region was implicated in shoot apex expression, while the -498 to -384 region was associated with cotyledon vein expression.

However, this approach lacks a previous *in-silico* analysis, thus losses resolution in the -1719 to -755 region where we could find 3 out of 4 CRERs identified in *BRL3* promoter (Figure 2.3). To address this limitation and gain deeper insight into the *cis*-regulatory regions identified through *in-silico* analysis, we utilized the transgenic lines previously generated by Salazar-Henao et al., 2016, and developed three

additional promoter deletion lines. These new lines were engineered to either retain or exclude the presence of the four CRERs identified in the *BRL3* promoter (Figure 2.4).

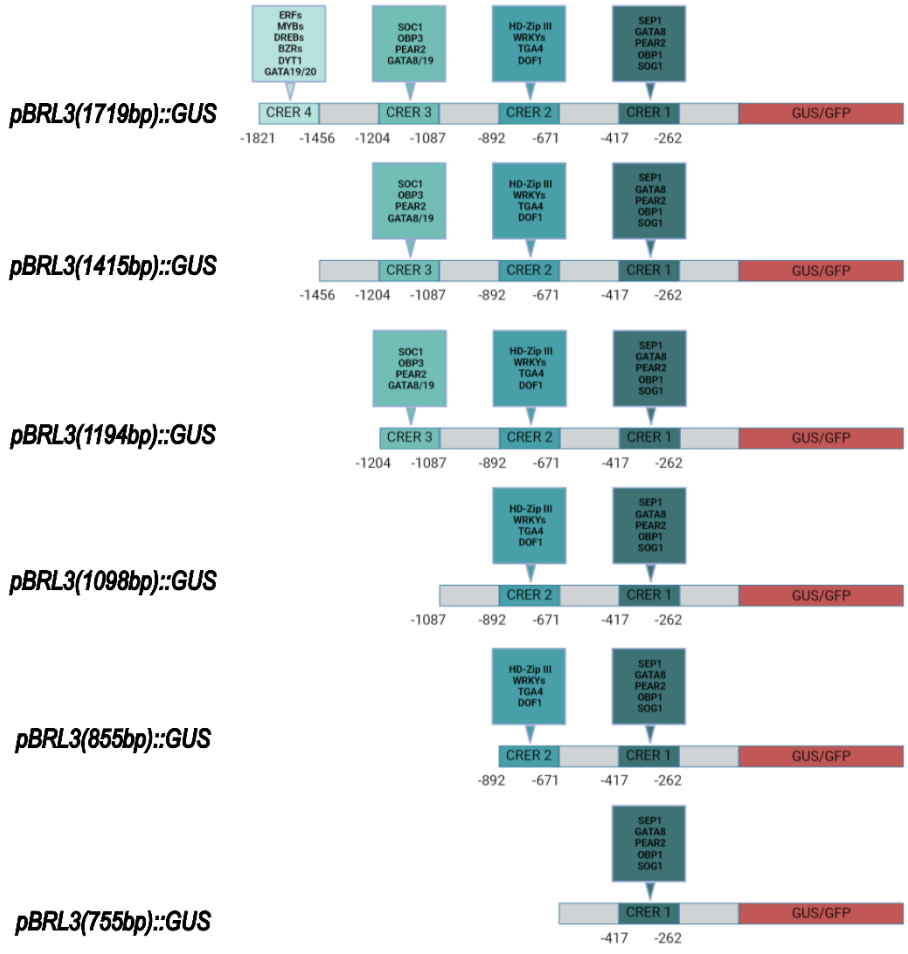


Figure 2.4 Refined promoter deletion analysis of *BRL3*. Schematic representation of *BRL3* promoter including the identified *cis*-regulatory enriched regions and the main TF families binding sites. The precise promoter length of each transgenic line is highlighted in bold.

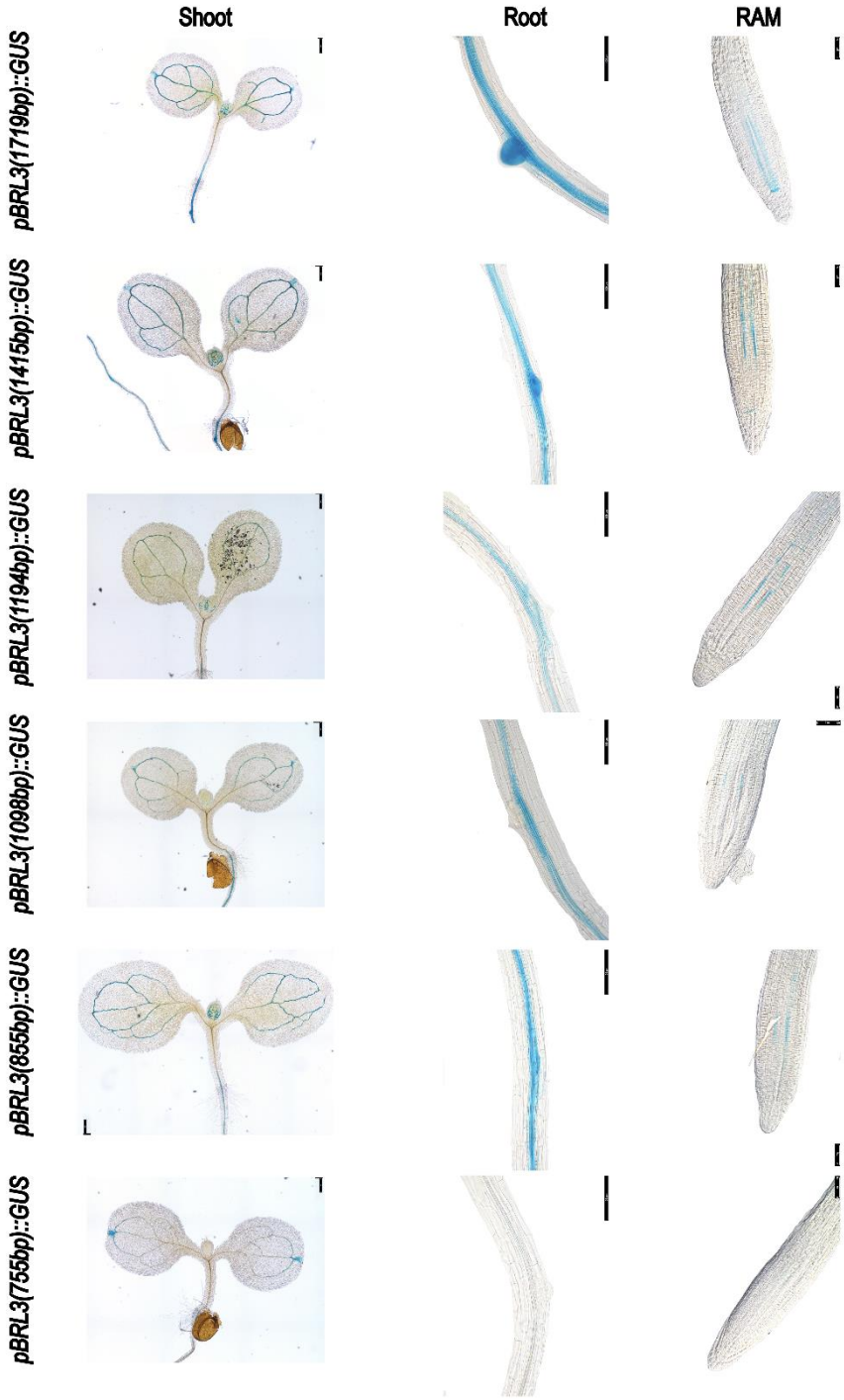


Figure 2.5 *BRL3* expression under different promoter lengths. GUS-stained 6-day-old seedlings showing *BRL3* expression under different promoter lengths (1719, 1415, 1194, 1098, 855, 755 bp) in shoot, mature root and root apical meristem (RAM). Scale bars: 5 mm, 109, and 50 µm.

Once the transgenic lines were generated, our initial focus was on examining the spatial distribution of *BRL3* expression. GUS staining was conducted throughout the entire plant in 6-day-old seedlings. Removal of 304 bp (*pBRL3(1415bp)::GUS*) resulted in a reduction of *BRL3* expression in the QC, while an additional deletion of 221 bp (*pBRL3(1194bp)::GUS*) completely abolished *BRL3* expression in this cell lineage. Furthermore, we pinpointed the specific *cis*-regulatory region crucial for *BRL3* expression in the root vasculature, a 100 bp module located within the -855 to -755 region (Figure 2.5).

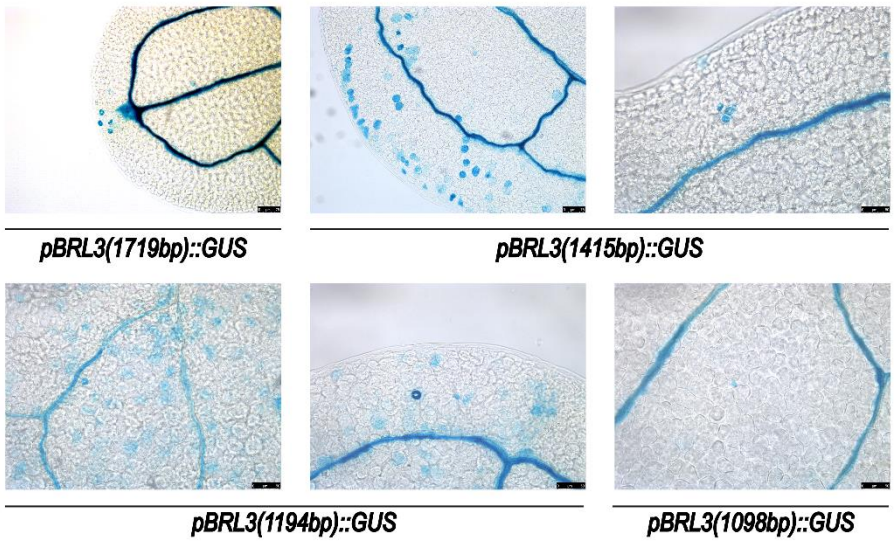


Figure 2.6 *BRL3* is expressed in the stomata. GUS-stained 6-day-old seedlings showing *BRL3* expression under different promoter lengths (1719, 1415, 1194, 1098 bp). Scale bar: 50, and 75 µm.

Interestingly, deletion of 304 bp (*pBRL3(1415bp)::GUS*) led to pronounced GUS staining in the cotyledons (Figure 2.6), a pattern also observed in the subsequent promoter deletion line (*pBRL3(1194bp)::GUS*). Upon closer examination of the cotyledons, we

uncovered BRL3 expression in the stomata. This expression was widespread in the aforementioned lines, while its presence in the stomata was minimal in the *pBRL3(1719bp)::GUS* and *pBRL3(1098bp)::GUS* lines (Figure 2.6).

2.2.3 *BRL3* promoter deletion analysis reveals *cis*-regulatory regions governing quiescent center and vascular initials *BRL3* expression

Due to the limited resolution of root meristem visualization achieved through GUS staining, we conducted confocal imaging of GFP in the same promoter deletion lines. Removal of 304 bp effectively prevented *BRL3* expression in the QC, whereas further deletion of 221 bp resulted in the complete elimination of *BRL3* expression in the vascular initials (Figure 2.7).

In summary, our findings indicate that *cis*-elements within the -1719 to -1415 region regulate *BRL3* expression in the QC, while those within the -1415 to -1194 region govern its expression in vascular initials. Additionally, *cis*-elements within the -855 to -755 region control root vascular expression, and those within the -755 to -384 region regulate protophloem expression. Notably, *BRL3* expression was observed in stomata, with deletion of 304 bp (*pBRL3(1415bp)::GUS*) enhancing its expression in these cells. This suggests a negative regulatory element for stomata expression within this *cis*-regulatory region (-1719 to -1415).

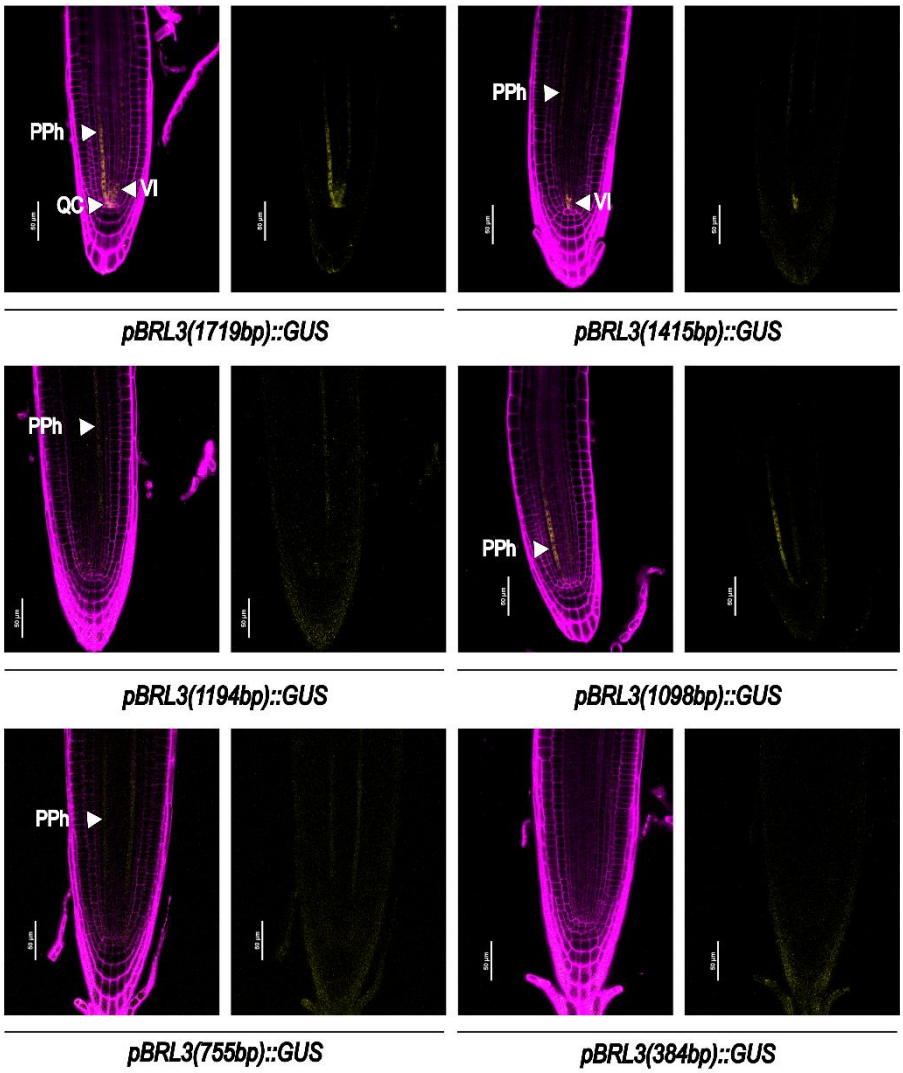


Figure 2.7 *BRL3* expression under different promoter lengths in the root apical meristem. Arabidopsis 6-day-old seedling roots stained with propidium iodide (magenta). GFP signal (yellow) shows the *BRL3* expression under different promoter lengths (1719, 1415, 1194, 1098, 755, 384 bp). The arrows indicate the different tissues where *BRL3* is expressed in the root meristem: Protophloem (PPh), Vascular Initials (VI) and Quiescent center (QC). Scale bar: 50µm.

2.2.4 *BRL3* expression is induced in the hypocotyl upon elevated temperatures: implication of KUA1 as putative mediator

As discussed in the introduction, BRL3 is known to be a receptor involved in abiotic stress adaptation. Consequently, after spatial analysis of *BRL3* expression, we aimed to determine whether *BRL3* undergoes transcriptional regulation in response to stress conditions, given its role in governing various abiotic stress-related phenotypes.

brl3 mutants exhibit impaired hypocotyl elongation under elevated temperatures, whereas its overexpression leads to hyperresponsiveness (Gupta et al., 2023). Hence, we wanted to explore whether *BRL3* expression is induced upon elevated temperatures. 6-day-old seedlings were subjected to continuous exposure to elevated temperatures (28°C), and GUS expression was assessed in the BRL3 transcriptional reporter line (*pBRL3(1719bp)::GUS*). Under control conditions, *BRL3* is expressed in the basal hypocotyl vasculature. However, upon exposure to elevated temperatures, *BRL3* expression was spatially induced, covering 34% of the hypocotyl compared to 17.13% coverage under control conditions (Figure 2.8a, b). Furthermore, upon quantification of GUS levels, *BRL3* expression was found to be induced in the basal hypocotyl vasculature under elevated temperatures, reaching a GUS mean intensity of 66.53 compared to 52.42 under control conditions (Figure 2.8c, d). Conversely, under elevated temperatures, *BRL3* expression in the root was reduced, with a GUS mean intensity of 46.1 compared to 93.36 under control conditions (Figure 2.8e, f).

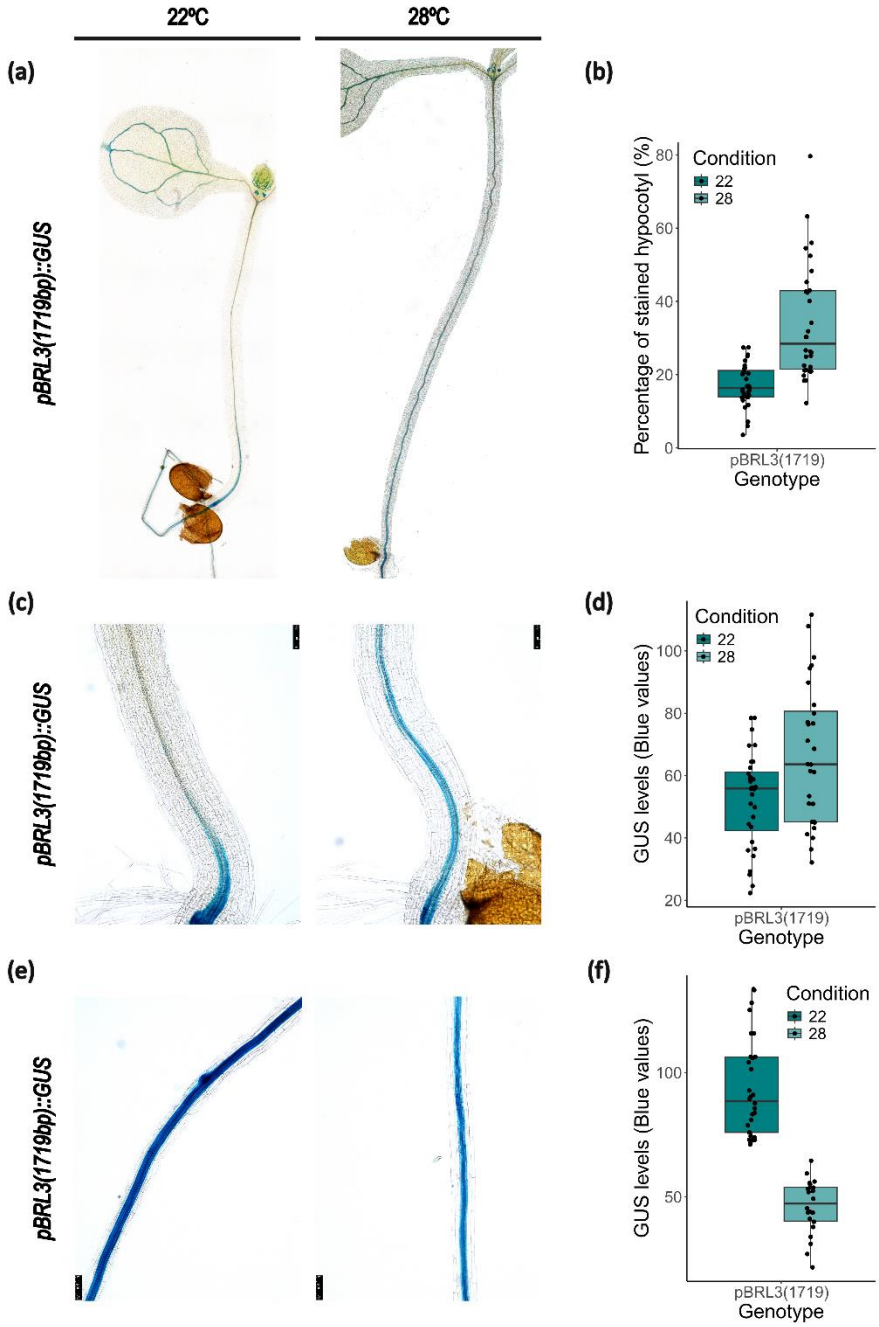


Figure 2.8 *BRL3* expression is induced in the hypocotyl and repressed in the root upon elevated temperature. GUS-stained 6-day-old seedlings showing *BRL3* expression under control conditions and elevated temperature in the hypocotyl (a,c) and the root (e). Scale bar: 75µm. (b) GUS levels quantification in the hypocotyl (b,d) and the root (f). Data from three independent biological replicates (n>22). One asterisk represents statistical significance differences (p-value<0.05) in a chi-squared test for survival ratios compared to control conditions.

Having established that *BRL3* is transcriptionally regulated under elevated temperatures, our next objective was to investigate which *cis*-regulatory elements are involved in this regulation. Promoter deletion lines were exposed to elevated temperatures, and GUS expression was monitored. The deletion of 304 bp showed no specific difference compared to the full-length transcriptional reporter line. However, a subsequent deletion of 221 bp abolished the transcriptional induction in the hypocotyl, while root repression persisted (Figure 2.9b). Contradictorily, our *in-silico* analysis did not reveal any *cis*-elements in the region from -1415 to -1194 (Figure 2.1, 2.2). Therefore, we re-evaluated this specific promoter region using RSAT with a Markov-chain background model of a low-order degree, while maintaining a stringent significance threshold (p-value<1e-5).

This analysis identified only two new *cis*-elements known to be bound by ZINC-FINGER HOMEODOMAIN PROTEIN 14 (ZHD14) and KUODA1 (KUA1) TFs (Figure 2.9a). Notably, the MYB TF KUA1, also referred to as MYBH, is implicated in hypocotyl elongation, and *mybh* mutants display defects in hypocotyl elongation (Kwon et al., 2013), suggesting KUA1 as a putative mediator of *BRL3* transcriptional regulation under elevated temperatures in the hypocotyl.

(a)

seq_id	ft_type	ft_name	strand	start	end	sequence	weight	Pval	ln_Pval	sig	rank	rank_pm
temperature	limit	START_END	D	-221	-1	.	0	0	0	0		
temperature	site	ZHD14	D	-102	-92	ATAATGCGGTA	9.4	7.1e-06	-11.861	5.151	1	1
temperature	site	KUA1	R	-72	-65	CATATCCG	7.2	8.4e-05	-9.379	4.073	2	1



(b)

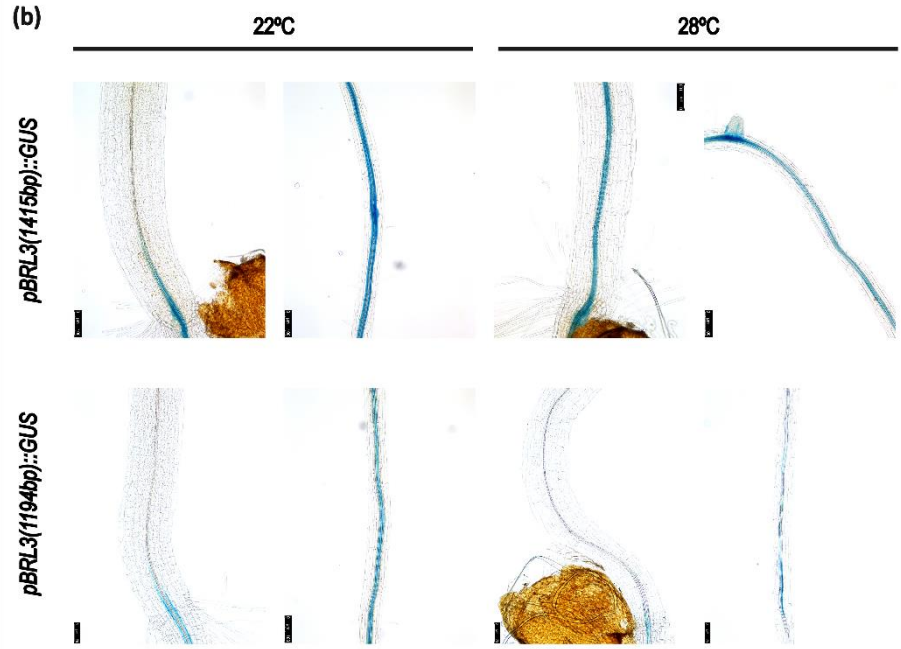


Figure 2.9 *BRL3* expression under different promoter lengths in the hypocotyl and root upon elevated temperatures. (a) *BRL3* promoter (region between -1415 and -1194) TF binding sites including information about the *cis*-element position, DNA strand, and sequence. Below schematic representation of *BRL3* promoter including the identified *cis*-regulatory regions, is included. (b) GUS-stained 6-day-old seedlings showing *BRL3* expression under control conditions and elevated temperature in the hypocotyl and the root. Scale bar: 75, and 100µm.

2.2.5 *BRL3* expression is induced in the root meristem following DNA damage: implication of SOG1 and ERF115 as putative mediators

BRL3 is also known to have a key role in DNA damage-induced QC divisions (Takahashi et al., 2023). Hence, we sought to investigate whether *BRL3* expression is induced upon DNA damage in the root meristem, where *brl3* mutants exhibit this defective response. 5-day-old seedlings of the BRL3 transcriptional reporter line were exposed or not to 24 hours of zeocin treatment, a DNA damage agent drug known to cause double-strand breaks (Chankova et al., 2007), followed by GUS staining (Figure 2.10a). Zeocin-induced DNA damage enhanced *BRL3* expression in the root meristem, where it is naturally expressed, with a GUS mean intensity of 17.86 compared to 15.2 under control conditions (Figure 2.10b). Interestingly, upon zeocin treatment, ectopic expression of *BRL3* was observed in the outer cell layers, such as the epidermis (Figure 2.10a, 2.11b).

To elucidate the *cis*-elements governing the regulatory mechanism of the BRL3 receptor, a comprehensive analysis of the *BRL3* promoter was conducted. *In-silico* analysis identified a conserved SOG1 TF DNA binding motif at -567 bp, consistent with ChIP-seq experiments conducted by Ogita et al., 2018. Additionally, *in-silico* analysis of the *BRL3* promoter identified a region from -1605 to -1529, containing binding motifs for known TFs related to BRs and DNA damage response, such as MYB (e.g., MYB56), ERF (e.g., ERF115), and BES1/BZR1 (Figure 2.11a).

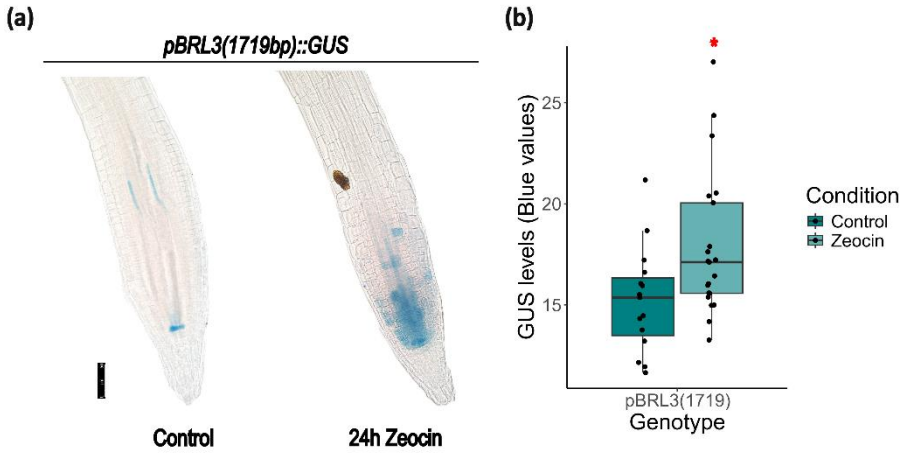


Figure 2.10 *BRL3* expression is induced in the root meristem upon DNA damage. (a) GUS-stained 6-day-old seedlings showing *BRL3* expression under control conditions and zeocin treatment. Scale bar: 50µm. (b) GUS levels quantification in the root meristem. Data from three independent biological replicates (n>15). One asterisk represents statistical significance differences (p-value<0.05) in a chi-squared test for survival ratios compared to control conditions.

Therefore, promoter deletion lines were tested in response to zeocin treatment and observed under confocal for a better resolution (Figure 2.11). Deletion of CRER4 (*pBRL3(1415bp)::GFP*) preserved the activation of *BRL3* upon DNA damage in the meristematic region, while inhibiting the ectopic expression observed in the epidermis, indicating the role of this enhancer region in epidermal *BRL3* induction (Figure 2.10b). Conversely, deletion of the -567 SOG1 binding site (*pBRL3(384bp)::GFP*) suppressed the meristematic upregulation of *BRL3* upon DNA damage, while its presence (*pBRL3(755bp)::GFP*) maintained it, highlighting the crucial role of this motif in controlling its meristematic activity. Taken together, these findings provide evidence that *BRL3* expression is upregulated in the root meristem, directly promoted by the action of SOG1, and is upregulated ectopically, specifically in the epidermis, putatively through ERF115 TF.

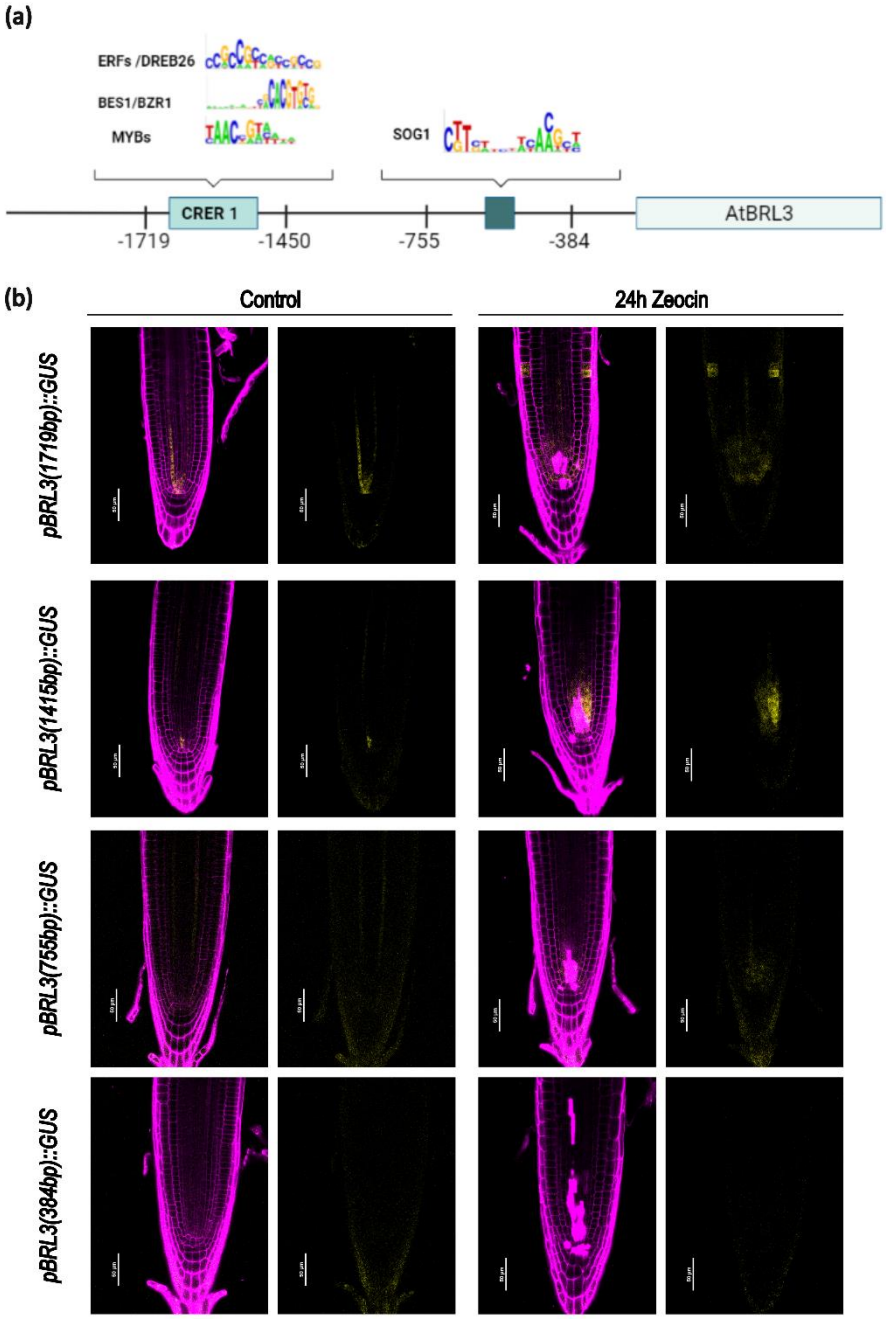


Figure 2.11 *BRL3* expression under different promoter lengths in the root apical meristem upon DNA damage. (a) Schematic representation of *BRL3* promoter including the identified *cis*-regulatory regions related to DNA damage regulators. (b) Arabidopsis 6-day-old seedling roots stained with propidium iodide (magenta). GFP signal (yellow) shows the *BRL3* expression under different promoter lengths (1719, 1415, 755, and 384 bp). Scale bar: 50µm.

2.2.6 HB15 is repressing *BRL3* transcriptionally through direct binding to its promoter

One of the primary objectives of this study was to enhance *BRL3* expression by genetically modifying *BRL3* promoter, while maintaining its responsiveness to environmental cues, thereby boosting plant´s ability to withstand abiotic stressors.

The adaptive responses mediated by BRL3 originate in its vascular domain, where it elicits a heightened thermomorphogenic response when expressed under the phloem companion cells-specific promoter SUCROSE-PROTON SYMPORTER 2 (pSUC2) and facilitates the mobilization and accumulation of osmoprotectants in the root through the phloem (Fàbregas et al., 2018; Gupta et al., 2023). Promoter deletion analysis identified a 100 bp region crucial for *BRL3* vascular expression (Figure 2.5). Within this promoter element, in silico analysis identified a HD-Zip III TF binding site, which was also conserved by another vascular-specific BR receptor, BRL1 (Figure 2.3b). This suggests that this specific *cis*-element plays an important role in ensuring proper vascular expression of *BRL3*. Consequently, we investigated whether HD-Zip III TFs are involved in the transcriptional regulation of *BRL3* vascular expression.

Through *in-silico* analysis, AtHB15, an HD-Zip III TF, was identified as putative *BRL3* transcriptional regulator (Figure 2.2a). HB15 is an homeobox HD-Zip III TF natively expressed in root vascular tissues and functionally characterized as a negative regulator of vascular development and secondary cell wall formation (Okashi-Ito et al., 2003; Kim et al., 2005; Du et al., 2015; Wei et al., 2023).

To elucidate whether HB15 regulates *BRL3* expression, a luciferase reporter assay was conducted. *Nicotiana benthamiana* (Nicotiana) leaves were co-agroinfiltrated with both *35S::HB15-GFP* (effector) and different *BRL3* promoter deletion constructs driving the luciferase reporter gene (*pBRL3(855bp)::LUC / pBRL3(755bp):.LUC / pBRL3(*100bp vascular cis-element*)::LUC*). An empty binary vector was co-agroinfiltrated with the different *BRL3* promoter deletion constructs as a control. Two days post-agroinfiltration, Nicotiana leaf disks were harvested and placed in a plate reader luminometer. Co-agroinfiltrated leaves with *35S::HB15-GFP* and *pBRL3(855bp)::LUC* exhibited a significant reduction in the luciferase activity compared to control leaves, a reduction not observed when the putative HB15 binding site was absent (*pBRL3(755bp)::LUC*) (Figure 2.12a). Similarly, co-agroinfiltration of *35S::HB15-GFP* and *pBRL3*(100bp vascular *cis*-element)::*LUC* also led to a significant reduction in the luciferase activity (Figure 2.12a), indicating that HB15 can bind to the 100 bp *cis*-element trans-acting as a repressor of *BRL3* expression.

Further validation of HB15 as a *BRL3* transcriptional repressor was conducted by generating Arabidopsis transgenic lines overexpressing *HB15* (*35S::HB15-GFP*). Confocal visualization of the resultant transgenic lines revealed HB15 protein confinement to the nucleus and its ubiquitous expression (Figure 2.12b). Quantitative Polymerase Chain Reaction (qPCR) analysis of the overexpressing line demonstrated a 3.5-fold upregulation compared to Columbia ecotype (Col-0) WT plants (Figure 2.12c). Consistent with the luciferase reporter assay, overexpression of *HB15* resulted in a 0.57-fold downregulation of *BRL3* compared to WT plants (Figure 2.12d).

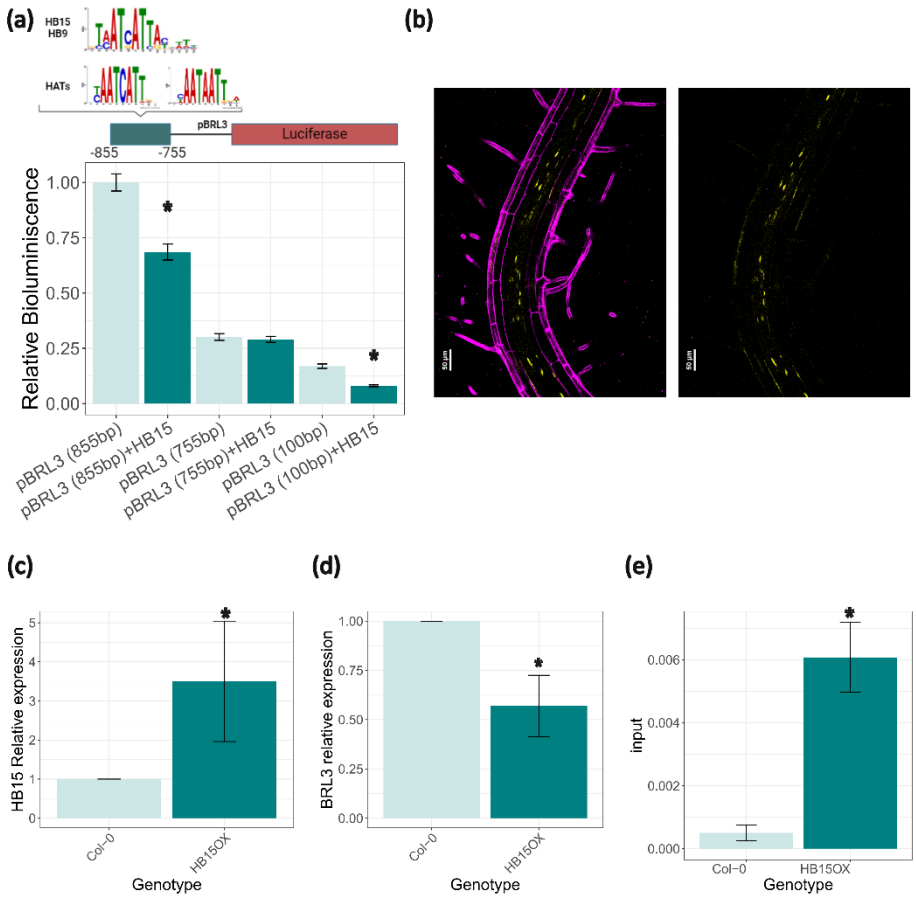


Figure 2.12 HB15 is a negative regulator of *BRL3* expression. (a) Expression of HB15 leads to *BRL3* inhibition. In the upper panel: schematic representation of *BRL3* promoter including the identified *cis*-regulatory regions related to *BRL3* vascular expression. In the lower panel: *BRL3* promoter with different lengths (855, 755 bp and the 100bp region including the HB15 *cis*-regulatory element) was fused to the luciferase reporter gene and co-transfected with empty binary vector or *35S::HB15-GFP* effector (+HB15) construct into Nicotiana leaves. Data from three independent biological replicates. One asterisk represents statistical significance differences (p-value<0.05) in a chi-squared test for luciferase activity between control leaves and leaves with the effector HB15 being expressed. (b) Arabidopsis *35S::HB15-GFP* 6-day-old seedling roots stained with propidium iodide (magenta). GFP signal (yellow) shows *HB15* expression. Scale bar: 50µm. (c, d) qRT-PCR analysis showing expression levels relative to WT (Col-0) of (c) *HB15* and (d) *BRL3*. Data from three independent biological replicates. One asterisk represents statistical significance differences (p-value<0.05) in a chi-squared test for *35S::HB15-GFP* expression levels compared to Col-0. (e) 20-day-old *35S::HB15-GFP* seedlings grown in MS media were used to extract genomic DNA, and chromatin fraction bound to HB15-GFP was immunoprecipitated with anti-GFP antibody. qPCR was conducted to amplify the 100 bp region including the HB15 *cis*-regulatory element. The recovery rate was determined against the input DNA.

To rule out the possibility of indirect transcriptional regulation of BRL3 by HB15, a chromatin immunoprecipitation assay followed by qPCR (ChIP-qPCR) was performed in the overexpressing line. ChIP-qPCR analysis revealed enrichment of HB15 in the *BRL3* promoter region spanning -855 to -755 bp (Figure 2.12e), consistent with previous DAP-Seq experiments conducted in O´Malley et al., 2016.

Taken together, these results indicate that HB15 directly binds to the *BRL3* promoter, specifically to the HD-Zip III preferentially recognized pseudopalindromic sequence TAAT(C/G)ATTA (Sessa et al., 2018) located within the 100 bp *cis*-element involved in *BRL3* vascular expression. This binding results in transcriptional repression of *BRL3*.

2.2.7 Several homeobox transcription factors are repressing *BRL3* transcriptionally

HB15 has been established as a negative regulator of *BRL3*, implying that mutations in HB15 could potentially enhance *BRL3* expression in the root vascular tissue, where *HB15* is natively expressed. To test this hypothesis, *athb15* mutants were crossed with the *BRL3* transcriptional reporter line (*pBRL3(1719bp)::GUS*). *GUS* expression was assessed in 6-day-old *pBRL3(1719bp)::GUS* x *athb15* seedlings (Figure 2.13b). While there was a slight increase in *GUS* expression observed throughout the root and hypocotyl vasculature of *pBRL3(1719bp)::GUS* x *athb15* seedlings (Figure 2.13a, b), it was not particularly pronounced.

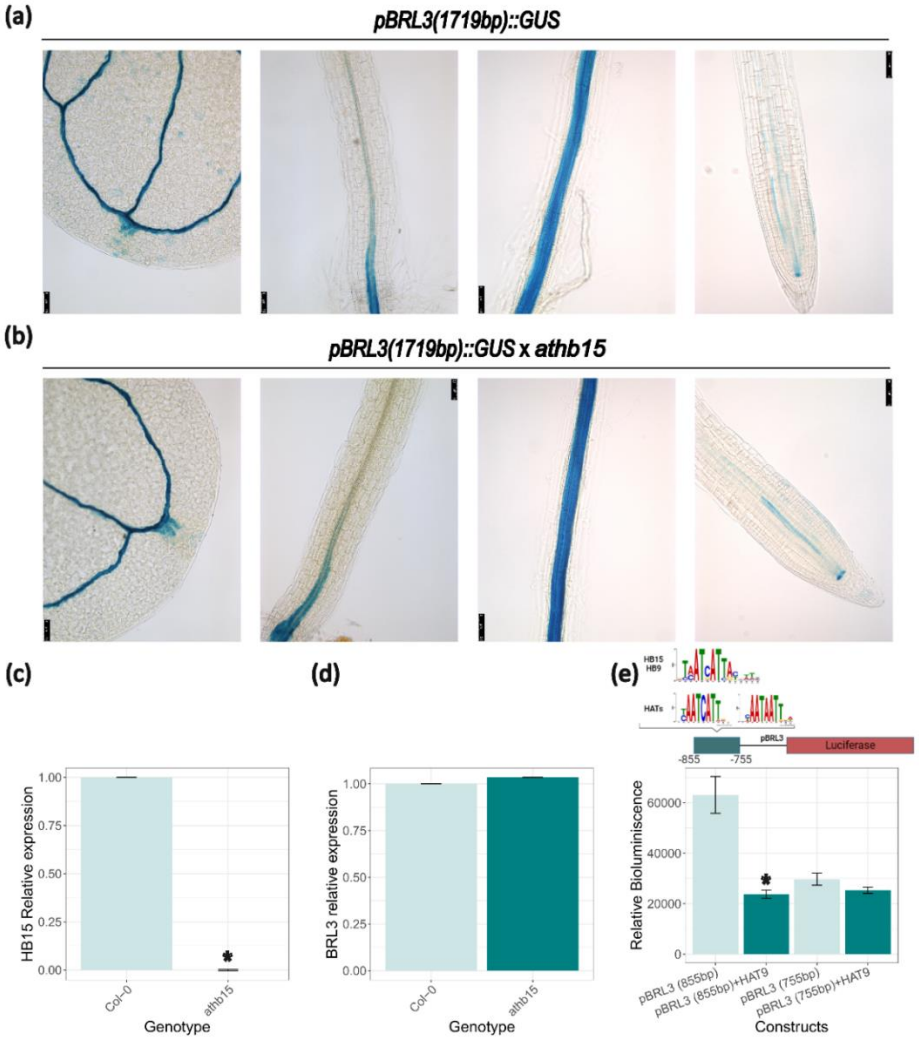


Figure 2.13 HAT9, together with HB15, is a negative regulator of *BRL3* expression. GUS-stained 6-day-old seedlings showing *BRL3* expression of pBRL3(1719)::GUS in Col-0 (a) and *athb15* mutant background (b). qRT-PCR analysis showing expression levels relative to WT (Col-0) of *HB15* (c) and *BRL3* (b). Data from three independent biological replicates. One asterisk represents statistical significance differences (p-value<0.05) in a chi-squared test for *athb15* expression levels compared to Col-0. (e) Expression of HAT9 leads to pBRL3 inhibition. In the upper panel: schematic representation of *BRL3* promoter including the identified *cis*-regulatory regions related to *BRL3* vascular expression. In the lower panel: *BRL3* promoter with different lengths (855 and 755 bp) was fused to the luciferase reporter gene and co-transfected with empty binary vector or *35S::HAT9-GFP* effector (+HAT9) construct into Nicotiana leaves. Data from three independent biological replicates. One asterisk represents statistical significance differences (p-value<0.05) in a chi-squared test for luciferase activity between control leaves and leaves with the effector HAT9 being expressed.

To further investigate whether *BRL3* expression was enhanced in the *athb15* mutant background, qPCR analysis was performed on *athb15* mutants. The analysis revealed a complete absence of HB15 transcript in the mutant, confirming a knockout mutation (Figure 2.13c). However, there was no statistically significant increase in *BRL3* transcript levels compared to WT levels (Figure 2.13d), suggesting that HB15 may not be the only transcriptional repressor binding to the 100 bp vascular *cis*-element. Interestingly, HB9 was also identified as a putative *BRL3* regulator through *in-silico* analysis, making it a potential candidate as an additional negative regulator (Figure 2.1a). Additionally, some HAT homeobox TFs share the DNA binding motif with HB9/15 and exhibit an additional DNA binding motif (AATAATT) (O´Malley et al., 2016), which was also found in the studied region. This suggests that HAT homeobox TFs could also act as additional *BRL3* repressors.

To assess whether HAT TFs could regulate *BRL3* expression, a luciferase reporter assay was performed. Nicotiana leaves were co-agroinfiltrated with *35S::HAT9-GFP* (effector) and various *BRL3* promoter deletion constructs driving the luciferase reporter gene (*pBRL3(855bp)::LUC / pBRL3(755bp)::LUC*). An empty binary vector served as a control for co-agroinfiltration with the different *BRL3* promoter deletion constructs. Two days post-agroinfiltration, Nicotiana leaf disks were collected and subjected to a plate reader luminometer. Co-agroinfiltrated leaves with *35S::HAT9-GFP* and *pBRL3(855bp)::LUC* demonstrated a significant reduction in luciferase activity compared to control leaves, a reduction not observed when the putative HAT TF binding sites were absent (*pBRL3(755bp)::LUC*) (Figure 2.13e). This result indicated that HAT9 can bind to *BRL3* promoter, acting as a *BRL3* repressor.

These results collectively suggest that HB15 is not the sole *BRL3* transcriptional repressor directly binding to the 100 bp vascular *cis*-element. Furthermore, HB9 or HAT TFs, particularly HAT9, could potentially bind to the same region, thereby negatively regulating *BRL3* expression in vascular tissues.

2.2.8 Engineering *BRL3* promoter to enhance its vascular expression

Several Homeobox TFs bind and negatively regulate *BRL3* expression by directly interacting with a specific 100-bp region in its promoter, which is crucial for *BRL3* vascular expression. This region, however, does not appear to be involved in the conditional regulation of *BRL3* expression by temperature or DNA damage. Consequently, genetic engineering of this 100-bp region in the *BRL3* promoter could potentially enhance its expression in transgene-free plants. To achieve this, a CRISPR-mediated *BRL3* promoter engineering approach was developed to generate allelic variation. Two different guide RNAs (gRNAs) were identified near the 100-bp region where the negative regulators bind: one spanning the *cis*-element associated with HAT TFs binding, and the other close to the HB15 or HB9 binding site (Figure 2.14a).

T1 Col-0 transformed plants carrying Cas9 and the gRNAs targeting the *BRL3* promoter binding box were obtained. Sequencing the T2 segregant population revealed two mutations of interest: a 4-bp deletion in the first gRNA site, removing a core *cis*-element of the HAT TF binding site, and a 45-bp deletion removing both HAT and HB TF binding sites (Figure

2.14b). Shoot samples from T2 segregant plants homozygous for these mutations and Col-0 plants of the same developmental stage were analyzed via qPCR. The 4-bp deletion resulted in a 2.4-fold upregulation of *BRL3*, while the 45-bp deletion did not significantly alter *BRL3* expression (Figure 2.14c). It is important to note that root sampling was not performed, and the analysis was conducted in a T2 segregant population. Therefore, further validation in T3 homozygous plants is necessary to confirm these findings.

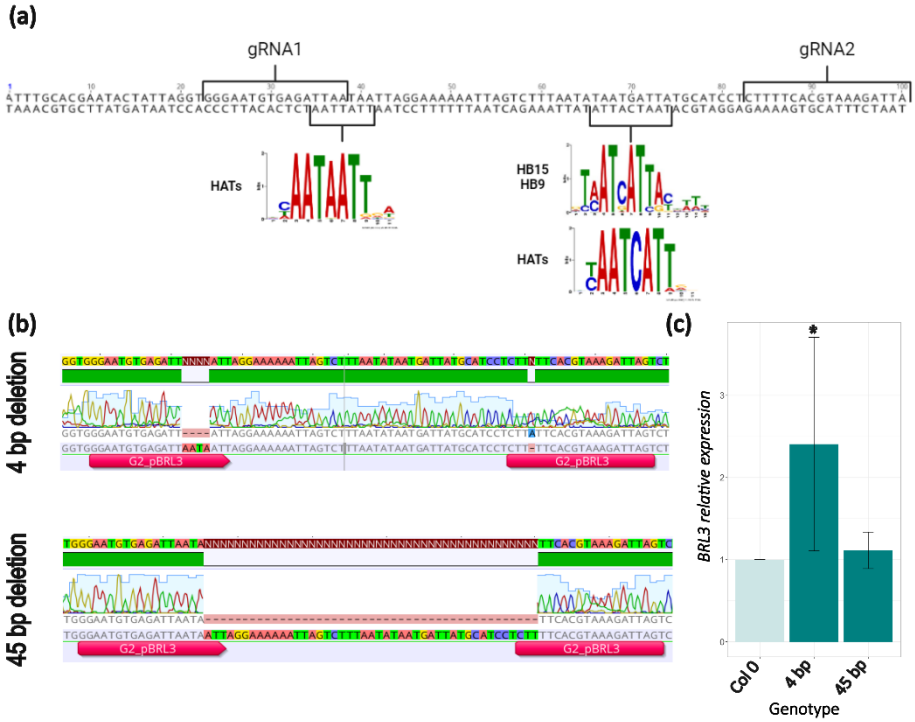


Figure 2.14 Engineering *BRL3* promoter to enhance its vascular expression. (a) Strategy for engineering the *cis*-elements responsible for HAT and HB TF binding, which negatively regulate *BRL3* expression. The promoter model highlights the positions of the HAT and HB binding sites and the gRNA positions. (b) Sequencing results from CRISPR-edited plants carrying 4-bp and 45-bp deletions spanning the HAT and HB binding sites. (c) qRT-PCR analysis showing *BRL3* relative expression levels in Col-0 and *BRL3* promoter-edited leaves. Data are from three independent biological replicates. One asterisk indicates statistically significant differences (p-value < 0.05) in a chi-squared test for *BRL3* expression levels compared to Col-0.

Chapter 3

Results

BRL3 DOWNSTREAM TRANSCRIPTION FACTORS MODULATE DROUGHT TOLERANCE IN *ARABIDOPSIS THALIANA*

3.1 Introduction

BRs play crucial roles in both plant growth and stress adaptation. The ability of plants to cope with abiotic stresses relies on a finetuned balance between growth and adaptation to stress. BRs exhibit antagonistic effects to ABA, a hormone pivotal for drought and osmotic stress adaptation while inhibiting plant growth (Cutler et al., 2010). Co-regulation of genes by both ABA and BRs emphasizes the complex interaction between these hormonal pathways. Studies on conserved motifs within genes responsive to ABA or BR treatments revealed enrichment of BRRE motifs in ABA-upregulated and BR-downregulated genes, while GAGA motifs were enriched in ABA-downregulated and BR-upregulated genes (Chung et al., 2014). Mutants insensitive to BRs, such as *bin2* mutants, exhibit heightened ABA sensitivity, highlighting the antagonistic role of these two hormones (Li et al., 2001). Further investigations established a molecular link between BIN2 and ABA signaling, where BIN2 inhibits BR signaling through phosphorylation of BES1/BZR1 while activating ABA-mediated stress responses by phosphorylating SnRK2 and ABI5 (Cai et al., 2014; Hu and Yu, 2014).

Besides BIN2 involvement in ABA signaling, BES1 emerges as a key player in promoting growth while antagonizing drought responses. BES1 directly interacts with DSK2, a ubiquitin-binding receptor involved in protein degradation pathway. During abiotic stress conditions, drought, or fixed-carbon starvation, BES1-DSK2 interaction leads to BES1 ATG8-mediated autophagy, reducing plant growth under drought stress conditions (Nolan et al., 2017). This study highlights the importance of BES1 posttranslational regulation upon stress conditions to avoid growth and prioritize the drought stress responses.

Furthermore, BES1 interacts with other TFs to modulate transcriptional control and balance BR-driven growth with ABA-driven drought stress responses. RD26 and BES1, for instance, act antagonistically in regulating gene expression. RD26 protein is accumulated upon high salt, drought and ABA treatment and function as a transcriptional activator of ABA-responsive genes (Fujita et al., 2004). BES1 inhibits *RD26* transcription, while RD26 is forming an inactive heterodimer with BES1 to inhibit the BES1-mediated BR-responsive genes transcriptional regulation. This complex regulation at transcriptional and protein level establishes a balance between growth and drought survival. Whereas constitutively active BES1 in *bes1-D* plants is resulting in drought susceptibility, low transcriptional activity of BES1 through RD26 leads to drought tolerance and growth penalization (Ye et al., 2017). RD26 is also phosphorylated and activated by BIN2 kinase, a negative regulator of BR signaling, promoting drought stress responses (Jiang et al., 2019). Similarly, TINY, an AP2/ERF family TF, interacts with BES1 to promote drought-responsive genes while inhibiting growth-related ones, with BIN2 also playing a role in stabilizing TINY (Xie et al., 2019). Moreover, WRKY46, WRKY54 and WRKY70 TFs synergize with BES1 to promote BR signaling and growth while inhibiting drought responses. These WRKY TFs are transcriptionally induced by BES1 and negatively regulated by BIN2 phosphorylation in a similar manner than BES1/BZR1 TFs, illustrating the complexity of the regulatory network (Chen et al., 2017).

Altogether, these findings suggest that BR signaling negatively regulates drought stress-responsive genes in an ABA-dependent or independent manner, promoting the overall growth of the plant. The role of BR signaling in growth promotion and their antagonistic function in drought

stress is further suggested by recent studies performed in our lab. BR loss-of-function mutants (such as *bri1* and *bak1*) were showing drought resistance phenotypes caused by a reduction in the overall growth, thus having a reduced exposure to the effect of drought, a known process called drought avoidance (Fàbregas et al., 2018).

However, BR application have resulted in increased tolerance to diverse abiotic stress, in maize (Anjum et al., 2011), Arabidopsis and *Brassica napus* (Kagale et al., 2007), suggesting a complex BR signaling network. An increased concentration of BRs in *DWF4* overexpressor plants also enhanced plant survival upon drought stress in *Brassica napus* (Shani et al., 2016). Overexpression of the vascular-specific BR receptor BRL3, enriched in the vasculature, also conferred drought resistance without affecting growth. The drought tolerance driven by BRL3 was achieved through an increase water stress-induced programmed cell death, enhanced hydrotropic response and the accumulation of osmoprotectants as raffinose, trehalose and proline (Fàbregas et al., 2018), leading to a higher survival rate after severe water deprivation. Finally, a study in tomato determined that exogenous application of BR was enhancing drought tolerance and up-regulated drought-related gene expression, while overexpressing *SlBRI1* resulted in increased H_2O_2 levels and drought susceptibility (Nie et al., 2019). These findings are suggesting that some of the drought tolerant phenotypes obtained by exogenous application of BRs or overexpression of biosynthetic enzymes are not driven by BRI1 signaling cascade including BES1 activation, but by BRL3-mediated signaling in a cell-specific manner.

In this chapter, our focus is on investigating the molecular pathway downstream of BR sensing that confers drought tolerance, specifically

through BRL3-specific signaling. Employing computational analysis, we initially selected genes exhibiting transcriptional deregulation by *BRL3* overexpression as well as similar tissue-specific expression pattern. Subsequently, through the generation of mutant and overexpression lines, we identified three TFs involved in drought adaptation and thermomorphogenesis. Following functional, transcriptional, and biochemical characterization of these TFs, a new molecular pathway mediated by BR signaling in drought adaptation, specifically by BRL3, is elucidated.

3.2 Results

3.2.1 Screening of genes transcriptionally regulated by BRL3 identifies three transcription factors involved in thermomorphogenesis and drought adaptation

To identify downstream components of the BRL3 signaling that could modulate the BR-mediated drought stress adaptation in Arabidopsis, a series of TFs were selected (Table 3.1) in the base of the following criteria: (I) Transcriptionally deregulated by the overexpression of *BRL3* in control or drought. (II) Being differentially regulated upon drought because of *BRL3* overexpression, e.g. upregulation in *BRL3* overexpressor but downregulation in WT between control and drought conditions. (III) Tissue specificity enrichment in the BRL3 native domain (Brady et al., 2007).

Table 3.1 Selection of BRL3-dowsntream TFs. In the table is included: The TF identification number; Gene name; Gene description; Log_2 fold change (LogFC) of *BRL3* overexpressor (BRL3OX) vs WT roots in control conditions; LogFC of BRL3OX vs WT roots in drought conditions; Interaction (Log (FCdrought/FCcontrol) in BRL3OX)) – ((Log (FCdrought/FCcontrol in WT)); Tissue specificity according to Brady et al., 2007 (APL: phloem + companion cells, J2661: pericycle, S17: phloem pole pericycle, S18: maturing xylem, and SUC2: phloem); Bibliography previously published.

TF ID	Gene name	Gene description	LogFC in BRL3OX control	LogFC in BRL3OX drought	LogFC BRL3OX interaction	Tissue specific (Brady et al., 2007)	References
TF1	*AT2G01430 (ATHB17)*	HD-ZIP TF; ABA salt and drought	6.3	6.4	-	-	(Park et al., 2013);(Zhao et al., 2017)
TF2	*AT5G62470 (MYB96)*	R2R3 MYB; ABA and drought	1.03	1.23	-	-	(Seo et al., 2009, 2010, 2011); (Lee S. B. et al., 2014, 2016); (Lee K. et al., 2015); (Lee H. G. et al., 2015, 2016, 2016, 2018, 2019, 2019); (Dai et al., 2020)
TF3	*AT5G05790*	Homeodomain like protein	-	-	-1.01	SUC2	Not previously decribed
TF4	*AT3G10910 (DAFL1)*	RING/U-box protein	0.7	-	-	SUC2	Not previously described
TF5	*AT3G04060 (NAC46)*	NAC domain protein; chlorophyll	0.73	-	-1.07	S18	(Cui et al., 2021)
TF6	*AT2G46640 (TAC1)*	Tiller Angle Control 1	-	-	-2.95	-	(Waite et al., 2018)
TF7	*AT2G20350*	ERF/AP2	-2.97	-	-	-	Not previously described
TF8	*AT3G24310 (MYB305)*	MYB protein	0.9	-	-	J2661	(Cheng et al., 2022)
TF9	*AT1G31050 (PFA1)*	bLHL;Lateral root and pericycle	0.7	0.93	-	J2661	(Zhang et al. 2021)
TF10	*AT2G22800 (HAT9)*	Homeobox	1.06	-	-	J2661/S17	Not previously decribed
TF11	*AT1G74370*	RING/U-box	-	-	1.15	-	Not previously decribed
TF12	*AT1G71692 (AGL12)*	MADS; cell differentiation; flowering	-	-	-0.6	APL/SUC2	(Tapia-Lopez et al. 2008)

Available T-DNA mutants corresponding to most of the selected TFs were ordered from the SALK collection, genotyped, and bred to achieve homozygosity (Table 3.2).

Table 3.2 Selected TFs T-DNA mutants. In the table is included: The TF identification number; gene name; SALK mutant name; identification number from NASC stock centre; and the primers used for genotyping.

TF ID	Mutant name	Mutants NASC ID	Primers for genotyping	
TF1	SALK_095524C	N657998	SALK_095524_LP	CGGGATTAAGGGTATGA
			SALK_095524_RP	TCCATTTCACTGATTGACACG
TF2	SALK_070557	N570557	SALKseq_070557_LP	TTGCTTGTAGTGGTGGTTGTG
			SALKseq_070557_RP	ACCAAACCCATTTGGACTTTC
TF3	SALK_031552C	N670503	SALK_031552_LP	AAAGCAATCGCATTGTTTTTG
			SALK_031552_RP	ACGTGGACTCACAACCTGATC
TF4	SALK_124824	N624824	SALK_124824_LP	TACGCTTGAGAAGCAGAGGAG
			SALK_124824_RP	GAAAATCTTTTGGCCTTGACC
TF5	SALK_107861C	N867711	SALK_107861_LP	CTACACACCACCCATTCATCC
			SALK_107861_RP	TAATTGTGGGGCTTTTTCAAC
TF6	-	-	-	-
TF7	-	-	-	-
TF8	SALK_058186	N558186	SALKseq_058186_LP	CTTCTCCGCACTGTTAGTTGG
			SALKseq_058186_RP	GAAAAGGGGTAACGAGAGCAC
TF9	-	-	-	-
TF10	SALK_049131C	N675016	SALK_049131_LP	CCTAAGCTTCTACCAGGCCTG
			SALK_049131_RP	GCAAACTCGATTAGTTCGACG
TF11	SALK_045398	N545398	SALKseq_045398_LP	AGGATTTGATGACAATGGCAC
			SALKseq_045398_RP	TTCACTTACAGGTTTGCGACC
TF12	-	-	-	-

BRL3-mediated signaling is essential for proper photomorphogenic response, as *brl3-2* seedlings are not able to elongate the hypocotyl at 28ºC (Gupta et al., 2023; Figure 3.1a). To rapid filter the selected TFs, six-day-old homozygous mutants were screened for their hypocotyl elongation under elevated temperatures (Figure 3.1b). All screened TF mutants displayed significant defects in hypocotyl elongation at 28ºC (Figure 3.1b), suggesting the effectiveness of computational analysis. However, this approach did not facilitate the rapid filtering of TFs for further investigation.

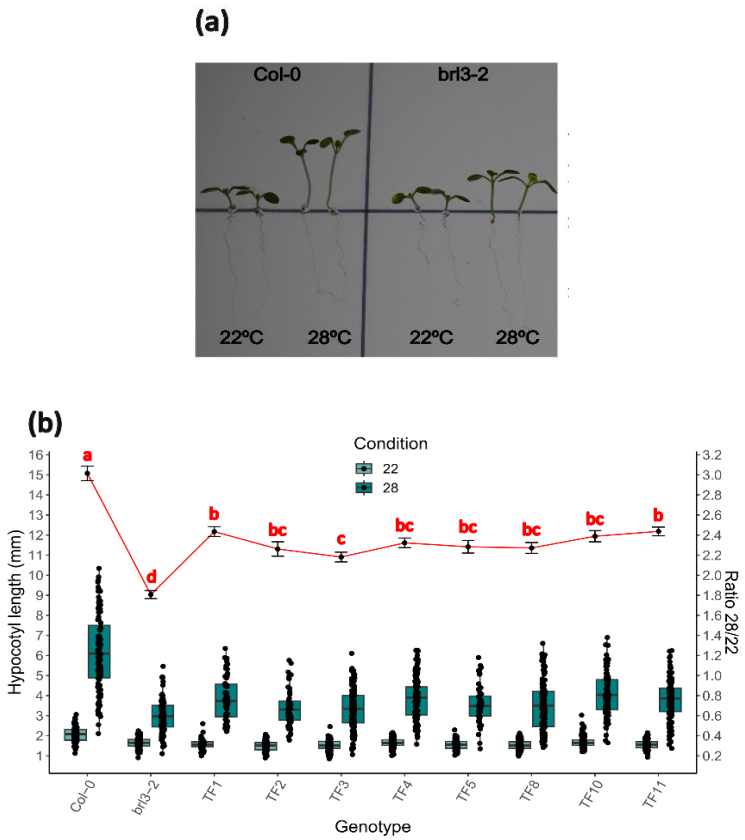


Figure 3.1 Thermomorphogenesis screening of TF T-DNA mutant lines. (a) Six-day-old seedling hypocotyl phenotype of Col-0 (left) and *brl3-2* (right) at 22ºC (left) and 28 ºC (right). (b) Boxplots of six-day-old hypocotyl length quantification in control (light blue) and elevated temperature (blue) conditions. Red line represents the ratio of hypocotyl length at 28 ºC/ hypocotyl length at 22ºC. Data from three independent biological replicates (n >107). Different letters represent statistical differences (p-value<0.05) in ANOVA plus Tukey´s HSD test.

To further filter the selected TFs, we generated overexpressing lines by constitutively activating them. This was achieved by transforming Col-0 Arabidopsis plants with *35S::TF* (genomic DNA coding sequence)-*GFP* constructs. We identified three independent lines and verified the subcellular localization along with the proper fusion of the TF with GFP by visualizing the roots of six-day-old seedlings under a confocal microscope (Figure 3.2). TF1, TF2, TF3, TF8, and TF10 showed enriched nuclear localization, while TF4, TF5, and TF11 displayed cytosolic expression. Following the identification of three independent lines exhibiting elevated constitutive expression, both T-DNA mutant lines and overexpressing lines for each TF were subjected to screening in a drought stress assay. This experiment was motivated by the previously reported drought-resistant phenotype of *BRL3* overexpressor plants (Fàbregas et al., 2018), aiming to unravel the molecular mechanism underlying the BRL3-mediated signaling pathway in abiotic stress adaptation. Two different drought stress assays were performed, wherein three-week-old Arabidopsis plants were subjected to severe drought stress by withholding water until Col-0 plants reached 5% of field capacity (FC). Drought survival rates were evaluated after a 10-day rewatering recovery period (Figures 3.3 and 3.4).



Figure 3.2 TF overexpressing lines. Six-day-old TF overexpressor (TF-OX) roots stained with propidium iodide (magenta). GFP signal (yellow) shows the TF localization. Scale bar: 50µm.

In both experiments, *BRL3* overexpressor plants were included as positive controls. Consistent with previous reports, in the first experiment (Figure 3.3), *BRL3* overexpressor plants exhibited a higher survival rate of 46.88%, contrasting with the 13.33% observed in Col-0 plants. Notably, both mutation and the overexpression of TF1 and TF3 was conferring drought susceptibility. These findings suggest that maintaining a precise balance of expression for these TFs is crucial for coping with drought stress. Interestingly, the overexpression of TF2 and TF8 was conferring drought tolerance, with an average survival rate of 46.64% and 49.33% respectively, while the mutation was resulting in drought susceptibility, with a survival rate of 6.45% and 3.13% respectively. These results suggest that TF2 and TF8 are positive regulators of drought adaptation.

In the second experiment (Figure 3.4), the positive control of *BRL3* overexpressor plants were again exhibiting higher survival rates in comparison with Col-0 plants. In this experiment, TF10 was showing the same tendency as TF2 and TF8, showing a drought tolerance when overexpressed (49.16% survival rate average) and susceptibility when mutated (15% survival rate average). This result suggests that TF10 is a positive regulator of drought adaptation.

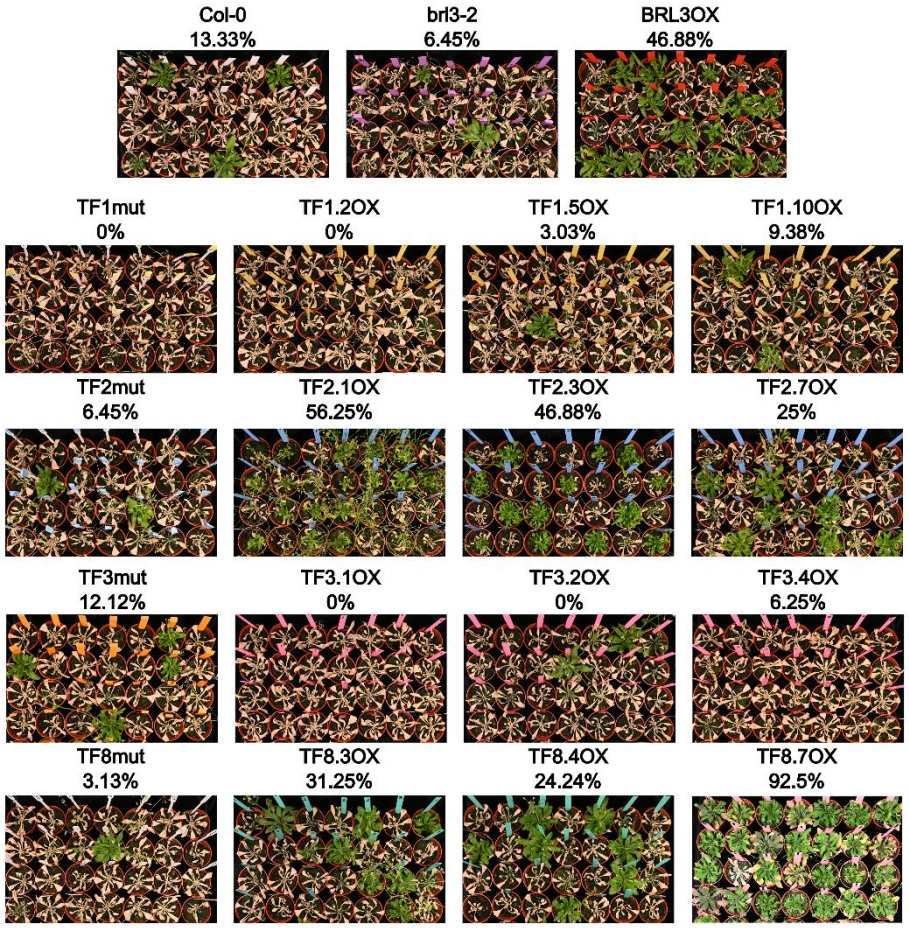


Figure 3.3 Overexpression of TF2 and TF8 confers drought tolerance. Plant phenotypes following a 10-day rewatering recovery period, initiated once Col-0 plants reached the 5% of FC. Plant survival percentages are included above the pictures. Data from one biological replicate.

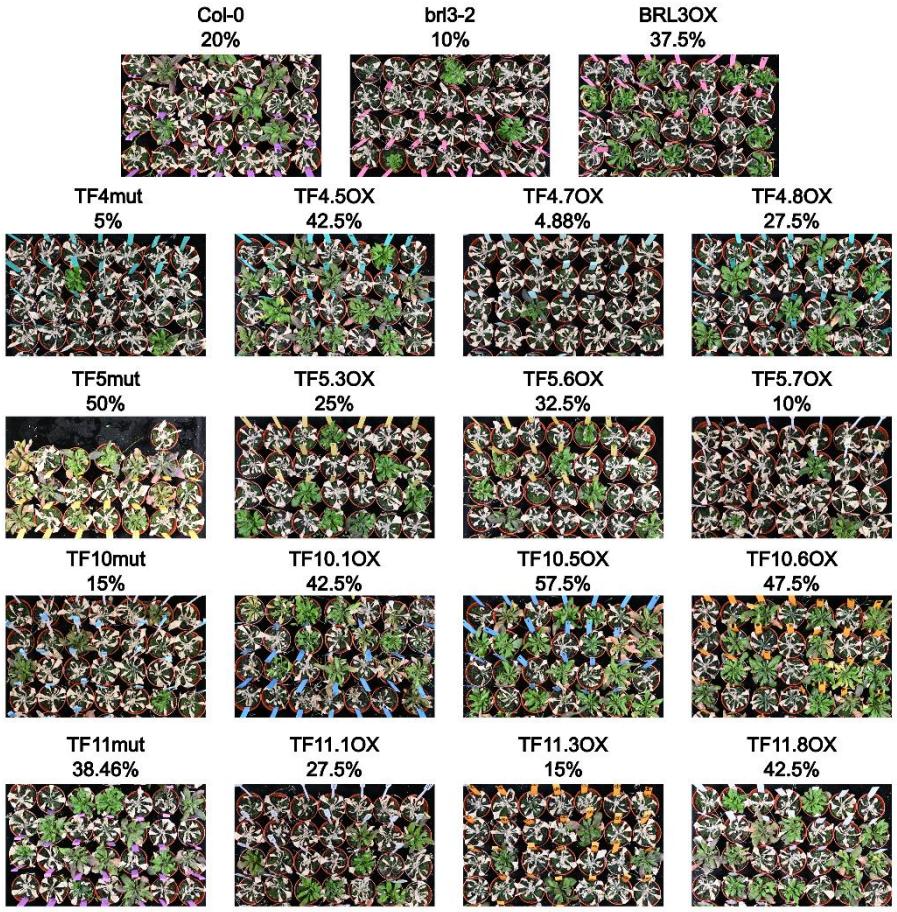


Figure 3.4 Overexpression of TF10 confers drought tolerance. Plant phenotypes following a 10-day rewatering recovery period, initiated once Col-0 plants reached the 5% of FC. Plant survival percentages are included above the pictures. Data from one biological replicate.

Taking together, these results prompt us to select for further analysis TF2 (MYB96), TF8 (MYB305) and TF10 (HAT9). These TFs emerged as putative positive regulators of both thermomorphogenesis and drought stress, exhibiting phenotypes also controlled by BRL3-mediated signaling.

In the following sections, each candidate TF will be further individually studied by functional, transcriptional, and biochemical characterization.

3.2.2 MYB96 is a BRL3-dowsntream transcription factor modulating abiotic stress adaptation

MYB96 is a R2R3-type MYB TF which positively regulates drought stress responses and lateral root formation through the integration of ABA and auxin signals (Seo et al., 2009). Later studies demonstrated that one of the main mechanisms to mediate the drought stress tolerance was through the regulation of ABA-mediated cuticular wax biosynthesis under drought stress conditions in Arabidopsis and *Camelina sativa* (Seo et al., 2011; Lee et al., 2014; Lee et al., 2016). However, no previous relation with BR signaling has been established. In a dataset previously published by our lab (Fàbregas et al., 2018), we found that *MYB96* is upregulated by the overexpression of *BRL3* in control (1.03 logFC) and drought stress conditions (1.23 logFC) (Table 3.1).

3.2.2.1 *MYB96* and *BRL3* are co-expressed in the root vascular initials and the guard cells

Upon constitutive activation of the *BRL3* receptor, the expression of *MYB96* is induced. To explore whether this transcriptional regulation occurs under normal conditions, we conducted an analysis into the native expression pattern of *MYB96*. Employing single-cell resolution transcriptomics and transcriptional reporter lines, we first analyzed *MYB96* expression in roots. Utilizing the single-cell atlas visualization tool from Tissue-Enrichment web tool (TOTEM) (Coleto-Alcudia et al., 2024), we observed *MYB96* expression is mainly enriched in root

vascular initials, epidermis initials, and mature endodermis, although with relatively low expression (Figure 3.5a).

Additionally, we constructed a fusion between a 2 Kb region upstream of the *MYB96* transcription starting site and the *GUS-GFP* coding sequence, generating the *pMYB96::GUS/GFP* construct which was introduced into the Col-0 ecotype. Analysis of the resulting transcriptional reporter lines via GUS staining revealed notable expression of *MYB96* in the mature endodermis (Figure 3.5b) and the root meristem (Figure 3.5c). Further visualization of *MYB96* expression using confocal microscopy to observe GFP fluorescence confirmed its presence in vascular initials, with a particularly enriched expression in epidermis initials (Figure 3.6).

Notably, *MYB96* expression was also detected in the cotyledon vasculature, epidermis and guard cells (Figure 3.5e), reinforced by the TOTEM tissue enrichment analysis where we could observe a *MYB96* expression enrichment in abaxial epidermis and guard cells (Figure 3.5d).

These findings, consistent with prior research (Seo et al., 2009), suggest potential co-expression of *MYB96* and *BRL3* in various tissues, including root vascular initials, root vasculature, and guard cells.

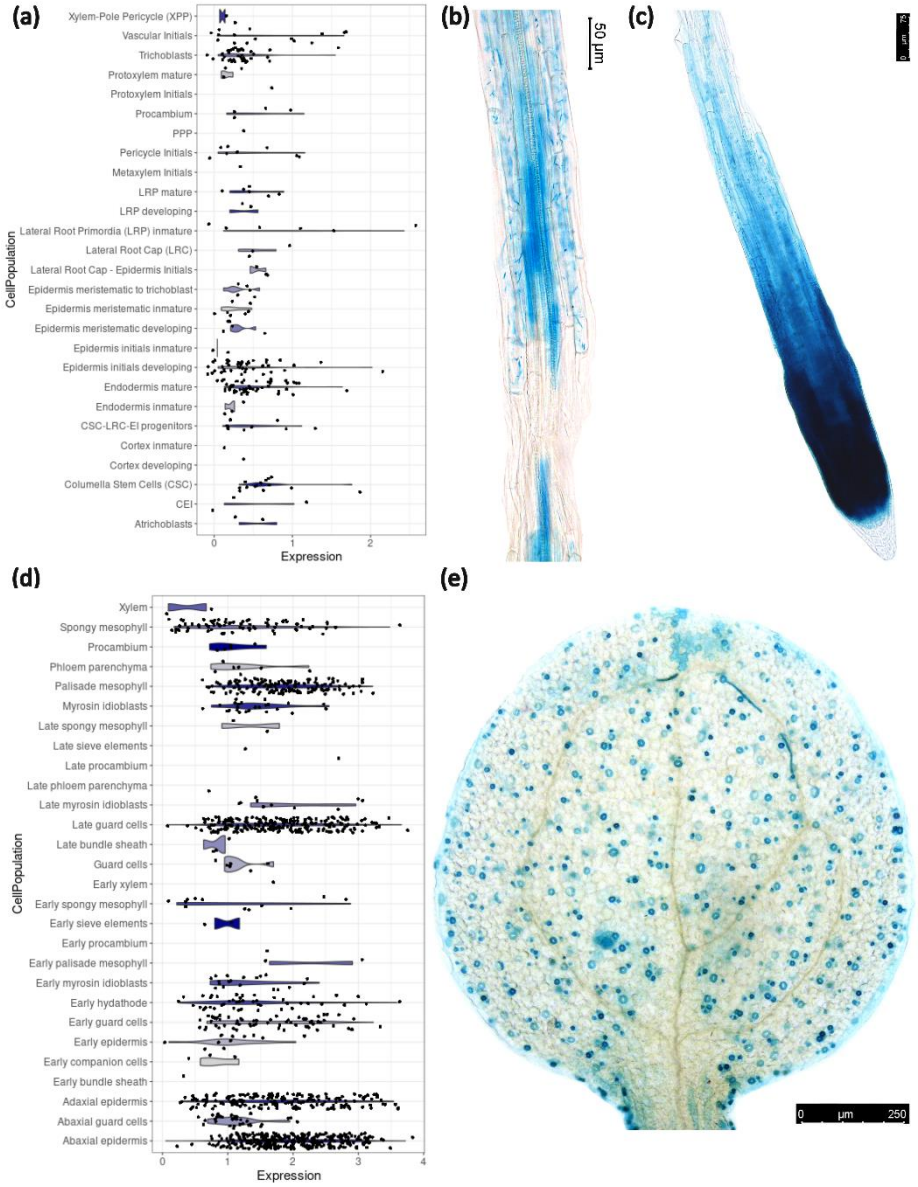


Figure 3.5 *MYB96* is natively expressed in the root meristem, mature endodermis and in the cotyledon vasculature, epidermis and guard cells. (a) Root cell population enrichment of *MYB96* expression. *pMYB96::GUS/GFP* expression in six-day-old GUS-stained seedlings in different plant tissues: (b) Mature root (Scale bar: 50 µm) and (c) primary root meristem (Scale bar: 75µm). (d) Shoot cell population enrichment of *MYB96* expression. (e) *pMYB96::GUS/GFP* expression in six-day-old GUS-stained cotyledon (Scale bar: 250 µm).

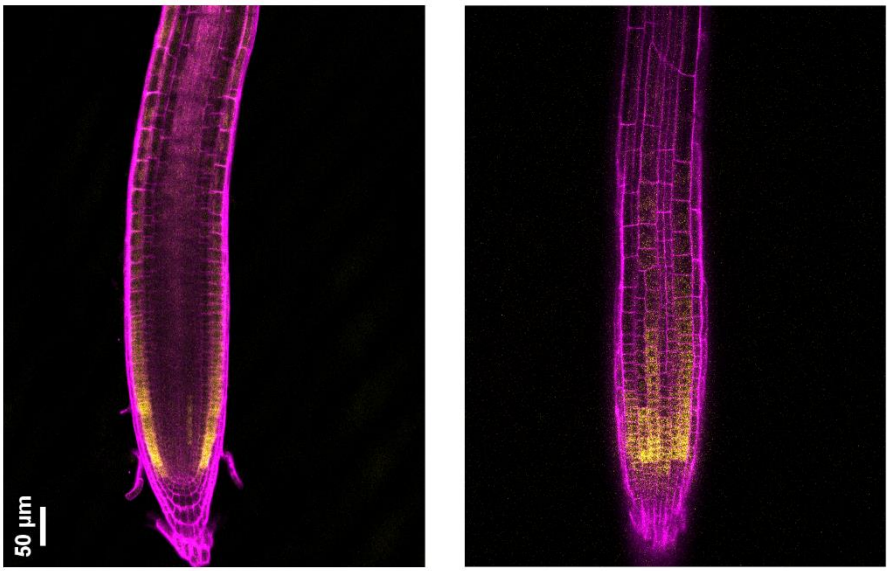


Figure 3.6 *MYB96* is expressed in the vascular initials and enriched in the epidermis initials. Arabidopsis *pMYB96::GUS/GFP* six-day-old seedling roots stained with propidium iodide (magenta). GFP signal (yellow) shows the *MYB96* native expression. Scale bar: 50µm.

3.2.2.2 Overexpression of *MYB96* results in drought tolerance and growth penalization

To assess the role of MYB96 in severe drought and growth in mature plants, three-week-old *MYB96* overexpressor plants were pictured, rosette area was measured, and then exposed to severe drought by withholding water until they reached the 5% of FC. Afterwards, plants were re-watered and plant survival was accounted after 10 days of recovery in normal water regime. *BRL3* overexpressor plants were showing a drought tolerance phenotype (Fàbregas et al., 2018), reaching 46.67% of survival in comparison with the 13.86% found in WT plants (Figure 3.7a, c).

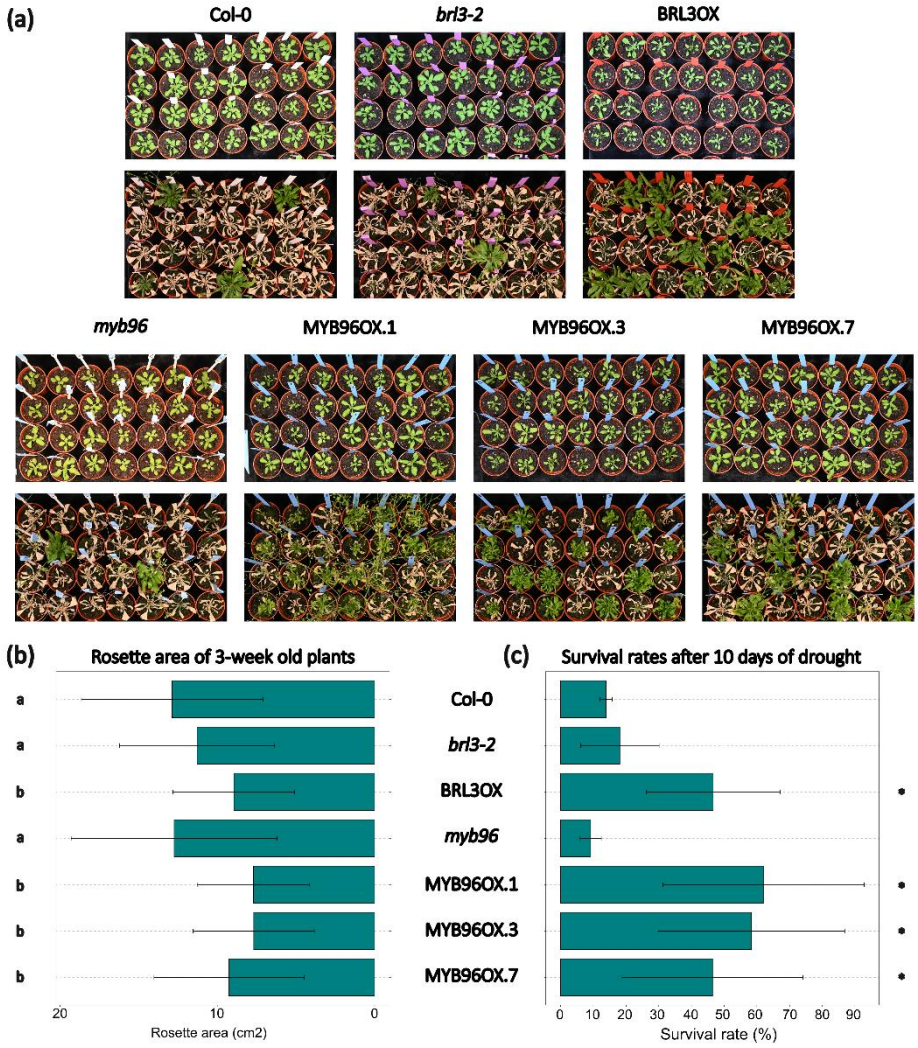


Figure 3.7 Overexpression of *MYB96* results in drought tolerance in Arabidopsis. (a) Three-week-old plant rosette phenotypes in control conditions (upper row) and after 10 days of rewatering (bottom row). Genotypes included are Col-0, *brl3-2* and *myb96* mutants, *BRL3* and *MYB96* overexpressors (BRL3OX and MYB96OX respectively). (b) Barplot of three-week-old Arabidopsis rosette area quantification. Data from three independent biological replicates (n>96). Different letters represent statistical significance differences (p-value<0.05) in ANOVA plus Tukey´s HSD test. (c) Drought survival rate after 10 days of rewatering. Data from three independent biological replicates (n>96). One asterisk represents statistical significance differences (p-value<0.05) in a chi-squared test for survival ratios compared to Col-0.

Notably, the overexpression of *MYB96* further enhanced drought tolerance, with a mean survival rate of 55.59% across three independent overexpressor lines (Figure 3.7a, c). Overexpression of *BRL3* and *MYB96* led to a notable reduction in the rosette area of three-week-old plants, measuring 3.87 and 4.06 cm^2 respectively, compared to the 5.76 cm^2 observed in WT plants (Figure 3.7b). This reduction exhibited a statistically significant and robust correlation (R^2 = 0.97, p-value= 4e-05) with survival rate (Figure 3.8), indicating a strong association between rosette area and plant survival under abiotic stress conditions. These findings suggest that the promotion of plant survival through *BRL3* and *MYB96* overexpression involves a trade-off with rosette area reduction and remarking their pivotal roles in facilitating adaptation to abiotic stressors.

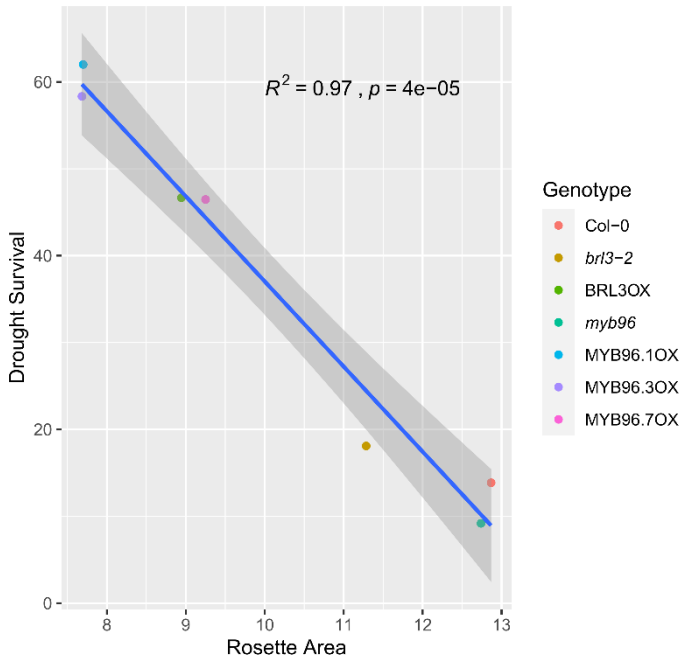


Figure 3.8 Correlation of drought survival and rosette area. The graph includes the coefficient of determination and the correlation p-value. The rosette area and drought survival rates are the mean from three independent biological replicates (n>96).

3.2.2.3 MYB96 exhibits dual phosphorylation states, and brassinosteroids play a role in stabilizing its dephosphorylated, active form via BIN2

The BR signaling cascade culminates in the dephosphorylation and stabilization of the BES1 and BZR1 TFs (Wang et al., 2002; Yin et al., 2002). Previous findings indicate that *MYB96* is transcriptionally upregulated upon overexpression of *BRL3* (Table 3.1) and through ABA signaling (Seo et al., 2009). Additionally, *MYB96* is co-expressed in the root and guard cells with BRL3 (Figure 2.5, 2.6, 3.5 and 3.6), and exhibits similar phenotypic traits, such as drought tolerance and growth arrest, when overexpress (Figure 3.7). Given these observations, we wanted to investigate whether BR signaling also contributes to the post-translational stabilization of MYB96 activity, similar to what occurs with the BR-related TFs BES1 and BZR1.

Previous studies indicated that MYB96 was stabilized by ABA signaling, which involves the degradation of the ubiquitin ligase MYB30-INTERACTING E3 LIGASE 1 (MIEL1). MIEL1 is responsible for ubiquitinating MYB96, marking it for degradation via proteasome-mediated proteolysis (Lee et al., 2016). However, the phosphorylation states of MYB96 were not previously reported. Total protein extracts from *MYB96* overexpressor seeds were subjected to western blot analysis using anti-GFP antibody (Figure 3.9). The analysis under control conditions (DMSO mock) revealed two phosphorylation states of MYB96, with the dephosphorylated state exhibiting higher stability (Figure 3.9a). Furthermore, we analyzed MYB96 phosphorylation states under BL treatment (10 nM) and demonstrate an

increase in dephosphorylation stability, with a phosphorylated/dephosphorylated ratio of 0.86 relative to the DMSO mock treatment (Figure 3.9a). In the absence of BR signaling, the GSK3-like kinase BIN2 is phosphorylating and inactivating BES1 and BZR1 by promoting their binding to 14-3-3 proteins, leading to their cytoplasmic retention and proteasome-mediated degradation (Li and Nam, 2002; Gampala et al., 2007; Peng et al., 2008). In the presence of BR signaling, BIN2 is dephosphorylated by BSUI and sent to proteasome-mediated degradation (Li and Nam, 2002; Peng et al., 2008). Therefore, we wanted to investigate whether the observed dephosphorylation of MYB96 induced by BL was mediated through the inhibition of BIN2 kinase activity.

To address this question, we analyzed the phosphorylation states of MYB96 under Bikinin treatment (50 μM), an inhibitor of BIN2 activity (De Rybel et al., 2009). Our results revealed an increase in dephosphorylation stability, with an even greater phosphorylated/dephosphorylated ratio of 0.66 relative to the DMSO mock treatment (Figure 3.9a). This suggests that inhibition of BIN2 kinase activity contributes to the dephosphorylation of MYB96, highlighting a potential regulatory mechanism by which BR signaling influences MYB96 activity.

Finally, to further support the idea that BR signaling reinforces MYB96 activity through the stabilization of its dephosphorylated form, we examined the phosphorylation states of MYB96 under MG132 treatment (50 μM), an inhibitor of the proteasome (Nolan et al., 2017). Our findings revealed that inhibiting the proteasome led to the stabilization of the

phosphorylated form of MYB96, resulting in a phosphorylated/dephosphorylated ratio of 2.02 (Figure 3.9b).

Collectively, these results suggest that BR signaling stabilizes the dephosphorylated and active form of MYB96 via BIN2 kinase. Conversely, in the absence of BR signaling, the phosphorylated form of MYB96 undergoes proteasome-mediated degradation.

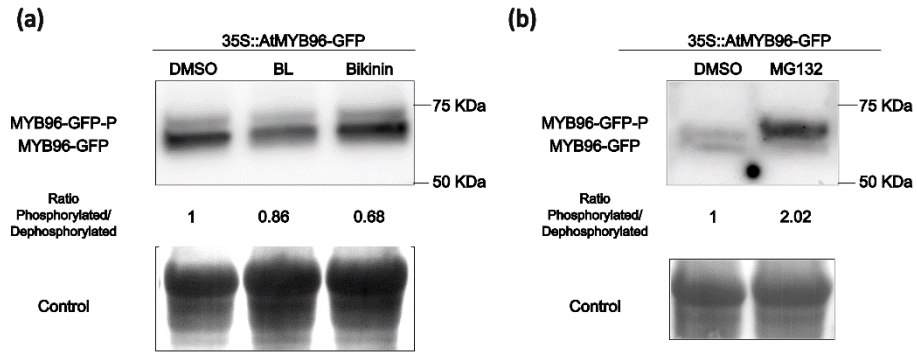


Figure 3.9 MYB96 dephosphorylated form is stabilized by BR signaling via BIN2. (a) Western blot analysis was conducted using total protein extracts derived from 12-day-old 35S::MYB96-GFP seedlings treated with liquid Dimethyl sulfoxide (DMSO), BL (10 nM) and Bikinin (50 μM) for 1 hour. Anti-GFP antibodies were used for detection. Control bands illustrating Rubisco levels were visualized through Ponceau staining. (b) Western blot analysis was conducted using total protein extracts derived from 12-day-old 35S::MYB96-GFP seedlings treated with liquid DMSO, and MG132 (50 μM) for 6 hours. Anti-GFP antibodies were used for detection. Control bands illustrating Rubisco levels were visualized through Ponceau staining. Data from three independent biological replicates with similar results and the ratio phosphorylated/dephosphorylated was quantified using ImageJ.

3.2.2.4 MYB96 interacts with BZR1 in the cytoplasm and the nucleus

Next, we explored if MYB96 can coordinate its transcriptional activity together with BR-related TF BES1 and BZR1. This was accomplished through *in vivo* co-immunoprecipitation assays using GFP-immunoprecipitated protein extracts obtained from *MYB96* overexpressor seedlings. The GFP antibody, successfully pulled down MYB96-GFP fusion (Figure 3.10a). Then, by using specific native antibodies for BZR1, this TF was detected in the MYB96-GFP pull down, indicating the interaction between these TFs (Figure 3.10a). However, by using native BES1 antibodies, this TF was not detected under the same conditions, suggesting MYB96 and BES1 are not interacting (Figure 3.10a). Moreover, we used 35S::GFP seedlings as negative control to confirm that BZR1 is not interacting with GFP under the same conditions (Figure 3.10b), suggesting specificity of the interaction between MYB96 and BZR1.

To further validate the interaction between MYB96 and BZR1, we employed Bimolecular Fluorescence Complementation (BiFC) assays. The BiFC assay was performed with the C-terminal and N-terminal of the YELLOW FLUORESCENT PROTEIN (YFPC and YFPN, respectively). Co-expression of *BZR1-YFPC* and *MYB96-YFPN* in Nicotiana leaves resulted in the reconstitution of YFP fluorescence in both the cytoplasm and nucleus (Figure 3.10c). This interaction was corroborated by the positive control, BZR1-YFPC and PIF4-YFPC (Oh et al., 2012), which also showed YFP fluorescence in the nucleus, while the negative control, BZR1-YFPC and AT2G01430-YFPN (TF1 from

the initial screening, considered a more suitable negative control than an empty vector YFPN due to nuclear subcellular localization [Figure 3.2] and to avoid free YFP), did not exhibit YFP fluorescence (Figure 3.10c). These results further support the interaction between MYB96 and BZR1 in the cytoplasm and nucleus.

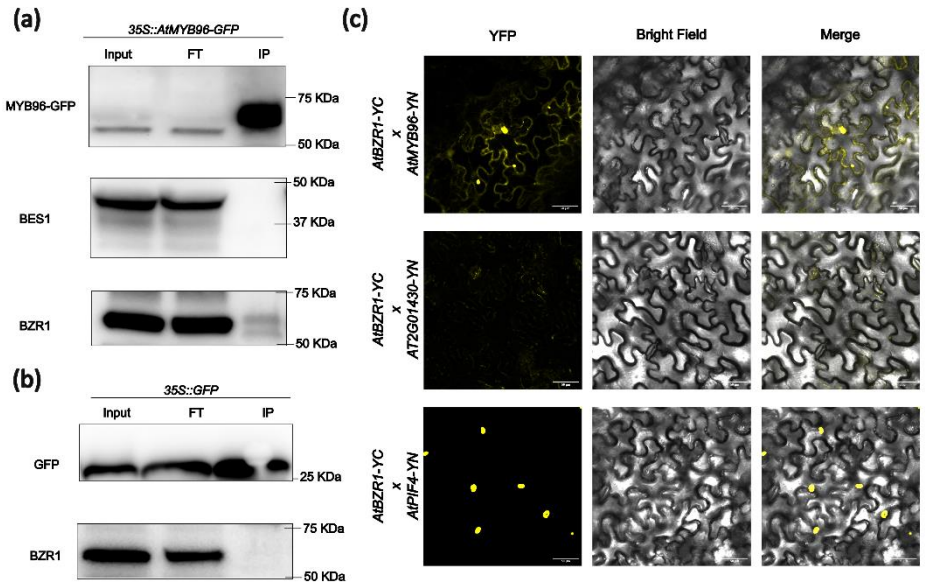


Figure 3.10 MYB96 interacts with BZR1 in the cytoplasm and in the nucleus. (a) Coimmunoprecipitation assays were conducted using GFP-immunoprecipitated protein extracts obtained from 12-day-old *MYB96* overexpressors. Anti-GFP, anti-BES1 and anti-BZR1antibodies were used for detection. (b) Coimmunoprecipitation assays were conducted using GFP-immunoprecipitated protein extracts obtained from 12-day-old *35S::GFP* seedlings, used as a negative control for the MYB96 and BZR1 coimmunoprecipitation. Anti-GFP and anti-BZR1 antibodies were used for detection. The coimmunoprecipitation experiments were repeated three times with similar results. (c) BiFC assays were conducted by co-expressing *BZR1-YFPC* and *MYB96-YFPN* (tested interaction), *AT2G01430-YFPN* (negative control), and *PIF4-YFPN* (positive control), in Nicotiana leaves. For each panel YFP, bright field, and merged images from confocal microscopy are shown. Data from three independent biological replicates.

3.2.2.4 MYB96, BZR1 and BRL3 coordinate transcriptionally responses to stress

To delve into the transcriptional coordination between MYB96 and BZR1 TFs, we studied the putative targets identified through DAP-seq experiments for MYB96 (O´Malley et al., 2016), and those for BZR1 identified via ChIP-chip experiments (Sun et al., 2010). By identifying a common set of genes among these targets, we conducted Gene Ontology Enrichment (GOE) analysis (Figure 3.11a). Our analysis revealed enrichment in several Gene Ontology (GO) categories associated with abiotic stress adaptation, including "Response to stress", "Response to abiotic stimulus", and "Response to oxygen-containing compounds" (Figure 3.11b). Within the genes associated with "Response to abiotic stimulus", we observed the presence of DREB TFs, such as *RELATED TO AP2 4* (*RAP2.4*), known for its role in enhancing plant tolerance to various abiotic stresses, including drought (Lata et al., 2011). Additionally, we identified several common targets involved in the synthesis of osmoprotectants, such as *GALACTINOL SYNTHASE 1* (*GolS1*), a crucial enzyme in raffinose synthesis, a well-established osmoprotectant in plant cells (Nishizawa et al., 2008).

Furthermore, to explore MYB96-mediated transcriptional regulation driven by BRL3 signaling, we investigated MYB96 targets that were deregulated by *BRL3* overexpression (Figure 3.11a). GOE analysis once again highlighted an enrichment in abiotic stress-related categories, such as "Response to stress", "Response to abiotic stimulus", and "Response to water deprivation" (Figure 3.11c). Within the genes associated with "Response to abiotic stimulus", we identified genes involved in drought

stress and osmotic stress adaptation, including *ABSCISIC ACID RESPONSIVE ELEMENT-BINDING FACTOR 2* (*ABF2*) (Yoshida et al., 2015). Additionally, we found *RBOHD*, which is involved in ROS production and mediates systemic signaling in various biotic and abiotic stresses (Martínez-Rivas et al., 2023).

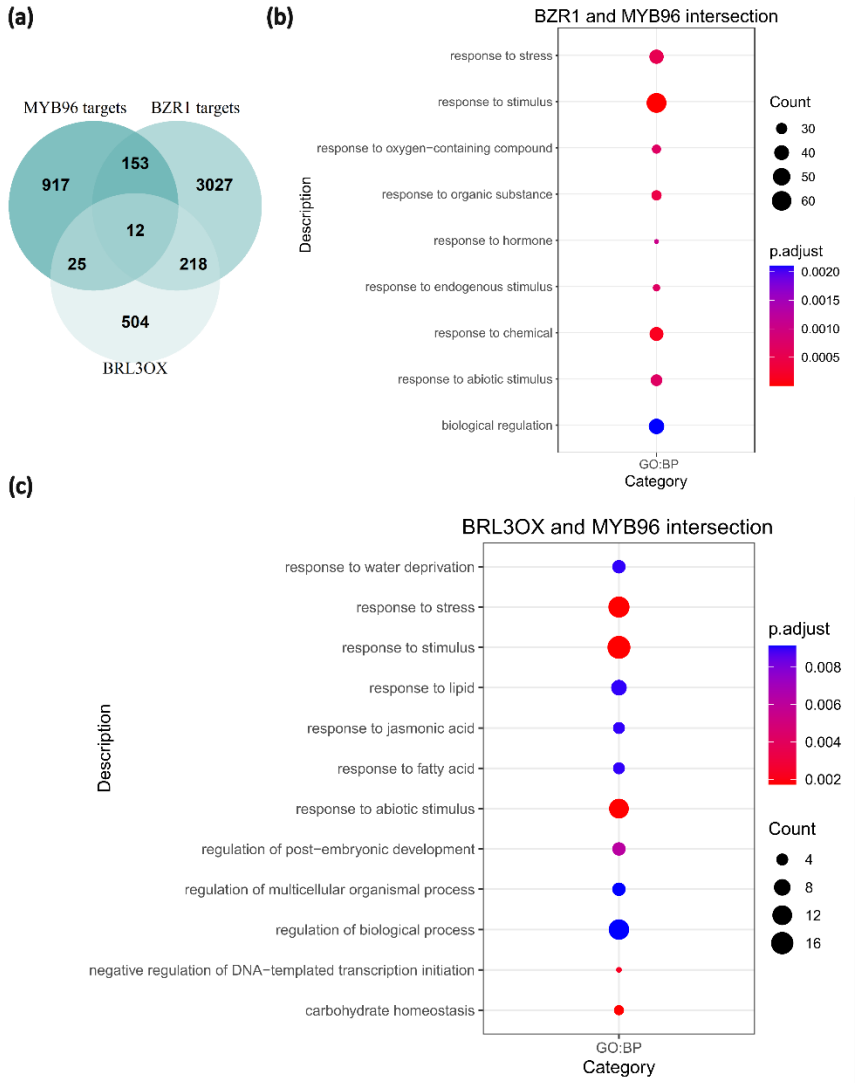


Figure 3.11 MYB96, BZR1 and BRL3 coordinate transcriptionally responses to abiotic stress. (a) Venn diagram of MYB96 targets, BZR1 targets and deregulated genes in *BRL3* overexpressor plants. GOE analysis of (b) MYB96 and BZR1 common targets and (c) MYB96 targets deregulated by the overexpression of *BRL3*.

Collectively, these findings suggest that MYB96, BZR1, and BRL3 may cooperatively regulate plant responses to abiotic stress by transcriptionally modulating genes involved in drought adaptation, osmoprotectant synthesis, and ROS production.

3.2.3 MYB305 is a BRL3-dowsntream transcription factor modulating abiotic stress adaptation

MYB305 (also called MYB71) is a R2R3-type MYB TF induced transcriptionally by ABA signaling and its overexpression induces hypersensitivity to ABA in terms of germination (Cheng et al., 2022). No previous relation with BR signaling or drought tolerance has been stablished. In a dataset previously published by our lab (Fàbregas et al., 2018), we found that *MYB305* is upregulated by the overexpression of *BRL3* receptor in control conditions (0.9 logFC) and it appeared to be tissue specific in "J2661" root cell population, belonging to pericycle cells according to Brady et al., 2007.

3.2.3.1 *MYB305* and *BRL3* are co-expressed in the phloem pole pericycle and the guard cells

Upon the constitutive activation of the BRL3 receptor, the expression of *MYB305* is induced. To investigate whether this transcriptional regulation occurs downstream basal BRL3 conditions, we conducted an analysis of the native expression pattern of *MYB305*. Utilizing TOTEM, we observed tissue-specific expression of *MYB305* enriched in the

phloem and xylem pole pericycle, as well as in the lateral root primordia (Figure 3.12a).

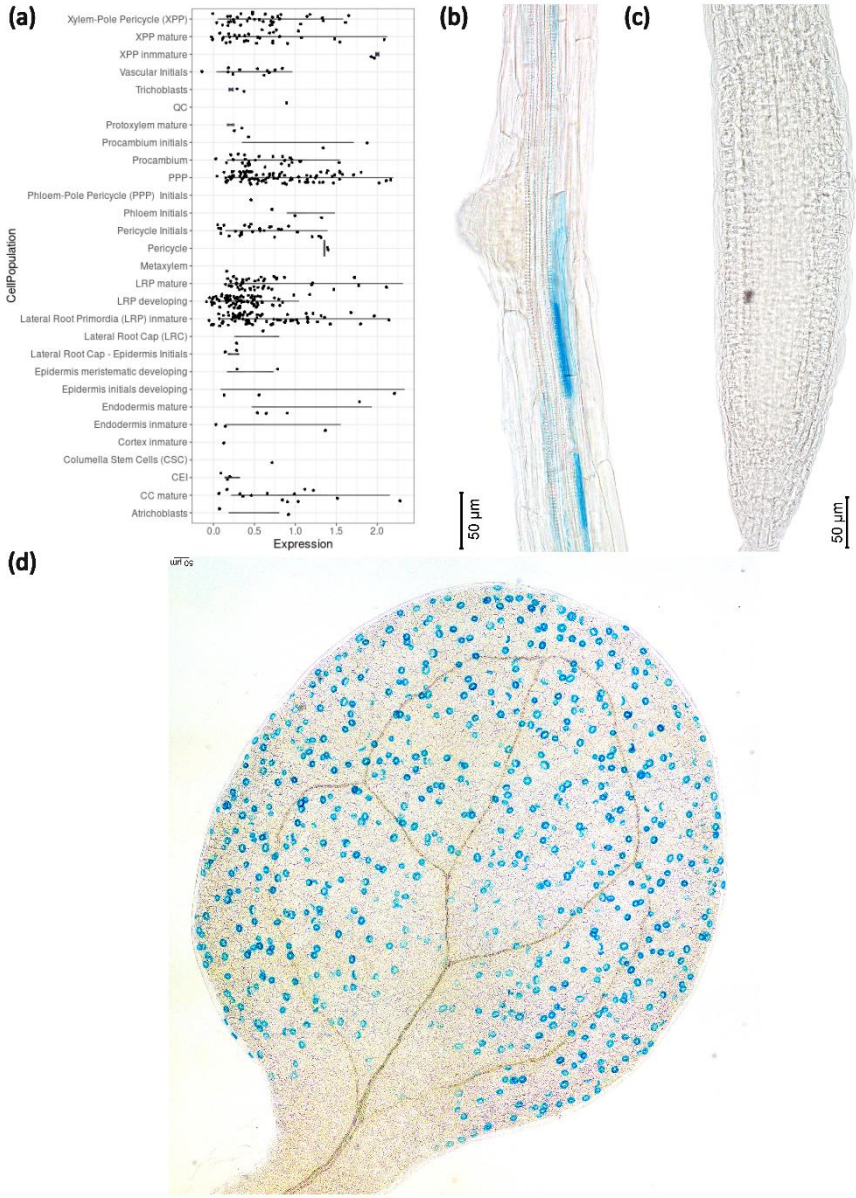


Figure 3.12 *MYB305* is natively expressed in mature root vasculature and in the guard cells. (a) Root cell population enrichment of *MYB305* expression. *pMYB305::GUS/GFP* expression in six-day-old GUS-stained seedlings in different plant tissues: (b) Mature root (Scale bar: 50 µm), (c) primary root meristem (Scale bar: 50µm), and (d) cotyledon (Scale bar: 50 µm).

Furthermore, we generated *pMYB305::GUS/GFP* transcriptional reporter lines (2 Kb promoter). Analysis of these reporter lines via GUS staining revealed tissue-specific expression of *MYB305* in the mature root vasculature (Figure 3.12b) and in the guard cells (Figure 3.12d) but absent from the root meristem (Figure 3.12c). In contrast with single-cell resolution transcriptomics (Figure 3.12a), we did not observe *MYB305* expression in the lateral root primordia (Figure 3.12b), however lateral roots emerge from pericycle, and the TOTEM could be detecting these specific cells.

Further visualization of *MYB305* expression using confocal microscopy to check GFP fluorescence demonstrated a precise expression pattern in the pericycle (Figure 3.13a, c). Consistent with the GUS staining results, *MYB305* expression was absent from the root meristem (Figure 3.13b, 3.12c).

These findings suggest a potential co-expression of MYB305 and BRL3 in the phloem pole pericycle and the guard cells.

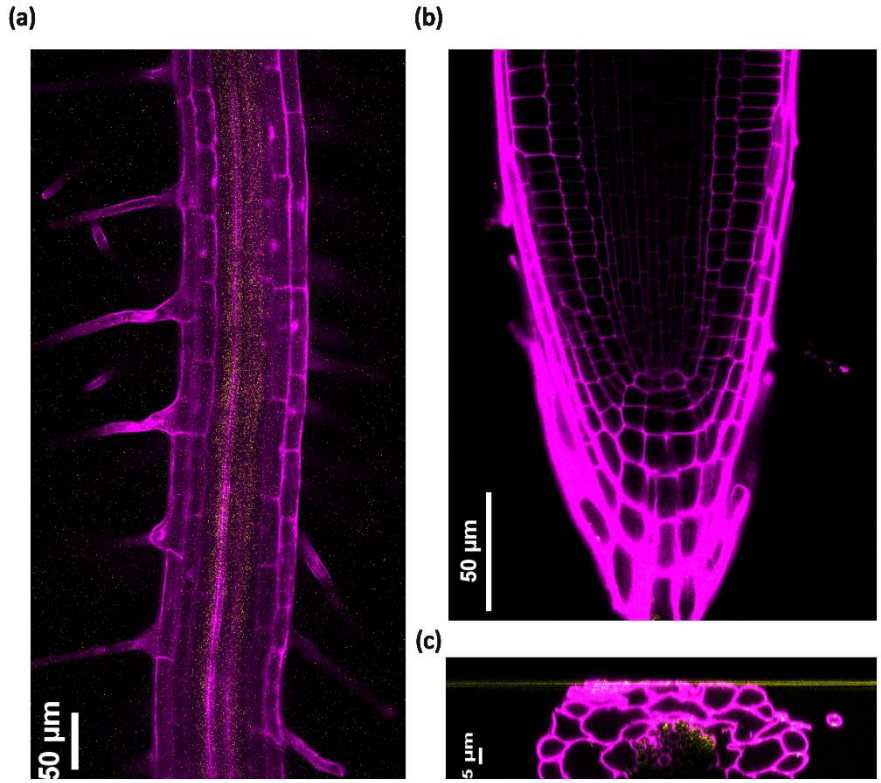


Figure 3.13 *MYB305* is expressed in the pericycle. *pMYB305::GUS/GFP* six-day-old seedling roots stained with propidium iodide (magenta). GFP signal (yellow) shows the *MYB305* native expression. Scale bar: 50µm and 5 µm.

3.2.3.2 Overexpression of *MYB305* confers drought tolerance

To evaluate the functional significance of MYB305 in drought tolerance and growth, we pictured and quantified the rosette area of three-week-old mutant and overexpressor plants. Subsequently, the plants were subjected to severe drought stress until Col-0 reached 5% FC. Following the severe drought period, plants were rewatered and after a recovery period of 10 days, plants were pictured, and survival rate was determined (Figure 3.14).

Interestingly, the overexpression of *MYB305* resulted in a drought resistant phenotype, with a mean survival rate of 53.43% across three independent lines, compared to Col-0 plants with a mean survival rate of 13.86% (Figure 3.14c). Notably, while one *MYB305* overexpressor line (MYB305.4OX) did not show a drought resistant phenotype, another (MYB305OX.7) exhibited the highest survival rate of 96.49% (Figure 3.14c), which correlated with higher *MYB305* expression levels as validated by confocal microscopy GFP visualization (Figure 3.2). Despite the *MYB305* overexpressor lines showing a reduction in rosette area compared to Col-0 plants, averaging 8.77 cm^2 compared to 12.9 cm^2 in Col-0 (Figure 3.14b), there was low correlation between survival rate and rosette area (Figure 3.15). These results suggest that overexpression of *MYB305* leads to a drought resistant mechanism involving active adaptation to abiotic stress rather than a phenotype characterized by drought avoidance through reduced growth.

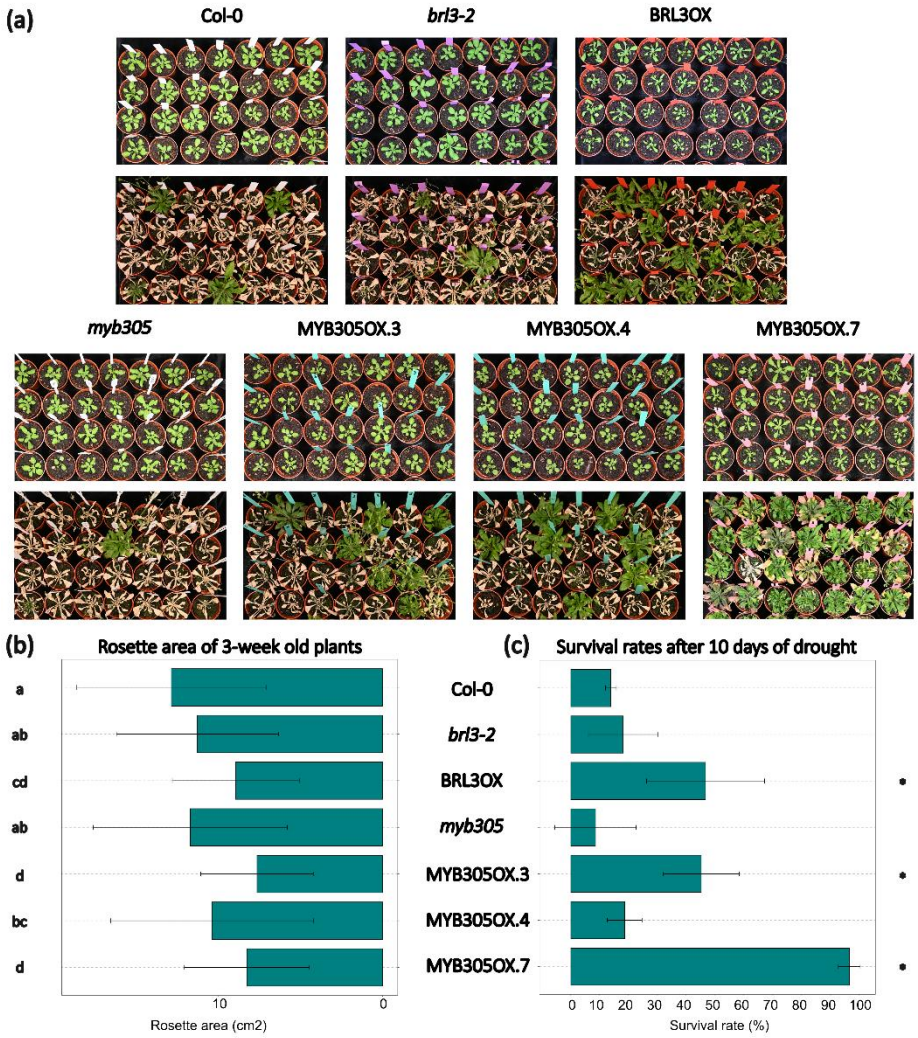


Figure 3.14 Overexpression of *MYB305* results in drought tolerance in Arabidopsis. (a) Three-week-old plant rosette phenotypes in control conditions (upper row) and after 10 days of rewatering (bottom row). (b) Barplot of three-week-old Arabidopsis rosette area quantification. Data from three independent biological replicates (n>94). Different letters represent statistical significance differences (p-value<0.05) in ANOVA plus Tukey´s HSD test. (c) Drought survival rate after 10 days of rewatering. Data from three independent biological replicates (n>94). One asterisk represents statistical significance differences (p-value<0.05) in a chi-squared test for survival ratios compared to WT.

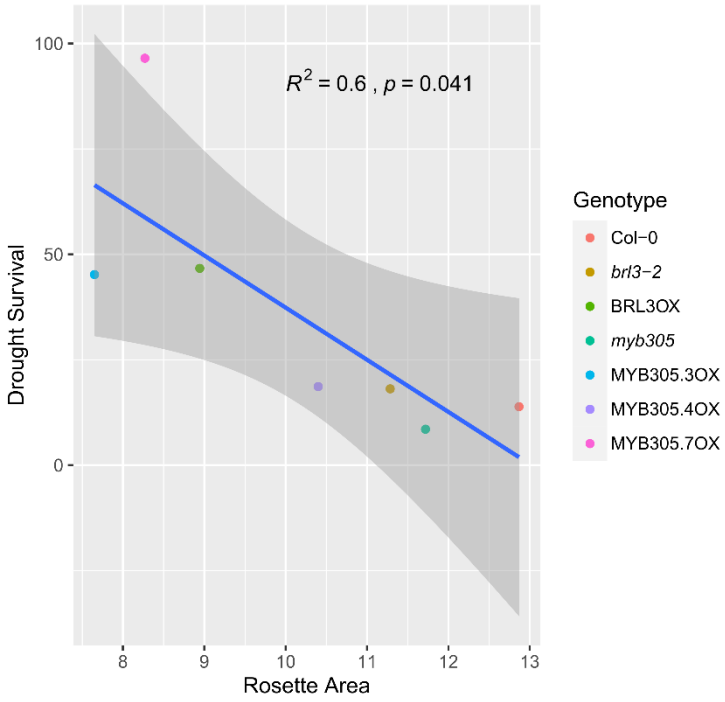


Figure 3.15 Correlation of drought survival and rosette area. The graph includes the coefficient of determination and the correlation p-value. The rosette area and drought survival rates are the mean from three independent biological replicates (n>94).

3.2.3.3 MYB305 is stabilized by BR signaling via BIN2, inhibiting its proteasome-mediated degradation, but not by ABA signaling

Prior findings revealed that *MYB305* is transcriptionally activated by both ABA signaling (Cheng et al., 2022) and *BRL3* overexpression (Table 3.1). Co-expression of *MYB305* and *BRL3* occurs notably in the phloem pole pericycle and guard cells (Figure 2.5, 2.6, 3.12, 3.13), with shared phenotypes upon overexpression, such as drought resistance and growth penalization (Figure 3.14). Therefore, we sought to investigate whether BR or ABA signaling played a role in MYB305 protein stability.

In contrast to MYB96 protein (Figure 3.9a), distinct phosphorylation states for MYB305 protein were not identified (Figure 3.16). However, BR signaling and BIN2 inhibition were found to stabilize MYB305 protein (Figure 3.16a), indicating a negative regulatory role of BIN2 kinase activity in MYB305 protein stability. This suggests the presence of different phosphorylation states, even if undetectable via western blot analysis.

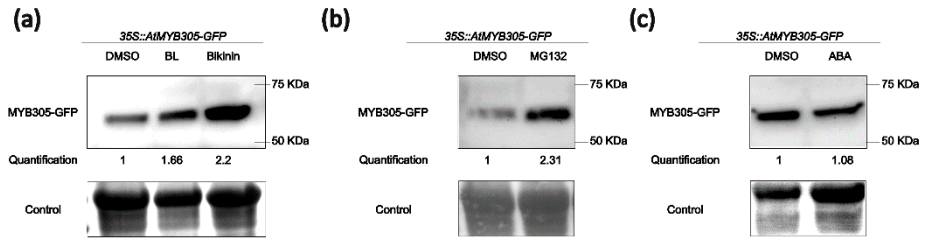


Figure 3.16 MYB305 is stabilized by BR signaling via BIN2, inhibiting the proteasome-mediated degradation, but not by ABA signaling. (a) Western blot analysis was conducted using total protein extracts derived from 12-day-old 35S::MYB305-GFP seedlings treated with liquid DMSO, BL (10 nM) and Bikinin (50 μM) for 1 hour. Anti-GFP antibodies were used for detection. Control bands illustrating Rubisco levels were visualized through Ponceau staining. (b) Western blot analysis was conducted using total protein extracts derived from 12-day-old 35S::MYB96-GFP seedlings treated with liquid DMSO, and MG132 (50 μM) for 6 hours. Anti-GFP antibodies were used for detection. Control bands illustrating Rubisco levels were visualized through Ponceau staining. (c) Western blot analysis was conducted using total protein extracts derived from 12-day-old 35S::MYB305-GFP seedlings treated with liquid DMSO, and ABA (50 mM) for 1 hour. Anti-GFP antibodies were used for detection. Control bands illustrating Rubisco levels were visualized through Ponceau staining. Data from three independent biological replicates with similar results. The protein abundance relative to the WT is quantified using ImageJ.

The protein stabilization induced by BR signaling was likely mediated by the inhibition of proteasome-mediated degradation, as treatment with MG132 also led to increased MYB305 protein abundance (Figure 3.16b). In this case, while ABA signaling transcriptionally induces *MYB305* expression, it does not induce its protein stability (Figure

3.16c). These findings suggest that the stabilization of MYB305 protein and prevention of its proteasome-mediated degradation are specific to BR signaling, rather than ABA signaling.

3.2.3.4 MYB305 interacts with BZR1 in the nucleus

Analysis of both in vivo co-immunoprecipitation and BiFC assays was conducted to explore the coordination of MYB305 with the BR-related TF BES1 and BZR1. Immunoprecipitation with GFP antibody successfully precipitated the MYB305-GFP fusion protein, which was confirmed by western blot detection (Figure 3.17a). BZR1, but not BES1, was detected in the MYB305-GFP pulldown by using their native antibodies (Figure 3.17a). This indicates a potential protein interaction between MYB305 and BZR1. Furthermore, as a negative control, in *35S::GFP* pulldown, the GFP antibody was able to detect free GFP but not BZR1 protein (Figure 3.17b).

Finally, to validate the Co-IP results and determine the subcellular localization of the interaction, BiFC assays were conducted by co-expressing *BZR1-YFPC* and *MYB305-YFPN* in Nicotiana leaves. This combination resulted in the reconstitution of YFP fluorescence in the nucleus, similar to the positive control where *BZR1-YFPC* was co-expressed with *PIF4-YFPN* (Figure 3.17c). As a negative control, the combination of BZR1-YFPC and AT2G01430-YFPN was included (Figure 3.17c). These findings confirm that MYB305 and BZR1 can interact in the nucleus.

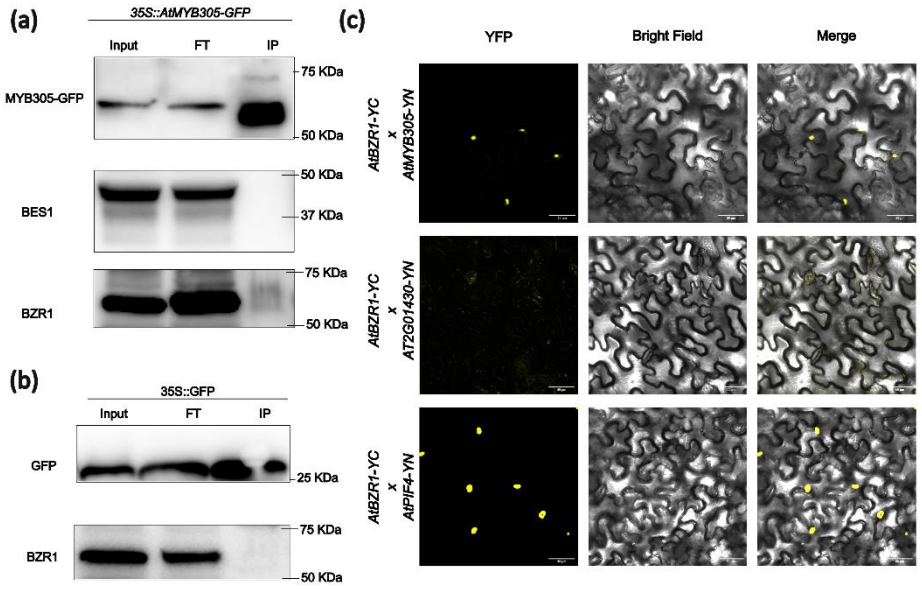


Figure 3.17 MYB305 interacts with BZR1 in the nucleus. (a) Coimmunoprecipitation assays were conducted using GFP-immunoprecipitated protein extracts obtained from 12-day-old 35S::MYB305-GFP seedlings. Anti-GFP, anti-BES1 and anti-BZR1antibodies were used for detection. (b) Coimmunoprecipitation assays were conducted using GFP-immunoprecipitated protein extracts obtained from 12-day-old 35S::GFP seedlings, used as a negative control for the MYB305 and BZR1 coimmunoprecipitation. Anti-GFP and anti-BZR1 antibodies were used for detection. (c) BiFC assays were conducted by co-expressing BZR1-YFPC and MYB305-YFPN (tested interaction), AT2G01430-YFPN (negative control), and PIF4-YFPN (positive control), in Nicotiana leaves. For each panel YFP, bright field, and merged images from confocal microscopy are shown. Data from three independent biological replicates with similar results

3.2.3.5 MYB305 transcriptionally regulates cellular responses to oxygen levels

Finally, to explore the functional role of MYB305 and its potential transcriptional coordination with BZR1, we examined the RNA-Seq dataset published by Cheng et al., 2022. Dexamethasone-inducible *MYB305* overexpressor lines were treated with dexamethasone and compared to non-treated plants, resulting in a total of 26 upregulated genes (Cheng et al., 2022).

After conducting GOE analysis of the 26 upregulated genes induced by *MYB305* overexpression, we observed a predominance of enriched categories related to "Responses/Cellular responses to hypoxia/oxygen levels" (Figure 3.18). Examination of the genes involved in these GO categories revealed the upregulation of several peroxidases, such as *PEROXIDASE 4* (*PER4*), which play a crucial role in regulating oxygen levels and reactive oxygen species under both abiotic and biotic stress conditions (Arnaud et al., 2017; Abuelsoud et al., 2020).

Furthermore, investigating the transcriptional coordination between MYB305 and BZR1, we intersected the 26 MYB305 upregulated genes with the BZR1 ChIP-chip dataset. Interestingly, we identified one common target gene, *CRUCIFERINA* (*CRU1*), a storage protein expressed in seeds and guard cells, which is essential for nutrient reservoir activity.

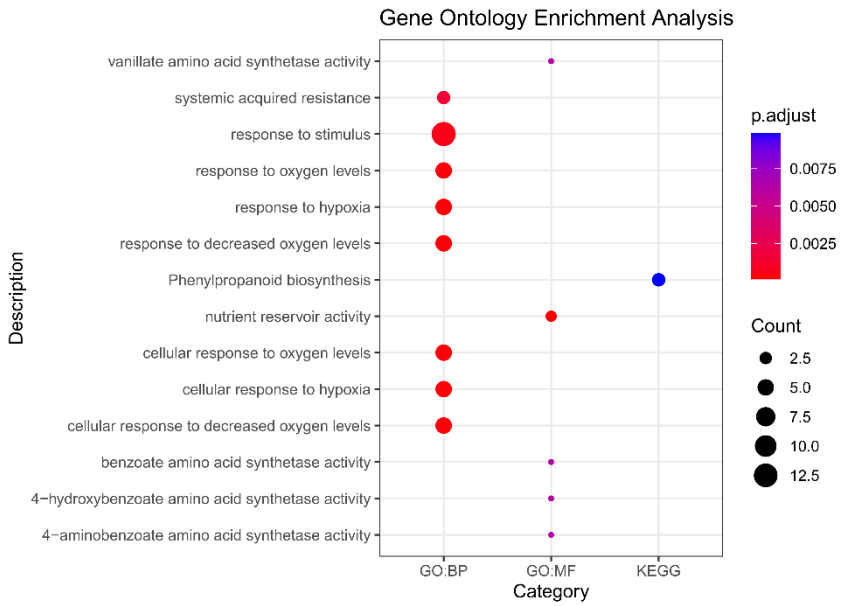


Figure 3.18 MYB305 transcriptionally regulates cellular responses to oxygen levels. GOE analysis of the upregulated genes in *MYB305* overexpression.

3.2.4 HAT9 is a BRL3-dowsntream transcription factor modulating abiotic stress adaptation

HAT9 is a homeobox-leucine zipper TF that has not been previously described. It was found to be transcriptionally induced by *BRL3* overexpression in control conditions (1.06 logFC), and to be specifically expressed in "J26612 and "S17" root cell populations, belonging to pericycle and phloem pole pericycle according to Brady et al., 2007.

3.2.4.1 *HAT9* and *BRL3* are co-expressed in the phloem pole pericycle and the cotyledon vasculature

As previously mentioned, *HAT9* is transcriptionally induced upon constitutive activation of *BRL3* (Table 3.1). However, we aimed to investigate whether this transcriptional activation could occur under native conditions. Thus, we examined the native expression domain of *HAT9* using TOTEM, which allowed us to analyze single-cell resolution transcriptomics. Our analysis revealed that *HAT9* expression was notably present in various root cell types, with enrichment observed in trichoblasts, phloem pole pericycle, lateral root primordia, and mature endodermis (Figure 3.19a).

Subsequently, we generated transcriptional reporter lines by fusing the 2 Kb *HAT9* promoter to *GUS/GFP* coding sequences. GUS staining of the resulting lines enabled us to identify *HAT9* expression in the root vasculature, while it was absent from the root meristem (Figure 3.19b, c). To further define the native expression domain of *HAT9*, we examined the transcriptional reporter lines using confocal microscopy to

assess GFP fluorescence. Our observations confirmed that *HAT9* expression in the root vasculature was predominantly confined to the endodermis and phloem pole pericycle, validating the findings from single-cell transcriptomics (Figure 3.20a, c, e). Additionally, absence from the root meristem was also confirmed through confocal microscopy (Figure 3.20b).

Shoot single-cell transcriptomics revealed *HAT9* enriched expression in the spongy mesophyll, where the vascular bundles are located (Figure3.19d), which was corroborated by transcriptional reporter lines showing *HAT9* expression in the cotyledon vasculature (Figure 3.19e).

These results suggest that *HAT9* and *BRL3* may potentially be co-expressed in the phloem pole pericycle and the cotyledon vasculature.

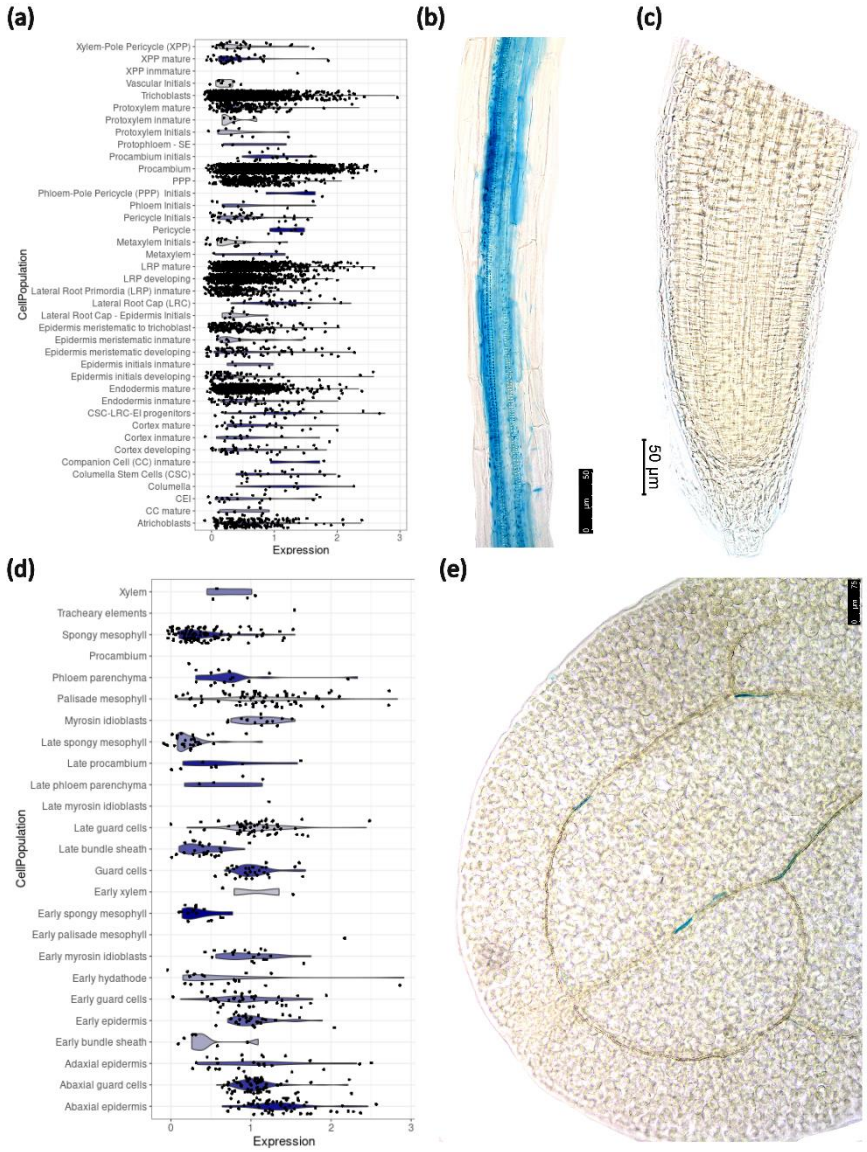


Figure 3.19 *HAT9* is natively expressed in mature root and cotyledon vasculature. (a) Root cell population enrichment of *HAT9* expression. *pHAT9::GUS/GFP* expression in six-day-old GUS-stained seedlings in different plant tissues: (b) Mature root (Scale bar: 50 µm), and (c) primary root meristem (Scale bar: 50µm). (d) Shoot cell population enrichment of *HAT9* expression. (e) *pHAT9::GUS/GFP* expression in six-day-old GUS-stained cotyledon (Scale bar: 75 µm).

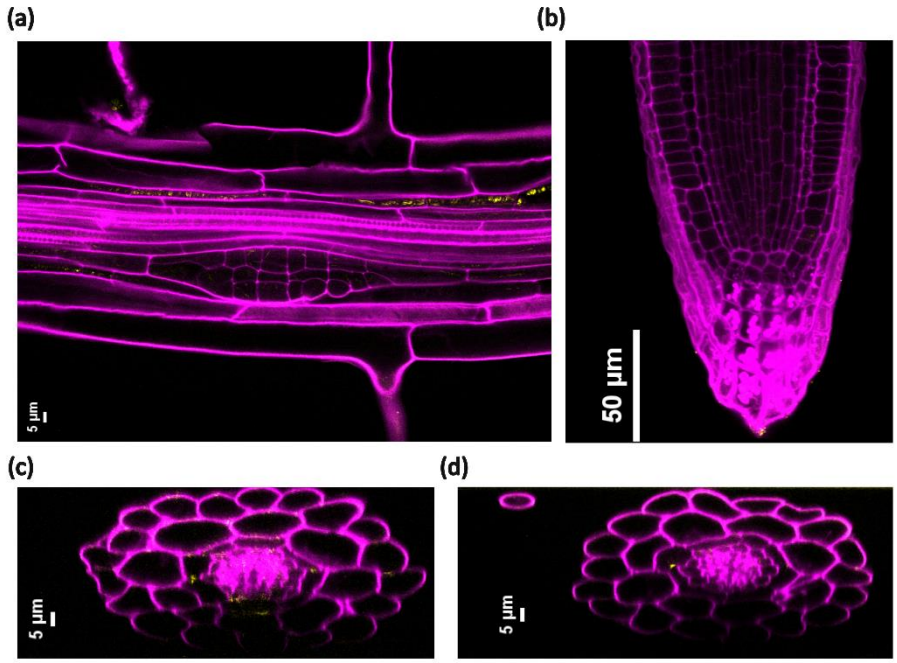


Figure 3.20 *HAT9* is expressed in the phloem pole pericycle, endodermis and lateral root primordia. *pHAT9::GUS/GFP* six-day-old seedling roots stained with propidium iodide (magenta). GFP signal (yellow) shows the *HAT9* native expression. Scale bar: 50µm and 5 µm.

3.2.4.2 Overexpression of *HAT9* confers drought tolerance and enhanced hydrotropic response

HAT9 is a homeobox-leucine zipper TF that has not been previously described. Therefore, to functionally characterize HAT9, we subjected mutant and overexpressor lines to various abiotic stress conditions.

Given the importance of hydrotropism in adapting to low water availability environments (Takahashi et al., 2002), we exposed six-day-old seedlings to sorbitol-supplemented media and measured root bending towards a non-supplemented media (Figure 3.21a). Our findings revealed that *BRL3* overexpression enhanced the hydrotropic response

compared to Col-0, consistent with previous reports (Fàbregas et al., 2018). Interestingly, overexpression of *HAT9* also resulted in an increased hydrotropic response (Figure 3.21b).

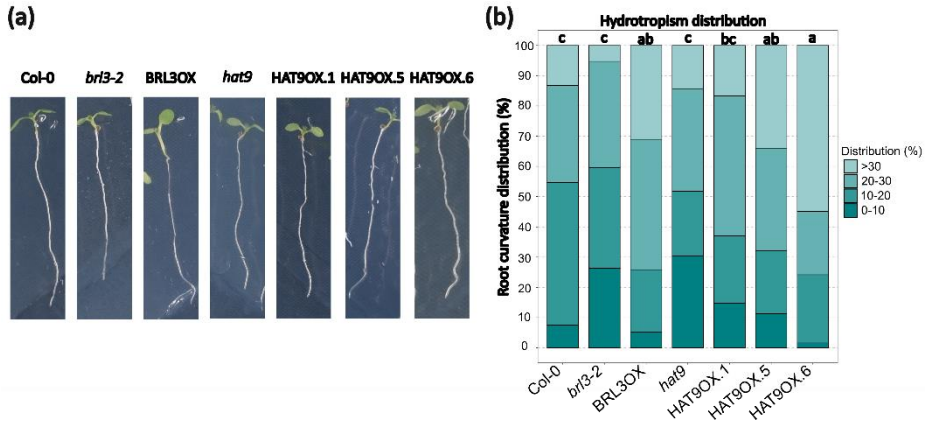


Figure 3.21 *HAT9* overexpression results in higher hydrotropic responses. (a) Arabidopsis six-day-old seedling exposed to 24 hours sorbitol-supplemented media (right part of the pictures) and the root bending towards a non-supplemented media (left part of the pictures). (b) Quantification and distribution of root hydrotropic angles. Different colors depict roots bending between 0º-10º, 10º-20º, 20º-30º and >30º categories. Data from three independent biological replicates (n>53). Different letters represent statistical significance differences (p-value<0.05) in ANOVA plus Tukey´s HSD test.

To investigate if HAT9 also plays a functional role in abiotic stress adaptation in mature plants and growth regulation, we photographed and measured the rosette area of three-week-old plants (Figure 3.22a). Subsequently, we exposed them to severe drought stress by withholding water until Col-0 reached 5% of FC. Following this stress period, we rewatered them and allowed a 10-day recovery period before accounting plant survival (Figure 3.22a, c).

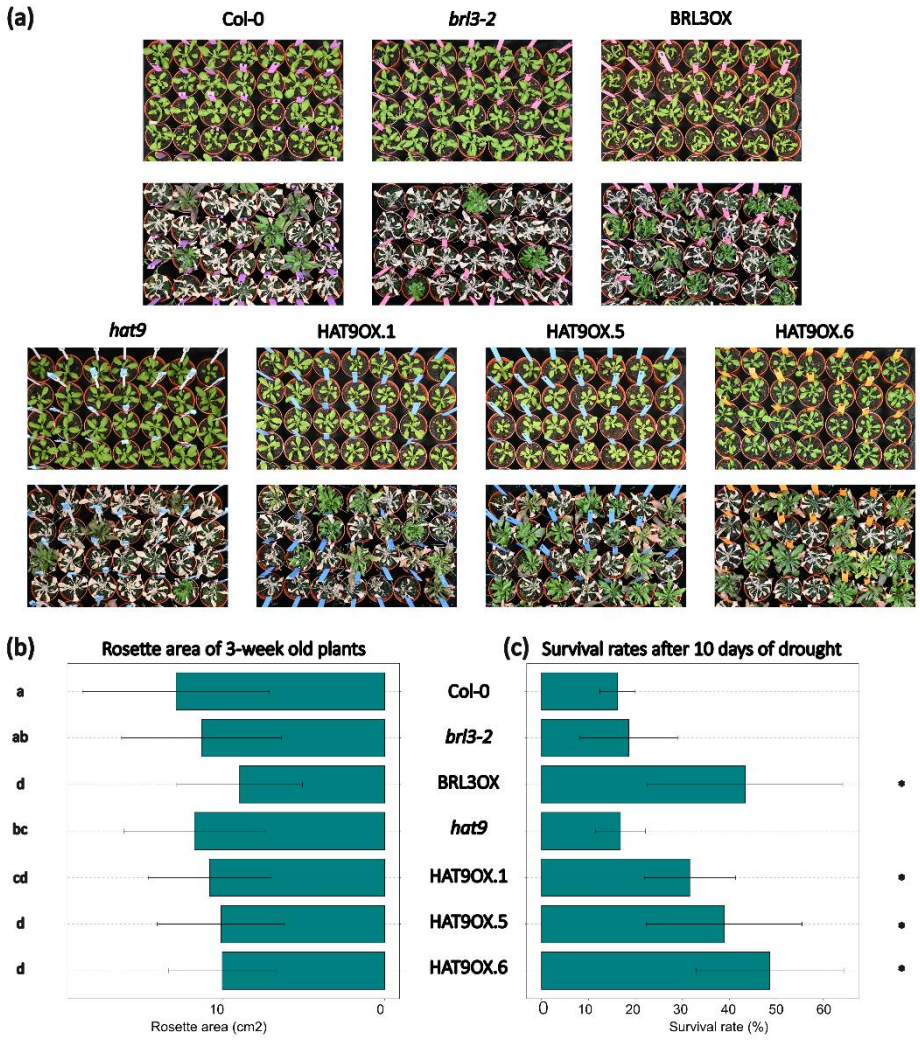


Figure 3.22 Overexpression of *HAT9* results in drought tolerance in Arabidopsis. (a) Three-week-old plant rosette phenotypes in control conditions (upper row) and after 10 days of rewatering (bottom row). (b) Barplot of three-week-old Arabidopsis rosette area quantification. Data from three independent biological replicates (n>109). Different letters represent statistical significance differences (p-value<0.05) in ANOVA plus Tukey´s HSD test. (c) Drought survival rate after 10 days of rewatering. Data from three independent biological replicates (n>109). One asterisk represents statistical significance differences (p-value<0.05) in a chi-squared test for survival ratios compared to Col-0.

Overexpression of *HAT9* resulted in drought tolerance, with an average survival rate of 39.71% across three independent lines, compared to the 16.21% survival rate of Col-0 plants (Figure 3.22c). Despite observing a statistically significant slight reduction in rosette area in the *HAT9* overexpressor lines compared to Col-0, measuring 10.3cm2 and 12.9cm2, respectively (Figure 3.22b), the difference was minimal and may not be the primary mechanism involved in drought adaptation. This is supported by the low correlation between rosette area and plant survival rate, as shown in Figure 3.23.

In summary, these findings indicate that overexpression of *HAT9* leads to improved adaptation to abiotic stresses such as hydrotropism and severe drought through an active molecular response, rather than simply avoiding stress due to growth penalties.

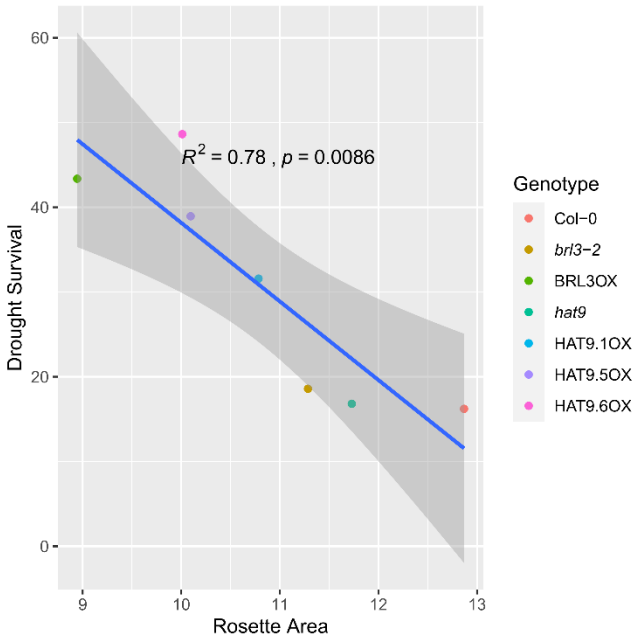


Figure 3.23 Correlation of drought survival and rosette area. The graph includes the coefficient of determination and the correlation p-value. The rosette area and drought survival rates are the mean from three independent biological replicates (n>109).

3.2.4.3 *HAT9* is transcriptionally induced by ABA signaling while its protein stability is enhanced by BR signaling via BIN2, inhibiting its proteasome-mediated degradation

Previous findings have shown that *HAT9* is transcriptionally induced by the overexpression of *BRL3* (Table 3.1). *HAT9* is also transcribed in the same *BRL3* native domain, including the phloem pole pericycle and the cotyledon vasculature (Figure 3.19, 3.20), and shares abiotic stress-related phenotypes when overexpressed, such as higher hydrotropic responses and drought tolerance (Figure 3.21, 3.22). Therefore, we aimed to examine the effect of BR signaling on HAT9 protein stability and the role of ABA in transcription and post-translation, given their widely recognized antagonistic effects during drought tolerance.

Initially, we investigated whether *HAT9* was transcriptionally regulated by ABA signaling. Six-day-old HAT9 transcriptional reporter lines were exposed to ABA treatment (50 mM), and GUS staining revealed significant induction of *GUS* expression in the root (Figure 3.24). This induction occurred specifically in the zone where ABA reduced root hair length but induced the differentiation of atrichoblasts into trichoblasts, thereby increasing root hair density (Lombardo et al., 2018).

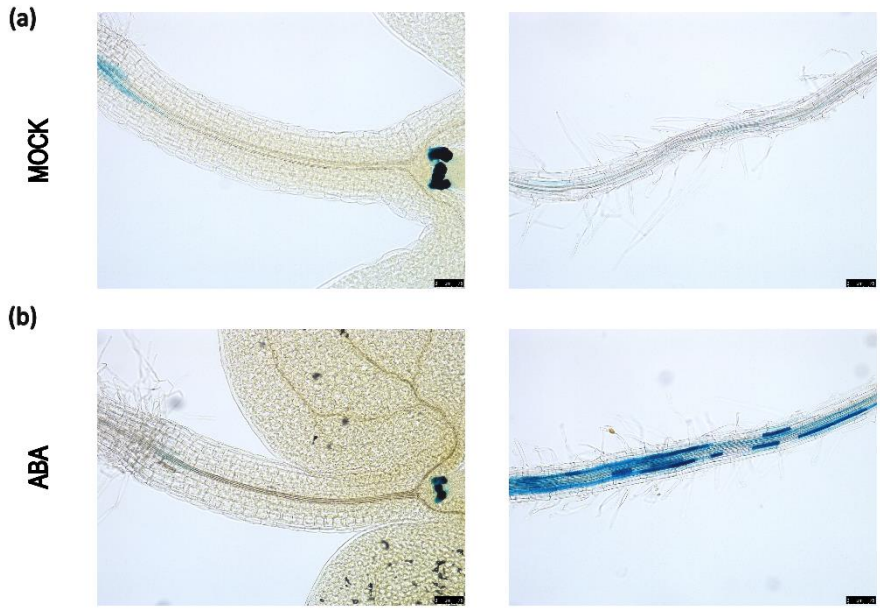


Figure 3.24 *HAT9* is transcriptionally induced by ABA. *pHAT9::GUS/GFP* expression in six-day-old GUS-stained seedlings in (b) control conditions and (c) upon 48 hours of ABA treatment (50mM). Scale bar: 75μm.

Subsequently, we explored the roles of ABA and BR in HAT9 protein stability. BR signaling via BIN2 markedly stabilized HAT9 protein, as treatment with BL and Bikinin substantially enhanced HAT9 protein content in *35S::HAT9-GFP* protein extracts (Figure 3.25a, b). However, ABA signaling did not lead to HAT9 accumulation, suggesting its involvement in transcriptional regulation rather than post-translational regulation (Figure 3.25c). To delineate the molecular mechanism by which BR signaling stabilized HAT9 protein, we analyzed HAT9 stability with the proteasome inhibitor MG132 and observed significant accumulation of HAT9 protein when proteasome activity was blocked (Figure 3.25b).

Taken together, these results confirm that ABA and BRL3 transcriptionally induce *HAT9* expression, while BR signaling via BIN2 prevents proteasome-mediated degradation of HAT9.

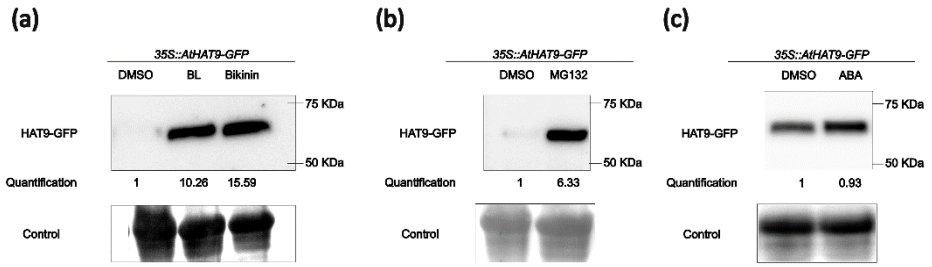


Figure 3.25 HAT9 is stabilized by BR signaling via BIN2, inhibiting the proteasome-mediated degradation, but not by ABA signaling. (a) Western blot analysis was conducted using total protein extracts derived from 12-day-old *35S::HAT9-GFP* seedlings treated with liquid DMSO, BL (10 nM) and Bikinin (50 µM) for 1 hour. Anti-GFP antibodies were used for detection. Control bands illustrating Rubisco levels were visualized through Ponceau staining. (b) Western blot analysis was conducted using total protein extracts derived from 12-day-old *35S::HAT9-GFP* seedlings treated with liquid DMSO, and MG132 (50 µM) for 6 hours. Anti-GFP antibodies were used for detection. Control bands illustrating Rubisco levels were visualized through Ponceau staining. (c) Western blot analysis was conducted using total protein extracts derived from 12-day-old *35S::HAT9-GFP* seedlings treated with liquid DMSO, and ABA (50 mM) for 1 hour. Anti-GFP antibodies were used for detection. Control bands illustrating Rubisco levels were visualized through Ponceau staining. Data from three independent biological replicates with similar results. The protein abundance relative to the WT is quantified using ImageJ.

3.2.4.4 HAT9 and BZR1 are interacting in the nucleus

Finally, to further elucidate the molecular mechanism of HAT9 in the context of BR signaling, we investigated whether its transcriptional activity could be coordinated with the BR-related TFs BES1 and BZR1. In vivo co-immunoprecipitation assays confirmed the interaction between HAT9 and BZR1, but not between HAT9 and BES1 (Figure

3.26a). Further validation by BiFC assays confined the HAT9-BZR1 interaction to the nucleus (Figure 3.26c).

These collective findings suggest that HAT9 and BZR1 may coordinate transcriptional responses by directly interacting in the nucleus.

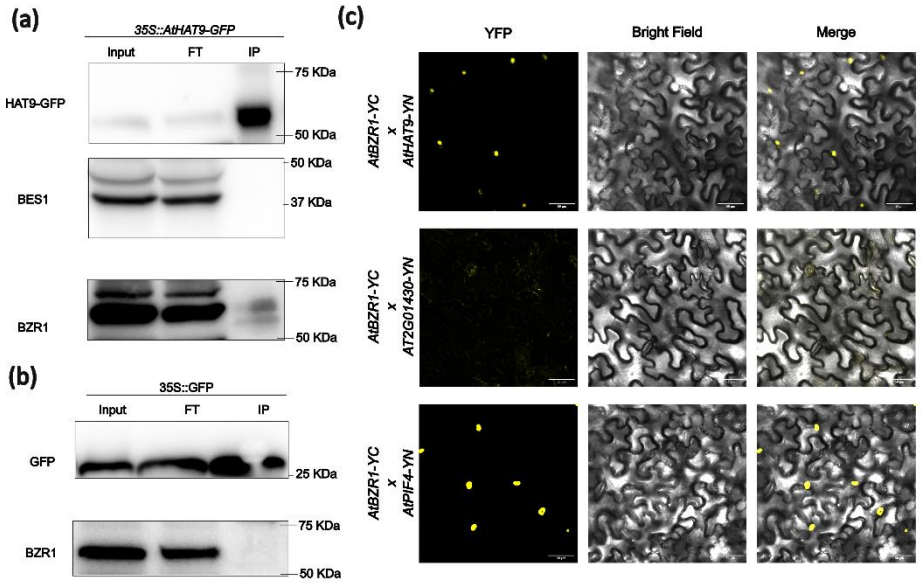


Figure 3.26 HAT9 interacts with BZR1 in the nucleus. (a) Coimmunoprecipitation assays were conducted using GFP-immunoprecipitated protein extracts obtained from 12-day-old *35S::HAT9 -GFP* seedlings. Anti-GFP, anti-BES1 and anti-BZR1antibodies were used for detection. (b) Coimmunoprecipitation assays were conducted using GFP-immunoprecipitated protein extracts obtained from 12-day-old *35S::GFP* seedlings, used as a negative control for the HAT9 and BZR1 coimmunoprecipitation. Anti-GFP and anti-BZR1 antibodies were used for detection. (c) BiFC assays were conducted by co-expressing *BZR1-YFPC* and *HAT9-YFPN* (tested interaction), *AT2G01430-YFPN* (negative control), and *PIF4-YFPN* (positive control), in Nicotiana leaves. For each panel YFP, bright field, and merged images from confocal microscopy are shown. Data from three independent biological replicates with similar results.

Chapter 4

Results

UNTARGETED MUTAGENESIS OF BRASSINOSTEROID RECEPTOR SBBRI1 CONFERS DROUGHT TOLERANCE BY ALTERING PHENYLPROPANOID METABOLISM IN *SORGHUM BICOLOR*

Part of this chapter is published in:

Fontanet-Manzaneque, J.B., Laibach, N., Herrero-García, I., Coleto-Alcudia, V., Blasco-Escámez, D., Zhang, C., Orduña, L., Alseekh, S., Miller, S., Bjarnholt, N., Fernie, A.R., Matus, J.T., & Caño-Delgado, A. I. (2023). Untargeted mutagenesis of brassinosteroid receptor SbBRI1 confers drought tolerance by altering phenylpropanoid metabolism in Sorghum bicolor. *Under review.*

4.1 Introduction

In the current context of the climate change emergency, drought is the most devastating environmental factor that significantly diminishes crop productivity, producing more annual loss in crop yield than all pathogens combined (Farooq et al., 2012; Beillouin et al., 2020; Gupta et al., 2020). Cereal grains serve as the primary source of dietary energy, carbohydrates, and plant proteins worldwide (Poutanen et al., 2022), and their growth is severely affected by water scarcity (Daryanto et al., 2016). Sorghum is the fifth most cultivated cereal crop globally (FAO 2020) and represents a staple food for millions of people within the semi-arid regions of Africa, Asia and Central America (Taylor et al., 2006; Proietti et al., 2015). Despites its reputation for drought resilience, Sorghum production can be severely hampered by drought, particularly during the anthesis and grain filling stages (Abreha et al., 2022). Multiple breeding programs have tried to exploit the potential traits conferring drought tolerance in Sorghum, specifically the stay-green traits, post-flowering drought adaptation expressed by delayed leaf senescence (Ochieng et al., 2020). Through these programs four major QTL, *Stg1, Stg2, Stg3, Stg4,* have been identified and mapped as causative factors for the expression of the stay-green trait in Sorghum (Xu et al., 2000; Sanchez et al., 2002). Further studies provided evidence linking these quantitative trait loci to increase grain yield under drought conditions (Borrell et al., 2014) and improvements in food and fodder quality (Blummel et al., 2015). However, the precise identification of genes responsible for regulating stay-green traits remains unclear, encouraging the functional and molecular characterization of these genes to gain a comprehensive understanding of the genetic controls involved.

BRs are plant steroid hormones that are essential for plant growth and development, including processes such as cell elongation, proliferation, and differentiation (Planas et al., 2019). In Arabidopsis, the primary receptor for BRs is a membrane-localized LRR receptor-like kinase BRI1 (Li and Chory, 1997). Upon hormone perception, BRI1 interacts with its co-receptor BAK1 (Li et al.,2002; Nam et al., 2002). The BRI1-BAK1 heterodimerization triggers a phosphorylation cascade which will control the expression of multiple BR-related genes through BES1 and BZR1 TF (Yin et al., 2002; Wang et al., 2002). Translational studies have demonstrated the conserved role of this receptor in the control of growth and development in crops (Nolan et al., 2020).

The phenotypic and molecular characterization of a rice dwarf mutant *d61* revealed the involvement of OsBRI1 in multiple developmental processes including overall growth, internode elongation, lamina joint vending, skotomorphogenesis and panicle development (Yamamuro et al., 2000). The barley "*uzu*" dwarf variety from Japan is known for its lodging resistance in intensive crop production. This variety was found to harbor a SNP in the *HvBRI1* gene. As a result, the "*uzu*" variety exhibited reduced sensitivity to BRs and increased levels of BRs, such as castasterone (Chono et al., 2003). In maize, a close relative of Sorghum, an RNA interference knockdown mutant was generated targeting the five maize homologs of BRI1. Specifically, a 498-bp fragment encoding LRRs 6 to 12 of the extracellular domain was targeted. The resulting RNA interference mutants were insensitive to BRs, and exhibited dwarf phenotype characterized by shortened internodes, dark green upright and twisted leaves, and decreased auricle formation. In addition, these maize mutants exhibited a reduced activation of BES1, as evidenced by a decreased accumulation of BES-

YFP in the nucleus (Kir et al., 2015). Our recent work pointed that the BRI1 receptor shares structurally and functionally conserved roles in Sorghum, playing an important role in root meristem and panicle development (Rico-Medina et al., 2024).

Despite these findings, whether BR-mediated signaling promotes or repress plant adaptation to stress is not clear. On one hand, physiological studies shown that exogenous BR application enhances drought tolerance to abiotic stresses in several crops (Anjum et al., 2011; Kagale et al., 2007). This could also be supported by finding that elevated BR levels in *DWF4* overexpressing plants enhanced drought survival in *Brassica napus* (Sahni et al., 2016). On the other hand, the phenotypes of plants with genetically manipulated BR receptors are somewhat controversial. Studies in tomato suggest that BR application enhances drought tolerance, while overexpressing *SlBRI1* increases susceptibility (Nie et al., 2019). Overexpression of ZmBRI1-downstream TF *ZmBES1/BZR1-1* resulted in drought susceptibility of transgenic Arabidopsis and rice (Feng et al., 2023).

In Arabidopsis, loss-of-function BR signaling mutants (*bri1*, *bak1*) showed increased drought resistance due to growth penalization, known as drought avoidance (Fàbregas et al., 2018). Constitutively active BES1 in *bes1-D* mutants confers drought susceptibility (Ye et al., 2017), while overexpression of *PLETHORA2*, a BZR1-inihibited TF, could partially rescue the *bes1-D* susceptibility (Zhao et al., 2023). In contrast, the vascular-specific BR receptor BRL3 positively regulates a myriad of plant adaptation traits including elevated temperatures and water scarcity as such its overexpression confers drought resistance without penalizing growth (Fàbregas et al., 2018; Gupta et al., 2023). These findings imply

a complex signal integration by BRI1-like family of receptors, in the control of plant adaptation to abiotic stress prompting us to investigate the downstream mechanisms of BR-regulated drought tolerance.

In the current study, we demonstrate that BRI1 signaling is negatively contributing to Sorghum´s ability to adapt to drought and osmotic stress. Our findings unveil that the Sorghum and Arabidopsis BRI1 (SbBRI1 and AtBRI1) proteins enhance susceptibility to drought while SbBRI1 is restoring osmotic stress insensitivity in Arabidopsis *bri1* mutants. Through a comprehensive analysis of *bri1* Sorghum mutants derived from an EMS-mutagenized population (Jiao et al., 2016), we show that BRI1 acts as a negative regulator of drought response in Sorghum. We further investigated this, by conducting a DAP-seq experiment to narrow down the direct targets of SbBRI1 using SbBRI1-downstream master regulator SbBES1/BZR1 (SbBES1). Our data analysis suggests that BRI1-driven BR signaling directly influences the expression of drought stress responsive genes, through direct binding of SbBES1. These findings not only enhance our understanding of BR signaling in monocots but also offer a valuable genetic resource for breeders seeking to improve drought adaptation.

4.2 Results

4.2.1 Sorghum BRI1 receptor is restoring Arabidopsis *bri1-301* insensitivity to osmotic stress

To determine the contribution and conservation of SbBRI1 receptor in abiotic stress adaptation, we first performed heterologous complementation of *bri1* Arabidopsis mutants with constitutively expressed SbBRI1 protein.

The SbBRI1 receptor shows a conserved protein structure compared to Arabidopsis and functionally complements *bri1-301* Arabidopsis mutant´s inability to dephosphorylate BRI1-downstream TF BES1 (Rico-Medina et al., 2024). Therefore, we wanted to examine its functional conservation and potential to complement Arabidopsis *bri1* mutant phenotypes in several abiotic stress traits. To this end, Arabidopsis WT Col-0 and *bri1* plants were transformed with *35S:SbBRI1-GFP* construct as previously described by Rico et al., 2024, and two T3 homozygous independent lines were selected for further analysis; these are from now on referred to as SbBRI1;*bri1* and SbBRI1;Col-0.

First, we determined the SbBRI1 receptor´s ability to sense osmotic stress and revert *bri1* insensitiveness in seedling stage. The root length of six-day-old plants was analyzed under control and osmotic stress conditions (Figure 4.1a, b). Osmotic stress triggers primary root growth inhibition (Rowe et al., 2016) and *bri1* mutants are less sensitive to sorbitol-induced osmotic stress not showing root growth penalization (Fàbregas et al., 2018). SbBRI1 was able to restore the root growth to

WT levels in control conditions, however resulted in a higher sensitivity to the osmotic stress than WT and *bri1* plants, as observed in the ratio Sorbitol/Control (Figure 4.1b). Overexpressing *SbBRI1* in the WT background resulted in an enhancement of primary root growth in control conditions and increased sensitivity to sorbitol, similarly to Arabidopsis plants constitutively expressing *AtBRI1*. Our results suggest a conserved role for SbBRI1 in promoting root growth in both control and osmotic stress conditions.

When plants sense water deficit, the root elongation zone undergoes cell death (Duan et al., 2010; Zhang et al., 2017). To further evaluate the function of SbBRI1 in sensing osmotic stress, we then quantify the cell death triggered by sorbitol treatment (Fàbregas et al., 2018). Five-day-old seedling were exposed to 24-hour sorbitol treatment and stained with Propidium Iodide (PI) to visualize the nuclei of death cells (Figure 4.1c, d). Confocal images analysis of the different heterologous complementation lines showed that while *SbBRI1-GFP* appeared ubiquitously expressed in the *bri1* background, it was also ubiquitously expressed in WT background but with an enrichment in epidermis and cortex cells, suggesting a *SbBRI1* silencing by endogenous AtBRI1 receptor. As previously reported, *bri1* plants showed a significant decreased in cell death in the root elongation zone in comparison to those of WT (Fàbregas et al., 2018) and SbBRI1 complemented the insensitivity reaching cell death WT ratios. However, both overexpressing *SbBRI1* or *AtBRI1* in WT background failed to increase the cell death ratios in the root when comparing it to WT. Conversely, our result suggests that a functional Sorghum receptor SbBRI1 can sense the osmotic stress in a similar manner to AtBRI1, reverting the insensitivity of *bri1*. However, higher levels of BRI1 receptor failed to

provoke cell death hypersensitivity under osmotic stress, in contrast with higher levels of BRL3, which enhance the cell death hypersensitivity in the root elongation zone (Fàbregas et al., 2018), supporting a differential role in abiotic stress sensing of both BR receptors.

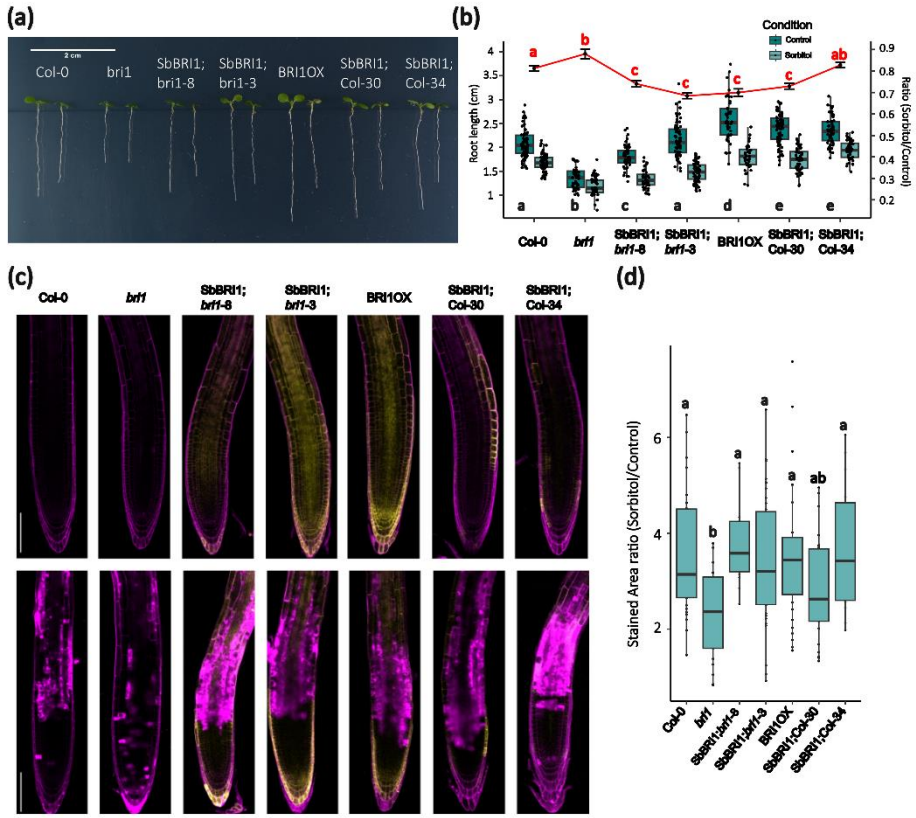


Figure 4.1 Sorghum BRI1 receptor is restoring Arabidopsis *bri1-301* insensitivity to osmotic stress. (a) six-day-old Arabidopsis seedlings in control (left) and osmotic stress (right) conditions. Scale bar: 2 cm. (b) Boxplot of Arabidopsis root length quantification in control (blue) and osmotic stress conditions (light blue). The red line represents the root length ratio of sorbitol against control. Data from three independent biological replicates (n>84). Different letters represent statistical significance differences (p-value<0.05) in ANOVA plus Tukey´s HSD test (c) six-day-old Arabidopsis seedling roots stained with propidium iodide (magenta) after 24 h in control (top) and osmotic stress (bottom). Yellow channel (GFP) shows the localization of SbBRI1 or AtBRI1 protein. Scale bar: 100 µm. (d) Boxplot of propidium iodide-stained area quantification, representing the ratio of sorbitol against control. Data from three independent biological replicates (n>15). Different letters represent statistical significance differences (p-value<0.05) in ANOVA plus Tukey´s HSD test.

4.2.2 Overexpression of *BRI1* results in drought susceptibility in *Arabidopsis thaliana*

To assess the role of SbBRI1 and AtBRI1 receptors in severe drought in mature plants, rosette areas from 3-weeks old plants were imaged and measured (Figure 4.2a, c), and then exposed to severe drought by withholding water until they reached 5% FC. By considering full (100%) FC, the maximum water content able to be retained in a drained soil, plants were re-watered, and the survival rate was measured (Figure 4.2b, c). *bri1* plants showed a remarkable drought avoidance phenotype (Fàbregas et al., 2018), reaching 86.4% of survival in comparison with the 30.8% found in WT plants. Even SbBRI1 was able to restore root growth in seedling stage (Figure 4.1a, b), was only able to partially restore the rosette area dwarfism of *bri1* plants in adult stage (Figure 4.2a, b). However, the partially restored rosette area resulted in a significantly decreased drought tolerance compared to *bri1-301* of 79.1 and 63 % in SbBRI1;*bri1*-8 and SbBRI1;*bri1*-3, respectively (Figure 4.2c).

Strikingly, when overexpressing *SbBRI1* or *AtBRI1* receptor in WT background, a dramatic decrease in drought tolerance was found in both lines, with a survival rate of 12.2% and 8.7%, respectively. However, overexpression of *AtBRI1* and *SbBRI1* did not result in a significant increase of the rosette area before the drought stress, impairing the BRI1-mediated drought susceptibility from the gain of plant growth.

Collectively, our results show that plants overexpressing these receptors perform oppositely in drought adaptation uncovering the differential roles of BRI1 and BRL3 receptors in abiotic stress adaptation.

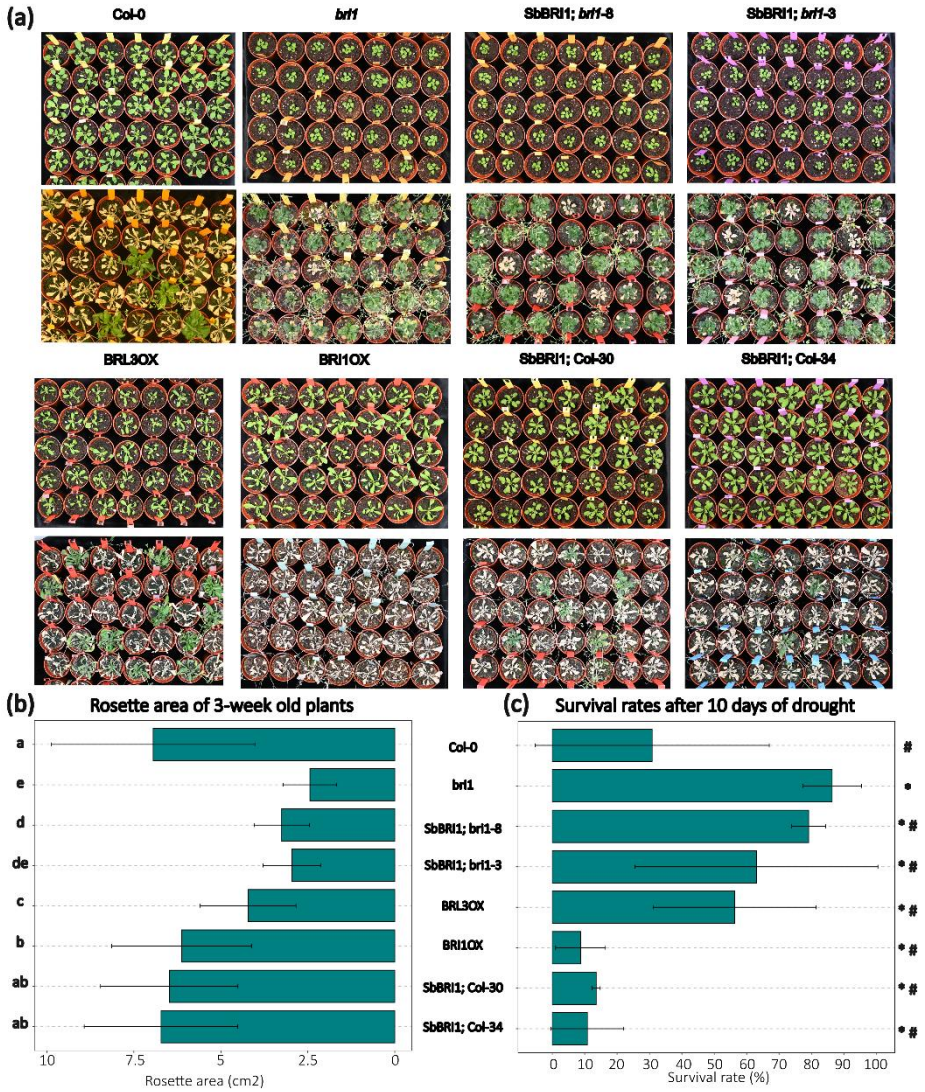


Figure 4.2 Overexpression of *BRI1* results in drought susceptibility in Arabidopsis. (a) Three-week-old plant rosette phenotypes in control conditions (upper row) and after 7 days of rewatering (bottom row). (b) Barplot of three-week-old Arabidopsis rosette area quantification. Data from three independent biological replicates (n>110). Different letters represent statistical significance differences (p-value<0.05) in ANOVA plus Tukey´s HSD test. (c) Drought survival rate after 7 days of rewatering. Data from three independent biological replicates (n>110). One asterisk or hash represent statistical significance differences (p-value<0.05) in a chi-squared test for survival ratios compared to WT or *bri1*, respectively.

4.2.3 Sorghum *bri1* mutants are less sensitive to osmotic stress

Next, we investigated the functional role of SbBRI1 receptor by analyzing Sorghum *bri1* mutants (*Sbbri1*) from a BTx623 tilling population (Jiao et al., 2016). We identified two different *Sbbri1* mutants carrying SNPs in the extracellular domain of SbBRI1 that show altered BL sensitivity and impaired meristematic and panicle development (Rico-Medina et al., 2024); we name these from now on NIL-*bri1*-72 and NIL-*bri1*-87. A hydroponic experiment was set up and carried out to evaluate the function of SbBRI1 in osmotic stress (Figure 4.3a, Material and Methods). All following experiments were conducted comparing mutagenized plants either carrying the mutation (NIL-*bri1*-72/87) or the WT allele (NIL-WT-72/87) of SbBRI1 after 2 backcrosses using the un-mutagenized accession BTx623 as a parent (Material and Methods).

Upon sorbitol treatment, five-day old NIL-*bri1*-72 plants showed increased growth of shoot and primary root compared to NIL-WT-72 (Figure 4.3a, b, c), the same was observed in shoots from NIL-*bri1*-87 (Figure 4.4). The primary root growth penalization upon osmotic stress is accompanied by a reduction of root meristem size (Liu et al., 2015). We performed a modified pseudo-Schiff Propidium Iodide staining (mPS-PI) to visualize the meristem, defined as the region where the first metaxylem cell doubles in size compared to its distal neighbor, of *Sbbri1* plants exposed to osmotic stress (Figure 4.3d). NIL-*bri1*-72 showed a smaller reduction of root meristem length upon osmotic stress than NIL-WT-72 (Figure 4.3e), even though the meristem width displayed no significant changes (Figure 4.3f). These results together with the

observed reduced sensitivity to osmotic stress of Sb*bri1* mutants support a conserved role of SbBRI1 receptor in plant abiotic stress adaptation.

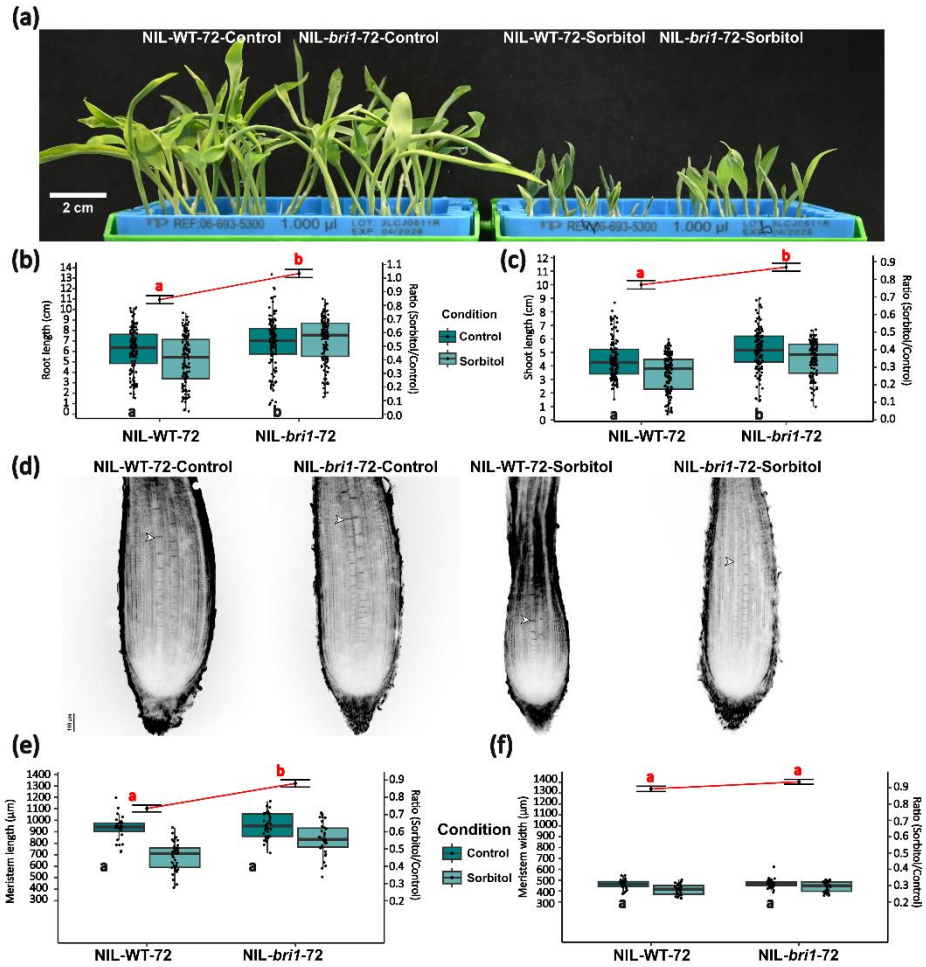


Figure 4.3 Sorghum *bri1* mutants are less sensitive to osmotic stress. (a) five-day-old Sorghum seedling phenotypes in control (left box) and osmotic stress conditions (right box). (b, c) Boxplots of five-day-old Sorghum root (b) and shoot (c) length quantification in control (blue) and osmotic stress (light blue) conditions. Red line represents the root (b) or shoot (c) length ratio of sorbitol against control. Data from three independent biological replicates (n >125). Different letters represent statistical significance differences (p-value<0.05) in ANOVA plus Tukey´s HSD test. (d) Sorghum seedling roots stained with propidium iodide (black) after 3 days in control (two left pictures) and osmotic stress (two right pictures) conditions. Scale bar: 100 µm. Arrowheads indicate the transition zone. (e, f) Boxplots of five-day-old Sorghum meristem length (e) and width (f) quantification in control (blue) and osmotic stress (light blue) conditions. Red line represents the meristem length (e) or width (f) ratio of sorbitol against control. Data from three independent biological replicates (n >28). Different letters represent statistical significance differences (p-value<0.05) in ANOVA plus Tukey´s HSD test.

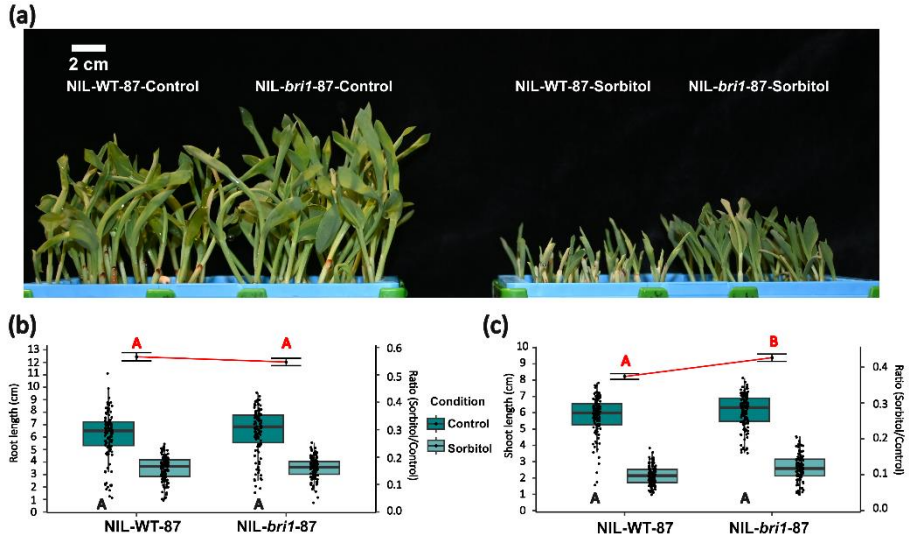


Figure 4.4 Sorghum NIL-*bri1*-87 mutants are less sensitive to osmotic stress. (a) 5-days old Sorghum seedling phenotypes in control (left box) and osmotic stress conditions (right box). (b, c) Boxplots of 5-days old Sorghum root (b) and shoot (c) length quantification in control (blue) and osmotic stress (light blue) conditions. Red line represents the root (b) or shoot (c) length ratio of sorbitol against control. Data from three independent biological replicates. Different letters represent statistical significance differences (p-value<0.05) in ANOVA plus Tukey´s HSD test.

4.2.4 Sorghum *bri1* mutants show increased tolerance to drought stress without penalizing growth

In contrast to Arabidopsis *bri1* mutants, *Sbbri1* mutant seedlings did not show any reduction of primary root and shoot growth in control conditions, in fact NIL-bri1-72 seedlings showed longer root and shoots in comparison with NIL-WT-72 (Figure 4.3b, c and Figure 4.4b, c). Nonetheless, the reduced sensitivity to osmotic stress conditions, prompted us to test these mutants in drought stress conditions (Figure 4.5).

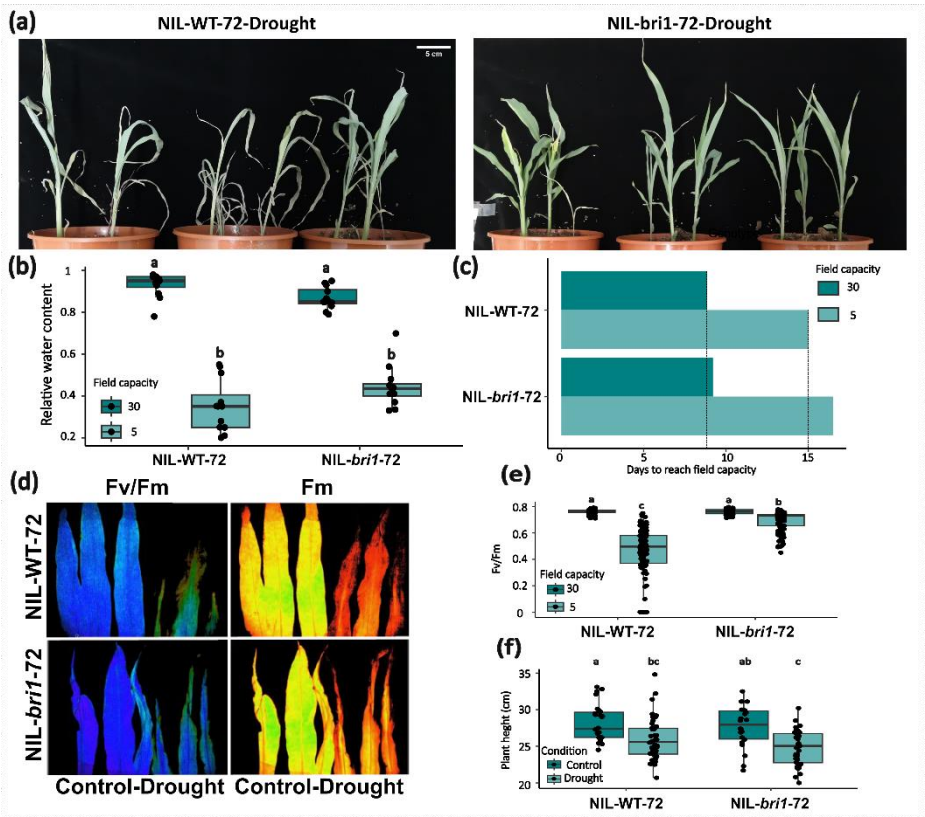


Figure 4.5 Sorghum *bri1* mutants are tolerant to drought stress without growth penalization. (a) Sorghum seedling phenotypes under drought stress conditions, specifically at 5% field capacity. Scale bar: 5cm. (b) Boxplot of relative water content of Sorghum seedlings at 30% (blue) and 5% (light blue) field capacity. Data from six independent biological replicates (n = 12). Different letters represent statistical significance differences (p-value<0.05) in ANOVA plus Tukey´s HSD test. (c) Barplot of days to reach 30% (blue) and 5% (light blue) field capacity. Dotted lines represent the average of WT plants to reach different field capacities. (d) Fv/Fm (left column) and Fm (right column) from Sorghum leaves in control conditions (three leaves on the left) and drought stress conditions (three leaves on the right). (e) Boxplot of Fv/Fm values at 30% (blue) and 5% (light blue) field capacity. Data from six independent biological replicates (n >114). Different letters represent statistical significance differences (p-value<0.05) in ANOVA plus Tukey´s HSD test. (f) Boxplot of plant height in control (blue) and drought stress conditions, specifically 5% FC (light blue). Data from six independent biological replicates (n >25). Different letters represent statistical significance differences (p-value<0.05) in ANOVA plus Tukey´s HSD test.

Thus, sixteen-day-old Sorghum plants grown in soil, were exposed to drought by withholding water until they reached the 5% FC (Figure 4.5a). To evaluate drought stress tolerance, we measured the time expend to reach a determined FC, the relative water content (RWC) in leaves, and as an indicator of the photosynthetic efficiency, the Fv/Fm ratio. At 30% of FC, NIL-WT-72 and NIL-*bri1*-72 had a RWC of 0.92 and 0.86, respectively (Figure 4.5b), and the Fv/Fm ratio was close to 0.8 in both cases (Figure 4.5d, e). This suggest that even though the water content in the soil was significantly lower, Sorghum seedlings were not exhibiting any phenotypic response to drought in the shoot. However, under a more severe drought scenario, at 5 % of FC, NIL-*bri1*-72 mutants had higher Fv/Fm ratios than the WT, thereby displaying a better photosynthetic efficiency (Figure 4.5d). In addition, NIL-*bri1*-72 mutants took longer to reach the 5% of the FC (Figure 4.5c), suggesting an improved water use efficiency, even though the RWC was not significantly higher once they reached this specific FC (Figure 4.5b). Finally, we measured the plant height of control and drought-stressed plants (Figure 4.5f) and did not see any growth penalty in the seedling stage under either control or drought stress conditions (thirty-day-old seedlings). The same trend in all the parameters measured was observed in the other independent mutant line NIL-*bri1*-87 (Figure 4.6).

Taken together, our results indicate that in opposition to Arabidopsis, abiotic stress tolerance of *Sbbri1* lines is not correlated with stunted growth.

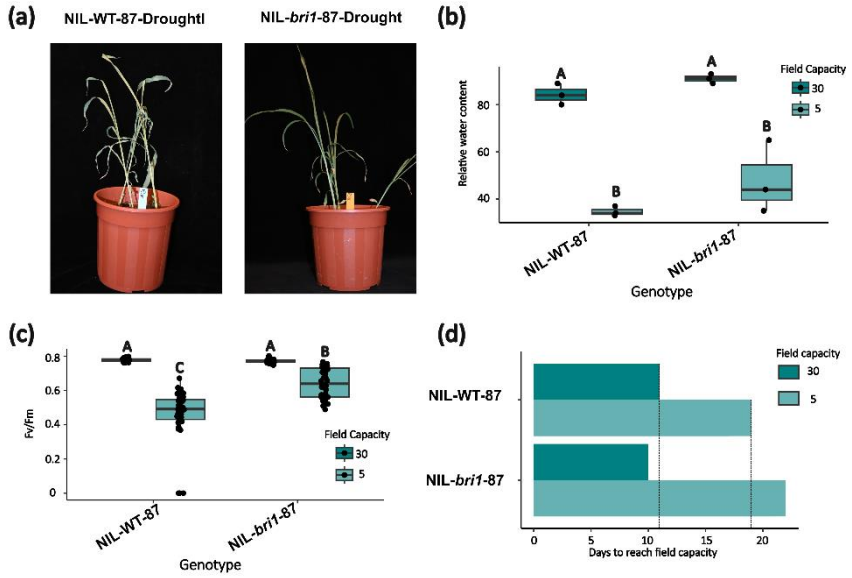


Figure 4.6 Sorghum NIL-*bri1*-87 mutants are tolerant to drought stress. (a) Sorghum seedling phenotypes under drought stress conditions, specifically at 5% of field capacity. (b) Boxplot of relative water content of Sorghum seedlings at 30% (blue) and 5% (light blue) of field capacity. Data from three independent biological replicates (n = 6). Different letters represent statistical significance differences (p-value<0.05) in ANOVA plus Tukey´s HSD test. (c) Boxplot of Fv/Fm values at 30% (blue) and 5% (light blue) field capacity. Data from three independent biological replicates. Different letters represent statistical significance differences (p-value<0.05) in ANOVA plus Tukey´s HSD test. (d) Barplot of days to reach 30% (blue) and 5% (light blue) of field capacity. Dotted lines represent the average of WT plants to reach different field capacities.

4.2.5 The cistrome of Sorghum BES1 shows functional conservation and transcription factor binding to the G-box element, regulating brassinosteroid biosynthesis

Analysis of both transcriptomic and metabolomic changes in root tissue from the drought experiment was carried to investigate the active biological parameters underlying the NIL-*bri1*-72 phenotype in drought

tolerance. Considering the background mutations of the EMS-mutagenized Sorghum mutants and WT plants, we firstly performed DAP-seq of the SbBRI1-downstream TF SbBES1 (Sobic.002G353200). This was conducted with the purpose of reinforcing the transcriptional changes observed in the RNA-Seq dataset.

SbBES1 was firstly expressed in Sorghum leaves by agroinfiltration, to ensure proper expression and localization of the recombinant protein. The SbBES1 protein was localized in the nuclei and the cytoplasm (Figure 4.8a), in accordance with previous studies performed in the plant model system Arabidopsis (Ryu et al., 2010). After validation of the subcellular localization of Sorghum SbBES1, DAP-seq experiments were performed to identify the putative SbBES1 direct targets by mapping the sequencing data in the Sorghum bicolor v3.1.1 (Phytozome genome ID:454) reference genome.

A total of 2255 peaks were detected with a significant enrichment compared to the Halo-input libraries, and the nearest genes were considered as SbBES1-bound. Binding peaks were selected in the base of bell shape peaks, the enrichment against the Halo-input signal and the presence of a motif, analyzed by motif k-mer identification in Multiple EM for Motif Elicitation (MEME) database (Figure 4.7a).

49.14% of peaks were upstream of the starting transcription site, while 25.1% inside the gene and 20.27% downstream of the stop codon (Figure 4.8b). Among all the detected peaks, 96.4% were present in the region of -20000 to 20000 bp relative to the transcription starting site (Figure 4.8b), but the majority of the peaks, 78.22%, were detected in the region of -5000 to 5000 bp, suggesting a higher transcriptional influence as you get closer to the transcriptional starting site.

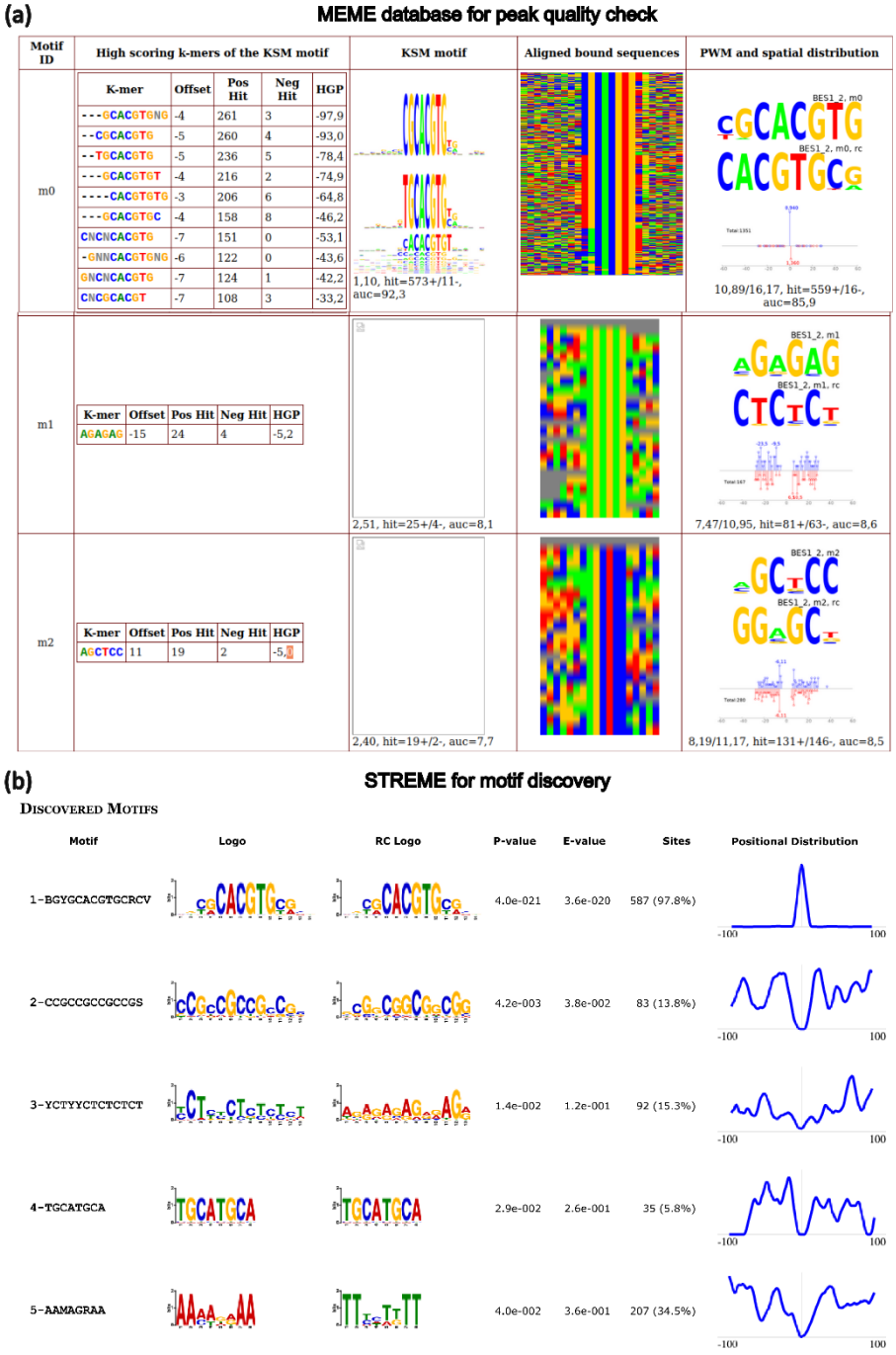


Figure 4.7 Consensus motif in TOP600 best scoring SbBES1 DAP-seq peaks. (a) MEME analysis results done for peak quality check. (b) STREME analysis results done for motif discovery.

After performing motif enrichment on the TOP600 best-scoring SbBES1 bound genes, we observed the enrichment of a G-box (CACGTG) element (Figure 4.8c), which is a type of E-box with two inverted repeats of the Brassinosteroid Responsive Element (BRRE) core element (CGTG). Both elements, BRRE and E-box, have previously been reported as a recognition site for Arabidopsis AtBES1 and AtBZR1 (Yin et al., 2005; Sun et al., 2010). The first motif discovery was done using STREME and the determination of the core binding sequence was determined by the positional distribution of the enriched promoter element, selecting the motif present in the summit peak (Figure 4.7b). By running the analysis in STREME and in additional databases, as RSAT, additional motifs appeared to be enriched, however the G-box was the only promoter element satisfying the positional distribution criteria (Figure 4.7b).

We also used their best-homolog match in Arabidopsis using the Phytozome database to observe the overlapping genes with the Arabidopsis BES1 and BZR1 targets determined by ChIP-chip and DAP-seq experiments, respectively (Yu et al., 2011; O´Malley et al., 2016). Out of 2255 Sorghum target genes we found 1489 Arabidopsis homologs, 11.21% of them to be common with AtBES1 or AtBZR1 targets (Figure 4.8d). After GOE of the common targets, we observed a KEGG enrichment of "Brassinosteroid biosynthesis" (Figure 4.8e), including the presence of the biosynthesis genes Sb*DWF4*, *CYTOCHROME P450 90D1* (Sb*CYP90D1*) and *CONSTITUTIVE PHOTOMORPHOGENIC DWARF* (Sb*CPD*), and signaling gene Sb*BRI1* (Figure 4.8f; *Sobic.001G445900, Sobic.003G030600, Sobic.005G030400 and Sobic.003G277900*, respectively).

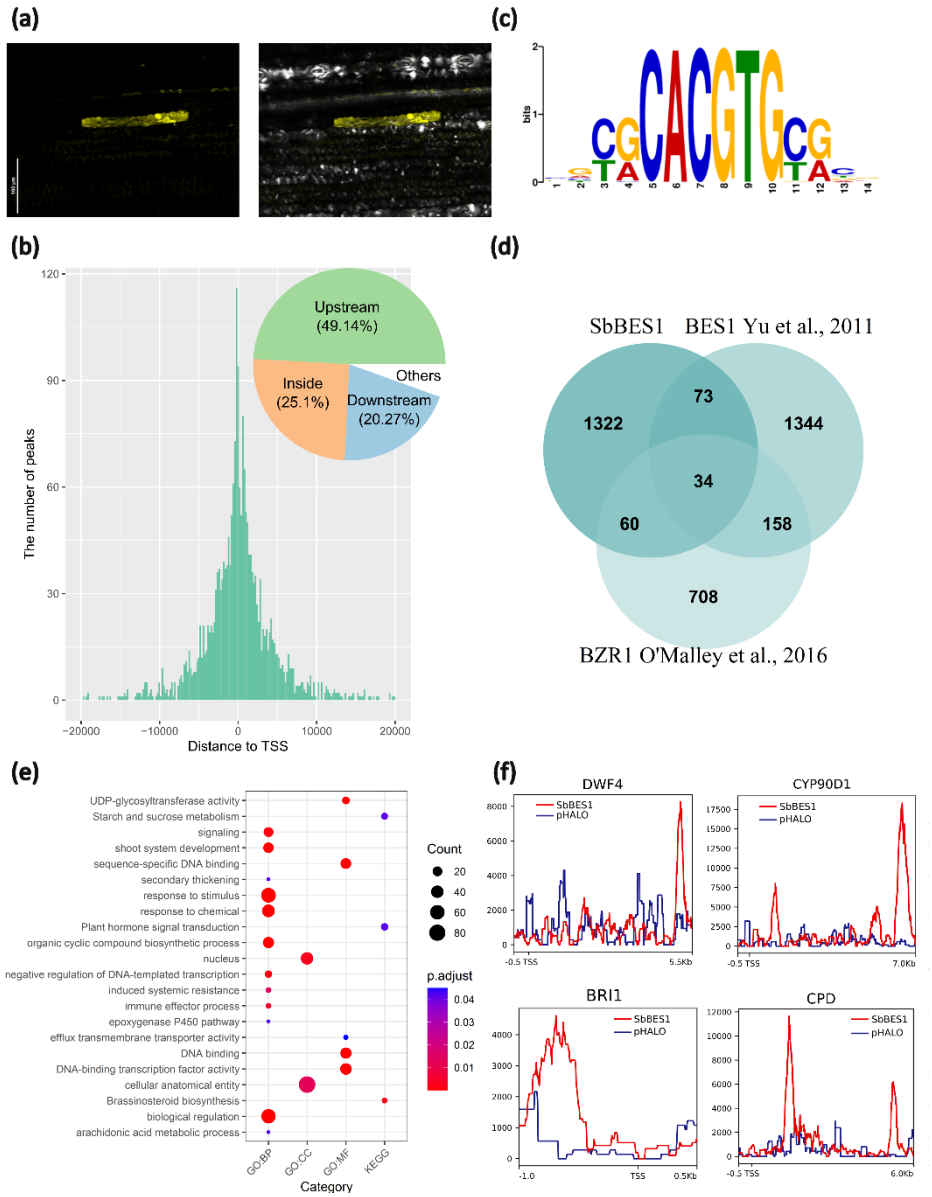


Figure 4.8 Functional conservation of SbBES1 in terms of DNA binding to E-box motifs and regulating brassinosteroid biosynthesis. (a) SbBES1 expression in Sorghum agroinfiltrated leaves. Yellow channel (GFP, left panel) shows SbBES1 protein localization and grey channel shows the bright field. The right panel is the composite image of fluorescence and bright field. Scale bar: 100 µm. (b) SbBES1 peak distribution regarding the distance from the transcription start site. The pie chart shows the percentage of peaks present in the upstream, downstream and inside the coding region of the nearest gene. "Others" pie category accounts for peaks overlapping start or stop codon. (c) Sequence logo of SbBES1 binding motif. (d) Venn diagram of SbBES1, AtBES1 and AtBZR1 targets. (e) GO enrichment analysis of SbBES1, AtBES1 and AtBZR1 target interaction by filtering out redundancy of enriched GO terms (threshold 0.5). Dot size corresponds to the number of bound/target genes enriched in the GO term while color corresponds to the adjusted p-value (FDR). (f) Density plot showing peak signals from pHALO input library (blue line) and SbBES1 DAP-library (red line) in different brassinosteroid biosynthesis and signaling genes (-1 kb and +7 kb from the transcription start site).

All these results point towards a functional conservation of SbBES1, sharing the same binding motif and having a conserved role in the regulation of BR biosynthesis.

After an analysis of all the SbBES1 targets, we could find GOE of biological processes involved in hormone perception such as " Response to brassinosteroid" and "Response to ABA", abiotic stress adaptation such as "Response to osmotic stress" and "Response to water", tolerance to stress responses such as "Regulation of flavonoid biosynthetic process" and "Regulation of anthocyanin metabolic process", and cell wall modification such as "Plant-type secondary cell wall biogenesis", "Phenylpropanoid biosynthesis" and "Lignin metabolic process" (Figure 4.9). Finally, we filtered the putative direct targets by distance, keeping those genes with binding in the proximal promoter (peaks from 0 to -2000 bp from the transcription start site), and inside the gene. In this subgroup we found significantly enriched biological processes related to lignin, flavonoid and phenylpropanoid metabolic processes (for proximal promoters), and response to abiotic stresses (water and osmotic) and BR biosynthesis (for peaks inside the genes) (Figure 4.10a, b).



Figure 4.9 Gene ontology enrichment analysis of Sorghum BES1 direct targets before peak positional filtering. GOE analysis of all Sorghum BES1 targets

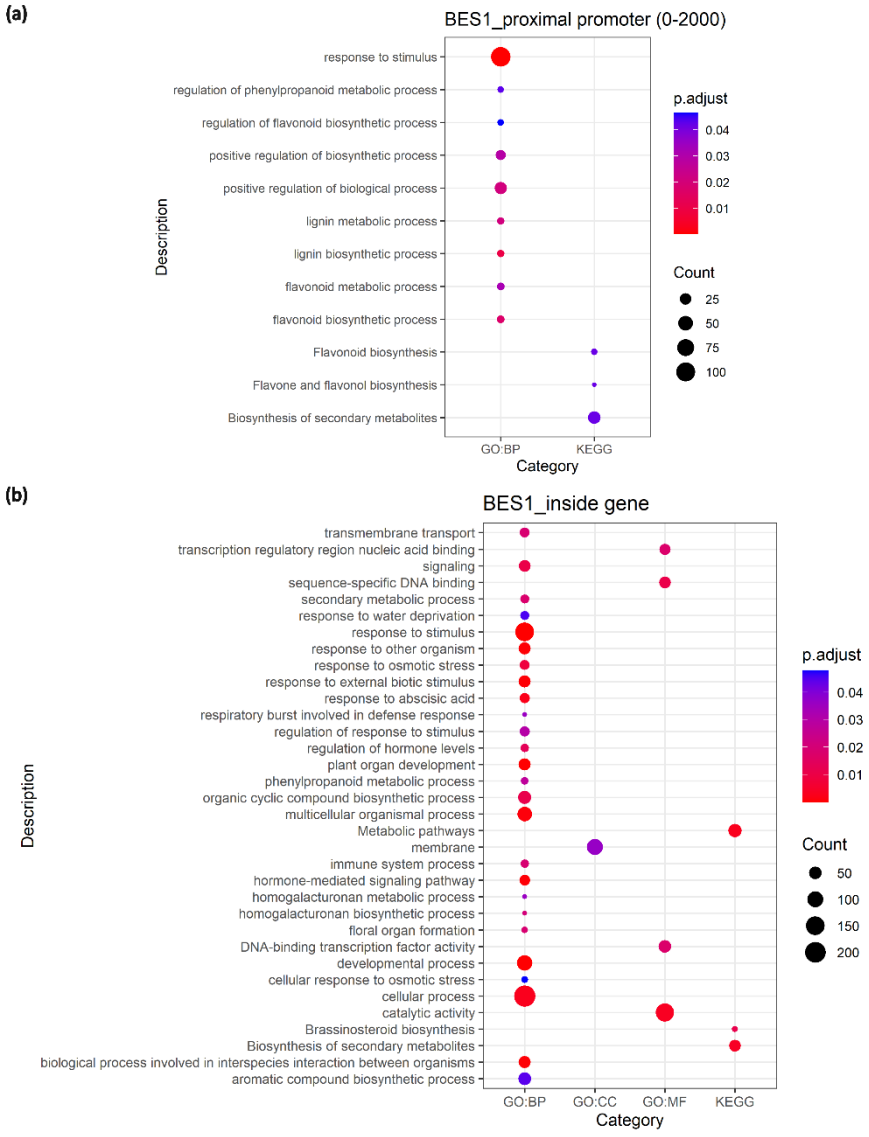


Figure 4.10 Gene ontology enrichment analysis of Sorghum BES1 direct targets after peak positional filtering. GOE analysis of BES1 targets (a) with peaks present in proximal promoter regions (-0 -2000 bp from ATG), and (b) with peaks present inside the coding sequence.

4.2.6 Sorghum *bri1* mutants exhibit distinctive transcriptional regulation of photosynthesis and lignification

We performed RNA sequencing (RNA-Seq) experiments of NIL-*bri1*-72 and NIL-WT-72 plants in control and drought stress conditions. Specifically, this was carried out at 30% FC, when the difference in measured drought indicators was not statistically significant.

Given the likely differences in background mutations among the employed lines and to retain only the data variance attributable to genotype and the treatment, a batch effect correction was applied to remove the variance accounted for by replication (Material and methods).

Subsequent differential expression analysis was conducted using the corrected data. When comparing *Sbbri1* vs WT, 79 deregulated genes in control conditions and 12 deregulated genes in drought were identified (Figure 4.11a). GOE analysis of the deregulated genes under control conditions unveiled that upregulated genes are enriched in categories such as “Plastid thylakoids” and “Photosystem II antenna complex”, while downregulated genes were significantly associated with the “Lignin metabolic process”, “Response to biotic stimulus” and “Response to wounding” (Figure 4.11b). The enrichment of GO categories such as “Plastid thylakoids” and “Photosystem II antenna complex” in non-photosynthetic root tissue could be explained by the incorporation of crown roots in the sampling, where photosynthesis can take place. Additionally, there was a noticeable enrichment of upregulated genes in “Sucrose synthase activity” and “Sugar

transmembrane transporter activity". The upregulation of genes associated with light capture in Photosystem 2, such as *LIGHT HARVESTING COMPLEX OF PHOTOSYSTEM 5* (Sb*LHCB5*) (*Sobic.005G087000*), and the increased activity of sucrose synthase, exemplified by *SUCROSE SYNTHASE 6* (Sb*SUS6*) (*Sobic.004G357600*), implies a stimulation of photosynthetic processes, leading to enhanced sucrose production. Notably, these alterations in gene expression are observed in the root, indicating a similar transcriptional response due to the *bri1* mutation, even in aerial tissues where photosynthesis takes place. Conversely, the downregulation of genes involved in lignin synthesis, such as *CINNAMATE 4-HYDROXYLASE* (Sb*C4H*) (*Sobic.004G141200*) and upregulation of monosaccharide transporter as *POLYOL/MONOSACCHARIDE TRANSPORTER 5* (Sb*PMT5*) (*Sobic.005G196700*), suggest that the synthesized sugars are not being utilized for lignin formation but rather being transported to other sink tissues. Under drought conditions the only enriched category was observed in downregulated genes involved in melatonin biosynthesis and metabolism (Figure 4.11b).

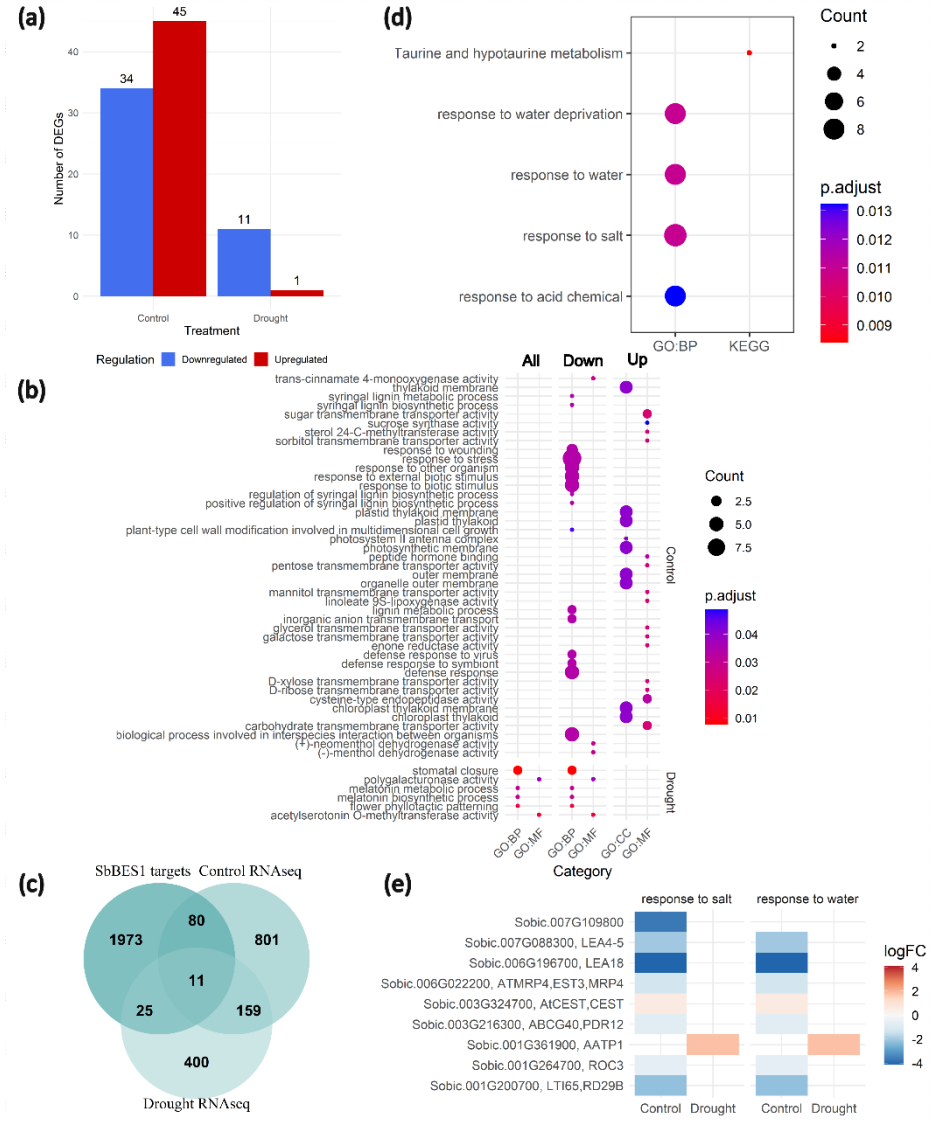


Figure 4.11 Sorghum *bri1* mutants exhibit distinctive transcriptional regulation of photosynthesis and sugar biosynthesis to enhance stress resilience. (a) Number of deregulated genes depending on their regulation when comparing *bri1* vs WT in control or drought stress conditions (FDR<0.05 and |logFC|>0.5). (b) GOE analysis of the different set of deregulated genes in *bri1* vs WT comparison. (c) Venn diagram of SbBES1 targets and deregulated genes in *bri1* vs WT comparison (p-value<0.05 and |logFC|>0.5). (d) GOE analysis of SbBES1 targets which are deregulated by *bri1* mutation. (e) Deployment of SbBES1 targets which are deregulated by *bri1* mutation belonging to "Response to water" and "Response to salt" GO categories. Color indicates logFC.

Next, to obtain a more comprehensive overview of transcriptional responses, we opted for selecting genes with p-values < 0.05, bypassing the consideration of the False Discovery Rate (FDR). This approach was taken because the mutational background could potentially hide transcriptional changes attributed to the *bri1* mutation. Subsequently, to strengthen the evidence for transcriptional alterations, this dataset was merged with the direct targets of SbBES1. Since SbBES1 functions as a downstream TF of SbBRI1, this combined dataset allowed us to identify a set of genes that were deregulated likely due to the *bri1* mutation and were also direct targets of SbBES1 (Figure 4.11c). Following the GOE analysis of this gene set, we observed an enrichment in categories involving "Response to salt" and "Response to water deprivation" (Figure 4.11d). We then deployed the genes belonging to these categories. We found that in control conditions *Sbbri1* mutants exhibited a downregulation of dehydrins and genes responsive to desiccation (such as several *LATE EMBRYOGENESIS ABUNDANT* (Sb*LEA*s) and *RESPONSIVE TO DESICCATION 29B* (Sb*RD29B*)) that typically respond to and accumulate under conditions of low water availability. In contrast, there was an upregulation of a chloroplast protein *CHLOROPLAST PROTEIN-ENHANCING STRESS TOLERANCE* (Sb*CEST*) known to enhance stress tolerance (Yokotani et al., 2010; Yu et al., 2018) (Figure 4.11e). These findings were further supported by analyzing strictly the *bri1* deregulated genes with FDR < 0.05, and that were targets of SbBES1 (Figure 4.12a). Following the GOE analysis of this gene set, we still observed an enrichment in categories involving "Response to water deprivation" (Figure 4.12b). An after the deployment of genes belonging to this category, we still observed that *Sbbri1* mutants

exhibited a downregulation of dehydrins such as Sb*LEA18* (Figure 4.12c).

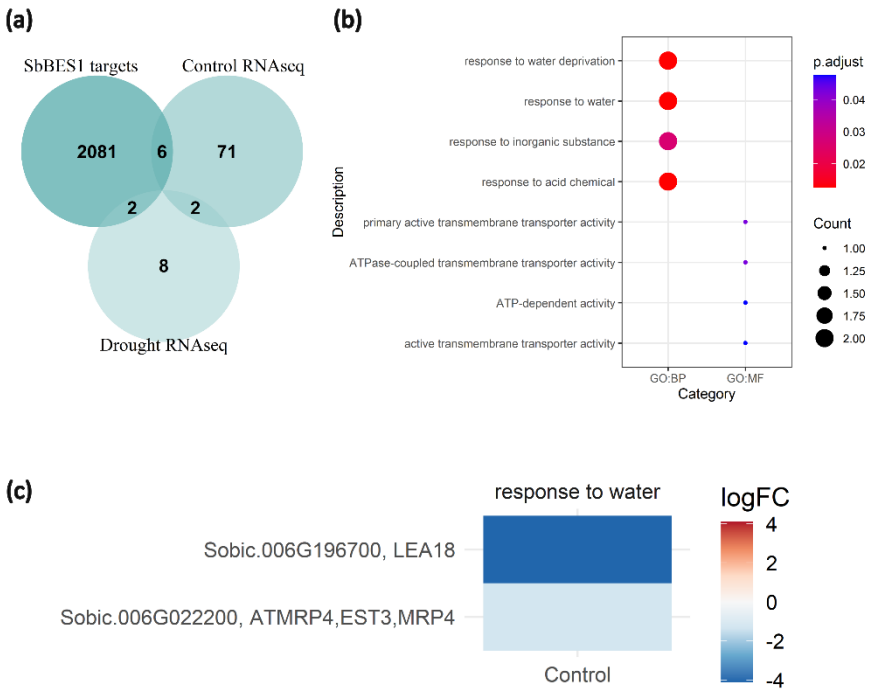


Figure 4.12 Differentially expressed genes in *bri1* mutants and SbBES1 target interaction. (a) Venn diagram of SbBES1 targets and deregulated genes in *bri1* vs WT comparison (FDR<0.05 and |logFC|>0.5). (b) GOE analysis of SbBES1 targets which are deregulated by *bri1* mutation. (c) Deployment of SbBES1 targets which are deregulated by *bri1* mutation belonging to "Response to water deprivation" GO category. Color indicates logFC.

4.2.7 Sorghum *bri1* lines are defective in the phenylpropanoid pathway, leading to reduced levels of lignin precursors and accumulation of flavone

Next, a metabolic profiling of NIL-*bri1*-72 and NIL-WT-72 was conducted under both control and drought stress conditions, using the same sample plant material as the RNA-Seq experiments. The metabolite profiles were mainly influenced by the treatment and secondly by the genotype, as shown by principal component analysis (Figure 4.13a, b). Similar to the transcriptomic analysis, the most significant differences in *Sbbri1* lines metabolite profiles were observed under control conditions, but these differences were restored to WT levels in the early stages of drought stress (Figure 4.13d).

Under control conditions, we observed a depletion of phenylalanine, a precursor in the phenylpropanoid biosynthesis pathway, along with various dipeptides derived from phenylalanine (such as phenylalanyphenylalanine, phenylalanyleucine, glycyl-L-phenylalanine) (Figure 4.14a, c). In downstream metabolic pathways, flavonols like quercetin were reduced, but conversely, there was an increase in flavone levels (Figure 4.14a). These findings are consistent with the transcriptomic changes, which indicated a downregulation of enzymes responsible for catalyzing the phenylpropanoid pathway, such as *CINNAMOYL-COA REDUCTASE* (Sb*CCR*) (*Sobic.007G141200*), and enzymes involved in the early stages of lignin formation, like SbC4H.

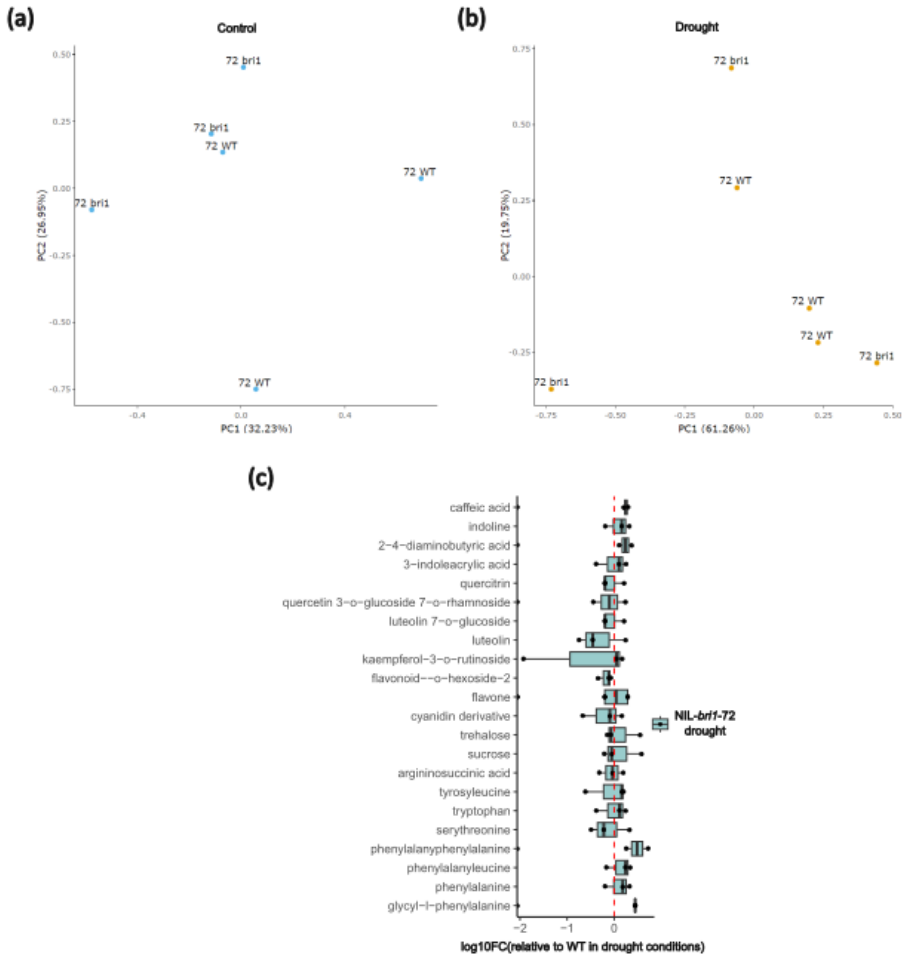


Figure 4.13 Metabolite distribution. (a, b) Principal component analysis and (c) boxplot of log(10)FC of all metabolites. (d) Boxplot of differentially accumulated metabolites when comparing *bri1* vs WT in drought conditions.

In early drought response, we detected a significant trend towards the accumulation of flavonoids, including flavonoid—*O*-hexoside-2 (Figure 4.14b), as well as non-significant increases in luteolin and quercitrin, all approaching WT levels (Figure 4.14d). These findings lead us to conclude that *Sbbri1* mutants have an impaired phenylpropanoid pathway under control conditions, resulting in flavone accumulation and lower levels of lignin, while early drought conditions, appears to restore flux through these metabolic pathways to WT levels.

Additionally, we did not detect higher levels of sugar in root tissue under control conditions (Figure 4.14a), despite transcriptional changes indicating sugar accumulation and transport in *Sbbri1* mutants (Figure 4.11b). This discrepancy can be explained by the fact that transcriptional promotion of photosynthesis and sugar biosynthesis in source tissues occurs more rapidly than sugar production or transport in sink tissues, such as the root. However, under early drought responses, there was a clear tendency to accumulate sugars like trehalose and sucrose (Figure 4.14b).

Furthermore, a significant decrease in tryptophan, which serves as the precursor for auxin biosynthesis, was observed in control conditions together with reduced levels of 3-indoleacrylic acid, an auxin that is metabolize from tryptophan (Figure 4.13a).

Finally, accumulation of 2,4-diaminobutyric acid (DAB), a structural isomer of the neurotoxic secondary metabolite β-*N*-methylamino-L-alanine (BMAA) (Kim et al., 2022), was found in control conditions.

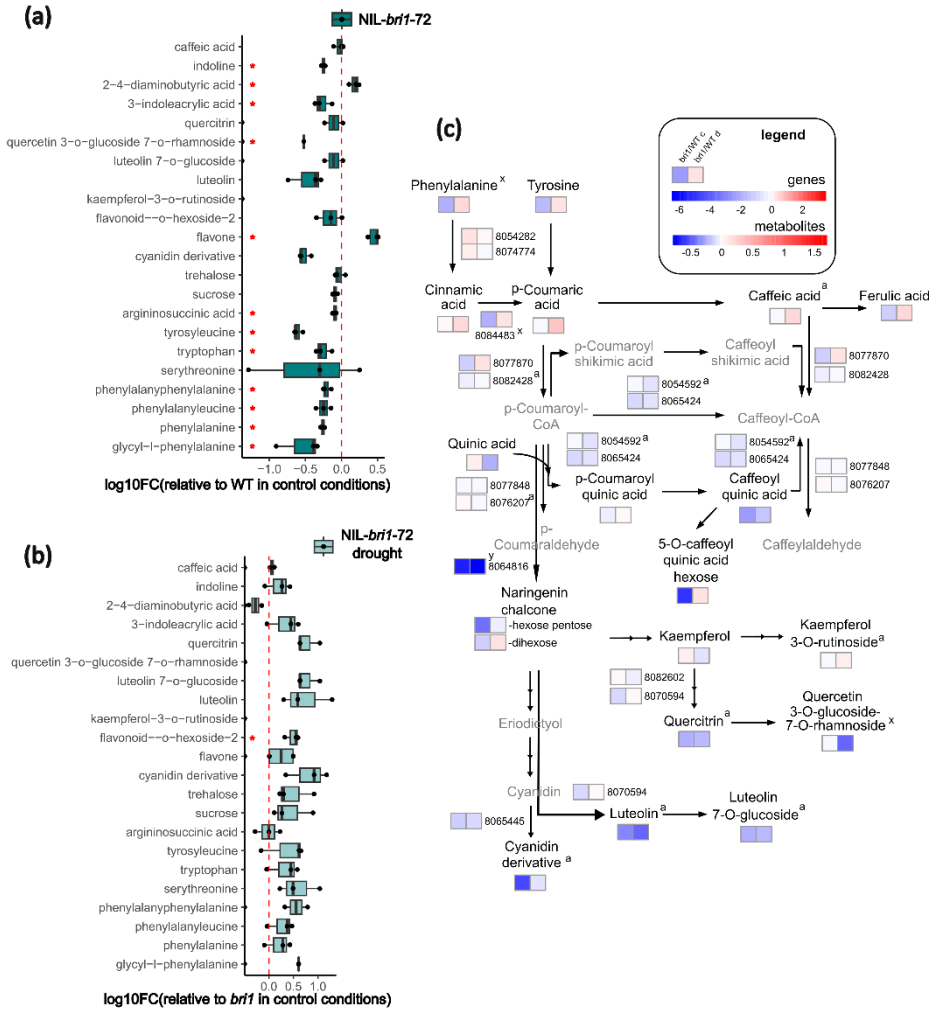


Figure 4.14 Sorghum *bri1* mutants exhibit alterations in the phenylpropanoid pathway, leading to reduced levels of lignin precursors and accumulation of flavone. (a) Boxplot of differentially accumulated metabolites when comparing *bri1* vs WT in control conditions (asterisks indicates significant differences with a p-value <0.05) (b) Boxplot of differentially accumulated metabolites when comparing *bri1* in drought conditions vs *bri1* in control conditions (asterisks indicates significant differences with a p-value <0.05). (c) Phenylpropanoid pathway containing significantly altered genes and metabolites. The genes IDs are Sobic.004G141200 (GeneID: 8084483, cinnamate-4-hydroxylase), Sobic.007G141200 (GeneID: 8076207/8077848, cinnamoyl-CoA reductase), Sobic.007G145600 (GeneID: 8077870/8082428, 4-coumarate:CoA ligase 2), Sobic.010G066601 (Gene ID: 8065424/8054592, HCT hydroxycinnamoyl-CoA shikimate/quinate hydroxycinnamoyl transferase), Sobic.005G136450 (GeneID: 8064816, Chalcone and stilbene synthase family protein), Sorbi.004G200800 (GeneID: 8070594/8082601,Cytochrome P450 superfamily protein) and Cyanidin derivatisation by Sobic.010G070200 (GeneID: 8065445, anthocyanidin 3-*O*-glucosyltransferase). Different letters indicate significant differences (Significant change in *bri1*/WT in control (x) or drought (y) and significant change in drought/control in WT (a) or *bri1* (b), p < 0.05).

Chapter 5

Results

ENHANCING EXPRESSION OF SORGHUM BRL RECEPTOR VIA EFFICIENT SORGHUM TRANSFORMATION USING A TERNARY VECTOR SYSTEM COMBINED WITH MORPHOGENIC REGULATORS

5.1 Introduction

Sorghum is a C4 monocotyledon crop widely grown in Africa and South Asia in arid and semi-arid regions for its use as a staple food and fodder. In addition, it is grown in countries such as the United States, Mexico, Brazil and Australia, mainly as animal feed. Together this makes Sorghum the 5th most important cereal crop in terms of production (Mullet et al., 2002; FAOSTAT, 2022).

Several studies rely on natural variation to find alleles to improve desirable traits for Sorghum breeding, including better quality grains or ability to tolerate drought stress (Ortiz et al., 2021; Xie et al., 2022). However, little progress has been made in genetic engineering of Sorghum by leveraging well-understood molecular pathways to accelerate the generation of Sorghum varieties better adapted to the current climate emergency. In the previous chapter, we successfully identified Sorghum plants with altered BRI1 signaling and improved drought tolerance through EMS mutagenesis. Considering the conserved mechanisms underlying Sorghum drought tolerance via BRI1 and the presence of BR receptors in Sorghum (Blasco-Escámez et al., 2017; Rico-Medina et al., 2024), along with the documented drought tolerance achieved by overexpressing Arabidopsis BRL3 (Fàbregas et al., 2018), our current study focuses on enhancing the expression of the putative vascular-specific Sorghum BRL receptor to develop drought-tolerant Sorghum cultivars.

Despite several years of study, Sorghum has been considered as a crop recalcitrant to genetic transformation because of low regeneration and

accumulation of phenolics during tissue culture (Visarada and Kishore, 2015).

Genetic transformation of Sorghum is traditionally done with microprojectile bombardment using immature embryos as explants. Initially, only 2 out of 600 embryos yielded transgenics, resulting in an unworkable 0.3% transformation efficiency (Casas et al., 1993). Since then, significant progress has been made in sorghum particle bombardment-mediated transformation, with reports up to 20.7% (Liu and Godwin, 2012).

Agrobacterium tumefaciens (Agrobacterium)-mediated transformation is however a preferred technology as particle bombardment can lead to structural genome rearrangements (Yue *et al*., 2022). In 2000 it was firstly reported the use of Agrobacterium to genetically transform sorghum immature embryos, obtaining very variable transformation efficiencies from 0.17 to 10.1 % (Zhao et al., 2000). The implementation of the use of morphogenic regulators was a breakthrough in immature embryo-based transformation in monocots. Agrobacterium-mediated transformation of maize *BABY BOOM (Bbm)* and *WUSCHEL2 (Wus2)* in maize inbred lines led to high transformation frequencies and genotype-flexibility of regeneration (Lowe et al. 2016). The morphogenic genes were used together with a novel ternary vector system. The latter allowed equipping Agrobacterium with extra virulence genes, improving the transfer DNA (T-DNA) delivery (Anand et al., 2018; Zhang et al., 2019). The combination of these two new techniques has led to an immature embryo-based and genotype-flexible sorghum transformation system, having the highest transformation frequency reported up to now of 69.7 % (Che et al. 2022).

Nonetheless, expressing *Bbm* and *Wus2* has a limitation. These morphogenic regulators have the desirable effect of boosting somatic embryo formation but also have undesirable pleiotropic effects when constitutively expressed in T0 plants. To avoid this limitation, several strategies were proposed such as a Cre/Lox-mediated excision system and a method designated as "altruistic transformation". The excision system is based on three expression cassettes containing *Bbm*, *Wus2* and a *CRE* recombinase, flanked by LoxP recombination target sites. *CRE* is driven by an inducible promoter, therefore resulting in an inducible system to excise the morphogenic expression cassettes (Gordon-Kamm et al., 2019). The "altruistic transformation" is based on a co-transformation system in which two Agrobacterium strains are used for transformation. The first strain will carry the "altruistic T-DNA" with morphogenic regulator expression cassette but lacking a selectable marker. The second will contain the gene of interest and the presence of a selectable marker. The concept is that morphogenic regulator proteins can move to neighboring cells, enhancing the somatic embryogenesis and non-morphogenic regulator containing cells will have the ability to be efficiently transformed through somatic embryo formation (Hoerster et al., 2020). In both systems regenerated plants carrying the gene of interest are generated that lack morphogenic regulators.

In this study, we evaluated morphogen-assisted transformation for Sorghum using the publicly available pVS1-VIR2 ternary vector system combined with a newly designed and compatible binary destination vector. We improved conditions for Agrobacterium co-cultivation and the pressure of the selectable agent in order to obtain significantly higher sorghum transformation efficiencies than those previously reported.

With the implementation of this new methodology, Sorghum plants with enhanced *BRL* expression have been produced and phenotypic analysis revealed a drought-tolerant phenotype associated with the higher expression of the vascular-enriched BR receptor, revealing that roles for BRL in Sorghum are conserved with those previously described in the model system Arabidopsis (Fàbregas et al., 2018).

For clarity, the Material and Methods section will be presented first.

5.2 Material and Methods

5.2.1 Sorghum transformation

The Materials and equipment for the Sorghum transformation are the following:

1. Laminar flow hood
2. Sorghum variety TX430
3. *Agrobacterium* EHA105 recA- (Rodrigues et al., 2021) containing pVS1-VIR2 construct (Zhang et al., 2019)
4. Horizontal shaker
5. Tools for embryo isolation and subcultures: dissecting lancet, scalpel and tweezers
6. 50 ml Falcon tubes
7. Plastic petri dishes: 90 and 150 mm of diameter
8. Different media, specified in Table 5.1
9. 2 ml microcentrifuge tubes
10. Sterilization solution (5% NaOCl + 0.01% Tween-20)

11. Sterile distilled water
12. Rotor wheel
13. Pipettes and pipette tips
14. Stereomicroscope (Leica)
15. Culture room at 24°C, 26°C and 28°C

Table 5.1 Medium composition for Sorghum transformation.

	Units	YP media	Infection media	Co-cultivation	Resting	Maturation I	Maturation II	Rooting
MS Basal Salt with vitamins	g		4.43	4.43	4.43			
MS Basal Salt	g					4.3	4.3	2.15
Yeast extract	g	5						
Peptone	g	10						
NaCl	g	5						
Sucrose	g		68.5	20	20		60	40
Glucose	g		36	10	10			
Myo-inositol	mg					250	100	50
Maltose	g					30		
L-proline	mg			700	700	690	700	
Casein hydrolysate	mg					1000		
Thiamine HCL	mg		1	1	1	1		
Ascorbic acid	mg			10	10			
MES	mg			500	500			
Cefotaxime	mg				100	100	100	
Vancomycine	mg				100	100	100	
Acetosyringone	µM		200	200	200			
CuSO4	mg					1.22	1.25	
IAA	mg						1	
Thidiazuron	mg						0.1	
ABA	mg						0.026	
BAP	mg					0.5		
Zeatin	mg						0.5	
2,4-D	mg		1.5	2	2	2		
MS-vitamins stock	ml						1	1
G418	mg						100 / 250	
Gelrite	g						3	3
Agar	g	12		8	8	8		
pH		6.8	5.2	5.8	5.8	5.8	5.8	5.8

The transformation methodology (Figure 5.1) is described in detail in the following sections.

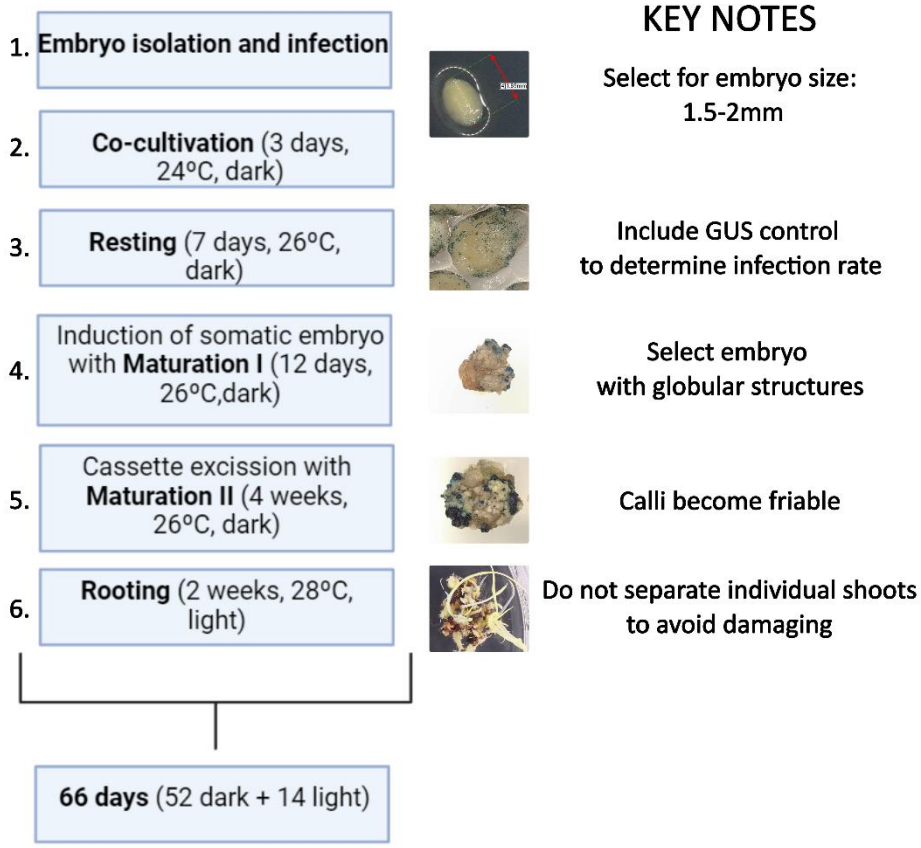


Figure 5.1: Flow chart of excision-based TX430 Sorghum transformation protocol. Left Panel: This flow chart delineates each stage of the protocol, specifying the time, temperature, and light conditions required at each step. The entire process spans a total of 66 days. Right Panel: Key notes highlighting critical points and considerations for each stage of the protocol are provided.

5.2.1.1 Collecting immature embryos from TX430 Sorghum plants

1. Fifteen days upon anthesis initiation, select for embryo size between 1.5-2 mm (Figure 5.1, 5.3b). Harvest the spikelets having embryos of the mentioned size. Carefully separate each seed of the spikelet by hand without harming them. This last step will facilitate embryo isolation.
2. Place the individual seeds in 50 ml conical centrifuge tubes and leave at 4 °C overnight.

5.2.1.2 Agrobacterium preparation

1. Schematic representation of the construct used in this work is in Figure 5.3a. We used two different Gene Of Interest:
    a. Zm*Ubi*$_{pro}$::GUS-intron-Bd*Ubi* T. This construct was used to monitor the Agrobacterium infection and the stable expression of our construct along the different transformation stages.
    b. Zm*Ubi*$_{pro}$-*SbBRL*-*GFP*-Bd*Ubi* T. This construct was used for obtaining SbBRL overexpressor lines.
2. Glycerol stock (*Agrobacterium* strain EHA105 recA- carrying the pVS1-VIR2 and the constructs specified above) was used to inoculate a plate with YP media (Table 5.1). Incubate 3 days at 28 °C in dark.

3. The day before transformation use the actively growing Agrobacterium to inoculate a freshly made plate with YP media. Incubate overnight at 28 °C in dark.
4. Prepare the *Agrobacterium* solution: the transformation day take a scoop of Agrobacterium and mix in a 50 ml conical centrifuge tube carrying 10 ml of Infection media (Table 5.1). Incubate minimum 2 hours at room temperature (RT) in a horizontal shaker at 200 rpm.

5.2.1.3 Sorghum seed sterilization and isolation of immature embryos

1. Sterilize seeds in 50 ml conical centrifuge tubes. Add 5% bleach and place the conical centrifuge tubes in a rotor wheel for 20 min. Wash the Sorghum seeds with sterile distilled water for 5 min in the rotor wheel 5 times.
2. Place seeds in big petri dishes and isolate embryos using tweezers and dissecting lancet (Figure 5.2). Place the isolated embryos in 2 ml microcentrifuge tube containing 1.75 ml of Infection media. Each infection tube should have 25 embryos.

5.2.1.4 Infection, co-cultivation and resting

1. Wash the embryos before infecting: take out all the Infection media from the infection tubes and add 1 ml of new Infection media. Invert the tube 3-4 times and pipette off the Infection media. Repeat this step.

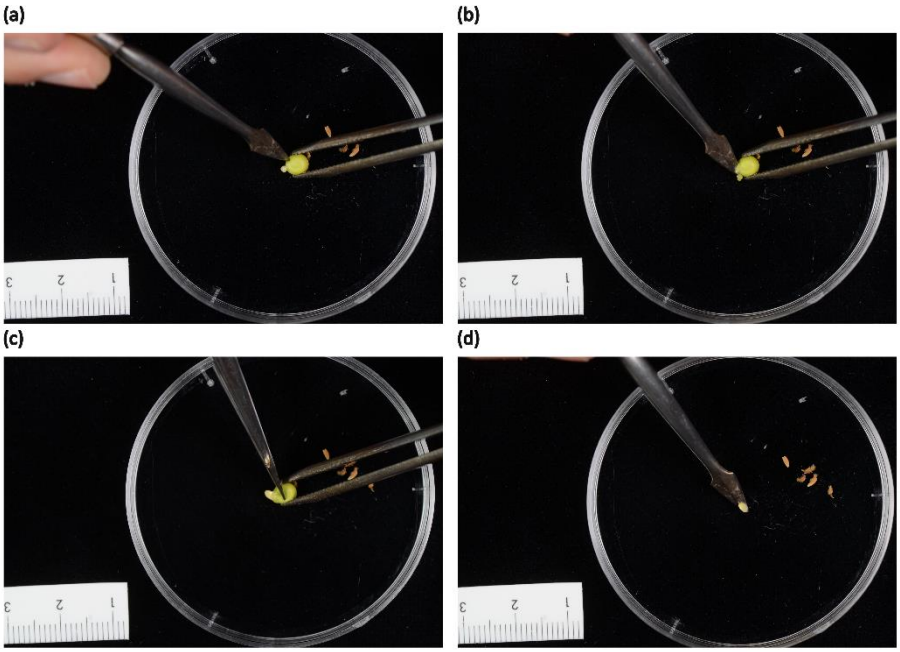


Figure 5.2: Immature Sorghum embryo isolation procedure. (a) Position the seed with tweezers, ensuring the embryo side (opposite the hilum) is facing upward. (b) Use a lancet to create a small aperture at the tip of the seed. (c) Gently press the lancet at the bottom of the seed, taking care to avoid damaging the embryo. (d) Extract the embryo with the tip of the lancet and transfer it into microcentrifuge tubes.

2. Add 1 ml of *Agrobacterium* solution. Before use, dilute the *Agrobacterium* solution in Infection media to an OD 0.3 in 550 nm wavelength. Invert tube 20 times and incubate at RT in dark for 5 min.
3. Take out 500 µl of *Agrobacterium* solution and poor the rest in a petri dish with Co-cultivation media (Table 5.1). Take off excess of *Agrobacterium* solution with a pipette and place the embryos with the scutellum side up and uniformly distributed.
4. Seal the plates with micropore and incubate them at 24°C in dark for 3 days.

5. After this step, transfer all the 25 embryos in a new petri dish containing Resting media (Table 5.1) to induce callus formation and incubate them at 26 C in dark for 7 days.
6. Check point: Include a GUS construct in parallel to your Gene of interest (GOI) construct and check for transient expression by performing a histochemical staining with x-Gluc (GUS staining) 7 days after infection (DAI) (Figure 5.3c).

5.2.1.5 Induction of somatic embryogenesis with Maturation media I

1. After resting for 7 days, transfer the embryos that have started the induction of callus to Maturation media I (Table 5.1). Remove the radicle from the embryo with scalpel and tweezers. Incubate them at 26 °C in the dark for 12 days. Discard the non-progressed embryos.
2. Check point: 14 DAI calli can be used to perform a GUS staining. The first GUS staining is informative in the infection efficiency of your transformation but can contain a GUS signal of transient expression. In the second GUS staining check the stable expression of your transgene. In a nice stable expression, you will see a change from single cell expression to cell clusters containing your transgene. In addition, the embryogenic tissue formation may be already appreciated (Figure 5.3d).

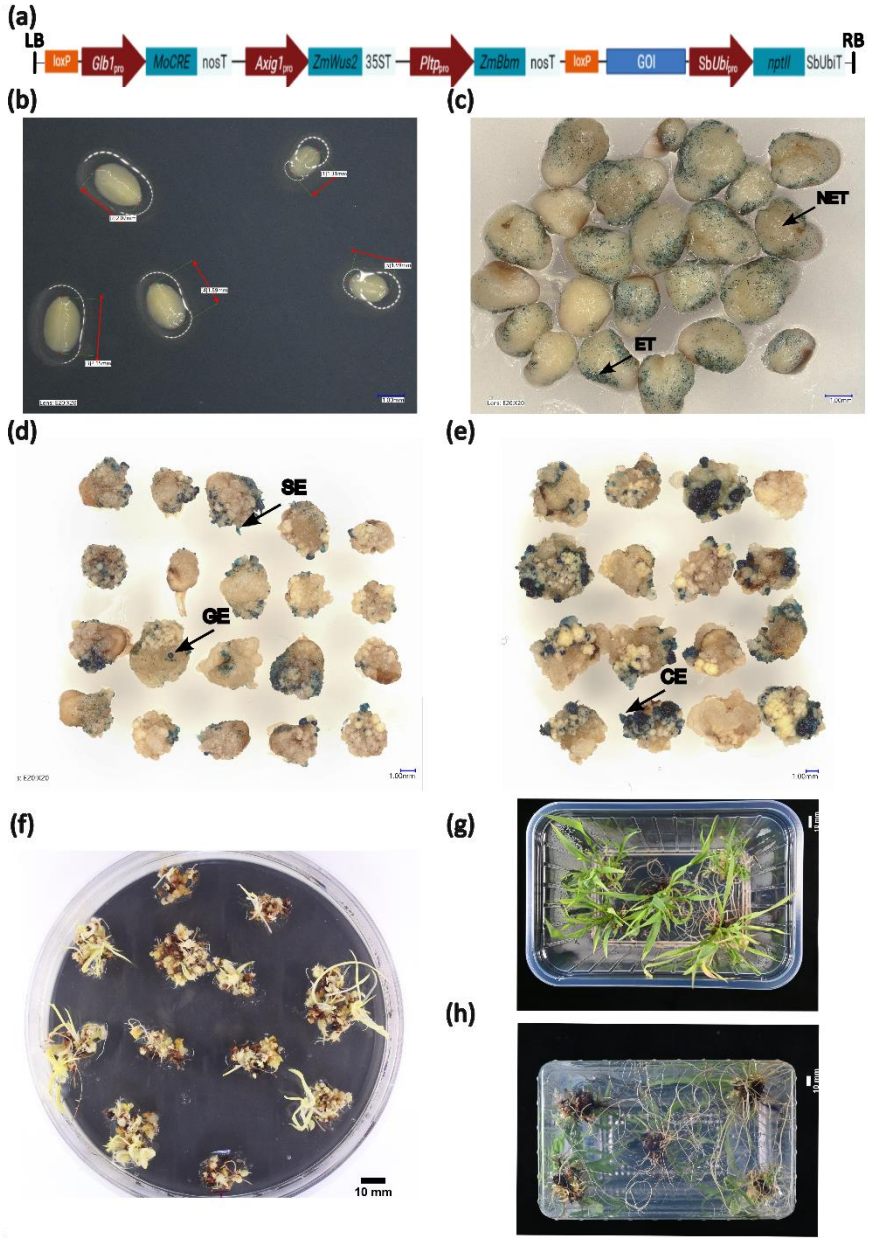


Figure 5.3 Schematic representation of the construct used in this work and tissue culture progression. (a) Excision-based construct using morphogenic regulators, ABA inducible MoCRE and nptII as a selection marker. (b) Isolated immature embryos ranging from 1.3 to 2.15 mm. (c-e) GUS-stained calli at 7, 14 and 21 days after infection. (c) Callus induction in resting medium 7 days after infection. It is noticeable the formation of embryogenic and non-embryogenic tissue (ET and NET) in the immature embryo scutellum. (d) Somatic embryogenesis induction in Maturation I medium 14 days after infection. There is already presence of globular embryos (GE) and scutellar embryos (SE) where GUS expression is present. (e) Somatic embryo maturation in Maturation I medium 21 days after infection and just before cassette excision. There is presence of coleoptilar embryos (CE) and the cell clusters expressing GUS are bigger. (f-h) Detailed pictures of calli overexpressing the membrane-protein in the GOI cassette 36 and 64 days after infection. (f) Germination of somatic embryos in Maturation II medium 36 days after infection. (g-h) Rooted plantlets in rooting media 64 days after infection.

5.2.1.6 Regeneration and rooting

1. After 12 days in Maturation media I, transfer all the calli to Maturation media II (Table 5.1) with 100 mg/L of Geneticin. Incubate them at 26 °C in dark for 14 days.
2. Check point: 21 DAI calli can be used to perform a GUS staining. After 7 days in Maturation media II, you can see already the selection effect in non-transformed cells (necrotic tissue). However, if clusters of living cells expressing your construct are visible is a good indication of stable expression of you construct including the selecting agent (Figure 5.3e).
3. After 14 days in Maturation media II, regenerant plants can be already observed (Figure 5.3f). Transfer the callus and the regenerant plants to new Maturation media II with 250 mg/L of Geneticin. At this stage the callus is very friable, therefore take care when subculturing and divide the callus in several pieces to allow proper growth of the regenerant plants. However, keep track of the regenerant plants and embryogenic tissue coming from the same callus to differentiate putative clones with the inserted T-DNA in the same genomic region. As callus are grown and divided into several pieces, they fill more space than before, therefore place around 10-12 callus per plate.
4. After 14 days pass calli and regenerant plants to Rooting media (Table 5.1) and incubate them at 28 °C in light regime until roots are well formed. After 14 days in Rooting media shoots will turn green and elongate and primary and secondary roots will be formed and elongated (Figure 5.3g, h).

5.2.1.7 Passing to soil T0 plants

The rooted plantlets are then transferred to soil using pre-wetted Jiffy-7 pellets and covered with a plastic box to maintain high humidity, aiding in their acclimatization from tissue culture to soil. These transgenic plantlets were maintained under controlled growth conditions, with a light intensity of 300 μE.m−2.s−1, a 16-hour light period at 26°C, and an 8-hour dark period at 22°C. The humidifying cover was removed after 3 days.

5.2.1.8 Genotyping and determining quality events

Stable T-DNA integration was determined by PCR using genomic DNA extracted from T0 plantlet leaves. Different PCRs were performed to test the presence of the GOI and the presence of the non-excised morphogenic regulators (Figure 5.4 and Table 5.4). The quality events (presence of *nptII* and absence of *MoCRE* and *GmR* [binary vector backbone]) were further analyzed by digital PCR (dPCR) to also determine the number of T-DNA copies (Table 5.2).

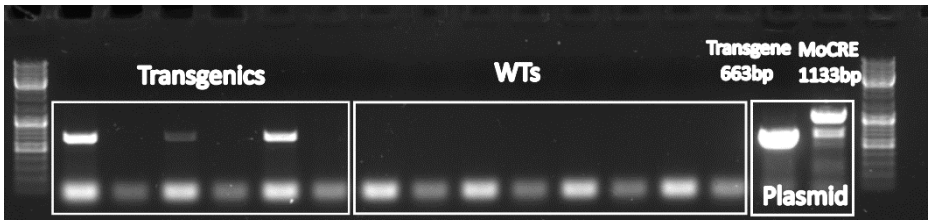


Figure 5.4 Gel electrophoresis of amplified DNA by PCR in transgenic and non-transgenic (WT) plants. Plasmid DNA was also amplified as a positive control. The amplicon length is 663 bp for the GOI region and 1133 bp for the excision cassette region

Table 5.2 Primers and probes used for determining T-DNA integration and gene copy number by PCR and digital PCR, respectively.

Primer ID	Sequence	Aim	Amplicon length
GFP Fw	CAA GCT GAC CCT GAA GTT CAT C	Pressence of transgene	663 bp
Bd*UBI10*T Rv	CGA CTA CTT CCA AGG GGC AG	Pressence of transgene	663bp
MoCRE Fw	ACC TCA TGG ACA TGT TCC GC	Pressence of BBM/WUS cassette	1133 bp
MoCRE Rv	TTC CAG GAG GCG AAC CAT TG	Pressence of BBM/WUS cassette	1133 bp
dPCR housekeeping Fw	TGA GGA CCC TTT TGA TCA GG	dPCR housekeeping Fw	135 bp
dPCR housekeeping Rv	CAA GCC TTC TTG CCA ATA GC	dPCR housekeeping Rv	135 bp
dPCR housekeeping Probe	TGG AGT TCA TGG GCA TCA TTG CA	dPCR housekeeping Probe	135 bp
dPCR nptII Fw	TTT CAT CGA CTG CGG TAG AC	dPCR nptII Fw	108 bp
dPCR nptII Rv	AGA AAC CTG TCA GCC CAT TC	dPCR nptII Rv	108 bp
dPCR nptII Probe	CAG GAC ATC GCC CTG GCA ACA CGC	dPCR nptII Probe	108 bp
dPCR MoCRE Fw	ATT GCA TAC AAC ACG CTC CT	dPCR MoCRE Fw	105 bp
dPCR MoCRE Rv	GGT CCT GCC AAT GTG GAT AA	dPCR MoCRE Rv	105 bp
dPCR MoCRE Probe	CGC GTG AAG GAC ATT AGC CGC ACCG	dPCR MoCRE Probe	105 bp
dPCR GmR Fw	AAG TAT GGG CAT CAT TCG CA	dPCR GmR Fw	115 bp
dPCR GmR Rv	ATG TTG GGA GTA GGT GGC TA	dPCR GmR Rv	115 bp
dPCR GmR Probe	GGC TCG GCC CTG ACC AAG TCA AAT CCA	dPCR GmR Probe	115 bp

In addition, the GOI used for this transformation was the membrane-localized Sorghum BRL receptor fused to GFP. Therefore, additional validation of proper transgene expression was done by visualizing GFP fluorescence under the confocal microscope. We could corroborate that the T0 plantlets were having the presence of plasma membrane-localized

protein fused to GFP (Figure 5.5a, b) and absence of GFP signal in non-transformed roots was observed (Figure 5.5c, d).ç

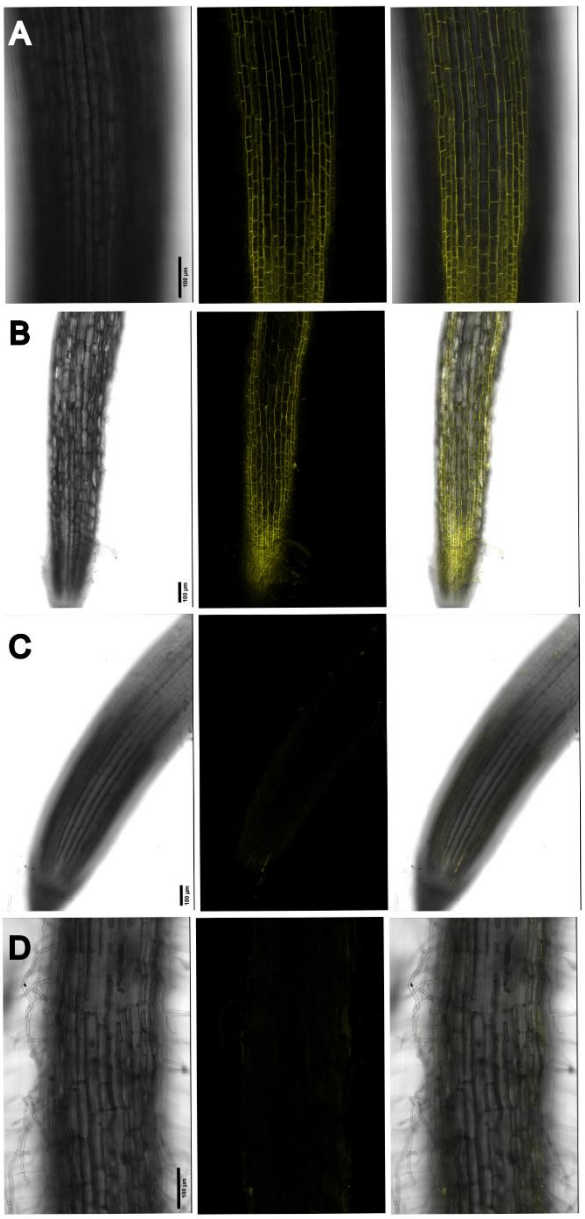


Figure 5.5 Confocal imaging pictures of transgenic roots with integrated membrane protein-GFP fusion and non-transgenic roots. Yellow channel (GFP) shows the localization of SbBRL protein and grey channel (bright field) shows the root tissue. (A) GFP presence in the mature root (B) and root meristem. (C) GFP absence in non-transgenic root meristem (D) and mature root. Images were acquired in FV1000 Olympus confocal microscope.

5.2.2 RNA *in situ* hybridization in Sorghum shoots

5.2.2.1 *In vitro* transcription of RNA probes

1. A specific region in the 3' and 5' UTR of our target genes, SbBRI1 and SbBRL, was identified. The specificity was confirmed using Nucleotide BLAST (NCBI).
2. The region of interest, spanning 150 to 250 bp, was amplified by PCR. The primers utilized in this study are detailed in Table 5.3.
3. PCR products were cloned into the pJET1.2 blunt vector using the pJET Kit (Thermo Fisher). Following E. coli transformation, colony PCRs were conducted to identify colonies containing both sense and antisense fragments of the genomic region.
4. Highly concentrated DNA was obtained by PCR amplification of the region of interest, using our resultant pJET plasmids as templates. The T7 promoter was incorporated for subsequent RNA synthesis.
5. DNA purification and concentration were carried out using the DNA Clean & Concentrator-5 kit (Zymo Research).
6. In vitro RNA transcription was performed using the MEGAscript T7 kit (Invitrogen), utilizing the concentrated DNA as a template. The protocol was executed according to the manufacturer's instructions.

Table 5.3 Primers used to generate RNA *in situ* hybridization probes for SbBRI1 and SbBRL.

Primer ID	Sequence	Aim	Amplicon length
BRI1 3´UTR Fw	GAGAAACTGCCCAGGGGTTA	BRI1 3´UTR probe	200 bp
BRI1 3´UTR Rv	GAAAAATCAACCTACTCCCATAGG	BRI1 3´UTR probe	200 bp
BRI1 5´UTR Fw	ATAGCAGCCCATTCCCTCCA	BRI1 5´UTR probe	150 bp
BRI1 5´UTR Rv	ACTAGCTATCGCGCTACCTT	BRI1 5´UTR probe	150 bp
BRL3 3´UTR Fw	AAAAAGGTGGCCTCCTCCTC	BRL3 3´UTR probe	223 bp
BRL3 3´UTR Rv	AAAGCTGTGGATCTGCGTCA	BRL3 3´UTR probe	223 bp
BRL3 5´UTR Fw	CCAATGGCGGGGTTCAGTAG	BRL3 5´UTR probe	237 bp
BRL3 5´UTR Rv	CGAAGAACCCAACCCCTCAT	BRL3 5´UTR probe	237 bp

5.2.2.2 Tissue fixation

1. BTx623 Sorghum seeds were planted in soil and allowed to grow for 12 days.
2. 12-day-old Sorghum seedlings were harvested for tissue fixation. Sections measuring 0.5 cm from the stem base, for visualizing the shoot apical meristem, and the region between 3.5 cm and 4 cm from the stem base, for radial shoot visualization, were excised and fixed in 4% paraformaldehyde. The samples were then incubated at 4ºC for 2 days.

5.2.2.3 Tissue dehydration and embedding

1. Fixed samples were dehydrated in an ethanol series according to the following steps:

    a. 1X PBS for 30 min at RT.

b. 1X PBS for 30 min at RT.
c. 15% EtOH for 30 min at RT.
d. 30% EtOH for 30 min at RT.
e. 50% EtOH for 30 min at RT.
f. 70% EtOH for 30 min at RT.
g. 85% EtOH for 30 min at RT.
h. 95% EtOH for 30 min at RT.
i. 100% EtOH for 30 min at RT.
j. 100% EtOH overnight at RT.

2. Dehydrated samples were prepared for paraplast embedding as follows:

    a. 100% EtOH for 2 hours at RT.
    b. 25% Histoclear/75% Ethanol for 1 hour at RT.
    c. 50% Histoclear/50% EtOH for 1 hour at RT.
    d. 75% Histoclear/25% EtOH for 1 hour at RT.
    e. 100% Histoclear for 1 hour at RT.
    f. 100% Histoclear for 1 hour at RT.
    g. 100% Histoclear for 1 hour at RT.
    h. Paraplast chips were added to approximately half the volume of the Histoclear and left for overnight.
    i. Samples were incubated at 60 ºC until Paraplast chips were dissolved.
    j. Freshly molten Paraplast at 60 ºC was replaced every evening and left overnight for 3 consecutive days.
    k. Paraplast blocks were created by pouring Paraplast with plant material into a mold and allowed to cool at 4ºC.

5.2.2.4 Tissue sectioning

1. Paraplast blocks were sectioned into slices of 8-10 μm and mounted in ProbeOn Plus slides (Fisher scientific).
2. Slides were positioned on slide warmer, and water was applied to the top of eac slide. Slides were then incubated overnight at 40ºC.

5.2.2.5 In situ hybridization: Deparaffinizing

1. Slides were arranged in stainless steel racks and subjected to different treatments.
2. Deparaffinization and rehydration:
    a. Histoclear for 10 min
    b. Histoclear for 10 min
    c. 100% EtOH for 30 s
    d. 100% EtOH for 30 s
    e. 95% EtOH for 30 s
    f. 70% EtOH for 30 s
    g. 50% EtOH for 30 s
    h. 30% EtOH for 30 s
    i. Deionized water for 30 s
    j. 1X PBS for 2 min
3. Permeabilization:
    a. 300 ml pronase buffer (50 mM Tris-Cl pH 7.5, 5 mM Ethylenediamine tetraacetic acid (EDTA)) + 930 μl pronase for 10 min
    b. 0.2% Glycine in 1XPBS for 2 min
    c. 1XPBS for 2 min
4. Re-fixation:

a. 3.7% formaldehyde in 1XPBS for 10 min
b. 1XPBS for 2 min

5. Acetylation
    a. 0.1M Triethanolamine briefly
    b. Slowly dribbling of 1.5 ml Acetic anhydride over slides
    c. 1XPBS for 2 min
6. Dehydration
    a. 30% EtOH for 30 s
    b. 50% EtOH for 30 s
    c. 70% EtOH for 30 s
    d. 95% EtOH for 30 s
    e. 100% EtOH for 1 minute
    f. 100% EtOH for 2 min

5.2.2.6 In situ hybridization: Hybridization, washing, antibody detection, mounting and visualization

1. Probes were prepared in a 1:100 v/v ratio (1 µL of probe to 100 µL of 50% formamide).
2. The probes were denatured at 95ºC for 3 min and then immediately placed on ice for 1 minute.
3. To the denatured probe, 150 µL of hybridization solution (as described in Zölner et al., 2021) was added.
4. Pair of slides were treated with the hybridization solution containing the probe, following the protocol outlined in Zölner et al., 2021, and placed in a humid chamber at 55ºC overnight.
5. The slides were washed with 0.2X SSC buffer (as described in Zölner et al., 2021) with gentle shaking at 55ºC for 1 hour. This washing step was repeated 3 times.

6. Following the washes, the slides were rinsed with 1XPBS for 5 min.
7. The slides were then treated with blocking solutions:
    a. Boehringer solution (as described in Zölner et al., 2021) for 45 min at RT.
    b. Bovine Serum Albumin (BSA) solution (as described in Zölner et al., 2021) for 45 min at RT.
8. Following the blocking process, each pair of slides was incubated with anti-digoxigenin alkaline phosphatase-conjugated antibody (Roche), diluted 1:1250 in BSA solution, for 2 hours at RT in a humid chamber.
9. After antibody incubation, slides were washed 4 times with BSA solution for 20 min each.
10. Additionally, the slides were washed with Buffer C (as described in Zölner et al., 2021) for 15 min.
11. The slides were then treated with 5-bromo-4-chloro-3-indolyl-phosphate in conjunction with nitro blue tetrazolium (NBT/BCIP Promega) for the colorimetric detection of the alkaline phosphatase-conjugated antibody for 12 hours at RT in dark conditions in a humid chamber.
12. Detection was stopped by rinsing twice in water for 3 min each.
13. Slides were then dehydrated through an alcohol series:
    a. 30% EtOH for 30 s
    b. 50% EtOH for 30 s
    c. 70% EtOH for 30 s
    d. 85% EtOH for 30 s
    e. 95% EtOH for 30 s
    f. 100% EtOH for 30 s

g. 100% EtOH for 30 s

14. Slides were rinsed twice in Histoclear for 5 min each.
15. Finally, slides were mounted using Permount (Fisher) and visualized under a Leica DM6 microscope.

5.3 Results

5.3.1 Sorghum BRL receptor is enriched in vascular tissues

To validate the tissue-specific expression of BR receptors in Sorghum, we conducted RNA *in situ* hybridization experiments to localize the transcripts of *SbBRI1* and *SbBRL* receptors in Sorghum shoots under control conditions using 12-day-old BTx623 Sorghum plants.

Prior to our main investigation, we assessed the quality of our sample treatments and the effectiveness of the technique by performing hybridization with RNA probes previously reported in maize for the *PLASTOCHRON 1* (*ZmPLA1*) and *ANGUSTIFOLIA3* (*ZmAN3/GIF1*) genes (Laureyns et al., 2022). To ensure the reliability of the test, we conducted a Nucleotide Blast analysis of the maize probes against the Sorghum genome, confirming their specificity for Sorghum homologs with 100% query coverage and 92% identity for *ZmPLA1*, and 100% query coverage and 96% identity for *ZmGIF1*. Consistent with the findings of Laureyns et al., 2022, we observed distinct expression patterns: *ZmPLA1* exhibited specific expression limited to the shoot

apical meristem (Figure 5.6b), while *ZmGIF1* displayed broader expression across all developing leaves (Figure 5.6a).

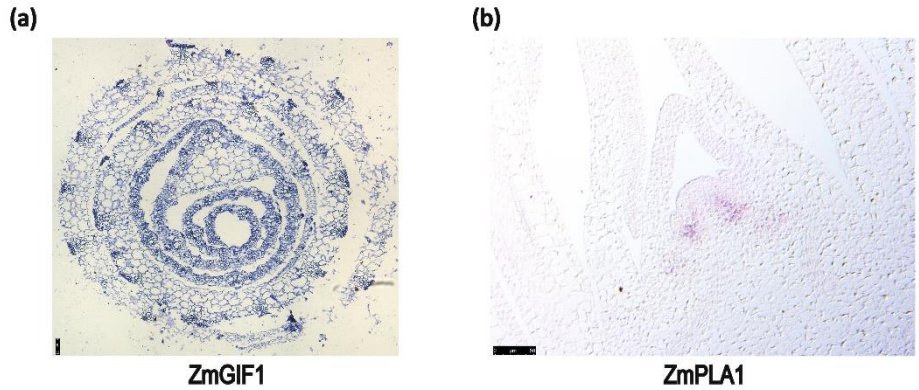


Figure 5.6 In situ hybridization of Zm*GIF1* and Zm*PLA1* RNA probes in Sorghum leaves and shoot apical meristem. (a) Sorghum shoots radial section showing *ZmGIF1* ubiquitous expression in all the developing leaves. Scale bar: 75 µm. (b) Sorghum shoot apical meristem transversal section showing *ZmPLA1* specific expression in the shoot apex. Scale bar: 50 µm.

Following the quality assessment, RNA probes were synthesized to target two 200 bp regions in the 5´ and 3´ UTR of *SbBRI1* and *SbBRL*. These probes were then used in RNA in situ hybridization experiments conducted on radial sections of Sorghum shoots and transverse sections of the Sorghum shoot apical meristem. The results revealed ubiquitous expression of *SbBRI1* throughout the developing leaves, with expression also detected in the shoot apical meristem (Figure 5.7a, 5.8b).

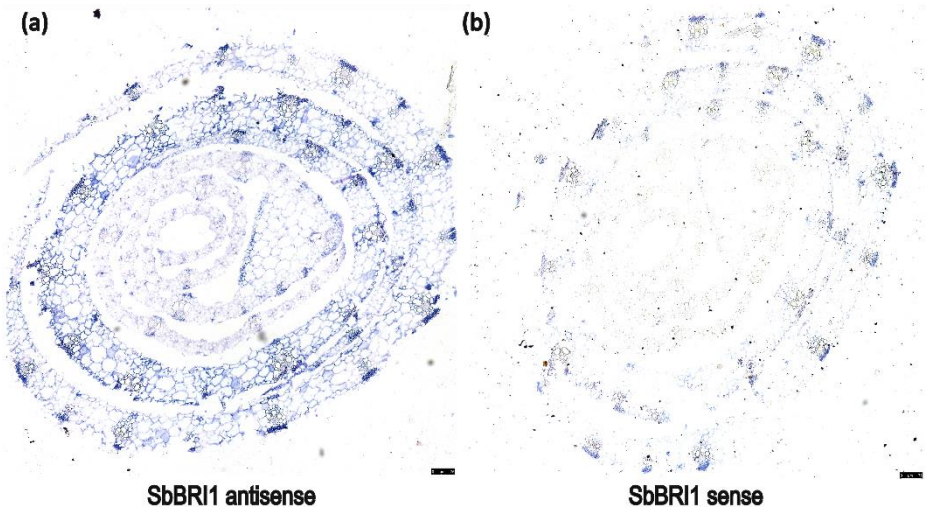


Figure 5.7 In situ hybridization of Sb*BRI1* shows *BRI1* ubiquitous expression. (a) Sorghum shoot radial section showing *SbBRI1* ubiquitous expression in all the developing leaves. Scale bar: 75 µm. (b) Sorghum shoot radial section showing the absence of expression by using the sense *SbBRI1* RNA probe. Scale bar: 75 µm.

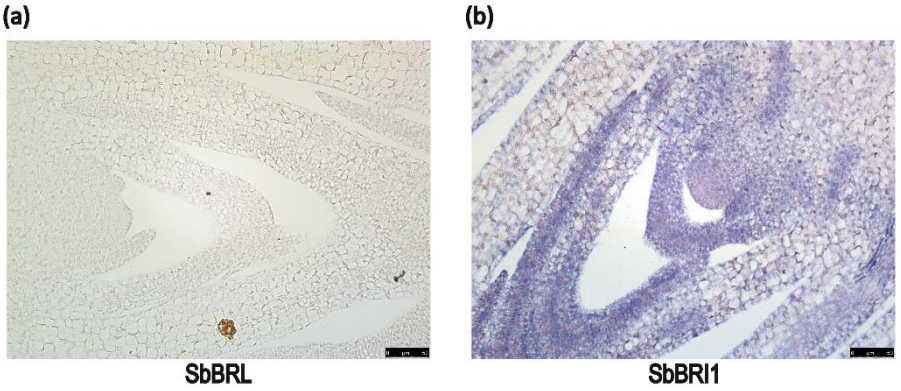


Figure 5.8 In situ hybridization of Sb*BRI1* and Sb*BRL* shows *BRI1* expression in the shoot apical meristem. (a) Sorghum shoot transversal section showing *SbBRL* absence of expression in the shoot apical meristem. Scale bar: 50 µm. (b) Sorghum shoot transversal section showing *SbBRI1* expression in the shoot apical meristem. Scale bar: 50 µm.

Importantly, it should be noted that in situ hybridization experiments using the sense probe exhibited background signal specifically in the dead and lignified sclerenchyma cells within the vascular bundles of the radial sections (Figure 5.7b, 5.9b, d).

In contrast to *SbBRI1*, *SbBRL* exhibited a distinct expression pattern in Sorghum shoots. Unlike *SbBRI1*, *SbBRL* was not detected in the shoot apical meristem; instead, it displayed enriched expression in the vascular bundles, particularly within the phloem and vascular bundle sheath (Figure 5.9c). Additionally, *SbBRL* expression was observed in the mesophyll cells, indicating a broader expression pattern compared to the native domains of *AtBRL1/3* (Figure 5.9a).

Given the conserved tissue specificity of *SbBRL* in vascular tissues, our aim was to extend the insight gained from Arabidopsis, where overexpression of the vascular-specific *AtBRL3* receptor has demonstrated drought tolerance without growth penalties (Fàbregas et al., 2018), to Sorghum. To accomplish this, we standardized the protocol for stable genetic transformation of Sorghum, as this procedure is not well-established in Europe.

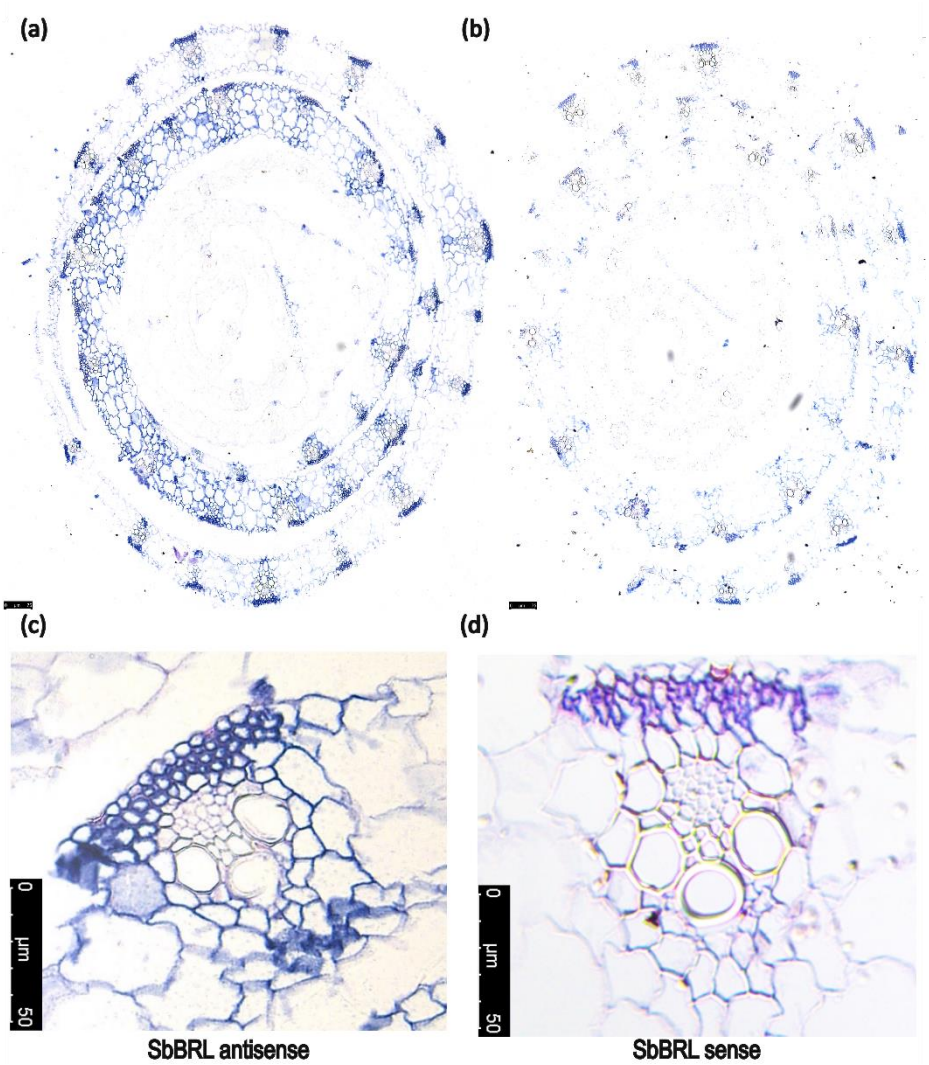


Figure 5.9 In situ hybridization of Sb*BRL* shows *BRL* enriched expression in the vascular bundle. (a, c) Sorghum shoot radial section showing *SbBRL* enriched expression in the vascular bundles, specifically in the phloem and the vascular bundle sheath, and in the mesophyll cells. Scale bar: 75 and 50 μm. (b, d) Sorghum shoot radial section showing the absence of expression by using the sense *SbBRL* RNA probe. Scale bar: 75 and 50 μm.

5.3.2 Optimizing conditions of Optical Density (OD) of Agrobacterium, co-cultivation time and temperature

In this study, we conducted an optimization of Agrobacterium infection by using the Agrobacterium strain EHA105 recA^{-} containing the ternary helper vector pVS1-VIR2. We evaluated adjustments of several factors: the optical density (OD) of the Agrobacterium culture, co-cultivation time, and temperature for co-cultivation. These adjustments were made to avoid Agrobacterium overgrowth, minimize the duration of infection and enhance the efficiency of transformation. Additionally, we evaluated a more acidic pH of the media, as it has been associated with virulence gene induction and facilitation of T-DNA transfer (Yuan et al., 2008; Wang et al 2018).

To evaluate these parameters, we employed embryos derived from three distinct panicles. The infection procedure was applied uniformly to all embryos using a construct carrying Zm*Ubi*$_{pro}$::*GUS* without the presence of morphogenic regulators. We tested different parameters during the experimentation: the OD of the Agrobacterium solution (0.3 and 0.7), co-cultivation incubation time (3 and 4 days), and incubation temperature (21 and 24 °C). Following the co-cultivation period of 3 or 4 days, embryos were transferred to resting media. Subsequently, 7 days after infection, GUS staining was carried out to assess the delivery of DNA (Figure 5.10a-h). This time frame allowed for the detection and visualization of the *GUS* gene expression, serving as an indicator of DNA transfer and integration.

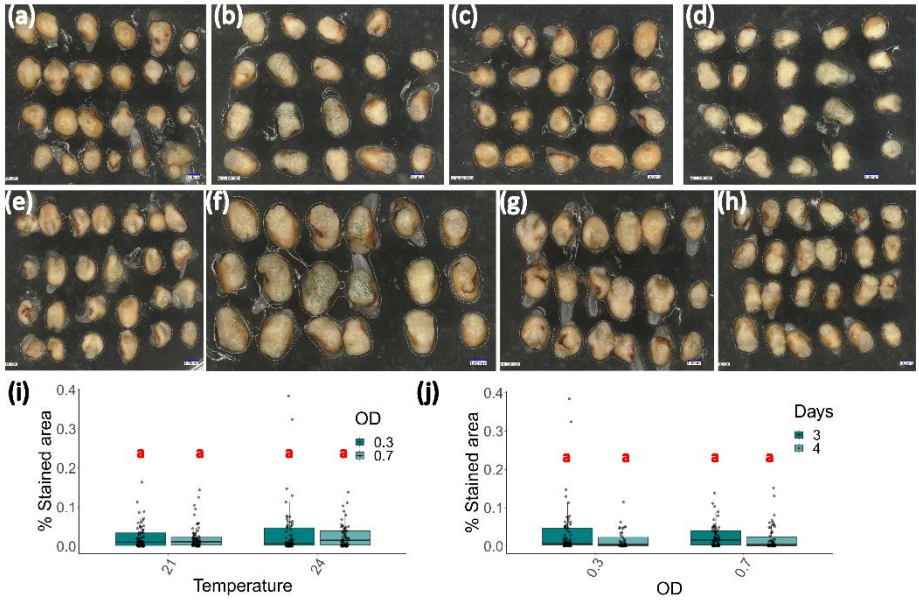


Figure 5.10 GUS-stained calli and quantification for optimization of infection conditions. (a-h) GUS-stained calli with different condition of pH, Optical density, and temperature. (a) pH 5.2, OD 0.3 and 21°C. (b) pH 5.8, OD 0.3 and 21°C. (c) pH 5.2, OD 0.7 and 21°C. (d) pH 5.8, OD 0.7, 21°C. (e) pH 5.2, OD 0.3 and 24°C. (f) pH 5.8, OD 0.3 and 24°C. (g) pH 5.2, OD 0.7 and 24°C. (h) pH 5.8, OD 0.7 and 24°C. (i, j) GUS quantification in GUS-stained percentage of callus growing at pH 5.8. Different letters represent statistical differences (p-value<0.05) in ANOVA plus Tukey´s HSD test.

Despite the reported enhancement of Agrobacterium virulence under acidic pH conditions, our observation revealed that embryos subjected to pH 5.2 during co-cultivation exhibited reduced callus development and no detectable *GUS* expression (Figure 5.10a, c, e and g).

Following the quantification of *GUS* expression levels (Figure 5.10i-j), a discernible trend emerged: greater expression was observed at OD 0.3 compared to OD 0.7, and at 3 days compared to 4 days. Nonetheless, an elevation in temperature (21 vs 24°C) did lead to a noticeable inclination towards enhanced GUS expression levels. However, it is worth noting that at 24 °C, favorable infection levels were achieved without encountering the anticipated problem of Agrobacterium overgrowth in

the co-cultivation or resting period, which might occur if these cultures were maintained at 28°C.

Hence, the optimized parameters for transformation consisted of a pH value of 5.8 for co-cultivation, an *Agrobacterium* OD of 0.3 and 3 days of co-cultivation period at 24 °C (Figure 5.10f).

5.3.3 Excision-based transformation system

Our novel methodology consists of two fundamental components. The primary element encompasses the excisable morphogenic gene cassette, with flanking loxP recombination sites, and three expression cassettes: *Axig1*$_{pro}$::*ZmWus2* and *Pltp*$_{pro}$::*ZmBbm* for morphogenic regulator expression, and *Glb1*$_{pro}$::*MoCRE* for recombinase expression, which facilitates cassette excision upon abscisic acid (ABA) induction. Notably, we employ non-constitutive promoters, maize phospholipid transferase protein promoter (*Pltp*$_{pro}$) driving *Bbm*, and auxin-inducible promoter (*Axig1*$_{pro}$) driving *Wus2*. The secondary element remains non-excised and houses the gene of interest (GOI), complete with its respective promoter and terminator, alongside the *nptII* selection marker (Figure 5.3a). It is noteworthy that the pVS1-VIR2 ternary vector, in conjunction with the *GRF4-GIF1* morphogenic regulator, has been documented to boost sorghum transformation efficiencies (Li et al., 2024). In line with this finding, we utilized the pVS1-VIR2 ternary vector along with a compatible binary destination vector, pG3K-WO-AG harboring the morphogenic regulators *ZmBbm* and *ZmWus2* together with a GreenGate-compatible cloning site.

The transformation process follows the workflow illustrated in Figure 5.1. Initial steps involve a co-cultivation period, previously optimized to enhance Agrobacterium T-DNA integration, followed by a resting period. During both phases, the presence of 2,4-D induces the expression of *Wus2*, initiating together with *Bbm* proembryo formation as early as 7 DAI (Figure 5.3c). Proembryos are characterized by the appearance of proliferative bulges at the scutellum epithelium (Wehbi et al., 2022). Notably, somatic embryo formation occurs as early as 14 DAI, with somatic embryos observed in the globular and scutellar stages (Figure 5.3d). Additionally, friable callus type II forms within the embryogenic tissue, where *GUS* expression is concentrated. This feature enables the initiation of *Bbm/Wus2* cassette excision as early as 21 DAI, mitigating their adverse effects in T0 plants. During this stage, transgenic cell proliferation and the presence of somatic embryos in the coleoptilar stage are evident (Figure 5.3e).

Following somatic embryo induction, calli are sub-cultured on culture media containing G418 selection (100 mg/L). In this media, the presence of ABA induces *MoCRE* expression, facilitating cassette excision. This step aims to maximize transgenic somatic embryos and excise morphogenic regulators, thereby facilitating transgenic embryo maturation and germination while minimizing non-transgenic embryo formation. The induction of excision at early somatic embryo stages allows for a substantial proportion of morphogenic regulator-free transgenic plantlets, achieving an excision efficiency of 67.7% based on one biological replicate (Table 5.5). After 14 days of sub-culture, the calli become highly friable, and a substantial number of somatic embryos have already germinated, exhibiting embryonic shoots and roots (Figure 5.3f). At this juncture, we increase the selection pressure (250 mg/L

G418) to ensure transgenic shoot formation and minimize escape frequency, achieving an average escape frequency of 1% based on two biological replicates (Table 5.5).

Table 5.5 Transformation efficiency, escape frequency and excision efficiency in Sorghum transformation protocol.

Genotype	Number of starting embryos	Embryos with at least one regenerated shoot (Efficiency percentage)	Total isolated plantlets (Efficiency percentage)	Number of escapes (Escape frequency)	MoCRE pressence on the analyzed plantlets (Excision efficiency)
TX430	250	77 (30.8%)	415 (166%)	6 (7%)	63 / 93 (67.7%)
TX430	125	29 (23.2%)	203 (162.4%)	0 (0%)	Not available

Finally, germinated somatic embryos are transferred to rooting media, where they spend two weeks under light conditions, inducing root formation and chlorophyll accumulation (Figure 5.3g, h). The total duration of the protocol is reduced to 66 days (Figure 5.1), compared to the 12-16 weeks required by conventional Agrobacterium or particle bombardment-based methods that do not incorporate morphogenic regulators (Liu and Godwin, 2012; Zhao et al., 2000).

The optimization of infection conditions and the introduction of this novel sorghum transformation method, combining *Bbm* and *Wus2* morphogenic regulators together with the ternary vector pVS1-VIR2, have enabled us to achieve a highly efficient transformation protocol. We achieved transformation efficiencies of 28.3% (based on embryos producing at least one regenerated shoot) and 164.8% (based on the total number of isolated plantlets) (Table 5.5). Moreover, the adaptability of

this vector system to include the Cas9 protein and guide RNAs within the GOI cassette opens up possibilities for producing marker/transgene-free genomic edited plants, addressing emerging concerns regarding genetically modified organisms in accordance with European regulations. This represents a significant milestone in advancing plant biotechnology within the European scientific community.

5.3.4 Overexpression of *SbBRL* promotes leaf epinasty

The resultant regenerant plants overexpressing *SbBRL* were transferred to soil, and their phenotypes were evaluated. A low proportion of regenerants carried the morphogenic regulators cassette or escaped transformation, as indicated in Table 5.5. The phenotypes of these T1 plants were assessed to avoid attributing traits that were not directly caused by the overexpression of *SbBRL*. T1 Sorghum plants carrying the morphogenic regulators exhibited pleiotropic defects in plant development, including dwarfism and absence of flowering (Figure 5.11b). Conversely, the escape plants did not display any remarkable phenotypes compared to Tx430 WT plants, except for their more vigorous growth (Figure 5.11a).

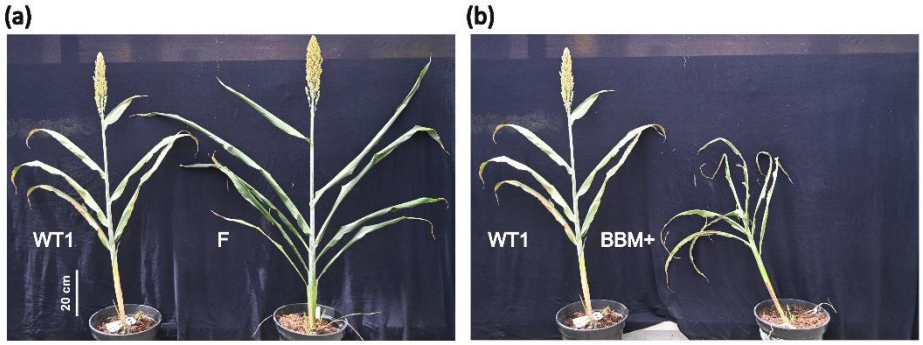


Figure 5.11 Presence of non-excised morphogenic regulators and escapes. Phenotypes observed in *ZmUbi::SbBRL-GFP* Sorghum transgenic plants carrying the morphogenic regulator cassette (b) and escapes (a).

When evaluating the phenotypes of the Sorghum *SbBRL* overexpressor T1 plants, we observed a drastic epinastic growth of the leaves and the absence of growth penalization compared to WT plants (Figure 5.12b). Additionally, we noted a reduction in yield attributed to a decrease in panicle size or grain number, indicating a lower fertility rate (Figure 5.12c). Despite confirming these plants as *SbBRL* overexpressors by PCR (Figure 5.4) or through confocal visualization of membrane-localized fluorescent protein in the roots (Figure 5.5), we sought to confirm proper protein translation in the organs exhibiting the drastic epinasty phenotypes. Therefore, total protein extracts from *SbBRL* T1 overexpressor leaves were subjected to western blot analysis using an anti-GFP antibody (Figure 5.12a). The analysis revealed the presence of the SbBRL-GFP fusion protein with the expected molecular size (129.234 KDa SbBRL + 27KDa GFP) (Figure 5.12a).

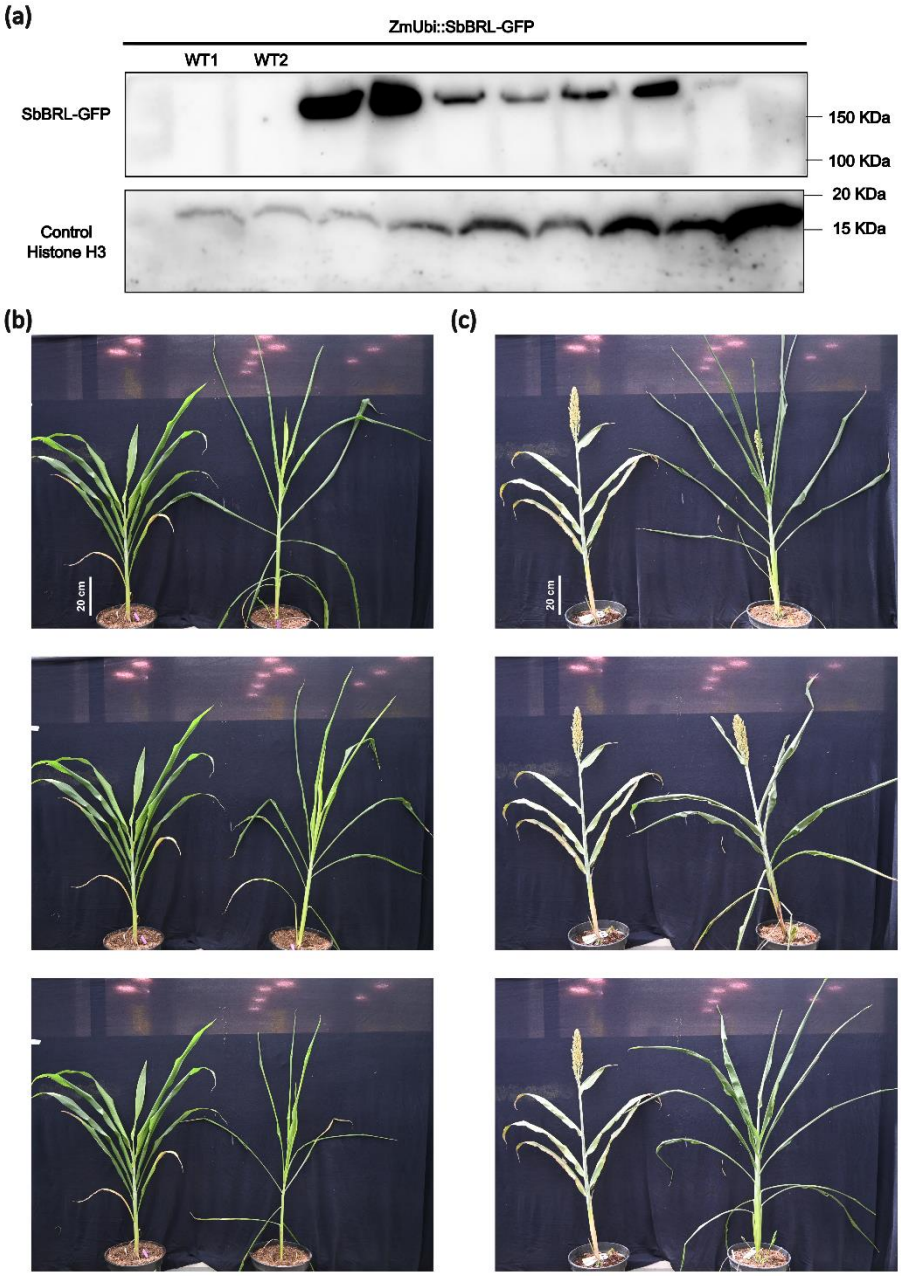


Figure 5.12 Sb*BRL* overexpressor plants show leaf epinasty phenotypes. (a) Western blot analysis was conducted using total protein extracts derived from ZmUbi::SbBRL-GFP Sorghum plants. Anti-GFP and anti-HIS3 antibodies were used for detection. Phenotypes observed in ZmUbi::SbBRL-GFP Sorghum transgenic plants at 1 month (b) and 3 months (c) after passing to soil the regenerants.

Finally, to further validate the functional role of the SbBRL-GFP fusion protein in sensing brassinosteroid hormones, roots from *SbBRL* T1 overexpressor plants were treated with BL. Upon BL treatment, the SbBRL-GFP protein exhibited significant internalization compared to non-treated roots (Figure 5.13).

Altogether, these results confirm that SbBRL is effectively overexpressed and functional across all plant organs and that its overexpression leads to leaf epinasty and a reduction in plant yield.

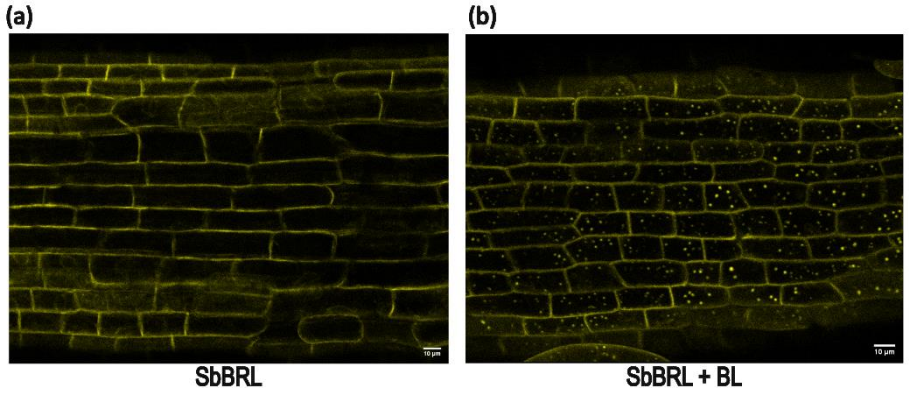


Figure 5.13 SbBRL protein is internalizing upon BL treatment. Confocal imaging pictures of transgenic roots with integrated SbBRL-GFP protein. Yellow channel (GFP) shows the localization of SbBRL protein. Scale bar: 10 μm.

Chapter 6

GENERAL DISCUSSION

6.1 Studying and engineering *BRL3* promoter to enhance abiotic stress adaptation in *Arabidopsis thaliana*

Cis-elements or introns located in proximal promoter regions are highly conserved across organisms and play a crucial role in driving gene expression and tissue specificity (Kim et al., 2006; Gallegos et al., 2017). Consistent with this, phylogenetic shadowing analysis of the *BRL3* promoter reveals conservation of the proximal promoter region, comprising -1000 bp from the transcription start site, across different *Brassicaceae* species (Figure 2.3a). Furthermore, a conserved 100 bp region between -855 and -755, shared by the vascular-specific BR receptors BRL1 and BRL3, is responsible for *BRL3* vascular expression (Figure 2.3b, 2.5). This reinforces the importance of core promoter *cis*-elements near the transcription start site for vascular-specific *BRL3* expression. We infer that this region is crucial for BRL3's role in abiotic stress adaptation, such as thermomorphogenesis and drought stress tolerance, as well as in vascular differentiation, due to the implication of BRL3 in these processes from the vasculature (Caño-Delgado et al., 2004; Fàbregas et al., 2013; Fàbregas et al., 2018; Gupta et al., 2023).

The removal of the 100 bp region resulted in the abolition of *BRL3* expression in the vasculature, suggesting the presence of transcriptional activators binding to *cis*-elements within this specific region. *In silico* analysis of this region identified HD-ZIP III TFs as putative mediators of its vascular expression. Therefore, we hypothesized that HD-ZIP III TFs could act as activators of *BRL3* expression.

HD-ZIP III TFs, a family composed of five members including HB15/CORONA, HB9/PHAVOLUTA, HB8, REVOLUTA, and PHABULOSA, are expressed in vascular cells and negatively regulate vascular cell division (Carlsbecker et al., 2010). Subsequent studies found that HD-ZIP III TFs increase BR levels through the transcriptional activation of BR biosynthesis genes and suppress periclinal division of stele vascular cells within the root apical meristem (Ohashi-Ito et al., 2023). In our study, we focused on the contribution of HB15 to *BRL3* expression, as DAP-seq analysis showed HB15 binding to this motif (O'Malley et al., 2016). Contrary to our expectations, we found that *BRL3* expression is repressed by HB15 TF through direct binding to the *BRL3* 100 bp *cis*-element responsible for vascular expression (Figure 2.12). Although *HB15* overexpression resulted in the downregulation of *BRL3* expression, *hb15* mutation was not sufficient to induce *BRL3* expression throughout the plant vasculature (Figure 2.13), suggesting the involvement of additional transcriptional repressors. Supported by several studies reporting that HD-ZIP III TFs act redundantly in various biological processes, such as vascular cell proliferation (Carlsbecker et al., 2010), we also found that *BRL3* expression is repressed by other HD-ZIP II TF binding to the same specific region, such as HAT9 (Figure 2.13).

However, we have yet to identify the transcriptional activators that could bind to this region. For instance, a study by Ohashi-Ito et al. (2023) identified a promoter region with HB15 and PHAVOLUTA binding sites predicted by DAP-seq analysis, but only PHAVOLUTA was found to be transcriptional activator. This further reinforces that HD-ZIP III TFs, even with redundant biological roles, can act as either repressors or activators of transcription. Given that PHAVOLUTA (also known as

HB9) could be a potential transcriptional activator, as predicted by the BRL3 promoter in silico analysis (Figure 2.1), we hypothesize that HD-ZIP III TFs tightly coordinate *BRL3* expression in the root vasculature, inferring a putative role for BRL3 in vascular differentiation or vascular cell divisions in the stele of the root meristem.

This hypothesis is corroborated by the CRISPR-mediated genetic engineering of the *BRL3* promoter, where deletion of the HATs *cis*-element resulted in upregulation of *BRL3*, while deletion of the HD-ZIP III *cis*-element did not increase expression, suggesting that HD-ZIP III TFs other than HB15 could be involved in *BRL3* activation (Figure 2.14). Further studies on PHAVOLUTA-mediated *BRL3* transcriptional regulation or *BRL3* root expression levels in T3 homozygous *BRL3* promoter-edited plants could further validate these hypotheses.

Besides the regulation of *BRL3* expression in the vasculature, we also identified several *cis*-elements involved in the regulation of *BRL3* expression in the root meristem. Our results indicate that *cis*-elements within the -1719 to -1415 region are essential for *BRL3* expression in the QC cells (Figure 2.7). Within this region, *in silico* analysis identified several components of the BR signaling and DNA damage response pathways, such as MYB56 (BRAVO; Villarrasa-Blasi et al., 2014), BES1 and BZR1, and ERF115 (Heyman et al., 2013).

The BRL1/BRL3/BAK1 complex has been shown to promote QC cell division activity upon BL treatment (Fàbregas et al., 2013), suggesting an important role for BRL3 in promoting cell division in this specific tissue. Furthermore, BRL3 is required for ERF115-mediated QC cell divisions upon DNA damage (Takahashi et al., 2024). BRs have been shown to induce *ERF115* expression in the QC, thereby promoting QC

cell divisions (Heyman et al., 2013). The presence of an ERF115 binding site in the region necessary for *BRL3* QC expression suggests that proper expression levels of *BRL3* in the QC, assured by ERF115, are necessary to sense DNA damage and respond by inducing *ERF115* expression, thus promoting QC divisions.

Additionally, BES1 and BZR1 have been shown to bind to this specific region and downregulate the expression of *BRL3* (Salazar-Henao et al., 2016). This indicates a regulatory mechanism where *BRL3* expression is tightly controlled by both activation and repression signals.

In conclusion, our working model proposes that ERF115 ensures *BRL3* expression in the QC to sense DNA damage and induce *ERF115* expression in a positive feedback loop. Meanwhile, BES1 and BZR1 downregulate *BRL3* expression levels once the BR signal has been transduced. This dual regulation ensures that *BRL3* is expressed at appropriate levels to maintain QC cell function and promote cell division in response to environmental and internal cues.

The working model is further validated by the finding that *BRL3* is transcriptionally induced upon DNA damage (Figure 2.10). The presence of the ERF115 *cis*-element was essential for inducing *BRL3* expression in the QC cells and ectopically, further supporting the idea that ERF115 directly binds to the *BRL3* promoter to enhance its QC expression. Additionally, the SOG1 *cis*-element, located in the -567 promoter region, is also required for *BRL3* induction in the meristem region, specifically in the vascular initials, aligning with other studies (Takahashi et al., 2024).

These results suggest that proper regulation of *BRL3* expression in the root meristem, under both control and DNA damage conditions, requires

the coordinated action of ERF115 and SOG1. ERF115 ensures *BRL3* expression in the QC cells, allowing the detection and response to DNA damage, while SOG1 contributes to *BRL3* regulation in the meristem vascular initials, highlighting a complex interplay between these TF to maintain *BRL3* expression and function in the root meristem.

In addition to *BRL3* upregulation upon DNA damage, we also observed its upregulation in response to elevated temperatures. BRL3 is known to be crucial for responding to elevated temperatures, including promoting hypocotyl and petiole elongation, a function mediated by phloem cells (Gupta et al., 2023). Interestingly, we observed differential regulation of *BRL3* expression in the shoot and root. Elevated temperatures activated *BRL3* expression in the hypocotyl vasculature but inhibited it in the root vasculature (Figure 2.8). This correlates with the different responses of roots and hypocotyls to elevated temperatures. While elevated temperatures clearly induce hypocotyl elongation, their effect on root elongation is variable, promoting elongation in Arabidopsis while reducing it in wheat (Gray et al., 1998; Martins et al., 2017; Benlloch-Gonzalez et al., 2014).

These findings support the hypothesis that *BRL3* expression is induced in the hypocotyl vasculature, where it triggers epidermal cell elongation from the phloem, while its repression in the root does not significantly impact root growth. Analysis of promoter deletion lines identified a region between -1415 and -1194 bp responsible for this differential expression upon elevated temperatures. In silico analysis identified the *cis*-element responsible for KUA1 binding within this region (Figure 2.9). KUA1, also known as MYBH, is a light signaling component negatively regulated by light. In the dark, KUA1 induces cell and

hypocotyl elongation via increased PIF4 TF activity (Kwon et al., 2013). KUA1 has also been found to induce cell expansion (Lu et al., 2014).

Therefore, these findings suggest that KUA1 could mediate the upregulation of *BRL3* in the hypocotyl under elevated temperatures or dark conditions, leading to cell expansion and thus promoting hypocotyl or petiole elongation.

BRL3 has also been shown to be important for drought adaptation in the vascular tissue, where it regulates the transcription of several osmoprotectant biosynthesis enzymes, promoting the accumulation of raffinose, trehalose, and proline (Salazar-Henao et al., 2016; Fàbregas et al., 2018). However, in this study, we report for the first time that *BRL3* is also expressed in the stomata, specifically in the guard cells (Figure 2.6). This finding further validates the role of BRL3 in drought adaptation and suggests its involvement in stomatal closure, a critical mechanism to prevent rapid water loss and death under drought conditions (Martin-StPaul et al., 2017).

In conclusion, our study underscores the critical role of conserved *cis*-elements within the proximal promoter region in regulating *BRL3* expression, essential for its functions in abiotic stress adaptation. The identified 100 bp region is crucial for *BRL3*'s vascular-specific expression, mediated by interactions with HD-ZIP II and III TFs, including both repressors like HB15 and HAT9, and potential activators such as PHAVOLUTA. Furthermore, we elucidate the intricate regulatory mechanisms involving ERF115 and SOG1 in the root meristem, ensuring *BRL3* expression in response to DNA damage and environmental cues. The differential expression of *BRL3* in response to elevated temperatures highlights its role in hypocotyl elongation,

mediated by the KUA1 *cis*-element. Additionally, the novel discovery of *BRL3* expression in guard cells expands its known function in drought adaptation by implicating it in stomatal closure. These findings provide a comprehensive understanding of the multifaceted regulatory network governing *BRL3* expression and its vital roles in plant development and stress responses.

6.2 BRL3 downstream transcription factors modulate drought stress tolerance in *Arabidopsis thaliana*

The interplay between ABA and BRs is crucial in regulating plant growth and drought tolerance, with evidence suggesting antagonistic interactions between the two hormone pathways. This crosstalk initiates at the receptor level, where the remorin gene *OsREM4.1*, upregulated by ABA, negatively regulates BR signaling by interacting with OsSERK1, thus impeding its interaction with OsBRI1 (Gui et al., 2016). ABA further counteracts BR signaling by inhibiting BES1 dephosphorylation and BR-responsive gene expression, particularly at BIN2 or upstream levels (Zhang et al., 2009). The dual role of BIN2, in negatively modulating BR signaling while promoting ABA signaling (Cai et al., 2014; Hu and Yu, 2014), and that of BES1, in interacting with other TFs to inhibit ABA-mediated stress responses (Ye et al., 2017; Xie et al., 2019), have been previously discussed.

Interestingly, despite the antagonistic relationship between ABA and BRs, BR application or upregulation of BR biosynthetic genes has been shown to enhance drought tolerance (Kagale et al., 2007; Anjum et al., 2011; Shani et al., 2016). While overexpression of *BRI1* or constitutive

activation of BES1 renders plants susceptible to drought (Ye et al., 2017; Nie et al., 2019), overexpression of *BRL3*, confers drought tolerance (Fàbregas et al., 2018). This suggests the involvement of a BRL3-mediated BR signaling pathway, potentially through non-canonical signal transduction via BES1, in promoting drought stress adaptation.

BRL3 exhibits tissue-specific expression, primarily in the phloem pole pericycle, root meristem (QC and protophloem), and guard cells, whereas BRI1 shows ubiquitous expression (Figure 2.5, 2.6; Caño-Delgado et al., 2004; Fàbregas et al., 2013; Salazar-Henao et al., 2016). While *brl3* mutants display no discernible phenotypes in root or shoot growth, they exhibit conditional phenotypes in abiotic stress adaptation, such as thermomorphogenesis responses and root hydrotropism under osmotic stress conditions (Gupta et al., 2023). This suggests that BRL3, from its native expression domain, could be involved in stress adaptation, whereas BRI1, ubiquitously expressed, together with BES1, will be involved in the control of growth in basal conditions (Planas-Riverola et al., 2019).

MYB96, MYB305 and HAT9, transcriptionally induced by BRL3 (Table 3.1), also exhibit tissue specificity overlapping with BRL3's native domains, such as the guard cells, in the case of MYB96 and MYB305 (Figure 3.5, 3.12), and the phloem pole pericycle, in the case of MYB305 and HAT9 (Figure 3.13, 3.20). Overexpression of *BRL3* or its downstream TFs results in improved drought adaptation, further confirming their functional relevance in stress response (Figure 3.7, 3.14, 3.22).

ABA and BRs have been previously described as positive regulators of stomatal closure, well known mechanism to cope with drought stress (Ha

et al., 2016). The ABA or *BRL3* overexpression induces transcriptionally MYB96 and MYB305 (Seo et al., 2009; Cheng et al., 2022; Table 3.1), and their specific expression in the guard cells, position these TFs as putative regulators of stomata aperture during drought stress adaptation. In addition, BR-mediated stomatal closure it is dependent on NADPH oxidase activity (Xia et al., 2014), and BR treatment induces transcriptionally *RBOHD* expression, increasing ROS in the stomata (Ha et al., 2016), and apoplastic hydrogen peroxide (Zhou et al., 2014), important mechanism for adaptation to drought, heat stress and oxidative damage. Interestingly, while analyzing RNA-seq and DAP-seq data, we observed that these MYB TFs were controlling the expression of genes involved in the reactive oxygen species productions, such as RBOHD in the case of MYB96, and PER4 in the case of MYB305 (Figure 3.11, 3.18). Taken together, these observations suggest that BR regulation of stomatal closure may be mediated by molecular mechanisms involving BRL3 and its downstream TFs MYB96 and MYB305, probably by modulating the ROS production in the guard cells.

Drought stress can also affect phloem transport because of viscosity build-up at the source tissues or by failing in the maintenance of cell turgor (Sevanto et al., 2014; Sevanto et al., 2018). The limitation of sugar loading in the phloem, during water scarcity, is a potential strategy to avoid excessive viscosity build-up, and allowing a better translocation of carbon assimilates (Stanfield et al., 2022). Overexpression of *BRL3*, under drought conditions, was resulting in a higher accumulation of osmoprotectants in the root, mainly composed of sugars, such as trehalose, sucrose, myo-inositol, and maltose, overcoming the limitations of sugar phloem loading under drought stress (Fàbregas et al., 2018). The co-expression of *BRL3*, *MYB305*, and *HAT9*, in the phloem

pole pericycle (Figure 3.13, 3.20), and their drought resistance phenotypes when overexpress (Figure 3.14, 3.22), suggest their putative role in regulating phloem transport under water limitation scenarios. In addition, long-distance phloem-transmitted asymmetric cytosolic Ca^{2+} signal is essential for water tracking, therefore regulating the root hydrotropism towards water availability (Shkolnik et al., 2018). Overexpression of *BRL3* and *HAT9* showed a higher hydrotropic response (Figure 3.21), reinforcing their role in phloem transport regulation. Root hairs are essential cells to increase the root surface for water uptake. Interestingly, sucrose, phloem-transported from source tissues, and ABA, regulate the root hair length, morphology, and density (Raya-Gonzalez et al., 2023). The induction of *HAT9* upon ABA treatment, specifically in the zone where the differentiation of atrichoblasts into trichoblasts occurs, thereby increasing root hair density (Figure 3.24), suggest again its role in phloem transport and root hair development, important processes in drought stress conditions.

Altogether, these results suggest that BRL3-mediated BR signaling, along with its downstream TFs MYB96, MYB305, and HAT9, may play critical roles in regulating stomatal closure, phloem transport, and root hydrotropism, thereby enhancing plant adaptation to drought stress.

The activity of BES1 and BZR1 TFs is tightly regulated by various post-translational modifications. In the absence of BRs, BIN2 kinase, a negative regulator of BR signaling, phosphorylates BES1 and BZR1, leading to their destabilization and subsequent degradation via the proteasome pathway (Li et al., 2002; He et al., 2002; Yin et al., 2002). This phosphorylation also prevents their binding to DNA and sequesters them in the cytoplasm through interaction with 14-3-3 proteins (Vert et

al., 2006; Gampala et al., 2007; Ryu et al., 2007). Upon BR presence, BIN2 is inactivated by BSUI phosphatase, allowing the dephosphorylation and activation of BES1 and BZR1 (Kim et al., 2009).

In our study, we observed a similar regulatory mechanism for MYB96, MYB305, and HAT9. MYB96 exhibited dual phosphorylation states, with BR signaling and BIN2 inhibition leading to its dephosphorylation (Figure 3.9). Conversely, inhibition of the proteasome resulted in the accumulation of its phosphorylated form (Figure 3.9). Same trend was observed in MYB305 and HAT9 (Figure3.16, 3.25), even we could not fully corroborate the dual phosphorylated states. These findings suggest that BRs induce the active dephosphorylated state of MYB96, MYB305, and HAT9 by inhibiting BIN2, while the phosphorylated forms are targeted for proteasome-mediated degradation.

Although proteasome-mediated degradation is typically driven by ubiquitination rather than phosphorylation (Kraft et al., 2010), our results suggest a potential mechanism whereby phosphorylation could promote the interaction of these TF with proteins involved in ubiquitin-mediated degradation pathways. For instance, BIN2-mediated phosphorylation of DSK2, ubiquitin receptor, enhances its interaction with ATG8, ubiquitin-like protein directing autophagosome formation and cargo recruitment, leading to autophagy-mediated degradation of BES1 (Nolan et al., 2017). Similarly, BIN2 phosphorylation of PUB40, a U-box ubiquitin E3 ligase, enhances its interaction with BZR1, promoting proteasome-mediated degradation (Kim et al., 2019). Thus, phosphorylation can indirectly drive ubiquitin-mediated proteolysis by facilitating the interaction of TFs with ubiquitin ligases.

The BR-induced dephosphorylation of MYB96, MYB305, and HAT9, along with their proteasome-mediated degradation in their phosphorylated state, suggests that phosphorylation may stabilize these TFs and facilitate their transcriptional activity, potentially through ubiquitin-mediated post-translational modifications. Indeed, MYB96 has been shown to undergo ubiquitination and proteasome-driven degradation by the RING-type E3 ligase MIEL1 (Lee et al., 2016), supporting the notion that ubiquitination may regulate the activity of these TFs, with phosphorylation potentially modulating their interaction with the ubiquitination machinery.

The functional modulation of TFs through protein-protein interactions is a crucial mechanism in the activation or repression of signal transduction (Singh et al., 2002; Alves et al., 2014). BES1 and BZR1 have been described to interact with many other TFs, in a synergistic or antagonistic manner, to regulate abiotic stress responses (Nolan et al., 2020). Interestingly, MYB96, MYB305, and HAT9 were found to interact specifically with BZR1 and not BES1 (Figure 3.10, 3.17, 3.26). While BES1 and its corresponding interactions have been widely associated with promoting growth at the expense of drought susceptibility (Ye et al., 2017; Xie et al., 2019), the role of BZR1 in this context remains elusive. This study marks the first report of the interaction between BZR1, and TFs involved in drought stress adaptation. Further investigation is needed to determine whether these interactions act antagonistically or synergistically. Nonetheless, these findings suggest that MYB96, MYB305, and HAT9 may cooperate with BZR1 to regulate drought stress responses through BRL3-mediated signal transduction.

In summary, the interplay between ABA and BRs is pivotal for plant growth and drought tolerance, with evidence supporting antagonistic interactions between these hormone pathways. Despite this antagonism, BR application enhances drought tolerance, suggesting a role for BR signaling in stress adaptation. BRL3, primarily expressed in vascular tissues, may be involved in the BR signaling-mediated stress adaptation, while BRI1 and BES1 will be involved in the control of growth in basal conditions. MYB96, MYB305, and HAT9, induced by BRL3, exhibit tissue-specific expression patterns overlapping with BRL3's domains, suggesting that they are downstream of the vascular-specific receptor. BRL3 signal transduction, through these TFs, may regulate processes such as stomatal closure and phloem transport during drought stress conditions. BR-driven dephosphorylation, through the inhibition of BIN2, regulates the stability of MYB96, MYB305, and HAT9 exhibiting similar regulatory mechanisms as BES1 and BZR1. Their interaction with BZR1, may further modulate their function in drought stress adaptation. In conclusion, our proposed model integrates ABA-BR crosstalk into a synergistic interaction by positively regulating the transcription and post-translational modification of MYB96, MYB305, and HAT9, thereby facilitating plant adaptation to drought stress (Figure 6.1)

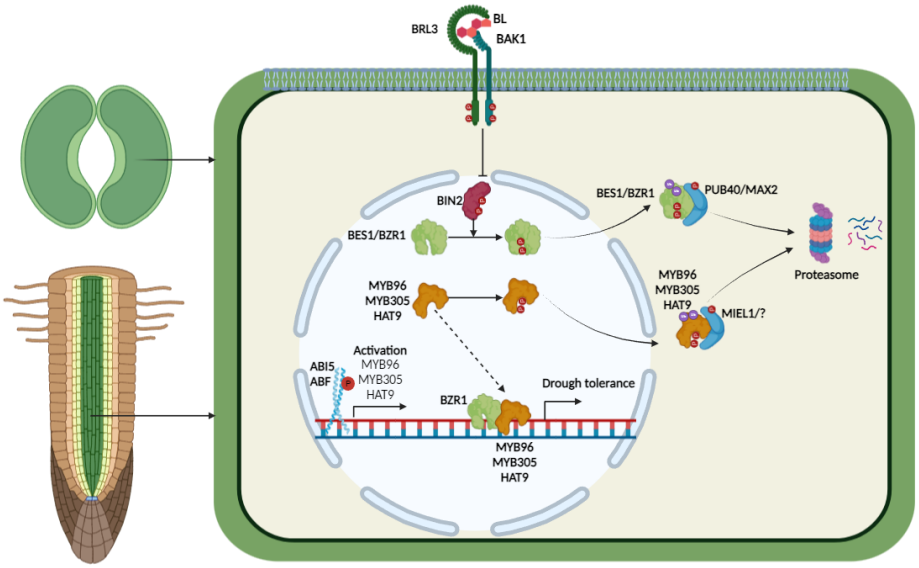


Figure 6.1 Working model of the activation of MYB96, MYB305, and HAT9 by BRL3 in guard cells and root vasculature. Upon drought stress, ABA and BRL3-mediated signaling activate MYB96, MYB305, and HAT9 transcriptionally. Additionally, BRL3 signaling inhibits BIN2, leading to the dephosphorylation of these TFs along with BES1 and BZR1. The dephosphorylated forms of MYB96, MYB305, and HAT9 then coordinate with BZR1 to modulate responses to cope with drought stress. Conversely, in the absence of BRs, the phosphorylated forms of these TFs are targeted for proteasome-mediated degradation, likely involving ubiquitination machinery.

6.3 Untargeted mutagenesis of brassinosteroid receptor SbBRI1 confers drought tolerance by altering phenylpropanoid metabolism in Sorghum bicolor.

Considerable research has delved into the role of BRs in plant adaptation to abiotic stresses. Nevertheless, an intricate regulation of drought responses arises depending on the way of modulating BR signaling. Notably, BR loss-of-function mutants, such as *bri1*, exhibit drought

resistance phenotypes attributed to reduced overall growth (Figure 4.2a), thereby reducing their susceptibility to drought (Figure 4.2b), a phenomenon known as “drought avoidance” (Fang et al., 2014). These BR-deficient mutants also exhibit a lower sensitivity to osmotic stress, resulting in a lower primary root growth reduction and osmotic-induced programmed cell death (Figure 4.1). In addition, complementation with the Sorghum BRI1 receptor, restores the sensitivity of Arabidopsis *bri1* mutants to osmotic stress (Figure 4.1). This complementation also correlates with an increased drought susceptibility, marked by a partial restoration of rosette area dwarfism (Figure 4.2). These findings imply that SbBRI1 shares conserved functions in terms of growth regulation and osmotic stress sensing.

The mechanism underlying the osmotic stress sensing could emerge through multiple pathways. Exposure to salt or osmotic stress increase reactive oxygen species concentration and may potentially lead to programmed cell death (Petrov et al., 2015). There is evidence suggesting that BRs interact with the reactive oxygen species signaling network, causing an increase in reactive oxygen species levels following exogenous applications in various organisms (Xia et al., 2014; Jiang et al., 2012; Zhu et al., 2013). Indeed, this BR-dependent reactive oxygen species induction was not triggered in *bri1-116* Arabidopsis mutants (Tian et al., 2018). Taken together, these observations suggest that the ability of the Sorghum BRI1 protein to sense osmotic stress in plants may be mediated by mechanisms involving reactive oxygen species production.

Conversely, the application of BRs has been shown to enhance tolerance to various abiotic stresses in maize, Arabidopsis, and *Brassica napus*

(Kagale et al., 2007; Anjum et al., 2011). Elevated BR concentration, as observed in DWF4 overexpressor plants, have also been linked to increased plant survival under drought stress in *Brassica napus* (Sahni et al., 2016). Our study reveals that the overexpression of different BR receptors in Arabidopsis yields distinct outcomes in drought stress adaptation, independent of growth promotion or arrest (Figure 4.2). Overexpression of the Arabidopsis or Sorghum BRI1 protein results in drought susceptibility uncoupled from growth promotion, while Arabidopsis BRL3 overexpressor plants showed drought resistance phenotypes (Figure 4.2). This suggests that the drought-tolerant phenotypes achieved through exogenous BR application, or the overexpression of biosynthetic enzymes are not primarily governed by the BRI1 signaling cascade but rather by BRL3 signaling. This finding aligns with previous studies wherein the overexpression of SlBRI1 in tomato led to increased hydrogen peroxide levels and heightened drought susceptibility, while the overexpression of BRL3 in Arabidopsis conferred an osmoprotectant signature in the root and drought tolerance (Nie et al., 2017; Fàbregas et al., 2018). In fact, BRI1 downstream signaling counteracts the ABA-mediated drought stress responses. BIN2 phosphorylates and stabilizes ABI5 and phosphorylates and activates SnRK2 to mediate ABA responses, while BR repress BIN2 activity (Hu et al., 2014; Cai et al., 2014). In contrast, application of 2,4-epibrassinolide improved drought tolerance in Nicotiana by upregulating BR-related genes as BRL3 (Khan et al., 2022).

It is important to highlight that both BRI1 and BRL3 receptors exhibit similarities within their respective signaling cascades. These similarities encompass elements such as BL perception and BAK1 heterodimerization (Caño-Delgado et al., 2004; Fàbregas et al., 2013),

and downstream processes, including BES1 dephosphorylation triggered by hormone perception or elevated temperatures (Yin et al., 2002; Gupta et al., 2023). Additionally, these two BR receptors share common phenotypical responses under condition of drought when constitutively expressed, where they display a less severe reduction of growth than WT plants (Xiang et al., 2021; Fàbregas et al., 2018). However, clearly divergent responses in terms of plant survival under extreme drought conditions, support a specific BRL3-mediated signaling pathway to address various abiotic stresses, as supported by our findings in Sorghum *Sbbri1* mutants. These plants exhibited heightened resilience to osmotic stress, evident in the mitigated reductions in shoot and root growth coupled with a lower reduction in root meristem (Figure 4.3). Remarkably, these BR-deficient mutants exhibited a higher drought tolerance, characterized by enhanced water usage and better photosynthetic performance. Nevertheless, during these seedling stage investigations, no discernible reduction was observed in root or shoot growth (Figure 4.3, 4.4). This absence of growth arrest contradicts the prospect of improved adaptability due to growth repression and suggests a direct negative role of BRI1 in abiotic stress adaptation.

Our data provides further evidence of the conservation of BRI1-downstream signaling in Sorghum. The SbBES1 TF downstream of SbBRI1 exhibits a conserved binding motif when compared to the Arabidopsis BES1 and BZR1 TF, leading to consistent transcriptional regulation of specific targets, particularly those involved in BR homeostasis (Figure 4.8c, d). Notably, it is essential to emphasize that most of the peaks identified in the genes associated with BR biosynthesis are located within the coding sequences (Figure 4.8f, 4.9c). These *cis*-elements found in the regions encoding amino acids, known as duons,

have previously been reported to function as transcriptional repressors of C4 genes (Reyna-Llorens et al., 2017). This suggests the negative transcriptional activity of SbBES1 on BR biosynthesis genes, aligning with the well-established concept of BR homeostasis driven by feedback inhibition of BR biosynthesis genes through the binding of Arabidopsis BES1 and BZR1 (He et al., 2005; Kim et al., 2006; Yu et al., 2011). Arabidopsis BES1 has also been related to the repression of ABA-mediated signaling upon drought stress, as observed in RD26 transcriptional repression or the cooperative action with WRKY46, WRKY54 and WRKY70 (Ye et al., 2017; Chen et al., 2017). Interestingly we could also find duons in genes related to categories such as “Response to water deprivation”, “Response to osmotic stress” and “Response to abscisic acid”, further suggesting the counteraction of SbBRI1 signaling through SbBES1 in ABA-mediated water stress responses (Figure 4.9c).

The present study, uncover that SbBES1 targets characterized by proximal promoter binding exhibited a significant enrichment in specific categories, including "Flavonoid biosynthesis," "Flavone and flavonol biosynthesis," and "Lignin biosynthesis" (Figure S4b). Notably, the downregulation of key components associated with early lignin formation, such as SbCCR and SbC4H, was observed in *Sbbri1* mutants. This downregulation was accompanied by decreased levels of lignin precursors, such as phenylalanine and its corresponding dipeptides (Figure 4.13a). These findings strongly suggest a positive regulation of lignin biosynthesis through the interaction of SbBRI1 signaling and SbBES1 transcriptional regulation, which aligns with prior research demonstrating lignocellulose accumulation in transgenic poplar through the overexpression of BR biosynthesis genes (Fan et al., 2020).

Furthermore, our study revealed that SbBES1 is associated with the inhibition of flavonoid biosynthesis under normal conditions, which corresponds to the observed overaccumulation of flavone in *Sbbri1* mutants (Figure 4.13a). This observation is consistent with earlier research in Arabidopsis, where defects in phenylpropanoid biosynthesis resulted in reduced lignin levels but an increased accumulation of flavonoids (Li et al., 2010). Additionally, under drought conditions, where active dephosphorylated BES1 is repressed to a greater extent (Chen et al., 2017), we noticed a trend towards further accumulation of flavonoids, including flavonoid-o-hexoside-2 (Figure 4.13a). These findings suggest that *Sbbri1* mutants exhibit enhanced photoprotection due to differential overaccumulation of flavones and flavonoids, a phenomenon previously reported to mitigate UV-B stress damage mediated by BES1 activity (Liang et al., 2020; Li et al., 2020). This, in turn, results in an improved photosynthetic rate under extremely dry conditions (Figure 4.5e, 4.6c).

In conclusion, our study unveils that the brassinosteroid receptor BRI1 pathway exerts a detrimental effect on drought tolerance. This effect is mediated through downstream SbBES1, which regulates phenylpropanoid transcription and mediates flavonoid and lignin production, contributing to improve photosynthetic efficiency (Figure 6.2).

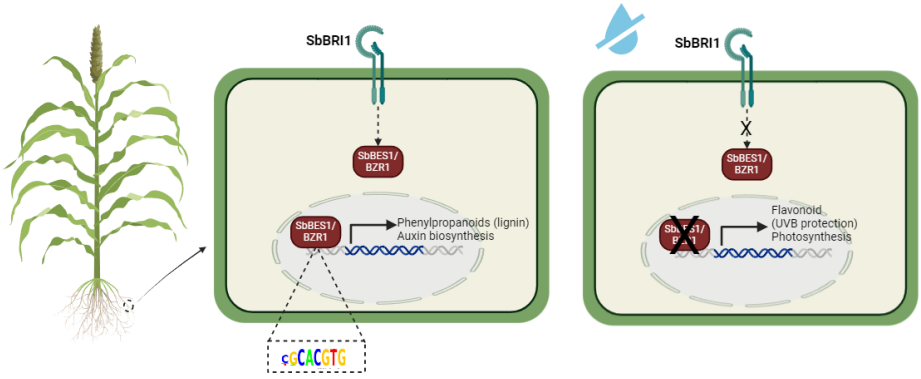


Figure 6.2 Working model of the Sorghum bicolor BRI1 receptor under control and drought stress conditions. Upon BR signaling sensed by SbBRI1 receptor, the SbBES1 TF promotes the activation of genes involved in phenylpropanoid and auxin metabolism. This activation positively regulates lignin content, contributing to overall plant growth and structural integrity. By modulating BRI1 receptor through EMS mutagenesis the signaling is compromised, leading to reduced activity of SbBES1. A less active SbBES1 triggers the activation of genes involved in flavonoid production. The increased flavonoid production provides UVB protection, enhancing the photosynthetic efficiency of Sorghum plants under drought stress conditions.

6.4 Enhancing expression of Sorghum BRL receptor via efficient Sorghum transformation using a ternary vector system combined with morphogenic regulators

Sorghum genetic transformation has historically faced challenges due to Sorghum's recalcitrance and low regeneration frequency (Belide et al., 2017). The adoption of Agrobacterium-mediated transformation has significantly improved regeneration frequencies, becoming the predominant transformation protocol, as evidenced by studies conducted by Anand et al. (2018), Che et al. (2018), Hoerster et al. (2020), Che et al. (2022), Johnson et al. (2023), and Wang et al. (2023). A common practice in monocot transformation studies involves the utilization of

LBA4404 Thy- Agrobacterium strains. This thymidine auxotrophic strain needs thymidine for its growth and proves advantageous in preventing excessive Agrobacterium proliferation during co-cultivation stages. The restricted growth of Agrobacterium, attributable to the absence of thymidine during the resting period, may contribute to the prolonged co-cultivation periods and elevated Agrobacterium solution OD observed in established Sorghum transformation protocols. However, the restricted availability of this strain poses limitations in the field of Sorghum transformation. In this study, we optimized Agrobacterium infection by employing the EHA105 strain, which is readily accessible but lacks thymidine auxotrophy, thus lacking the growth-limiting advantage. Through optimization, we demonstrated that reducing the co-cultivation temperature to 24°C—an intermediate temperature between common maize (21°C) (Aesaert et al., 2022) and Sorghum (28°C) (Aregawi et al., 2021) co-cultivation temperatures—and decreasing the co-cultivation duration to 3 days—a timeframe more akin to maize transformation protocols (Aesaert et al., 2022) compared to the 6 days typically employed in Sorghum transformation procedures (Aregawi et al., 2021)—effectively mitigates Agrobacterium overgrowth, facilitating proper infection and cassette integration. These adjustments align more closely with the framework employed in the latest published transformation protocols, further reinforcing the notion that reduced temperatures and incubation times are adequate for efficient Agrobacterium DNA delivery (Li et al., 2024). Further standardization of Agrobacterium infection revealed that, contrary to the reported enhancement of Agrobacterium virulence under acidic pH (Yuan et al., 2008; Wang et al., 2018), embryos subjected to a pH of 5.2 exhibited reduced callus development and no detectable GUS expression (Figure

5.10a, c, e, g). This indicates that pH is a limiting factor in callus cell proliferation and that a more acidic pH negatively impacts the plant material rather than improving the transfer of T-DNA in Sorghum immature embryos.

It is important to highlight that in our excision-based transformation system, we strategically incorporated morphogenic regulators, specifically BBM and WUS, known for their pivotal role in promoting somatic embryogenesis (Zuo et al., 2002; Lowe et al., 2016; Horstman et al., 2017; Chen et al., 2022). These regulators were driven by non-constitutive promoters: the maize phospholipid transferase protein promoter ($Pltp_{pro}$) for BBM and the auxin-inducible promoter ($Axig1_{pro}$) for WUS. This approach, proven effective in inducing somatic embryogenesis in maize (Jones et al., 2019), was adapted to enhance the somatic embryogenesis process in our Sorghum transformation protocol.

By integrating these morphogenic regulators into our protocol, we significantly simplified the transformation process, reducing the total duration to just 66 days. This represents a substantial improvement over conventional methods, such as Agrobacterium or particle-bombardment-based techniques that do not incorporate morphogenic regulators (Liu and Godwin, 2012; Zhao et al., 2000).

Significantly, our transformation methodology stands out for its incorporation of a binary vector containing the morphogenic regulators BBM and WUS, alongside the ternary helper vector pVS1-VIR2. This strategic combination, like the approach detailed by Li et al., 2024, has led to a remarkable 164.8% enhancement in transformation efficiency. This represents a substantial 2.36-fold increase compared to the previously reported highest Sorghum transformation efficiency (Che et

al., 2022). Notably, Li et al., 2024, achieved transformation efficiencies of 39.68% using a similar combination of GRF4-GIF1 with pVS1-VIR2, which closely aligns with our own achievement of 30.8% transformation efficiency with BBM and WUS. The development of this transformation technology has enabled us to genetically engineer BR receptors in Sorghum.

In monocot crops, the pursuit of semi-dwarf cereal cultivars to mitigate plant lodging has prompted research into brassinosteroid signaling, particularly focusing on mutations in the BRI1 receptor (Gruszka et al., 2020). The functional conservation of the BRI1 receptor has been demonstrated in several monocot crops, including maize, barley, and rice, where it plays crucial roles in plant growth, such as cell elongation, and various developmental processes, such as skotomorphogenesis (Kir et al., 2015; Chono et al., 2003; Yamamuro et al., 2000). However, knowledge regarding homologs of BR receptors in monocot species is limited. Despite this, BRL3 has been identified in Arabidopsis and shown to actively participate, in an antagonistic manner with BRI1, in the adaptation to various abiotic stresses, including elevated temperatures, osmotic stress, drought, elevated CO_2, and DNA damage responses (Gupta et al., 2023; Fàbregas et al., 2018; Takahashi et al., 2024). Given the current context of climate change, we aim to investigate further the role of BRL receptors in Sorghum.

BR receptor homologs have been identified in Sorghum, including homologs for BRI1 and BRL2, along with a single homolog for BRL1 and BRL3 (Blasco-Escámez et al., 2017). However, it is not known if the tissue specificity of the BR receptors is conserved in Sorghum, which could indicate differential functions of these receptors. In Arabidopsis,

while BRI1 is ubiquitously expressed, the other functional receptors, BRL1 and BRL3, exhibit tissue-specific expression, predominantly in the vascular tissues and the root meristem (Caño-Delgado et al., 2004; Fàbregas et al., 2013; Salazar-Henao et al., 2016).

Further investigation of the BRL3 native domain in Arabidopsis revealed expression in the stomata (Figure 2.6).

In this study, we confirmed the expected tissue-specific expression of SbBRL, the Sorghum homolog of Arabidopsis BRL1 and BRL3, which is enriched in shoot vascular bundles, particularly in the phloem and the vascular bundle sheath (Figure 5.9). Interestingly, the expression of SbBRL was absent from the shoot apical meristem and the leaf primordia (Figure 5.8), whereas BRI1 was ubiquitously expressed in the shoot apical meristem, leaf primordia, and more differentiated leaves (Figure 5.7, 5.8). However, in contrast to the native expression pattern of Arabidopsis BRL3 and BRL1, SbBRL exhibited mesophyll expression in the differentiated leaves of the P4 stage (Figure 5.9).

Given the positive role of Arabidopsis BRL3 in abiotic stress adaptation and the conservation of SbBRL in vascular-enriched expression, our objective was to overexpress SbBRL in Sorghum plants to potentially generate drought resistant crops without compromising overall growth. The successful overexpression of SbBRL was confirmed through PCR (Figure 5.4), confocal microscopy (Figure 5.5), and western blot analysis (Figure 5.12). Additionally, the internalization of SbBRL upon BR application was observed (Figure 5.13), a mechanism also documented in the BRI1 receptor in Arabidopsis, where BR perception triggers the ubiquitination and subsequent endocytosis of the BRI1 receptor (Zhou et al., 2018).

Remarkably, overexpression of SbBRL did not hinder overall growth but did induce leaf epinasty in Sorghum plants. Previous studies on tomato and Arabidopsis have also documented that BRL3 overexpression or BR application induces leaf epinasty, further supporting our phenotypic observations (Fàbregas et al., 2018; Schlagnhaufer et al., 1985). Leaf epinasty and stomatal closure are well-known mechanisms employed by plants in water deficit conditions to regulate water loss and prevent leaf overheating (Ruiz-Sanchez et al., 2020). This suggests that SbBRL, by regulating cell expansion, may contribute to the modulation of drought stress adaptation mechanisms to minimize water loss. Similar mechanisms have been observed in Arabidopsis, where BRL3 is capable of regulating cell expansion under elevated temperatures (Gupta et al., 2023).

By standardizing and enhancing Sorghum transformation, and overexpressing the vascular-enriched BR receptor SbBRL, as a proof of concept, we have enabled the generation of drought-resistant Sorghum plants through stable genetic transformation in Europe, addressing the challenges posed by climate change in crop production.

CONCLUSIONS

1. Tissue-specific expression of *BRL3* is intricately regulated by various *cis*-elements within its 5´ promoter region, and this expression is modulated by different environmental stresses and HD ZIP III TFs.

a. *Cis*-element regulation of tissue-specific expression

i. The 1719 – 1415 bp region (from the transcription start site) of the 5´ promoter is necessary for QC-specific expression

ii. The 1415-1194 bp region (from the transcription start site) of the 5´ promoter is necessary for vascular initials-specific expression

iii. The 855-755 bp region (from the transcription start site) of the 5´ promoter is necessary for vascular-specific expression

iv. The 755-384 bp region (from the transcription start site) of the 5´ promoter is necessary for protophloem-specific expression as previously reported by Salazar-Henao et al., 2016.

v. *BRL3* is specifically expressed in the stomata

b. Environmental stress regulation

i. *BRL3* expression is induced in the hypocotyl upon elevated temperatures, mediated by promoter

elements in the 1415-1194 bp region (from the transcription start site) of the 5´ promoter, where a KUA1 binding site was predicted by *in-silico* analysis.

ii. *BRL3* expression is induced in the QC and ectopically in the root meristem upon DNA-damage, mediated by promoter elements in the 1719-1415 bp region (from the transcription start site) of the 5´ promoter, where a ERF115 binding site was predicted.

iii. *BRL3* expression is induced in the vascular initials of the root meristem upon DNA-damage, mediated by promoter elements in the 755-384 bp region (from the transcription start site) of the 5´ promoter, where a SOG1 binding site was predicted and confirmed by Takahashi et al., 2024

c. HD-ZIP III and homeobox TFs regulation

i. HB15 TF acts as a negative regulator of *BRL3* expression by directly binding to the *BRL3* promoter region necessary for vascular expression in Arabidopsis.

ii. HAT9 is also a negative regulator of *BRL3* expression, as deducted by luciferase reporter assays and CRIPSR-mediated deletion of the *BRL3* promoter *cis*-element where HAT9 putatively binds, resulting in up-regulation of *BRL3* expression in the shoots.

2. **Overexpression of BRL3-regulated TFs MYB96, MYB305 and HAT9 confers drought tolerance in *Arabidopsis thaliana*.**

    a. MYB96, MYB305 and HAT9 are upregulated by the overexpression of BRL3 and co-localized with BRL3.

    b. Overexpression of MYB96, MYB305 and HAT9 results in high survival rates upon extreme drought

    c. BRs induce the protein stability of MYB96, MYB305 and HAT9, inhibiting their proteasome-mediated degradation.

    d. MYB96, MYB305 and HAT9 interact with BZR1 BR-related TF.

3. **Untargeted mutagenesis of SbBRI1 receptor confers drought and osmotic stress tolerance in *Sorghum bicolor.***

    a. BRI1 receptor is a negative regulator of drought stress as confirmed by overexpression and mutation in Arabidopsis and mutation in *Sorghum bicolor*.

    b. SbBRI1 regulates osmotic stress and drought stress in Sorghum bicolor

c. SbBES1 shows functional conservation in Sorghum bicolor and regulates brassinosteroid biosynthesis

d. Sorghum *bri1* mutants exhibit distinctive transcriptional regulation of photosynthesis and lignification

e. Sorghum *bri1* mutants are defective in the phenylpropanoid pathway

4. The use of morphogenic regulators in combination with ternary vectors system enhance the efficiency of Sorghum transformation.

a. The use of *Bbm* and *Wus2* in combination with the ternary vector system enhance the transformation efficiency of *Sorghum bicolor*

5. Sorghum BRL receptor is a vascular-enriched BR receptor and its overexpression results in leaf epinasty.

a. Sorghum BRL receptor is enriched in the vascular bundles, specifically in the vascular bundle sheath and the phloem.

b. Overexpression of *BRL* receptor results in leaf epinasty.

c. BL treatment enhances BRL receptor internalization

6. **This thesis demonstrates the effectiveness of using Arabidopsis screenings to identify molecular components of drought tolerance and the potential of Sorghum as a model cereal for translating research into agronomically valuable crops. By bridging basic and applied science, this work validates that findings in Arabidopsis can be successfully applied to enhance drought tolerance in important crops like Sorghum. This not only underscores the value of Arabidopsis as a genetic model but also highlights the practical implications for improving crop resilience in the face of climate change. Overall, this research paves the way for developing drought-resistant crop varieties, contributing significantly to agricultural sustainability.**

MATERIAL AND METHODS

Chapter 2: Studying and engineering BRL3 promoter to enhance abiotic stress adaptation in *Arabidopsis thaliana*

Plant material

The studies were conducted using Arabidopsis, Col-0. The genotypes utilized in this study included Col-0 WT (Col-0), and *athb15-1* (Du et al., 2015). BRL3 transcriptional reporter lines were created by constructing vectors containing the genomic promoter sequence of the TF (1415, 11941, and 855 bp from the ATG starting codon) fused to GUS GFP coding sequences in the pGWB632 backbone (developed by the Tsuyoshi Nakagawa laboratory), and subsequently transforming them into the Col-0. The BRL3 transcriptional reporter lines containing 1719, 1098, 755, and 384 bp promoter fragments were obtained from Salazar-Henao et al., 2016. *HB15* overexpressor lines were generated by constructing vectors containing the genomic coding sequence of the TF fused to GFP and driven by the constitutive 35S promoter in the pGWB405 backbone (also developed by the Tsuyoshi Nakagawa laboratory), followed by transformation into the Col-0.

Engineering BRL3 promoter by CRISPR-Cas9 system

Target pBRL3 mutants in the ATHB binding domain region were made by one round of CRISPR/Cas9-targeted mutagenesis using two sgRNAs

with guide sequences GGAATGTGAGATTAATAATT (gRNA1) and ACTAATCTTTACGTGAAAAG (gRNA2). To do so, we used the pDGE Dicot Genome Editing Kit form Stuttmann lab (Ordon et al., 2016; Stuttmann et al., 2021). The sgRNAs were inserted into the shuttle vectors pDGE332 for G1 and pDGE334 for G2 and both were then inserted into the binary vector pDGE666, containing both, Phosphinothricin (PPT) resistance selection and Fluorescence-Accumulating Seed Technology (FAST) red colorimetric selection. Binary vector pDGE666 was transformed by electroporation into Agrobacterium gv. 3101 and this was used for Arabidopsis floral dip transformation. After that, transformant T1 seeds were screened by FAST fluorescence selection in Stereomicroscope Olympus SZX16 using an RFP filter with 530-580 nm excitation and long path emission after 575 nm. Seeds were germinated in PPT for double verification and transferred to soil after 10 days. Adult plants were genotyped and screened for 1) modifications of the gRNA1 and 2) big deletion of the 45bp cassette between sgRNAs, that should modify the ATHB binding motifs. Finally, T2 seeds were collected and counter-screened against red fluorescence, keeping only the seeds that did not glow. Those seeds were CAS9 free and kept the T1 modifications that will be fixed in T3.

BRL3 promoter *in silico* analysis and phylogenetic shadowing.

We conducted an in-silico analysis of the 2Kb BRL3 promoter region using the RSAT (Turatsinze et al., 2008). RSAT employs statistical

inference to identify putative binding sites for TFs within the query sequence, also identifying CRERs. We utilized the 2Kb 5' upstream non-coding region of BRL3 and a series of TF position-based matrices retrieved from various databases, including Cis-BP, JASPAR, and DAP-seq (O'Malley et al., 2016). This analysis used a high-order degree Markov-chain background model (Thijs et al., 2001), applying a stringent significance threshold (p-value < 1e-5).

We also employed a phylogenetic shadowing strategy to discover conserved regions essential for BRL3 expression regulation across various species and within different Arabidopsis BR receptors of the same family (Castrillo et al., 2011). To achieve this, we compared the 2Kb promoter regions of BRL3 orthologs across six species within the Brassicaceae family: *Arabidopsis thaliana*, *Arabidopsis lyrata*, *Boechera stricta*, *Eutrema salsugineum*, *Capsella rubella*, and *Capsella grandiflora*. These sequences were retrieved from Phytozome (https://phytozome-next.jgi.doe.gov/) and aligned using the DiAlign software (Al Ait et al., 2013).

GUS staining

6-day-old seedlings were submerged in ice-cold acetone (90% v/v) and incubated for 20 min on ice. Subsequently, the acetone was rinsed twice with 1xPBS. The seedlings were then immersed in a GUS solution composed of 100mM sodium phosphate buffer (pH=7.2), 10mM sodium EDTA, 0.1% Triton X-100, 1mg/ml 5-bromo-4-chloro-3-indolyl-beta-D-glucorince (Xglu; Duchefa, Harrlem, NL), 10mM potassium

ferrocyanide, and potassium ferricyanide, and incubated at 37ºC overnight. After incubation, the seedlings were rinsed twice with 1xPBS and left overnight in 70% ethanol (v/v). Finally, the seedlings were mounted on slides, covered with chloral hydrate, and observed under a stereomicroscope the following day.

In the case of GUS staining in elevated temperature, seedlings were grown in half strength Murashige and Skoog media supplemented with vitamins and grown vertically in long day conditions (16 hours light [70µmol m^{-2} s^{-1}], 8 hours dark), at control (22 °C) or elevated (28 °C) temperature for 6 days. Subsequently, GUS staining was conducted following the protocol previously described.

In the case of GUS staining under DNA-damage, 5-day-old seedlings were treated with 2µg/ml of zeocin (Duchefa) for 24 hours. Subsequently, GUS staining was conducted following the protocol previously described.

The GUS quantification was performed as previously described in Bèziat et al., 2017.

Luciferase reporter assay

Nicotiana leaves were co-agroinfiltrated with both 35S::HB15-GFP or 35S::HAT9-GFP (effectors) and different BRL3 promoter deletion constructs driving the luciferase reporter gene (pBRL3(855bp)::LUC / pBRL3(755bp):.LUC / pBRL3(100bp vascular *cis*-element)::LUC). An empty binary vector was co-agroinfiltrated with the different BRL3

promoter deletion constructs as a control. Two days post-agroinfiltration, Nicotiana 0.5-cm-diameter leaf disks were harvested and placed in a 96-well plate containing 165 µl of 0.5× MS liquid medium and 35 µl of 1× D-Luciferin substrate (20 µg/ml; Promega). Luminescence was measured using a plate reader luminometer. Each well contained one leaf disk, with at least 12 replicate disks per sample. The average luminescence values were calculated to determine the activation of the BRL3 promoter by the effector constructs.

Chromatin immunoprecipitation assay

2 mg of 10-day-old 35S-HB15-GFP seedlings were collected. Chromatin immunoprecipitation assay was performed as described in Gendrel et al., 2005. Chromatin bound to HB15-GFP fusion protein was immunoprecipitated using Living Colors GFP Monoclonal Antibody (Clontech).

Detection by qPCR was performed on a LightCycler 480 System (Roche) using SYBR Green I master mix (Roche) in 96-well plate. The primers used for the ChIP-qPCR were:

pBRL3 Fw TGCACGAATACTATTAGGTGGGA

pBRL3 Rv AGAGGAGAAAAAGCTAAAGAAGACA

Chapter 3: BRL3 downstream transcription factors modulate drought stress tolerance in *Arabidopsis thaliana*

Plant material

The studies were conducted using Arabidopsis, Col-0 ecotype. The genotypes utilized in this study included Col-0 WT (Col-0), *brl3-2* (Caño-Delgado et al., 2004), and *35S::AtBRL3-GFP* (BRL3OX, Fàbregas et al., 2018). Mutant lines for BRL3-downstream TFs were obtained from the SALK institution (Table 3.2). Overexpressor lines were generated by constructing vectors containing the genomic coding sequence of the TF fused to GFP and driven by the constitutive *35S* promoter in the pGWB405 backbone (developed by the Tsuyoshi Nakagawa laboratory), followed by transformation into the Col-0. Transcriptional reporter lines were created by constructing vectors containing the genomic promoter sequence of the TF (2Kb upstream sequence from the ATG starting codon) fused to GUS and GFP coding sequences in the pGWB632 backbone (also developed by the Tsuyoshi Nakagawa laboratory), and subsequently transforming them into the Col-0 ecotype.

Thermomorphogenesis

For thermomorphogenic hypocotyl elongation analysis, seedlings were grown in half strength Murashige and Skoog media supplemented with vitamins and grown horizontally in long day conditions (16 hours light

[70µmol m^{-2} s^{-1}], 8 hours dark), at control (22 °C) or elevated (28 °C) temperature for 6 days and then photographed. Hypocotyl length was measured with ImageJ software.

Drought stress in adult plants

Seeds were plated on half strength Murashige and Skoog media supplemented with vitamins and grown vertically at 22 ºC in long day conditions (16 hours light, 8 hours dark).

10-day-old seedlings were individually transferred to pots containing 30 ± 1g of substrate (peat, vermiculite, perlite in a 12:1:0.5 proportion). 3-week-old plants were exposed to drought by withholding water until Col-0 plants reached 5% FC on average. Plants were rewatered, and after 10 days of recovery, photographed and counted manually for plant survival. For the rosette area calculation, 3-week-old plants were photographed and measured individually for rosette area using ImageJ.

Hydrotropism

Seeds were plated on half strength Murashige and Skoog media supplemented with vitamins and grown vertically at 22 ºC in long day conditions (16 hours light, 8 hours dark) for 6 days. Following this, the lower part of the agar from the plates was removed, and half strength Murashige and Skoog media supplemented with vitamins containing 270mM sorbitol was added, to mimic a low water availability media. To

minimize the effect of gravitropism, the media was positioned at 45º. Root angle was measured with ImageJ software.

GUS staining

6-day-old seedlings were submerged in ice-cold acetone (90% v/v) and incubated for 20 min on ice. Subsequently, the acetone was rinsed twice with 1xPBS. The seedlings were then immersed in a GUS solution composed of 100mM sodium phosphate buffer (pH=7.2), 10mM sodium EDTA, 0.1% Triton X-100, 1mg/ml 5-bromo-4-chloro-3-indolyl-beta-D-glucorince (Xglu; Duchefa, Harrlem, NL), 10mM potassium ferrocyanide, and potassium ferricyanide, and incubated at 37ºC overnight. After incubation, the seedlings were rinsed twice with 1xPBS and left overnight in 70% ethanol (v/v). Finally, the seedlings were mounted on slides, covered with chloral hydrate, and observed under a DM6 epifluorescence vertical microscope (Leica) the following day.

In the case of *pHAT9::GUS/GFP* lines treated with ABA, 4-day-old seedlings were transferred to Murashige and Skoog media supplemented with vitamins containing 50mM of ABA for 2 consecutive days. Subsequently, GUS staining was conducted following the protocol previously described.

Western blot

12-day-old seedlings (TF overexpressor), grown vertically in half strength Murashige and Skoog media supplemented with vitamins, were collected and placed in liquid half strength Murashige and Skoog media supplemented with vitamins containing the different treatments:

- Mock: DMSO, adding the same volume and incubating the same time as in the treatment.
- Hormones: BL (10 nM) or ABA (50 mM) for 1 hour
- Bikinin (50µM) for 1 hour
- MG132 (50µM) for 6 hours, preceded of a 5 min infiltration by vacuum.

Following the treatment, plant material was collected, dried, fast frozen and grinded in liquid nitrogen. Protein extraction buffer (150mM NaCl, 50mM Tris-HCl pH=8, 1% Triton X-100), supplemented with 1x protease inhibitor and phosphatase inhibitor cocktail (Roche), was added, and followed by centrifugation of 10 min at 5000 g at 4ºC. Supernatant was collected and the centrifugation step repeated. After collecting supernatant, 40 µl were boiled for 3 min at 95ºC and loaded into an SDS-PAGE 4-20% gel and run at 100V. After wet transference at 100V for 1 hour, Ponceau staining was performed to assessed if the same protein quantity was loaded in all the different treatments and conditions. For TF-GFP fusion detection, α-GFP-HRP (Miltenyi) antibodies diluted at 1:5000 in 1% milk in TBS-T were incubated at 4 ºC overnight. TF-GFP bands were detected using Chemi-doc Touch (Biorad).

Co-immunoprecipitation

12-day-old seedlings (TF overexpressors), grown vertically in half strength Murashige and Skoog media supplemented with vitamins, were collected, fast frozen and grinded in liquid nitrogen. Protein extraction buffer (150mM NaCl, 50mM Tris-HCl pH=8, 1% Triton X-100), supplemented with 1x protease inhibitor and phosphatase inhibitor cocktail (Roche), was added, followed by centrifugation of 10 min at 5000 g at 4ºC. Supernatant was collected and the centrifugation step repeated. 50 µl of the supernatant was collected to use it as an input for western blot visualization. After collecting 1 ml of supernatant, 50 µl of anti-GFP beads (Miltenyi), were added and incubated at 4ºC in a rotator wheel for 1 hour. After incubation, µColumn were placed on the µMACS Separator (Miltenyi) and 200 µl of protein extraction buffer was applied to equilibrate the column. The 1 ml sample lysate was applied to the µColumn, and the flowthrough was collected for western blot visualization, which was considered the flowtr. µColumn were washed 4 times with 200 µl of Wash buffer 1, and once with 100 µl of Wash buffer 2. 20 µl of Elution buffer, previously kept at 95ºC, was applied onto the center of the column, and incubate it at RT for 5 min. Finally, 50 µl of Elution buffer was applied onto the center of the column and the eluates were collected. The input, flowthrough, and IP eluate were boiled for 3 min at 95ºC and loaded into an SDS-PAGE 4-20% gel and run at 100V. Wet transference at 100V for 1 hour was performed. For TF-GFP fusion detection, α-GFP-HRP (Miltenyi) antibody was used in 1:5000 dilution in 1% milk in TBST. For BES1 detection, primary α-BES1 (kindly provided by Yanhai Yin) antibody in 1:2000 in 5% milk in

TBST, and secondary α-Rabbit-HRP (ThermoFisher) antibody in 1:10000 in 1% milk in TBST, were used. For BZR1 detection, primary α-BZR1 (Abiocode) antibody in 1:2000 in 5% milk in TBST, and secondary α-Rabbit-HRP (ThermoFisher) antibody in 1:10000 in 1% milk in TBST, were used.

Bimolecular fluorescence complementation

The genomic coding sequence of BZR1, MYB96, MYB305, HAT9, and AT2G01430, were inserted by LR clonase recombination into BiFC binary expression vectors pGTQL1221YC and pGTQL1211YN. Plasmids were transformed into the A. tumefaciens GV3101 strain by electroporation and infiltrated into Nicotiana leaves. Three to five days after infiltration, leaves were observed under an Olympus FV1000 inverted confocal microscope.

Gene ontology enrichment analysis and Venn diagrams

GOE analysis and KEGG pathway enrichment analysis were performed with the “gprofiler2” package of R. Venn diagrams were plotted with “VennDiagram” package in R. “ggplot2” package in R was used for the rest of the plots.

Chapter 4: Untargeted mutagenesis of brassinosteroid receptor SbBRI1 confers drought tolerance by altering phenylpropanoid metabolism in *Sorghum bicolor*

Plant material

Sorghum accession BTx623 EMS-mutagenized collection was obtained via Cropping Systems Research Laboratory from U.S. Department of Agriculture, Lubbock, Texas (Jiao et al., 2016). From 2 different M4 pool of seeds (ARS72 and ARS87) we genotyped and selected the plants carrying SNPs causing amino acid substitution in the extracellular region of SbBRI1 protein. We performed 2 backcrosses using unmutagenized accession BTx623 as a parent to reduce the amount of background mutations. All the phenotypical and multiomic analysis was performed in BC2F3 EMS-mutagenized plants carrying or lacking the SNP in the extracellular region of SbBRI1, therefore assuming that they are near isogenic lines.

Additional studies were conducted with Arabidopsis, Col-0. The genotypes used in this study are Col-0 WT (Col-0), *bri1-301* (*bri1*, Xu et al., 2008), 35S::AtBRI1-GFP (BRI1OX, Geldner et al., 2007), 35S::SbBRI1-GFP; Columbia-0 (SbBRI1;Col-30 and SbBRI1;Col-34) and 35S::SbBRI1-GFP;*bri1-301* (SbBRI1;*bri1-8* and SbBRI1;*bri1-3*).

Sorbitol sensitivity in root Arabidopsis seedlings

Arabidopsis seeds were surface sterilized with 35% commercial bleach for 5 min and washed with water 5 consecutive times. Seeds were stratified at 4 degrees in water for 48 hours. Seeds were plated on half strength Murashige and Skoog media supplemented with vitamins and grown vertically at 22 degrees in long day conditions (16 hours light, 8 hours dark).

For the root length assay, four-day-old seedlings were transferred to either control or sorbitol supplemented media (270 mM Sorbitol) and root length was measured at day 6.

For cell death damage visualization in the root meristem, five-day-old seedlings were transferred to either control or sorbitol supplemented media (270 mM Sorbitol) and roots were stained with propidium iodide and visualized in confocal microscope (FV1000 Olympus) at day 6. Cell death damage was measured by intensity mean of propidium iodide in a region of interest of 400 µm x 140 µm starting from the QC, using ImageJ.

Drought stress in Arabidopsis adult plants

Arabidopsis seeds were surface sterilized, plated and grown as described in sorbitol sensitivity assays. ten-day-old seedlings were individually transferred to pots containing 30 ± 1g of substrate (peat, vermiculite, perlite in a 12:1:0.5 proportion). Three-week-old plants were exposed to

drought by withholding water until Col-0 plants reached 5% FC on average. Plants were rewatered, and after 7 days of recovery, photographed and counted manually for plant survival. For the rosette area calculation, three-week-old plants were photographed and measured individually for rosette area using ImageJ.

Sorbitol sensitivity in Sorghum seedlings

Sorghum seeds were surface sterilized in 50% commercial bleach and 0.01% Tween 20 for 5 min and washed with water 5 consecutive times. Seeds were placed in a petri dish containing sterile water and germinated at 28 degrees under long day conditions. Two-day-old seedlings were selected for homogeneous germination and transferred to a hydroponic system either in control conditions (quarter strength Murashige and Skoog media supplemented with vitamins) or osmotic stress conditions (supplemented with Sorbitol 270mM). The hydroponic system was composed by a pipette tip rack box (165 x 120 x 80 mm) with plastic mesh (3.5 nominal aperture) on top of it as a support for the seedlings. Roots and shoots were pictured and measured at day 5, and the root tip was cut and fixed in 50% methanol and 10% acetic acid at 4°C for at least 24 hours. Fixed root tips were used to visualize the root meristem and they were stained using modified pseudo-Schiff propidium iodide method, as described in Rico-Medina et al., 2023. Stained roots were visualized in confocal microscope (FV1000 Olympus).

Drought stress in Sorghum seedlings

Sorghum seeds were sterilized and germinated as described previously. Two-day-old homogenously germinated seedlings were transferred to pots containing 500 ± 1g of substrate. Three individual seedlings were transferred to a single pot. Eight-day-old seedlings were exposed to drought by withholding water and several parameters were monitored along the drought time course. For FC calculations, pots were weighed along the time course to determine the time needed to reach a specific FC. For photosynthetic efficiency and RWC leaf samples were taken at 30 and 5% FC. Photosynthetic efficiency was calculated taking the variable and the maxima fluorescence using the MAXI version of the IMAGING-PAM (Heinz Walz GmbH). RWC was calculated by measuring the fresh weight, saturated weight, and dry weight of the leaves. Plants were photographed at 5% FC.

DNA affinity purification sequencing (DAP-seq)

Transient expression in Sorghum leaves. SbBES1-GFP was transiently expressed in Sorghum leaves, to ensure proper expression and localization, as described in Miller et al., 2023.

Plasmid preparation. SbBES1 coding sequence was synthesized in Twist Bioscience ® after codon optimization, including the stop codon and flanked by Gateway sites. SbBES1 coding sequence was transferred into the Gateway-compatible pIX-HALO expression vector (Bartlett et al., 2017), which contains an N-terminal HaloTag affinity tag sequence.

Sorghum genomic DNA extraction was conducted as in Thomas et al., 1993.

DAP-seq was conducted as in Barlett et al., 2017, with modifications as described below:

Genomic DNA library preparation. Genomic DNA was sonicated to obtain 200bp fragments on a Covaris Focus-ultrasonicator instrument. Fragments were selected by AMPure XP beads for removing small fragments (less than 100 bp). Beads with correct size fragments were washed twice with 80% ethanol, then resuspend in elution buffer after ethanol evaporation. Selected fragments were processed in the following three steps, including: i) end repair, ii) adding A-tail, and iii) adapter ligation. Two cleaning processes, following the instruction of QIAquick PCR Purification Kit (Cat No./ID: 28104), were required among these three steps. After the adapter ligation, fragments fused with adapters were purified and washed with AMPure XP beads and 80% ethanol for removing unattached adapters. Resuspended ligated fragments were quantified by Qubit and were confirmed by bioanalyzer analysis.

Protein preparation. The SbBES1-pHALO recombinant plasmid and an empty pIX-HALO plasmid (generating only the HALO peptide when translated) were *in vitro* translated with TNT Coupled Reticulocyte Lysate System (Promega). Two replicates were performed for each plasmid. the pIX-HALO plasmid was used as the ‘input’ control.

DAP-seq library preparation. Washed Halo-Tag beads were mixed with the *in vitro* translated proteins to pull down the Halo-Tag fused SbBES1 protein. Each pulled-down protein reaction was mixed with 500ng genomic DNA libraries for SbBES1 binding. The bound DNA was washed by PBST for 6 times, then released from Halo-Tag beads by

denaturation at high temperature (98 ºC). The eluted DNA was enriched by PCR amplification to generate the sequencing libraries. The enriched DAP-seq libraries were purified and washed with AMPure XP beads and 80% ethanol for removing indexes. Resuspended DAP-seq libraries were quantified by Qubit and were confirmed by bioanalyzer analysis.

DAP-seq library sequencing. DAP-seq libraries were sequenced on an Illumina NextSeq 550 (sequencing of libraries was set at 40 million and 1x75bp single-end reads). As a negative control, the 'input' (pIX-HALO expression vector without any insertion of opening reading frame) was accounted for possible non-specific DNA binding in the reaction mixture and copy number variations at specific genomic loci.

Sequencing analysis. DAP-seq reads were mapped to the Sorghum v3.1.1 (Phytozome genome ID:454) reference genome using bowtie2 (Langmead & Salzberg, 2012), version 2.0-beta7, with default parameters and post-processing to remove reads that have MAPQ scores lower than 30. Peak detection was performed using GEM peak caller (Guo et al., 2012) version 3.4 with the 12X.v2 genome assembly using the following parameters: '-q 2 -t 1 -k_min 6 -kmax 20 -k_seqs 600 -k_neg_dinu_shuffle'. A more detailed list of the GEM peak caller parameters is present in the Table S3. The replicates were analyzed as multi-replicates with the GEM replicate mode. Peak summits called by GEM were associated with the closest gene model in the custom annotation file using the BioConductor package ChIPpeakAnno (Zhu et al., 2010) with default parameters (i.e., NearestLocation). *De novo motif* discovery was performed by retrieving 200bp sequences centered at GEM-identified binding events for the 600 most enriched peaks and running STREME in MEME suit 5.5.3 with most default parameters.

Transcriptomic profiling analysis

RNA extraction. For RNA-Seq analysis, Sorghum roots in control conditions and drought stress conditions (30% FC) were detached from mature plants and freeze in liquid nitrogen. RNA was extracted with Maxwell® 16 LEV Plant RNA Kit (Promega) and quality checked using Bioanalyzer.

Preparation of the sequencing libraries. Stranded cDNA libraries were prepared with TrueSeq Stranded mRNA KIT (Illumina). Paired-end sequencing, with 100-bp reads, was performed in Illumina NextSeq2000 sequencer, with 33M of minimum sequencing depth. Raw reads were quality-checked using FastQC tool (v0.11.2), trimmed 13bp at the 3' end quality-trimmed and filtered at a minimum quality score of 28 (Phred+33, minimum read length of 75bp) using trimmomatic software (v0.38). Filtered reads were mapped to the Sorghum v3.0.1 genome release using HISAT2 (2.1.0) aligner and quantified at a gene level using FeatureCount software (v1.6.2) on the Sorghum v3.1.1 annotation file (Phytozome).

Batch correction. Batch effect was checked with batchQC function from "BatchQC" package in R, before and after batch correction. The batch effect or variability explained by the replicate was corrected with ComBat_seq function from "sva" package in R.

RNA-Seq data analysis. For differential expression, samples were TMM normalized and statistical values calculated with the "EdgeR" package in R. Differentially expressed genes were identified in pairwise comparisons between genotypes or treatments. Results were filtered for adjusted p-value (FDR) < 0.05 and |logFC| > 0.5. For the evaluation of

differential drought response between WT and *bri1* roots, a lineal model accounting for the interaction genotype and drought was constructed with "EdgeR" package. A gene was considered to be affected by the interaction if adjusted p-value (FDR) < 0.05. GOE analysis and KEGG pathway enrichment analysis were performed with the "gprofiler2" package of R. Venn diagrams were plotted with "VennDiagram" package in R. "ggplot2" package in R was used for the rest of the plots.

Metabolite profiling analysis

Metabolite Extraction and Quantification. The whole metabolite extraction and quantification pipeline followed the guidelines as described in Giavalisco et al. (2011) and Salem et al. (2020). Briefly, 10-25 mg of fresh plant tissue was harvested and immediately frozen in N2, and ground using zirconia beads with the help of Tissue Lyser Mixer-Mill (Qiagen) 3 min at 25 Hz. After samples were extracted in 100% cold methanol, they were centrifuged for 10 min at 14000 rpm (RT) and 3:1 chloroform was added. After vortexing thoroughly, 1:1 volume of water was added and the samples were subsequently vortexed and centrifuged. The semi-polar phase was used for analysis of semi-polar secondary and primary metabolites. For secondary semi-polar metabolites, the dried polar aliquots were resuspended in water:methanol (1:1 v/v).

Analysis of semi-polar metabolites was performed using a Thermo Q Exactive Focus coupled to a reverse-phase C18 column. The column was maintained at 40°C with a flow rate of 400 µl/min, and the eluent system consisted of water (eluent A) and acetonitrile (eluent B), both containing

0.1% formic acid. Mass spectra were acquired in full scan mode over a range of 100-1500 m/z using data-independent acquisition (DIA) with high-energy collisional dissociation (HCD) energy set at 30 eV in positive mode.

For primary metabolite metabolites, the dried polar was derivatized as described in Lisec et al. (2006). Derivatization was carried out at 37°C for 120 min using 40 µl of 20 mg/ml methoxyamine hydrochloride in pyridine, followed by a 30-min treatment at 37°C with 70 µl of trimethylsilyl-*N*-methyl trifluoroacetamide (MSTFA). The derivatized samples (1 µl) were injected in splitless mode into a gas chromatograph coupled to a time-of-flight mass spectrometer (Pegasus HT TOF-MS). Gas chromatography was performed on a 30-m DB-35 column using helium as the carrier gas. The initial temperature of the oven was 85°C, and it was ramped up at a rate of 15°C/min to a final temperature of 360°C. Mass spectra were recorded in the range of 70-600 m/z at a rate of 20 scans/s.

Data Processing and Compound Annotation. LC-MS full scan data were processed using MS Refiner (Expressionist 14.0). Processing of chromatograms, peak detection, and integration were performed using RefinerMS (version 5.3; GeneData). Metabolite identification and annotation were performed using in-house reference compound library, tandem MS (MS/MS) fragmentation, and metabolomics databases (Alseekh et al., 2021). For the annotation of metabolites measured by GC-MS the Golm Metabolome Database was used (Kopka et al., 2005). For the integration of transcriptomic and metabolic data, Paintomics4 (https://www.paintomics.org/) (Liu et al. 2022) was used.

Chapter 5: Enhancing expression of Sorghum BRL receptor via efficient Sorghum transformation using a ternary vector system combined with morphogenic regulators

For clarity and to highlight the establishment of the transformation protocol as a significant result, the Materials and Methods section of Chapter 5 has been integrated into the Results section.

BIBLIOGRAPHY

Abdel-Ghany, S. E., Ullah, F., Ben-Hur, A., & Reddy, A. S. (2020). Transcriptome analysis of drought-resistant and drought-sensitive Sorghum (Sorghum bicolor) genotypes in response to PEG-induced drought stress. *International Journal of Molecular Sciences*, *21*(3), 772.

Able, J. A., Rathus, C., & Godwin, I. D. (2001). The investigation of optimal bombardment parameters for transient and stable transgene expression in Sorghum. *In Vitro Cellular & Developmental Biology-Plant*, *37*, 341-348.

Abreha, K. B., Enyew, M., Carlsson, A. S., Vetukuri, R. R., Feyissa, T., Motlhaodi, T., Ng´uni, D., & Geleta, M. (2022). Sorghum in dryland: morphological, physiological, and molecular responses of Sorghum under drought stress. *Planta*, *255*, 1-23.

Abuelsoud, W., Cortleven, A., & Schmülling, T. (2020). Photoperiod stress induces an oxidative burst-like response and is associated with increased apoplastic peroxidase and decreased catalase activities. *Journal of plant physiology*, *253*, 153252.

Adam, D. (2021). How far will global population rise? Researchers can't agree. Nature, 597(7877), 462-465.

Aesaert, S., Impens, L., Coussens, G., Van Lerberge, E., Vanderhaeghen, R., Desmet, L., Vanhevel, Y., Bossuyt, S., Wambua, A.N., Van Lijsebettens, M., Inze, D., De Keyser, E., Jacobs, T.B., Karimi, M., & Pauwels, L. (2022). Optimized transformation and gene editing of the

B104 public maize inbred by improved tissue culture and use of morphogenic regulators. *Frontiers in Plant Science*, *13*, 883847.

Ainsworth, E. A., & Rogers, A. (2007). The response of photosynthesis and stomatal conductance to rising [CO2]: mechanisms and environmental interactions. *Plant, cell & environment*, *30*(3), 258-270.

Al Ait, L., Yamak, Z., & Morgenstern, B. (2013). DIALIGN at GOBICS—multiple sequence alignment using various sources of external information. *Nucleic acids research*, *41*(W1), W3-W7.

Ali, B., Hayat, S., Fariduddin, Q., & Ahmad, A. (2008). 24-Epibrassinolide protects against the stress generated by salinity and nickel in Brassica juncea. *Chemosphere*, *72*(9), 1387-1392.

Ali, M. A., Azeem, F., Nawaz, M. A., Acet, T., Abbas, A., Imran, Q. M., Shah, K.H., Rehman, H.M., Chung, G., Yang, S.H., & Bohlmann, H. (2018). Transcription factors WRKY11 and WRKY17 are involved in abiotic stress responses in Arabidopsis. *Journal of plant physiology*, *226*, 12-21.

Alseekh, S., Aharoni, A., Brotman, Y., Contrepois, K., D'Auria, J., Ewald, J., Fraser, P.D., Giavalisco, P., Hall, R.D., Heinemann, M., Link, H., Luo, J., Neumann, S., Nielsen, J., Perez de Souza, L., Saito, K., Sauer, U., Schroeder, F.C., Schuster, S., Siuzdak, G., Skirycz, A., Sumner, L.W., Snyder, M.P., Tang, H., Tohge, T., Wang, Y., Wen, W., Wu, S., Xu, G., Zamboni, N. & Fernie, A. R. (2021). Mass spectrometry-based metabolomics: a guide for annotation, quantification and best reporting practices. *Nature methods*, *18*(7), 747-756.

Alves, M. S., Dadalto, S. P., Gonçalves, A. B., De Souza, G. B., Barros, V. A., & Fietto, L. G. (2014). Transcription factor functional protein-protein interactions in plant defense responses. *Proteomes*, *2*(1), 85-106.

Amraee, L., Rahmani, F., & Mandoulakani, B. A. (2019). 24-Epibrassinolide alters DNA cytosine methylation of Linum usitatissimum L. under salinity stress. *Plant physiology and biochemistry*, *139*, 478-484.

Anand, A., Bass, S. H., Wu, E., Wang, N., McBride, K. E., Annaluru, N., Miller, M., Hua, M., & Jones, T. J. (2018). An improved ternary vector system for Agrobacterium-mediated rapid maize transformation. *Plant molecular biology*, *97*, 187-200.

Anjum, S. A., Wang, L. C., Farooq, M., Hussain, M., Xue, L. L., & Zou, C. M. (2011). Brassinolide application improves the drought tolerance in maize through modulation of enzymatic antioxidants and leaf gas exchange. *Journal of Agronomy and crop science*, *197*(3), 177-185.

Aregawi, K., Shen, J., Pierroz, G., Sharma, M. K., Dahlberg, J., Owiti, J., & Lemaux, P. G. (2022). Morphogene-assisted transformation of Sorghum bicolor allows more efficient genome editing. Plant Biotechnology Journal, 20(4), 748-760.

Arnaud, D., Lee, S., Takebayashi, Y., Choi, D., Choi, J., Sakakibara, H., & Hwang, I. (2017). Cytokinin-mediated regulation of reactive oxygen species homeostasis modulates stomatal immunity in Arabidopsis. *The Plant Cell*, *29*(3), 543-559.

Bai, M. Y., Fan, M., Oh, E., & Wang, Z. Y. (2012). A triple helix-loop-helix/basic helix-loop-helix cascade controls cell elongation downstream

of multiple hormonal and environmental signaling pathways in Arabidopsis. *The Plant Cell*, *24*(12), 4917-4929.

Bai, M. Y., Zhang, L. Y., Gampala, S. S., Zhu, S. W., Song, W. Y., Chong, K., & Wang, Z. Y. (2007). Functions of OsBZR1 and 14-3-3 proteins in brassinosteroid signaling in rice. *Proceedings of the National Academy of Sciences*, *104*(34), 13839-13844.

Bajguz, A., Chmur, M., & Gruszka, D. (2020). Comprehensive overview of the brassinosteroid biosynthesis pathways: substrates, products, inhibitors, and connections. *Frontiers in plant science*, *11*, 535077.

Bao, F., Shen, J., Brady, S. R., Muday, G. K., Asami, T., & Yang, Z. (2004). Brassinosteroids interact with auxin to promote lateral root development in Arabidopsis. *Plant physiology*, *134*(4), 1624-1631.

Bao, S. G., Shi, J. X., Luo, F., Ding, B., Hao, J. Y., Xie, X. D., & Sun, S. J. (2017). Overexpression of Sorghum WINL1 gene confers drought tolerance in Arabidopsis thaliana through the regulation of cuticular biosynthesis. *Plant Cell, Tissue and Organ Culture (PCTOC)*, *128*, 347-356.

Barnabás, B., Jäger, K., & Fehér, A. (2008). The effect of drought and heat stress on reproductive processes in cereals. *Plant, cell & environment*, *31*(1), 11-38.

Bartlett, A., O'Malley, R. C., Huang, S. S. C., Galli, M., Nery, J. R., Gallavotti, A., & Ecker, J. R. (2017). Mapping genome-wide transcription-factor binding sites using DAP-seq. *Nature protocols*, *12*(8), 1659-1672.

Bayu, W., Rethman, N. F. G., Hammes, P. S., Pieterse, P. A., Grimbeek, J., & Van Der Linde, M. (2005). Water stress affects the germination, emergence, and growth of different Sorghum cultivars. *SINET: Ethiopian Journal of Science*, *28*(2), 119-128.

Beillouin, D., Schauberger, B., Bastos, A., Ciais, P., & Makowski, D. (2020). Impact of extreme weather conditions on European crop production in 2018. *Philosophical Transactions of the Royal Society B*, *375*(1810), 20190510.

Belide, S., Vanhercke, T., Petrie, J. R., & Singh, S. P. (2017). Robust genetic transformation of Sorghum (Sorghum bicolor L.) using differentiating embryogenic callus induced from immature embryos. *Plant methods*, *13*, 1-12.

Benlloch-Gonzalez, M., Bochicchio, R., Berger, J., Bramley, H., & Palta, J. A. (2014). High temperature reduces the positive effect of elevated CO2 on wheat root system growth. *Field Crops Research*, *165*, 71-79.

Besson-Bard, A., Pugin, A., & Wendehenne, D. (2008). New insights into nitric oxide signaling in plants. *Annu. Rev. Plant Biol.*, *59*, 21-39.

Betegón-Putze, I., Mercadal, J., Bosch, N., Planas-Riverola, A., Marquès-Bueno, M., Vilarrasa-Blasi, J., ... & Caño-Delgado, A. I. (2021). Precise transcriptional control of cellular quiescence by BRAVO/WOX5 complex in Arabidopsis roots. *Molecular Systems Biology*, *17*(6), e9864.

Béziat, C., Kleine-Vehn, J., & Feraru, E. (2017). Histochemical staining of β-glucuronidase and its spatial quantification. *Plant Hormones: Methods and Protocols*, 73-80.

Bihani, P., Char, B., & Bhargava, S. (2011). Transgenic expression of Sorghum DREB2 in rice improves tolerance and yield under water limitation. *The Journal of Agricultural Science*, *149*(1), 95-101.

Blanco-Tourinan, N., Rana, S., Nolan, T. M., Li, K., Vukasinovic, N., Hsu, C. W., Russinova, E., & Hardtke, C. (2024). The brassinosteroid receptor gene BRI1 safeguards cell-autonomous brassinosteroid signaling across tissues. *bioRxiv*, 2024-05.

Blasco-Escámez, D., Lozano-Elena, F., Fàbregas, N., & Caño-Delgado, A. I. (2017). The primary root of Sorghum bicolor (L. Moench) as a model system to study brassinosteroid signaling in crops. *Brassinosteroids: Methods and Protocols*, 181-192.

Blümmel, M., Deshpande, S., Kholova, J., & Vadez, V. (2015). Introgression of staygreen QLT's for concomitant improvement of food and fodder traits in Sorghum bicolor. *Field Crops Research*, *180*, 228-237.

Borrell, A. K., Hammer, G. L., & Henzell, R. G. (2000). Does maintaining green leaf area in Sorghum improve yield under drought? II. Dry matter production and yield. *Crop science*, *40*(4), 1037-1048.

Borrell, A. K., van Oosterom, E. J., Mullet, J. E., George-Jaeggli, B., Jordan, D. R., Klein, P. E., & Hammer, G. L. (2014). Stay-green alleles individually enhance grain yield in Sorghum under drought by modifying canopy development and water uptake patterns. *New Phytologist*, *203*(3), 817-830.

Borrell, A. K., Wong, A. C., George-Jaeggli, B., van Oosterom, E. J., Mace, E. S., Godwin, I. D., Liu, G., Mullet, J.E., Klein, P.E., Hammer, G.L., McLean, G., Hunt, C., & Jordan, D. R. (2022). Genetic

modification of PIN genes induces causal mechanisms of stay-green drought adaptation phenotype. *Journal of Experimental Botany*, *73*(19), 6711-6726.

Botella, J. R. (2019). Now for the hard ones: is there a limit on CRISPR genome editing in crops?. *Journal of Experimental Botany*, *70*(3), 734-737.

Boutilier, K., Offringa, R., Sharma, V. K., Kieft, H., Ouellet, T., Zhang, L., Hattori, J., Liu, C.M., Van Lammeren, A.A.M., Miki, B.L.A., Custers, J.B.M., & van Lookeren Campagne, M. M. (2002). Ectopic expression of BABY BOOM triggers a conversion from vegetative to embryonic growth. *The Plant Cell*, *14*(8), 1737-1749.

Brady, S. M., Orlando, D. A., Lee, J. Y., Wang, J. Y., Koch, J., Dinneny, J. R., Mace, D., Ohler, U., & Benfey, P. N. (2007). A high-resolution root spatiotemporal map reveals dominant expression patterns. *Science*, *318*(5851), 801-806.

Brettell, R. I. S., Wernicke, W., & Thomas, E. (1980). Embryogenesis from cultured immature inflorescences of Sorghum bicolor. *Protoplasma*, *104*, 141-148.

Buchanan, B. B., Gruissem, W., & Jones, R. L. (Eds.). (2015). *Biochemistry and molecular biology of plants*. John wiley & sons.

Cai, T., Daly, B., & Butler, L. (1987). Callus induction and plant regeneration from shoot portions of mature embryos of high tannin Sorghums. *Plant cell, tissue and organ culture*, *9*, 245-252.

Cai, Z., Liu, J., Wang, H., Yang, C., Chen, Y., Li, Y., Pan, S., Dong, R., Tang, G., Barajas-Lopez, J., Fujii, H., & Wang, X. (2014). GSK3-like kinases positively modulate abscisic acid signaling through phosphorylating subgroup III SnRK2s in Arabidopsis. *Proceedings of the National Academy of Sciences*, *111*(26), 9651-9656.

Caño-Delgado A., Yin Y., Yu C., Vafeados D., Mora-García S., Cheng J.C., Nam K.H., Li J., Chory J. (2004). BRL1 and BRL3 are novel brassinosteroid receptors that function in vascular differentiation in Arabidopsis. Development **131**: 5341–5351.

Carlsbecker, A., Lee, J. Y., Roberts, C. J., Dettmer, J., Lehesranta, S., Zhou, J., Lindgren, O., Moreno-Risueno, M.A., Vatén, A., Thitamadee, S., Campilho, A., Sebastian, J., Bowman, J.L., Helariutta, Y., & Benfey, P. N. (2010). Cell signalling by microRNA165/6 directs gene dose-dependent root cell fate. *Nature*, *465*(7296), 316-321.

Casas, A. M., Kononowicz, A. K., Zehr, U. B., Tomes, D. T., Axtell, J. D., Butler, L. G., Bressan, R.A., & Hasegawa, P. M. (1993). Transgenic Sorghum plants via microprojectile bombardment. *Proceedings of the National Academy of Sciences*, *90*(23), 11212-11216.

Castorina, G., Persico, M., Zilio, M., Sangiorgio, S., Carabelli, L., & Consonni, G. (2018). The maize lilliputian1 (lil1) gene, encoding a brassinosteroid cytochrome P450 C-6 oxidase, is involved in plant growth and drought response. *Annals of botany*, *122*(2), 227-238.

Castrillo, G., Turck, F., Leveugle, M., Lecharny, A., Carbonero, P., Coupland, G., Paz-Ares, J., & Oñate-Sánchez, L. (2011). Speeding cis-trans regulation discovery by phylogenomic analyses coupled with

screenings of an arrayed library of Arabidopsis transcription factors. *PloS one*, *6*(6), e21524.

Chaiwanon, J., & Wang, Z. Y. (2015). Spatiotemporal brassinosteroid signaling and antagonism with auxin pattern stem cell dynamics in Arabidopsis roots. *Current Biology*, *25*(8), 1031-1042.

Chankova, S. G., Dimova, E., Dimitrova, M., & Bryant, P. E. (2007). Induction of DNA double-strand breaks by zeocin in Chlamydomonas reinhardtii and the role of increased DNA double-strand breaks rejoining in the formation of an adaptive response. *Radiation and environmental biophysics*, *46*, 409-416.

Che P, Anand A, Wu E, Sander JD, Simon MK, Zhu W, Sigmund AL, Zastrow-Hayes G, Miller M, Liu D, Lawit SJ, Zhao ZY, Albertsen MC, Jones TJ. (2018). Developing a flexible, high-efficiency Agrobacterium-mediated Sorghum transformation system with broad application. *Plant biotechnology journal*, *16*(7), 1388-1395.

Che, P., Wu, E., Simon, M. K., Anand, A., Lowe, K., Gao, H., Sigmund, A.L., Yang, M., Albersten, M.C., Gordon-Kamm, W., & Jones, T. J. (2022). Wuschel2 enables highly efficient CRISPR/Cas-targeted genome editing during rapid de novo shoot regeneration in Sorghum. *Communications Biology*, *5*(1), 344.

Chen, B., Maas, L., Figueiredo, D., Zhong, Y., Reis, R., Li, M., Horstman, A., Riksen, T., Weemen, M., Liu, H., Siemons, C., Chen, S., Angenent, G.C., & Boutilier, K. (2022). BABY BOOM regulates early embryo and endosperm development. *Proceedings of the National Academy of Sciences*, *119*(25), e2201761119.

Chen, E., Yang, X., Liu, R., Zhang, M., Zhang, M., Zhou, F., Li, D., Hu, H., & Li, C. (2022). GhBEE3-Like gene regulated by brassinosteroids is involved in cotton drought tolerance. *Frontiers in Plant Science*, *13*, 1019146.

Chen, J., Nolan, T. M., Ye, H., Zhang, M., Tong, H., Xin, P., Chu, J., Li, Z., & Yin, Y. (2017). Arabidopsis WRKY46, WRKY54, and WRKY70 transcription factors are involved in brassinosteroid-regulated plant growth and drought responses. *The Plant Cell*, *29*(6), 1425-1439.

Chen, L., Yang, H., Fang, Y., Guo, W., Chen, H., Zhang, X., Dai, W., Chen, S., Hao, Q., Yuan, S., Zhang, C., Huang, Y., Shan, Z., Yang, Z., Qiu, D., Liu, X., Phan, L.S., Zhou, X., & Cao, D. (2021). Overexpression of GmMYB14 improves high-density yield and drought tolerance of soybean through regulating plant architecture mediated by the brassinosteroid pathway. *Plant biotechnology journal*, *19*(4), 702-716.

Chen, X., Wu, Q., Gao, Y., Zhang, J., Wang, Y., Zhang, R., Zhou, Y., Xiao, M., Xu, W., & Huang, R. (2020). The role of deep roots in Sorghum yield production under drought conditions. *Agronomy*, *10*(4), 611.

Cheng, Y., Ma, Y., Zhang, N., Lin, R., Yuan, Y., Tian, H., Hussain, S., Chen, S., Yang, W., Cai, L., Li, Y., Wang, X., Wang, T., & Wang, S. (2022). The R2R3 MYB transcription factor MYB71 regulates abscisic acid response in Arabidopsis. *Plants*, *11*(10), 1369.

Choe, S., Dilkes, B. P., Fujioka, S., Takatsuto, S., Sakurai, A., & Feldmann, K. A. (1998). The DWF4 gene of Arabidopsis encodes a cytochrome P450 that mediates multiple 22α-hydroxylation steps in brassinosteroid biosynthesis. *The Plant Cell*, *10*(2), 231-243.

Chono, M., Honda, I., Zeniya, H., Yoneyama, K., Saisho, D., Takeda, K., Takatsuto, S., Hoshino, T., & Watanabe, Y. (2003). A semidwarf phenotype of barley uzu results from a nucleotide substitution in the gene encoding a putative brassinosteroid receptor. *Plant physiology*, *133*(3), 1209-1219.

Chung, Y., Kwon, S. I., & Choe, S. (2014). Antagonistic regulation of Arabidopsis growth by brassinosteroids and abiotic stresses. *Molecules and cells*, *37*(11), 795-803.

Clouse, S. D. (1996). Molecular genetic studies confirm the role of brassinosteroids in plant growth and development.

Clouse, S. D., & Sasse, J. M. (1998). Brassinosteroids: essential regulators of plant growth and development. *Annual review of plant biology*, *49*(1), 427-451.

Clouse, S. D., Hall, A. F., Langford, M., McMorris, T. C., & Baker, M. E. (1993). Physiological and molecular effects of brassinosteroids on Arabidopsis thaliana. *Journal of Plant Growth Regulation*, *12*, 61-66.

Clouse, S. D., Langford, M., & McMorris, T. C. (1996). A brassinosteroid-insensitive mutant in Arabidopsis thaliana exhibits multiple defects in growth and development. *Plant physiology*, *111*(3), 671-678.

Cohen, I., Zandalinas, S. I., Huck, C., Fritschi, F. B., & Mittler, R. (2021). Meta-analysis of drought and heat stress combination impact on crop yield and yield components. *Physiologia Plantarum*, *171*(1), 66-76.

Coleto-Alcudia, V., Lozano-Elena, F., Vera, G., Betegón-Putze, I., Gupta, A., Efroni, I., & Cano-Delgado, A. I. (2024). TOTEM: A web TOol for Tissue-EnrichMent analysis on gene lists. *bioRxiv*, 2024-04.

Cui, F., Liu, L., Zhao, Q., Zhang, Z., Li, Q., Lin, B., Wu, Y., Tang, S., & Xie, Q. (2012). Arabidopsis ubiquitin conjugase UBC32 is an ERAD component that functions in brassinosteroid-mediated salt stress tolerance. *The Plant Cell*, *24*(1), 233-244.

Cui, X. Y., Gao, Y., Guo, J., Yu, T. F., Zheng, W. J., Liu, Y. W., Chen, J., Xu, Z.S., & Ma, Y. Z. (2019). BES/BZR transcription factor TaBZR2 positively regulates drought responses by activation of TaGST1. *Plant physiology*, *180*(1), 605-620.

Cui, X., Zhao, P., Li, Y., Xie, L., Li, Q., Yan, J., Chen, Q., Gao, S., Sun, M., Yang, B., Rehmani, M. S., & Jiang, Y. Q. (2021). Rapeseed NAC46 positively regulates hypersensitive response-like cell death and chlorophyll degradation. *Environmental and Experimental Botany*, *189*, 104536.

Cutler, S. R., Rodriguez, P. L., Finkelstein, R. R., & Abrams, S. R. (2010). Abscisic acid: emergence of a core signaling network. *Annual review of plant biology*, *61*, 651-679.

Dai, X., Liu, N., Wang, L., Li, J., Zheng, X., Xiang, F., & Liu, Z. (2020). MYB94 and MYB96 additively inhibit callus formation via directly repressing LBD29 expression in Arabidopsis thaliana. *Plant science*, *293*, 110323.

Daryanto, S., Wang, L., & Jacinthe, P. A. (2016). Global synthesis of drought effects on maize and wheat production. *PloS one*, *11*(5), e0156362.

Davis, K. F., Chiarelli, D. D., Rulli, M. C., Chhatre, A., Richter, B., Singh, D., & DeFries, R. (2018). Alternative cereals can improve water use and nutrient supply in India. *Science advances*, *4*(7), eaao1108.

De Lucas, M., Daviere, J. M., Rodríguez-Falcón, M., Pontin, M., Iglesias-Pedraz, J. M., Lorrain, S., Fankhauser, C., Blázquez, M.A., Titarenko, E., & Prat, S. (2008). A molecular framework for light and gibberellin control of cell elongation. *Nature*, *451*(7177), 480-484.

De Rybel, B., Audenaert, D., Vert, G., Rozhon, W., Mayerhofer, J., Peelman, F., Coutuer, S., Denayer, T., Jansen, L., Nguyen, L., Vanhoutte, I., Beemster, G.T.S., Vleminckx, K., Joank, C., Chory, J., Inzé, D., Russinova, E., & Beeckman, T. (2009). Chemical inhibition of a subset of Arabidopsis thaliana GSK3-like kinases activates brassinosteroid signaling. *Chemistry & biology*, *16*(6), 594-604.

DeFries, R., Liang, S., Chhatre, A., Davis, K. F., Ghosh, S., Rao, N. D., & Singh, D. (2023). Climate resilience of dry season cereals in India. *Scientific Reports*, *13*(1), 9960.

Dicko, M. H., Gruppen, H., Traoré, A. S., Voragen, A. G., & van Berkel, W. J. (2006). Phenolic compounds and related enzymes as determinants of Sorghum for food use. *Biotechnology and Molecular Biology Review*, *1*(1), 20-37.

Dietz, K. J., Zörb, C., & Geilfus, C. M. (2021). Drought and crop yield. *Plant Biology*, *23*(6), 881-893.

Divi, U. K., Rahman, T., & Krishna, P. (2010). Brassinosteroid-mediated stress tolerance in Arabidopsis shows interactions with abscisic acid, ethylene and salicylic acid pathways. *BMC plant biology*, *10*, 1-14.

Dong, N., Yin, W., Liu, D., Zhang, X., Yu, Z., Huang, W., Liu, J., Yang, Y., Meng, W., Niu, M., & Tong, H. (2020). Regulation of brassinosteroid signaling and salt resistance by SERK2 and potential utilization for crop improvement in rice. *Frontiers in Plant Science*, *11*, 621859.

Du, Q., Avci, U., Li, S., Gallego-Giraldo, L., Pattathil, S., Qi, L., Hahn, M.G., & Wang, H. (2015). Activation of miR165b represses At HB 15 expression and induces pith secondary wall development in A rabidopsis. *The Plant Journal*, *83*(3), 388-400.

Duan, F., Ding, J., Lee, D., Lu, X., Feng, Y., & Song, W. (2017). Overexpression of SoCYP85A1, a spinach cytochrome p450 gene in transgenic tobacco enhances root development and drought stress tolerance. *Frontiers in plant science*, *8*, 1909.

Duan, Y., Zhang, W., Li, B., Wang, Y., Li, K., Sodmergen, Han, C., Zhang, Y. & Li, X. (2010). An endoplasmic reticulum response pathway mediates programmed cell death of root tip induced by water stress in Arabidopsis. *New Phytologist*, *186*(3), 681-695.

Elkonin, L. A., & Pakhomova, N. V. (2000). Influence of nitrogen and phosphorus on induction embryogenic callus of Sorghum. *Plant cell, tissue and organ culture*, *61*, 115-123.

Fàbregas, N., Li, N., Boeren, S., Nash, T. E., Goshe, M. B., Clouse, S. D., Vries, S., & Caño-Delgado, A. I. (2013). The BRASSINOSTEROID INSENSITIVE1–LIKE3 signalosome complex regulates Arabidopsis root development. *The Plant Cell*, *25*(9), 3377-3388.

Fàbregas, N., Lozano-Elena, F., Blasco-Escámez, D., Tohge, T., Martínez-Andújar, C., Albacete, A., Osorio, S., Bustamante, M., Riechmann, J. L., Nomura, T., Yokota, T., Conesa, A., Perez-Alfocea,

F., Fernie, A.R., & Caño-Delgado, A. I. (2018). Overexpression of the vascular brassinosteroid receptor BRL3 confers drought resistance without penalizing plant growth. *Nature communications*, *9*(1), 4680.

Fan, C., Yu, H., Qin, S., Li, Y., Alam, A., Xu, C., Fan, D., Zhang, Q., Wang, Y., Zhu, W., Peng, L. & Luo, K. (2020). Brassinosteroid overproduction improves lignocellulose quantity and quality to maximize bioethanol yield under green-like biomass process in transgenic poplar. *Biotechnology for biofuels*, *13*(1), 1-17.

Farooq, M., Hussain, M., Wahid, A., & Siddique, K. H. M. (2012). Drought stress in plants: an overview. *Plant responses to drought stress: From morphological to molecular features*, 1-33.

Feng, Q., Ou, Y., Han, Y., de Dios, V. R., Wang, L., Zhang, Q., & Yao, Y. (2021). The brassinosteroid biosynthesis enzyme gene PeCPD improves plant growth and salt tolerance in Populus tomentosa. *Industrial Crops and Products*, *162*, 113218.

Feng, W., Zhang, H., Cao, Y., Liu, Y., Zhao, Y., Sun, F., Yang, Q., Zhang, X., Zhang, Y., Whang, Y., Li, W., Lu, Y., Fu, F., & Yu, H. (2023). Maize ZmBES1/BZR1-1 transcription factor negatively regulates drought tolerance. *Plant Physiology and Biochemistry*, *205*, 108188.

Feng, Y., Yin, Y., & Fei, S. (2015). Down-regulation of BdBRI1, a putative brassinosteroid receptor gene produces a dwarf phenotype with enhanced drought tolerance in Brachypodium distachyon. *Plant Science*, *234*, 163-173.

Flinn, B., Dale, S., Disharoon, A., & Kresovich, S. (2020). Comparative analysis of in vitro responses and regeneration between diverse bioenergy Sorghum genotypes. *Plants*, *9*(2), 248.

Fracasso, A., Trindade, L. M., & Amaducci, S. (2016). Drought stress tolerance strategies revealed by RNA-Seq in two Sorghum genotypes with contrasting WUE. *BMC Plant Biology*, *16*, 1-18.

Fridman, Y., & Savaldi-Goldstein, S. (2013). Brassinosteroids in growth control: how, when and where. *Plant Science*, *209*, 24-31.

Friedrichsen, D. M., Joazeiro, C. A., Li, J., Hunter, T., & Chory, J. (2000). Brassinosteroid-insensitive-1 is a ubiquitously expressed leucine-rich repeat receptor serine/threonine kinase. *Plant physiology*, *123*(4), 1247-1256.

Fujita, M., Fujita, Y., Maruyama, K., Seki, M., Hiratsu, K., Ohme-Takagi, M., Tran, L.S.P., Yamaguchi-Shinozaki, K., & Shinozaki, K. (2004). A dehydration-induced NAC protein, RD26, is involved in a novel ABA-dependent stress-signaling pathway. *The Plant Journal*, *39*(6), 863-876.

Gallegos, J. E., & Rose, A. B. (2017). Intron DNA sequences can be more important than the proximal promoter in determining the site of transcript initiation. *The Plant Cell*, *29*(4), 843-853.

Gampala, S. S., Kim, T. W., He, J. X., Tang, W., Deng, Z., Bai, M. Y., Guan, S., Lalonde, S., Sun, Y., Gendron, J.M., Chen, H., Shibagaki, N., Ferl, R.J., Erhardt, D., Chong, K., Burlingame, A.L., & Wang, Z. Y. (2007). An essential role for 14-3-3 proteins in brassinosteroid signal transduction in Arabidopsis. *Developmental cell*, *13*(2), 177-189.

Gao, Q. M., Venugopal, S., Navarre, D., & Kachroo, A. (2011). Low oleic acid-derived repression of jasmonic acid-inducible defense responses requires the WRKY50 and WRKY51 proteins. *Plant physiology*, *155*(1), 464-476.

Gao, X., Zhang, J. Q., Zhang, X., Zhou, J., Jiang, Z., Huang, P., Tang, Z., Bao, Y., Cheng, J., Tang, H., Zhang, W., Zhang, H., & Huang, J. (2019). Rice qGL3/OsPPKL1 functions with the GSK3/SHAGGY-like kinase OsGSK3 to modulate brassinosteroid signaling. *The Plant Cell*, *31*(5), 1077-1093.

Gao, Z., Xie, X., Ling, Y., Muthukrishnan, S., & Liang, G. H. (2005). Agrobacterium tumefaciens-mediated Sorghum transformation using a mannose selection system. *Plant Biotechnology Journal*, *3*(6), 591-599.

Geldner, N., Hyman, D. L., Wang, X., Schumacher, K., & Chory, J. (2007). Endosomal signaling of plant steroid receptor kinase BRI1. *Genes & development*, *21*(13), 1598-1602.

Gendrel, A. V., Lippman, Z., Martienssen, R., & Colot, V. (2005). Profiling histone modification patterns in plants using genomic tiling microarrays. *Nature methods*, *2*(3), 213-218.

Giavalisco, P., Li, Y., Matthes, A., Eckhardt, A., Hubberten, H. M., Hesse, H., Segu, S., Hummel, J., Köhl, K. & Willmitzer, L. (2011). Elemental formula annotation of polar and lipophilic metabolites using 13C, 15N and 34S isotope labelling, in combination with high-resolution mass spectrometry. *The Plant Journal*, *68*(2), 364-376.

González-García, M. P., Vilarrasa-Blasi, J., Zhiponova, M., Divol, F., Mora-García, S., Russinova, E., & Caño-Delgado, A. I. (2011).

Brassinosteroids control meristem size by promoting cell cycle progression in Arabidopsis roots. *Development*, *138*(5), 849-859.

Gordon-Kamm B, Sardesai N, Arling M, Lowe K, Hoerster G, Betts S, Jones AT. Using Morphogenic Genes to Improve Recovery and Regeneration of Transgenic Plants. Plants (Basel). 2019 Feb 11;8(2):38. doi: 10.3390/plants8020038. PMID: 30754699; PMCID: PMC6409764.

Graeff, M., Rana, S., Marhava, P., Moret, B., & Hardtke, C. S. (2020). Local and systemic effects of brassinosteroid perception in developing phloem. *Current Biology*, *30*(9), 1626-1638.

Graeff, M., Rana, S., Wendrich, J. R., Dorier, J., Eekhout, T., Fandino, A. C. A., Guex, N., Bassel, G.W., De Rybel, B., & Hardtke, C. S. (2021). A single-cell morpho-transcriptomic map of brassinosteroid action in the Arabidopsis root. *Molecular plant*, *14*(12), 1985-1999.

Gray, W. M., Östin, A., Sandberg, G., Romano, C. P., & Estelle, M. (1998). High temperature promotes auxin-mediated hypocotyl elongation in Arabidopsis. *Proceedings of the National Academy of Sciences*, *95*(12), 7197-7202.

Grove, M. D., Spencer, G. F., Rohwedder, W. K., Mandava, N., Worley, J. F., Warthen Jr, J. D., Steffens, G.L., Flippen-Anderson, J.L., & Cook Jr, J. C. (1979). Brassinolide, a plant growth-promoting steroid isolated from Brassica napus pollen. *Nature*, *281*(5728), 216-217.

Gruszka, D. (2020). Exploring the brassinosteroid signaling in monocots reveals novel components of the pathway and implications for plant breeding. *International journal of molecular sciences*, *21*(1), 354.

Gui, J., Zheng, S., Liu, C., Shen, J., Li, J., & Li, L. (2016). OsREM4. 1 interacts with OsSERK1 to coordinate the interlinking between abscisic acid and brassinosteroid signaling in rice. *Developmental cell*, *38*(2), 201-213.

Guigou, M., Lareo, C., Pérez, L. V., Lluberas, M. E., Vázquez, D., & Ferrari, M. D. (2011). Bioethanol production from sweet Sorghum: Evaluation of post-harvest treatments on sugar extraction and fermentation. *Biomass and Bioenergy*, *35*(7), 3058-3062.

Guo, H., Li, L., Aluru, M., Aluru, S., & Yin, Y. (2013). Mechanisms and networks for brassinosteroid regulated gene expression. *Current opinion in plant biology*, *16*(5), 545-553.

Gupta, A., Medina, A. R., Elena, F. L., Bueno, M. M., Fontanet, J. B., Fàbregas, N., Alseekh, S. Fernie, A. R. & Cano-Delgado, A. I. (2023). Brassinosteroid receptor BRL3 triggers systemic plant adaptation to elevated temperature from the phloem cells. *bioRxiv*, 2023-03.

Gupta, A., Rico-Medina, A., & Caño-Delgado, A. I. (2020). The physiology of plant responses to drought. *Science*, *368*(6488), 266-269.

Gupta, A., Rico-Medina, A., Lozano-Elena, F., Marqués-Bueno, M., Fontanet-Manzaneque, J.B., Fàbregas, N., Alseekh, S., Fernie, A.R., & Caño-Delgado, A. I. (2023). Brassinosteroid receptor BRL3 triggers systemic plant adaptation to elevated temperature from the phloem cells. *bioRxiv*, 2023-03.

Ha, Y., Shang, Y., & Nam, K. H. (2016). Brassinosteroids modulate ABA-induced stomatal closure in Arabidopsis. *Journal of Experimental Botany*, erw385.

Hacham, Y., Holland, N., Butterfield, C., Ubeda-Tomas, S., Bennett, M. J., Chory, J., & Savaldi-Goldstein, S. (2011). Brassinosteroid perception in the epidermis controls root meristem size. *Development*, *138*(5), 839-848.

Hagio, T. (2002). Adventitious shoot regeneration from immature embryos of Sorghum. *Plant cell, Tissue and organ culture*, *68*, 65-72.

Han, Y. J., Kim, Y. S., Hwang, O. J., Roh, J., Ganguly, K., Kim, S. K., Hwang, I., & Kim, J. I. (2017). Overexpression of Arabidopsis thaliana brassinosteroid-related acyltransferase 1 gene induces brassinosteroid-deficient phenotypes in creeping bentgrass. *PLoS One*, *12*(10), e0187378.

Harris, K., Subudhi, P. K., Borrell, A., Jordan, D., Rosenow, D., Nguyen, H., Klein, P., Klein, R., & Mullet, J. (2007). Sorghum stay-green QTL individually reduce post-flowering drought-induced leaf senescence. *Journal of experimental botany*, *58*(2), 327-338.

Hayat, S., Hasan, S. A., Yusuf, M., Hayat, Q., & Ahmad, A. (2010). Effect of 28-homobrassinolide on photosynthesis, fluorescence and antioxidant system in the presence or absence of salinity and temperature in Vigna radiata. *Environmental and Experimental Botany*, *69*(2), 105-112.

Hayat, S., Maheshwari, P., Wani, A. S., Irfan, M., Alyemeni, M. N., & Ahmad, A. (2012). Comparative effect of 28 homobrassinolide and salicylic acid in the amelioration of NaCl stress in Brassica juncea L. *Plant physiology and biochemistry*, *53*, 61-68.

He J.X., Gendron J.M., Yang Y., Li J., Wang Z.Y. (2002). The GSK3-like kinase BIN2 phosphorylates and destabilizes BZR1, a positive

regulator of the brassinosteroid signaling pathway in Arabidopsis. Proc. Natl. Acad. Sci. USA **99**: 10185–10190.

He, J. X., Gendron, J. M., Sun, Y., Gampala, S. S., Gendron, N., Sun, C. Q., & Wang, Z. Y. (2005). BZR1 is a transcriptional repressor with dual roles in brassinosteroid homeostasis and growth responses. *Science*, *307*(5715), 1634-1638.

He, J. X., Gendron, J. M., Yang, Y., Li, J., & Wang, Z. Y. (2002). The GSK3-like kinase BIN2 phosphorylates and destabilizes BZR1, a positive regulator of the brassinosteroid signaling pathway in Arabidopsis. *Proceedings of the National Academy of Sciences*, *99*(15), 10185-10190.

He, Z., Wang, Z. Y., Li, J., Zhu, Q., Lamb, C., Ronald, P., & Chory, J. (2000). Perception of brassinosteroids by the extracellular domain of the receptor kinase BRI1. *Science*, *288*(5475), 2360-2363.

Heyman, J., Cools, T., Vandenbussche, F., Heyndrickx, K. S., Van Leene, J., Vercauteren, I., Vanderauwera, S., Vandepoele, K., De Jaeger, G., Van Der Straeten, D., & De Veylder, L. (2013). ERF115 controls root quiescent center cell division and stem cell replenishment. *Science*, *342*(6160), 860-863.

Hoerster, G., Wang, N., Ryan, L., Wu, E., Anand, A., McBride, K., Lowe, K. et al. (2020) Use of non-integrating Zm-Wus2 vectors to enhance maize transformation. In Vitro Cell. Dev. Biol. Plant, 56, 265–279.

Högy, P., Wieser, H., Köhler, P., Schwadorf, K., Breuer, J., Franzaring, J., Muntifering, A., & Fangmeier, A. (2009). Effects of elevated CO2 on

grain yield and quality of wheat: results from a 3-year free-air CO2 enrichment experiment. *Plant Biology*, *11*, 60-69.

Horstman, A., Li, M., Heidmann, I., Weemen, M., Chen, B., Muino, J. M., Angenent, G.C., & Boutilier, K. (2017). The BABY BOOM transcription factor activates the LEC1-ABI3-FUS3-LEC2 network to induce somatic embryogenesis. *Plant physiology*, *175*(2), 848-857.

Howe, A., Sato, S., Dweikat, I., Fromm, M., & Clemente, T. (2006). Rapid and reproducible Agrobacterium-mediated transformation of Sorghum. *Plant Cell Reports*, *25*, 784-791.

Hu, Y., & Yu, D. (2014). BRASSINOSTEROID INSENSITIVE2 interacts with ABSCISIC ACID INSENSITIVE5 to mediate the antagonism of brassinosteroids to abscisic acid during seed germination in Arabidopsis. *The Plant Cell*, *26*(11), 4394-4408.

Ikeda, M., Fujiwara, S., Mitsuda, N., & Ohme-Takagi, M. (2012). A triantagonistic basic helix-loop-helix system regulates cell elongation in Arabidopsis. *The Plant Cell*, *24*(11), 4483-4497.

Ikeda, M., Mitsuda, N., & Ohme-Takagi, M. (2013). ATBS1 INTERACTING FACTORs negatively regulate Arabidopsis cell elongation in the triantagonistic bHLH system. *Plant signaling & behavior*, *8*(3), e23448.

Imkampe, J., Halter, T., Huang, S., Schulze, S., Mazzotta, S., Schmidt, N., Manstretta, R., Postel, S., Wierzba, M., Yang, Y., Van Dongen, W.M.A.M., Stahl, M., Zipfel, C., Goshe, M.B., Clouse, S., De Vries, S.C., Tax, F., Wang, X., & Kemmerling, B. (2017). The Arabidopsis leucine-rich repeat receptor kinase BIR3 negatively regulates BAK1

receptor complex formation and stabilizes BAK1. *The Plant Cell*, *29*(9), 2285-2303.

Impa, S. M., Perumal, R., Bean, S. R., Sunoj, V. J., & Jagadish, S. K. (2019). Water deficit and heat stress induced alterations in grain physico-chemical characteristics and micronutrient composition in field grown grain Sorghum. *Journal of Cereal Science*, *86*, 124-131.

Intergovernmental Panel on Climate Change (IPCC) (2023). Summary for Policymakers. In: Climate Change 2023: Synthesis Report. A Report of the Intergovernmental Panel on Climate Change. Contribution of Working Groups I, II and III to the Sixth Assessment Report of the Intergovernmental Panel on Climate Change. II and III to the Sixth Assessment Report of the Intergovernmental Panel on Climate Change.

Izadi-Darbandi, A., Alameldin, H., Namjoo, N., & Ahmad, K. (2023). Introducing Sorghum DREB2 gene in maize (Zea mays L.) to improve drought and salinity tolerance. *Biotechnology and Applied Biochemistry*, *70*(4), 1480-1488.

Jagadish, S. K. (2020). Heat stress during flowering in cereals–effects and adaptation strategies. *New Phytologist*, *226*(6), 1567-1572.

Jaillais, Y., Hothorn, M., Belkhadir, Y., Dabi, T., Nimchuk, Z. L., Meyerowitz, E. M., & Chory, J. (2011). Tyrosine phosphorylation controls brassinosteroid receptor activation by triggering membrane release of its kinase inhibitor. *Genes & development*, *25*(3), 232-237.

Jiang, H., Tang, B., Xie, Z., Nolan, T., Ye, H., Song, G. Y., Walley, J., & Yin, Y. (2019). GSK 3-like kinase BIN 2 phosphorylates RD 26 to potentiate drought signaling in Arabidopsis. *The Plant Journal*, *100*(5), 923-937.

Jiang, Y. P., Cheng, F., Zhou, Y. H., Xia, X. J., Mao, W. H., Shi, K., Chen, Z. X. & Yu, J. Q. (2012). Hydrogen peroxide functions as a secondary messenger for brassinosteroids-induced CO2 assimilation and carbohydrate metabolism in Cucumis sativus. *Journal of Zhejiang University Science B*, *13*, 811-823.

Jiang, Y., & Deyholos, M. K. (2009). Functional characterization of Arabidopsis NaCl-inducible WRKY25 and WRKY33 transcription factors in abiotic stresses. *Plant molecular biology*, *69*, 91-105.

Jiang, Y., Liang, G., & Yu, D. (2012). Activated expression of WRKY57 confers drought tolerance in Arabidopsis. *Molecular plant*, *5*(6), 1375-1388.

Jiao, Y., Burke, J., Chopra, R., Burow, G., Chen, J., Wang, B., Hayes, C., Emendack, Y., Ware, D. & Xin, Z. (2016). A Sorghum mutant resource as an efficient platform for gene discovery in grasses. *The Plant Cell*, *28*(7), 1551-1562.

Jin, X., Zheng, Y., Wang, J., Chen, W., Yang, Z., Chen, Y., Yang, Y., Lu, G., & Sun, B. (2023). SbNAC9 improves drought tolerance by enhancing scavenging ability of reactive oxygen species and activating stress-responsive genes of Sorghum. *International Journal of Molecular Sciences*, *24*(3), 2401.

Johnson, K., Cao Chu, U., Anthony, G., Wu, E., Che, P., & Jones, T. J. (2023). Rapid and highly efficient morphogenic gene-mediated hexaploid wheat transformation. *Frontiers in Plant Science*, *14*, 1151762.

Johnson, S. M., Cummins, I., Lim, F. L., Slabas, A. R., & Knight, M. R. (2015). Transcriptomic analysis comparing stay-green and senescent

Sorghum bicolor lines identifies a role for proline biosynthesis in the stay-green trait. *Journal of Experimental Botany*, *66*(22), 7061-7073.

Johnson, S. M., Lim, F. L., Finkler, A., Fromm, H., Slabas, A. R., & Knight, M. R. (2014). Transcriptomic analysis of Sorghum bicolor responding to combined heat and drought stress. *BMC genomics*, *15*, 1-19.

Jones, T., Lowe, K., Hoerster, G., Anand, A., Wu, E., Wang, N., Arling, M., Lenderts, B., & Gordon-Kamm, W. (2019). Maize transformation using the morphogenic genes Baby Boom and Wuschel2. *Transgenic Plants: Methods and Protocols*, 81-93.

Jordan, D. R., Hunt, C. H., Cruickshank, A. W., Borrell, A. K., & Henzell, R. G. (2012). The relationship between the stay-green trait and grain yield in elite Sorghum hybrids grown in a range of environments. *Crop Science*, *52*(3), 1153-1161.

Journot-Catalino, N., Somssich, I. E., Roby, D., & Kroj, T. (2006). The transcription factors WRKY11 and WRKY17 act as negative regulators of basal resistance in Arabidopsis thaliana. *The Plant Cell*, *18*(11), 3289-3302.

Kaeppler, H. F., & Pedersen, J. F. (1997). Evaluation of 41 elite and exotic inbred Sorghum genotypes for high quality callus production. *Plant cell, tissue and organ culture*, *48*, 71-75.

Kagale, S., Divi, U. K., Krochko, J. E., Keller, W. A., & Krishna, P. (2007). Brassinosteroid confers tolerance in Arabidopsis thaliana and Brassica napus to a range of abiotic stresses. *Planta*, *225*, 353-364.

Kang, H. G., & Singh, K. B. (2000). Characterization of salicylic acid-responsive, Arabidopsis Dof domain proteins: overexpression of OBP3 leads to growth defects. *The Plant Journal*, *21*(4), 329-339.

Kang, Y. H., Breda, A., & Hardtke, C. S. (2017). Brassinosteroid signaling directs formative cell divisions and protophloem differentiation in Arabidopsis root meristems. *Development*, *144*(2), 272-280.

Kanwar, M. K., Bajguz, A., Zhou, J., & Bhardwaj, R. (2017). Analysis of brassinosteroids in plants. *Journal of plant growth regulation*, *36*, 1002-1030.

Karthikeyan, A. S., Ballachanda, D. N., & Raghothama, K. G. (2009). Promoter deletion analysis elucidates the role of cis elements and 5'UTR intron in spatiotemporal regulation of AtPht1; 4 expression in Arabidopsis. *Physiologia plantarum*, *136*(1), 10-18.

Kauschmann, A., Jessop, A., Koncz, C., Szekeres, M., Willmitzer, L., & Altmann, T. (1996). Genetic evidence for an essential role of brassinosteroids in plant development. *The Plant Journal*, *9*(5), 701-713.

Kazama, D., Itakura, M., Kurusu, T., Mitsuda, N., Ohme-Takagi, M., & Tada, Y. (2013). Identification of chimeric repressors that confer salt and osmotic stress tolerance in Arabidopsis. *Plants*, *2*(4), 769-785.

Kemmerling, B., Halter, T., Mazzotta, S., Mosher, S., & Nürnberger, T. (2011). A genome-wide survey for Arabidopsis leucine-rich repeat receptor kinases implicated in plant immunity. *Frontiers in Plant Science*, *2*, 88.

Khan, R., Ma, X., Hussain, Q., Asim, M., Iqbal, A., Ren, X., Shah, S., Chen, K. & Shi, Y. (2022). Application of 2, 4-Epibrassinolide Improves Drought Tolerance in Tobacco through Physiological and Biochemical Mechanisms. *Biology*, *11*(8), 1192.

Kim T.W., Guan S., Burlingame A.L., Wang Z.Y. (2011). The CDG1 kinase mediates brassinosteroid signal transduction from BRI1 receptor kinase to BSU1 phosphatase and GSK3-like kinase BIN2. Mol. Cell **43**: 561–571.

Kim, D. W., Lee, S. H., Choi, S. B., Won, S. K., Heo, Y. K., Cho, M., Park, Y.I., & Cho, H. T. (2006). Functional conservation of a root hair cell-specific cis-element in angiosperms with different root hair distribution patterns. *The Plant Cell*, *18*(11), 2958-2970.

Kim, E. J., Lee, S. H., Park, C. H., Kim, S. H., Hsu, C. C., Xu, S., Wang, Z.Y., Kim, S.K., & Kim, T. W. (2019). Plant U-Box40 mediates degradation of the brassinosteroid-responsive transcription factor BZR1 in Arabidopsis roots. *The Plant Cell*, *31*(4), 791-808.

Kim, H. B., Kwon, M., Ryu, H., Fujioka, S., Takatsuto, S., Yoshida, S., An, C. S., Lee, I., Hwang, I. & Choe, S. (2006). The regulation of DWARF4 expression is likely a critical mechanism in maintaining the homeostasis of bioactive brassinosteroids in Arabidopsis. *Plant physiology*, *140*(2), 548-557.

Kim, J., Jung, J. H., Reyes, J. L., Kim, Y. S., Kim, S. Y., Chung, K. S., Kim, J.A., Lee, M., Lee, Y., Kim, V.N., Chua, N.H., & Park, C. M. (2005). microRNA-directed cleavage of ATHB15 mRNA regulates vascular development in Arabidopsis inflorescence stems. *The Plant Journal*, *42*(1), 84-94.

Kim, S. Y., Hedberg, P., Winder, M., & Rydberg, S. (2022). Evidence of 2, 4-diaminobutyric acid (DAB) production as a defense mechanism in diatom Thalassiosira pseudonana. *Aquatic Toxicology*, *249*, 106210.

Kim, T. W., Guan, S., Sun, Y., Deng, Z., Tang, W., Shang, J. X., Sun, Y., Burlingame, A.L., & Wang, Z. Y. (2009). Brassinosteroid signal transduction from cell-surface receptor kinases to nuclear transcription factors. *Nature cell biology*, *11*(10), 1254-1260.

Kinoshita, T., Caño-Delgado, A., Seto, H., Hiranuma, S., Fujioka, S., Yoshida, S., & Chory, J. (2005). Binding of brassinosteroids to the extracellular domain of plant receptor kinase BRI1. *Nature*, *433*(7022), 167-171.

Kir, G., Ye, H., Nelissen, H., Neelakandan, A. K., Kusnandar, A. S., Luo, A., Inzé, D., Sylvester, A. W., Yin, Y. & Becraft, P. W. (2015). RNA interference knockdown of BRASSINOSTEROID INSENSITIVE1 in maize reveals novel functions for brassinosteroid signaling in controlling plant architecture. *Plant Physiology*, *169*(1), 826-839.

Koka, C. V., Cerny, R. E., Gardner, R. G., Noguchi, T., Fujioka, S., Takatsuto, S., Yoshida, S., & Clouse, S. D. (2000). A putative role for the tomato genes DUMPY and CURL-3 in brassinosteroid biosynthesis and response. *Plant physiology*, *122*(1), 85-98.

Komari, T. (1990). Transformation of cultured cells of Chenopodium quinoa by binary vectors that carry a fragment of DNA from the virulence region of pTiBo542. *Plant Cell Reports*, *9*, 303-306.

Komari, T., Takakura, Y., Ueki, J., Kato, N., Ishida, Y., & Hiei, Y. (2006). Binary vectors and super-binary vectors. *Agrobacterium protocols*, 15-42.

Kopka, J., Schauer, N., Krueger, S., Birkemeyer, C., Usadel, B., Bergmüller, E., Dörmann, P., Weckwerth, W., Gibon, Y., Stitt, M., Willmitzer, L., Fernie, A.R. & Steinhauser, D. (2005). GMD@ CSB. DB: the Golm metabolome database. *Bioinformatics*, *21*(8), 1635-1638.

Kraft, C., Peter, M., & Hofmann, K. (2010). Selective autophagy: ubiquitin-mediated recognition and beyond. *Nature cell biology*, *12*(9), 836-841.

Krupa, K. N., Dalawai, N., Shashidhar, H. E., Harinikumar, K. M., Manojkumar, H. B., Bharani, S., & Turaidar, V. (2017). Mechanisms of drought tolerance in Sorghum: a review. *International Journal of Pure and Applied Bioscience*, *5*(4), 221-237.

Kwon, Y., Kim, J. H., Nguyen, H. N., Jikumaru, Y., Kamiya, Y., Hong, S. W., & Lee, H. (2013). A novel Arabidopsis MYB-like transcription factor, MYBH, regulates hypocotyl elongation by enhancing auxin accumulation. *Journal of experimental botany*, *64*(12), 3911-3922.

Lata, C., & Prasad, M. (2011). Role of DREBs in regulation of abiotic stress responses in plants. *Journal of experimental botany*, *62*(14), 4731-4748.

Laureyns, R., Joossens, J., Herwegh, D., Pevernagie, J., Pavie, B., Demuynck, K., Debray, K., Coussens, G., Pauwels, L., Van Hautegem, T., Bontinck, M., Strable, J., & Nelissen, H. (2022). An *in situ* sequencing approach maps PLASTOCHRON1 at the boundary between indeterminate and determinate cells. *Plant Physiology*, *188*(2), 782-794.

Lee, H. G., & Seo, P. J. (2016). The Arabidopsis MIEL1 E3 ligase negatively regulates ABA signalling by promoting protein turnover of MYB96. *Nature Communications*, *7*(1), 12525.

Lee, H. G., & Seo, P. J. (2019). MYB96 recruits the HDA15 protein to suppress negative regulators of ABA signaling in Arabidopsis. *Nature Communications*, *10*(1), 1713.

Lee, H. G., Kim, H., Suh, M. C., Kim, H. U., & Seo, P. J. (2018). The MYB96 transcription factor regulates triacylglycerol accumulation by activating DGAT1 and PDAT1 expression in Arabidopsis seeds. *Plant and Cell Physiology*, *59*(7), 1432-1442.

Lee, H. G., Lee, K., & Seo, P. J. (2015). The Arabidopsis MYB96 transcription factor plays a role in seed dormancy. *Plant molecular biology*, *87*, 371-381.

Lee, H. G., Mas, P., & Seo, P. J. (2016). MYB96 shapes the circadian gating of ABA signaling in Arabidopsis. *Scientific reports*, *6*(1), 17754.

Lee, H. G., Park, M. E., Park, B. Y., Kim, H. U., & Seo, P. J. (2019). The Arabidopsis MYB96 transcription factor mediates ABA-dependent triacylglycerol accumulation in vegetative tissues under drought stress conditions. *Plants*, *8*(9), 296.

Lee, J., & Lee, I. (2010). Regulation and function of SOC1, a flowering pathway integrator. *Journal of experimental botany*, *61*(9), 2247-2254.

Lee, K., Lee, H. G., Yoon, S., Kim, H. U., & Seo, P. J. (2015). The Arabidopsis MYB96 transcription factor is a positive regulator of ABSCISIC ACID-INSENSITIVE4 in the control of seed germination. *Plant Physiology*, *168*(2), 677-689.

Lee, S. B., Kim, H. U., & Suh, M. C. (2016). MYB94 and MYB96 additively activate cuticular wax biosynthesis in Arabidopsis. *Plant and Cell Physiology*, *57*(11), 2300-2311.

Lee, S. B., Kim, H., Kim, R. J., & Suh, M. C. (2014). Overexpression of Arabidopsis MYB96 confers drought resistance in Camelina sativa via cuticular wax accumulation. *Plant Cell Reports*, *33*, 1535-1546.

Li J., Nam K.H., Vafeados D., Chory J. (2001). BIN2, a new brassinosteroid-insensitive locus in Arabidopsis. Plant Physiol. **127**: 14–22.

Li, D., Wang, L., Wang, M., Xu, Y. Y., Luo, W., Liu, Y. J., Xu, Z.H., Li, J., & Chong, K. (2009). Engineering OsBAK1 gene as a molecular tool to improve rice architecture for high yield. *Plant biotechnology journal*, *7*(8), 791-806.

Li, H., Han, X., Liu, X., Zhou, M., Ren, W., Zhao, B., Ju, C., Liu, Y., & Zhao, J. (2019). A leucine-rich repeat-receptor-like kinase gene SbER2–1 from Sorghum (Sorghum bicolor L.) confers drought tolerance in maize. *BMC genomics*, *20*, 1-15.

Li, H., Li, D., Yang, Z., Zeng, Q., Luo, Y., & He, N. (2020). Flavones produced by mulberry flavone synthase type I constitute a defense line against the ultraviolet-B stress. *Plants*, *9*(2), 215.

Li, J., & Chory, J. (1997). A putative leucine-rich repeat receptor kinase involved in brassinosteroid signal transduction. *Cell*, *90*(5), 929-938.

Li, J., & Nam, K. H. (2002). Regulation of brassinosteroid signaling by a GSK3/SHAGGY-like kinase. *Science*, *295*(5558), 1299-1301.

Li, J., Nagpal, P., Vitart, V., McMorris, T. C., & Chory, J. (1996). A role for brassinosteroids in light-dependent development of Arabidopsis. *Science*, *272*(5260), 398-401.

Li, J., Nam, K. H., Vafeados, D., & Chory, J. (2001). BIN2, a new brassinosteroid-insensitive locus in Arabidopsis. *Plant physiology*, *127*(1), 14-22.

Li, J., Pan, W., Zhang, S., Ma, G., Li, A., Zhang, H., & Liu, L. (2024). A rapid and highly efficient Sorghum transformation strategy using GRF4-GIF1/ternary vector system. *The Plant Journal*, *117*(5), 1604-1613.

Li, J., Wen, J., Lease, K. A., Doke, J. T., Tax, F. E., & Walker, J. C. (2002). BAK1, an Arabidopsis LRR receptor-like protein kinase, interacts with BRI1 and modulates brassinosteroid signaling. *Cell*, *110*(2), 213-222.

Li, L., Ye, H., Guo, H., & Yin, Y. (2010). Arabidopsis IWS1 interacts with transcription factor BES1 and is involved in plant steroid hormone brassinosteroid regulated gene expression. *Proceedings of the national academy of sciences*, *107*(8), 3918-3923.

Li, L., Yu, X., Thompson, A., Guo, M., Yoshida, S., Asami, T., Chory, J., & Yin, Y. (2009). Arabidopsis MYB30 is a direct target of BES1 and cooperates with BES1 to regulate brassinosteroid-induced gene expression. *The Plant Journal*, *58*(2), 275-286.

Li, Q. F., Wang, C., Jiang, L., Li, S., Sun, S. S., & He, J. X. (2012). An interaction between BZR1 and DELLAs mediates direct signaling crosstalk between brassinosteroids and gibberellins in Arabidopsis. *Science signaling*, *5*(244), ra72-ra72.

Li, X., Bonawitz, N. D., Weng, J. K., & Chapple, C. (2010). The growth reduction associated with repressed lignin biosynthesis in Arabidopsis thaliana is independent of flavonoids. *The plant cell*, *22*(5), 1620-1632.

Liang, T., Shi, C., Peng, Y., Tan, H., Xin, P., Yang, Y., Wang, F., Li, X., Chu, J., Huang, J., Yin, Y. & Liu, H. (2020). Brassinosteroid-activated BRI1-EMS-SUPPRESSOR 1 inhibits flavonoid biosynthesis and coordinates growth and UV-B stress responses in plants. *Plant Cell*, *32*(10), 3224-3239.

Lisec, J., Hoffmann, F., Schmitt, C., & Jaeger, C. (2016). Extending the dynamic range in metabolomics experiments by automatic correction of peaks exceeding the detection limit. *Analytical chemistry*, *88*(15), 7487-7492.

Liu, G., & Godwin, I. D. (2012). Highly efficient Sorghum transformation. *Plant cell reports*, *31*, 999-1007.

Liu, G., Gilding, E. K., & Godwin, I. D. (2015). A robust tissue culture system for Sorghum [Sorghum bicolor (L.) Moench]. *South African Journal of Botany*, *98*, 157-160.

Liu, J., Chen, J., Zheng, X., Wu, F., Lin, Q., Heng, Y., Tian, P., Cheng, Z., Yu, X., Zhou, K., Zhang, X., Guo, X., Wang, J., Wang, H., & Wan, J. (2017). GW5 acts in the brassinosteroid signalling pathway to regulate grain width and weight in rice. *Nature plants*, *3*(5), 1-7.

Liu, L., Sun, Y., Di, P., Cui, Y., Meng, Q., Wu, X., Chen, Y., & Yuan, J. (2022). Overexpression of a Zea mays Brassinosteroid-signaling kinase gene ZmBSK1 confers salt stress tolerance in maize. *Frontiers in Plant Science*, *13*, 894710.

Liu, L., Xiang, Y., Yan, J., Di, P., Li, J., Sun, X., Han, G., Ni, L., Jiang, M., Yuan, J., & Zhang, A. (2021). BRASSINOSTEROID-SIGNALING KINASE 1 phosphorylating CALCIUM/CALMODULIN-

DEPENDENT PROTEIN KINASE functions in drought tolerance in maize. *New Phytologist*, *231*(2), 695-712.

Liu, T., Salguero, P., Petek, M., Martinez-Mira, C., Balzano-Nogueira, L., Ramšak, Ž., Mclntyre, L., Gruden, K., Tarazona, S. & Conesa, A. (2022). PaintOmics 4: new tools for the integrative analysis of multi-omics datasets supported by multiple pathway databases. *Nucleic Acids Research*, *50*(W1), W551-W559.

Liu, W., Li, R. J., Han, T. T., Cai, W., Fu, Z. W., & Lu, Y. T. (2015). Salt stress reduces root meristem size by nitric oxide-mediated modulation of auxin accumulation and signaling in Arabidopsis. *Plant physiology*, *168*(1), 343-356.

Lombardo, M. C., & Lamattina, L. (2018). Abscisic acid and nitric oxide modulate cytoskeleton organization, root hair growth and ectopic hair formation in Arabidopsis. *Nitric Oxide*, *80*, 89-97.

Lowe, K., La Rota, M., Hoerster, G., Hastings, C., Wang, N., Chamberlin, M., Wu, E., Jones, T., & Gordon-Kamm, W. (2018). Rapid genotype "independent" Zea mays L.(maize) transformation via direct somatic embryogenesis. In Vitro Cellular & Developmental Biology-Plant, 54, 240-252.

Lowe K, Wu E, Wang N, Hoerster G, Hastings C, Cho MJ, Scelonge C, Lenderts B, Chamberlin M, Cushatt J, Wang L, Ryan L, Khan T, Chow-Yiu J, Hua W, Yu M, Banh J, Bao Z, Brink K, Igo E, Rudrappa B, Shamseer PM, Bruce W, Newman L, Shen B, Zheng P, Bidney D, Falco C, Register J, Zhao ZY, Xu D, Jones T, Gordon-Kamm W. (2016). Morphogenic regulators Baby boom and Wuschel improve monocot transformation. *The Plant Cell*, *28*(9), 1998-2015.

Lozano-Elena, F., Fàbregas, N., Coleto-Alcudia, V., & Caño-Delgado, A. I. (2022). Analysis of metabolic dynamics during drought stress in Arabidopsis plants. *Scientific Data*, *9*(1), 90.

Lu, D., Wang, T., Persson, S., Mueller-Roeber, B., & Schippers, J. H. (2014). Transcriptional control of ROS homeostasis by KUODA1 regulates cell expansion during leaf development. *Nature communications*, *5*(1), 3767.

Lu, M., Zhang, D. F., Shi, Y. S., Song, Y. C., Wang, T. Y., & Li, Y. (2013). Expression of SbSNAC1, a NAC transcription factor from Sorghum, confers drought tolerance to transgenic Arabidopsis. *Plant Cell, Tissue and Organ Culture (PCTOC)*, *115*, 443-455.

Mace, E. S., Singh, V., Van Oosterom, E. J., Hammer, G. L., Hunt, C. H., & Jordan, D. R. (2012). QTL for nodal root angle in Sorghum (Sorghum bicolor L. Moench) co-locate with QTL for traits associated with drought adaptation. *Theoretical and Applied Genetics*, *124*, 97-109.

Mandava, N. B. (1988). Plant growth-promoting brassinosteroids. *Annual review of plant physiology and plant molecular biology*, *39*(1), 23-52.

Martínez, C., Espinosa-Ruíz, A., de Lucas, M., Bernardo-García, S., Franco-Zorrilla, J. M., & Prat, S. (2018). PIF 4-induced BR synthesis is critical to diurnal and thermomorphogenic growth. *The EMBO journal*, *37*(23), e99552.

Martins, S., Montiel-Jorda, A., Cayrel, A., Huguet, S., Roux, C. P. L., Ljung, K., & Vert, G. (2017). Brassinosteroid signaling-dependent root responses to prolonged elevated ambient temperature. *Nature communications*, *8*(1), 309.

Martin-StPaul, N., Delzon, S., & Cochard, H. (2017). Plant resistance to drought depends on timely stomatal closure. *Ecology letters*, *20*(11), 1437-1447.

Mcgrath, J. M., & Lobell, D. B. (2013). Reduction of transpiration and altered nutrient allocation contribute to nutrient decline of crops grown in elevated CO2 concentrations. *Plant, Cell & Environment*, *36*(3), 697-705.

Miller, S., Rønager, A., Holm, R., Fontanet-Manzaneque, J. B., Caño-Delgado, A. I., & Bjarnholt, N. (2023). New methods for Sorghum transformation in temperate climates. *AoB Plants*, *15*(3), plad030.

Mittler, R., Vanderauwera, S., Suzuki, N., Miller, G. A. D., Tognetti, V. B., Vandepoele, K., Gollery, M., Shulaev, V., & Van Breusegem, F. (2011). ROS signaling: the new wave? *Trends in plant science*, *16*(6), 300-309.

Miyashima, S., Roszak, P., Sevilem, I., Toyokura, K., Blob, B., Heo, J. O., Mellor, N., Help-Rinta-Rahko, H., Otero, S., Smet, W., Boekschoten, M., Hooiveld, G., Hashimoto, K., Smetana, O., Siligato, R., Wallner, E.S., Mähönen, A.P., Kondo, Y., Melnyk, C.W., Greb, T., Nakajima, K., Sozzani, R., Bishopp, A., De Rybel, B., & Helariutta, Y. (2019). Mobile PEAR transcription factors integrate positional cues to prime cambial growth. Nature, 565(7740), 490-494.

Montoya, T., Nomura, T., Farrar, K., Kaneta, T., Yokota, T., & Bishop, G. J. (2002). Cloning the tomato curl3 gene highlights the putative dual role of the leucine-rich repeat receptor kinase tBRI1/SR160 in plant steroid hormone and peptide hormone signaling. *The Plant Cell*, *14*(12), 3163-3176.

Mora-García, S., Vert, G., Yin, Y., Caño-Delgado, A., Cheong, H., & Chory, J. (2004). Nuclear protein phosphatases with Kelch-repeat domains modulate the response to brassinosteroids in Arabidopsis. *Genes & development*, *18*(4), 448-460.

Mullet, J. E., Klein, R. R., & Klein, P. E. (2002). Sorghum bicolor—an important species for comparative grass genomics and a source of beneficial genes for agriculture. *Current opinion in plant biology*, *5*(2), 118-121.

Mussig, C., Shin, G. H., & Altmann, T. (2003). Brassinosteroids promote root growth in Arabidopsis. *Plant Physiology*, *133*(3), 1261-1271.

Nakamura, A., Fujioka, S., Sunohara, H., Kamiya, N., Hong, Z., Inukai, Y., Miura, K., Takatsuto, S., Yoshida, S., Ueguchi-Tanaka, M., Hasegawa, Y., Kitano, H., & Matsuoka, M. (2006). The role of OsBRI1 and its homologous genes, OsBRL1 and OsBRL3, in rice. *Plant physiology*, *140*(2), 580-590.

Nam, K. H., & Li, J. (2002). BRI1/BAK1, a receptor kinase pair mediating brassinosteroid signaling. *Cell*, *110*(2), 203-212.

Nawy, T., Lee, J. Y., Colinas, J., Wang, J. Y., Thongrod, S. C., Malamy, J. E., Birnbaum, K., & Benfey, P. N. (2005). Transcriptional profile of the Arabidopsis root quiescent center. *The Plant Cell*, *17*(7), 1908-1925.

Nelson-Vasilchik, K., Hague, J., Mookkan, M., Zhang, Z. J., & Kausch, A. (2018). Transformation of recalcitrant Sorghum varieties facilitated by baby boom and Wuschel2. *Current Protocols in Plant Biology*, *3*(4), e20076.

Nemhauser, J. L., Mockler, T. C., & Chory, J. (2004). Interdependency of brassinosteroid and auxin signaling in Arabidopsis. *PLoS biology*, *2*(9), e258.

Nguyen, T. V., Thanh Thu, T., Claeys, M., & Angenon, G. (2007). Agrobacterium-mediated transformation of Sorghum (Sorghum bicolor (L.) Moench) using an improved in vitro regeneration system. *Plant cell, tissue and organ culture*, *91*, 155-164.

Nie, S., Huang, S., Wang, S., Cheng, D., Liu, J., Lv, S., Li, Q. & Wang, X. (2017). Enhancing brassinosteroid signaling via overexpression of tomato (Solanum lycopersicum) SlBRI1 improves major agronomic traits. *Frontiers in plant science*, *8*, 1386.

Nie, S., Huang, S., Wang, S., Mao, Y., Liu, J., Ma, R., & Wang, X. (2019). Enhanced brassinosteroid signaling intensity via SlBRI1 overexpression negatively regulates drought resistance in a manner opposite of that via exogenous BR application in tomato. *Plant Physiology and Biochemistry*, *138*, 36-47.

Nishizawa, A., Yabuta, Y., & Shigeoka, S. (2008). Galactinol and raffinose constitute a novel function to protect plants from oxidative damage. *Plant physiology*, *147*(3), 1251-1263.

Nolan, T. M., Brennan, B., Yang, M., Chen, J., Zhang, M., Li, Z., Wang, X., Bassham, D.C., Walley, J., & Yin, Y. (2017). Selective autophagy of BES1 mediated by DSK2 balances plant growth and survival. *Developmental cell*, *41*(1), 33-46.

Nolan, T. M., Vukašinović, N., Liu, D., Russinova, E., & Yin, Y. (2020). Brassinosteroids: multidimensional regulators of plant growth, development, and stress responses. *The Plant Cell*, *32*(2), 295-318.

O'Malley, R. C., Huang, S. S. C., Song, L., Lewsey, M. G., Bartlett, A., Nery, J. R., Galli, M., Gallavotti, A., & Ecker, J. R. (2016). Cistrome and epicistrome features shape the regulatory DNA landscape. Cell, 165(5), 1280-1292.

.

Ochieng, G., Ngugi, K., Wamalwa, L. N., Manyasa, E., Muchira, N., Nyamongo, D., & Odeny, D. A. (2021). Novel sources of drought tolerance from landraces and wild Sorghum relatives. *Crop Science*, *61*(1), 104-118.

Ogita, N., Okushima, Y., Tokizawa, M., Yamamoto, Y. Y., Tanaka, M., Seki, M., ... & Umeda, M. (2018). Identifying the target genes of SUPPRESSOR OF GAMMA RESPONSE 1, a master transcription factor controlling DNA damage response in Arabidopsis. *The Plant Journal*, *94*(3), 439-453.

Yoshiyama, K. O., Kobayashi, J., Ogita, N., Ueda, M., Kimura, S., Maki, H., & Umeda, M. (2013). ATM-mediated phosphorylation of SOG1 is essential for the DNA damage response in Arabidopsis. *EMBO reports*, *14*(9), 817-822.

Ogita, N., Okushima, Y., Tokizawa, M., Yamamoto, Y. Y., Tanaka, M., Seki, M., Makita, Y., Matsui, M., Okamoto-Yoshiyama, K., Sakamoto, T., Kurata, T., Hiruma, K., Saijo, Y., Takahashi, N., & Umeda, M. (2018). Identifying the target genes of SUPPRESSOR OF GAMMA RESPONSE 1, a master transcription factor controlling DNA damage response in Arabidopsis. *The Plant Journal*, *94*(3), 439-453.

Oh, E., Zhu, J. Y., & Wang, Z. Y. (2012). Interaction between BZR1 and PIF4 integrates brassinosteroid and environmental responses. *Nature cell biology*, *14*(8), 802-809.

Oh, E., Zhu, J. Y., Bai, M. Y., Arenhart, R. A., Sun, Y., & Wang, Z. Y. (2014). Cell elongation is regulated through a central circuit of interacting transcription factors in the Arabidopsis hypocotyl. *elife*, *3*, e03031.

Oh, E., Zhu, J. Y., Ryu, H., Hwang, I., & Wang, Z. Y. (2014). TOPLESS mediates brassinosteroid-induced transcriptional repression through interaction with BZR1. *Nature communications*, *5*(1), 4140.

OHASHI-ITO, K., & FUKUDA, H. (2003). HD-Zip III homeobox genes that include a novel member, ZeHB-13 (Zinnia). *Plant and cell physiology*, *44*(12), 1350-1358.

Ohashi-Ito, K., Iwamoto, K., Yamagami, A., Nakano, T., & Fukuda, H. (2023). HD-ZIP III-dependent local promotion of brassinosteroid synthesis suppresses vascular cell division in Arabidopsis root apical meristem. *Proceedings of the National Academy of Sciences*, *120*(15), e2216632120.

Omer, R. A., Asami, P., & Birungi, J. (2018). Callus induction and plant regeneration from immature embryos of sweet Sorghum (Sorghum bicolor Moench). *Biotechnology (Faisalabad, Pakistan)*, *17*(1).

Ordon, J., Gantner, J., Kemna, J., Schwalgun, L., Reschke, M., Streubel, J., Boch, J., & Stuttmann, J. (2017). Generation of chromosomal deletions in dicotyledonous plants employing a user-friendly genome editing toolkit. *The Plant Journal*, *89*(1), 155-168.

Ortiz, D., & Salas-Fernandez, M. G. (2022). Dissecting the genetic control of natural variation in Sorghum photosynthetic response to drought stress. *Journal of experimental botany*, *73*(10), 3251-3267.

Park, M. Y., Kim, S. A., Lee, S. J., & Kim, S. Y. (2013). ATHB17 is a positive regulator of abscisic acid response during early seedling growth. *Molecules and Cells*, *35*, 125-133.

Paterson, A. H., Bowers, J. E., Bruggmann, R., Dubchak, I., Grimwood, J., Gundlach, H., ... & Rokhsar, D. S. (2009). The Sorghum bicolor genome and the diversification of grasses. *Nature*, *457*(7229), 551-556.

Pavelescu, I., Vilarrasa-Blasi, J., Planas-Riverola, A., González-García, M. P., Caño-Delgado, A. I., & Ibañes, M. (2018). A Sizer model for cell differentiation in Arabidopsis thaliana root growth. *Molecular systems biology*, *14*(1), e7687.

Peng, P., Yan, Z., Zhu, Y., & Li, J. (2008). Regulation of the Arabidopsis GSK3-like kinase BRASSINOSTEROID-INSENSITIVE 2 through proteasome-mediated protein degradation. *Molecular plant*, *1*(2), 338-346.

Pennisi, E. (2009). How Sorghum withstands heat and drought. *Science*, *323*(5914), 573-573.

Petrov, V., Hille, J., Mueller-Roeber, B., & Gechev, T. S. (2015). ROS-mediated abiotic stress-induced programmed cell death in plants. *Frontiers in plant science*, *6*, 69.

Planas-Riverola, A., Gupta, A., Betegón-Putze, I., Bosch, N., Ibañes, M., & Caño-Delgado, A. I. (2019). Brassinosteroid signaling in plant development and adaptation to stress. *Development*, *146*(5), dev151894.

Podia, V., Chatzopoulos, D., Milioni, D., Stravopodis, D. J., Dervisi, I., Roussis, A., Roubelakis-Angelakis, K.A., & Haralampidis, K. (2023). GUS reporter-aided promoter deletion analysis of A. thaliana POLYAMINE OXIDASE 3. *International Journal of Molecular Sciences*, *24*(3), 2317.

Poutanen, K. S., Kårlund, A. O., Gómez-Gallego, C., Johansson, D. P., Scheers, N. M., Marklinder, I. M., Eriksen, A. K., Silventoinen, P. C., Nordlund, E., Sozer, N., Hanhineva, K. J., Kolehmainen, M. & Landberg, R. (2022). Grains–a major source of sustainable protein for health. *Nutrition reviews*, *80*(6), 1648-1663.

Proietti, I., Frazzoli, C., & Mantovani, A. (2015). Exploiting nutritional value of staple foods in the world's semi-arid areas: Risks, benefits, challenges and opportunities of Sorghum. In *Healthcare* (Vol. 3, No. 2, pp. 172-193). MDPI.

Queiroz, M. S., Oliveira, C. E., Steiner, F., Zuffo, A. M., Zoz, T., Vendruscolo, E. P., Eduardo, P., & Menis, F. T. (2019). Drought stresses on seed germination and early growth of maize and Sorghum. *Journal of Agricultural Science*, *11*(2), 310.

Raghuwanshi, A., & Birch, R. G. (2010). Genetic transformation of sweet Sorghum. *Plant cell reports*, *29*, 997-1005.

Raya-González, J., Prado-Rodríguez, J. C., Ruiz-Herrera, L. F., & López-Bucio, J. (2023). Loss-of-function of MEDIATOR 12 or 13 subunits causes the swelling of root hairs in response to sucrose and abscisic acid in Arabidopsis. *Plant Signaling & Behavior*, *18*(1), 2191460.

Reyna-Llorens, I., Burgess, S. J., Reeves, G., Singh, P., Stevenson, S. R., Williams, B. P., Stanley, S. & Hibberd, J. M. (2018). Ancient duons may underpin spatial patterning of gene expression in C4 leaves. *Proceedings of the National Academy of Sciences*, *115*(8), 1931-1936.

Rezaei, E. E., Webber, H., Asseng, S., Boote, K., Durand, J. L., Ewert, F., Martre, P., & MacCarthy, D. S. (2023). Climate change impacts on crop yields. *Nature Reviews Earth & Environment*, *4*(12), 831-846.

Rezaei, E. E., Webber, H., Gaiser, T., Naab, J., & Ewert, F. (2015). Heat stress in cereals: Mechanisms and modelling. *European Journal of Agronomy*, *64*, 98-113.

Rico-Medina, A., Blasco-Escámez, D., Fontanet-Manzaneque, J.B., Martignago, D., Lozano-Elena, F. and Caño-Delgado, A.I. (2023). Molecular and physiological characterization of Brassinoteroid receptor BRI1 mutants in *Sorghum bicolor*. Under submission.

Riechmann, J. L., Heard, J., Martin, G., Reuber, L., Jiang, C. Z., Keddie, J., Adam, L., Pineda, O., Ratcliffe, O.J., Samaha, R.R., Creelman, R., Pilgrim, M., Broun, P., Zhang, J.Z., Ghandehari, D., Sherman, B.K., & Yu. G.L. (2000). Arabidopsis transcription factors: genome-wide comparative analysis among eukaryotes. *science*, *290*(5499), 2105-2110.

Rivas, F. J. M., Fernie, A. R., & Aarabi, F. (2023). Roles and Regulation of the RBOHD Enzyme in Initiating ROS-Mediated Systemic Signaling During Biotic and Abiotic Stress. *Plant Stress*, 100327.

Rodrigues, S. D., Karimi, M., Impens, L., Van Lerberge, E., Coussens, G., Aesaert, S., Rombaut, D., Holtappels, D., Ibrahim, H.M.M., Van Montagu, M., Wagemans, J., Jacobs, T.B., De Coninck, B., & Pauwels,

L. (2021). Efficient CRISPR-mediated base editing in Agrobacterium spp. *Proceedings of the National Academy of Sciences*, *118*(2), e2013338118.

Rodríguez-Leal, D., Lemmon, Z. H., Man, J., Bartlett, M. E., & Lippman, Z. B. (2017). Engineering quantitative trait variation for crop improvement by genome editing. *Cell*, *171*(2), 470-480.

Rowe, J. H., Topping, J. F., Liu, J., & Lindsey, K. (2016). Abscisic acid regulates root growth under osmotic stress conditions via an interacting hormonal network with cytokinin, ethylene and auxin. *New Phytologist*, *211*(1), 225-239.

Ruiz-Sánchez, M. C., Domingo, R., Torrecillas, A., & Pérez-Pastor, A. (2000). Water stress preconditioning to improve drought resistance in young apricot plants. *Plant science*, *156*(2), 245-251.

Ryu, H., Cho, H., Bae, W., & Hwang, I. (2014). Control of early seedling development by BES1/TPL/HDA19-mediated epigenetic regulation of ABI3. *Nature communications*, *5*(1), 4138.

Ryu, H., Kim, K., Cho, H., & Hwang, I. (2010). Predominant actions of cytosolic BSU1 and nuclear BIN2 regulate subcellular localization of BES1 in brassinosteroid signaling. *Molecules and cells*, *29*, 291-296.

Sahni, S., Prasad, B. D., Liu, Q., Grbic, V., Sharpe, A., Singh, S. P., & Krishna, P. (2016). Overexpression of the brassinosteroid biosynthetic gene DWF4 in Brassica napus simultaneously increases seed yield and stress tolerance. *Scientific Reports*, *6*(1), 28298.

Salazar-Henao, J. E., Lehner, R., Betegón-Putze, I., Vilarrasa-Blasi, J., & Caño-Delgado, A. I. (2016). BES1 regulates the localization of the

brassinosteroid receptor BRL3 within the provascular tissue of the Arabidopsis primary root. *Journal of experimental botany*, *67*(17), 4951-4961.

Salem, M. A., Perez de Souza, L., Serag, A., Fernie, A. R., Farag, M. A., Ezzat, S. M., & Alseekh, S. (2020). Metabolomics in the context of plant natural products research: From sample preparation to metabolite analysis. *Metabolites*, *10*(1), 37.

Sanchez, A. C., Subudhi, P. K., Rosenow, D. T., & Nguyen, H. T. (2002). Mapping QTLs associated with drought resistance in Sorghum (Sorghum bicolor L. Moench). *Plant molecular biology*, *48*, 713-726.

Sarshad, A., Talei, D., Torabi, M., Rafiei, F., & Nejatkhah, P. (2021). Morphological and biochemical responses of Sorghum bicolor (L.) Moench under drought stress. *SN Applied Sciences*, *3*(1), 81.

Savaldi-Goldstein, S., Peto, C., & Chory, J. (2007). The epidermis both drives and restricts plant shoot growth. *Nature*, *446*(7132), 199-202.

Schilbach, S., Hantsche, M., Tegunov, D., Dienemann, C., Wigge, C., Urlaub, H., & Cramer, P. (2017). Structures of transcription pre-initiation complex with TFIIH and Mediator. *Nature*, *551*(7679), 204-209.

Schlagnhaufer, C. D., & Arteca, R. N. (1985). Brassinosteroid-induced epinasty in tomato plants. *Plant physiology*, *78*(2), 300-303.

Sehgal, A., Sita, K., Siddique, K. H., Kumar, R., Bhogireddy, S., Varshney, R. K., Hanumantharao, B., Nair, R.M., Prasad, P.V.V., & Nayyar, H. (2018). Drought or/and heat-stress effects on seed filling in

food crops: impacts on functional biochemistry, seed yields, and nutritional quality. *Frontiers in plant science*, *9*, 1705.

Seo, P. J., & Park, C. M. (2010). MYB96-mediated abscisic acid signals induce pathogen resistance response by promoting salicylic acid biosynthesis in Arabidopsis. *New phytologist*, *186*(2), 471-483.

Seo, P. J., Lee, S. B., Suh, M. C., Park, M. J., Go, Y. S., & Park, C. M. (2011). The MYB96 transcription factor regulates cuticular wax biosynthesis under drought conditions in Arabidopsis. *The Plant Cell*, *23*(3), 1138-1152.

Seo, P. J., Xiang, F., Qiao, M., Park, J. Y., Lee, Y. N., Kim, S. G., Lee, Y. H., Park, W.J., & Park, C. M. (2009). The MYB96 transcription factor mediates abscisic acid signaling during drought stress response in Arabidopsis. *Plant physiology*, *151*(1), 275-289.

Sevanto, S. (2014). Phloem transport and drought. *Journal of experimental botany*, *65*(7), 1751-1759.

Sevanto, S. (2018). Drought impacts on phloem transport. *Current Opinion in Plant Biology*, *43*, 76-81.

Sharma, B., Joshi, D., Yadav, P. K., Gupta, A. K., & Bhatt, T. K. (2016). Role of ubiquitin-mediated degradation system in plant biology. *Frontiers in plant science*, *7*, 806.

Shkolnik, D., Nuriel, R., Bonza, M. C., Costa, A., & Fromm, H. (2018). MIZ1 regulates ECA1 to generate a slow, long-distance phloem-transmitted Ca2+ signal essential for root water tracking in Arabidopsis. *Proceedings of the National Academy of Sciences*, *115*(31), 8031-8036.

Silva, T. N., Kelly, M. E., & Vermerris, W. (2020). Use of Sorghum bicolor leaf whorl explants to expedite regeneration and increase transformation throughput. *Plant Cell, Tissue and Organ Culture (PCTOC)*, *141*(2), 243-255.

Singh, K. B. (1998). Transcriptional regulation in plants: the importance of combinatorial control. *Plant Physiology*, *118*(4), 1111-1120.

Singh, K. B., Foley, R. C., & Oñate-Sánchez, L. (2002). Transcription factors in plant defense and stress responses. *Current opinion in plant biology*, *5*(5), 430-436.

Singh, V., van Oosterom, E. J., Jordan, D. R., Hunt, C. H., & Hammer, G. L. (2011). Genetic variability and control of nodal root angle in Sorghum. *Crop Science*, *51*(5), 2011-2020.

Skirycz, A., Radziejwoski, A., Busch, W., Hannah, M. A., Czeszejko, J., Kwaśniewski, M., Zanor, M.I., Lohmann J.U., De Veylder, L., Witt, I., & Mueller-Roeber, B. (2008). The DOF transcription factor OBP1 is involved in cell cycle regulation in Arabidopsis thaliana. The Plant Journal, 56(5), 779-792.

Smith, R. L., Hoveland, C. S., & Hanna, W. W. (1989). Water stress and temperature in relation to seed germination of pearl millet and Sorghum. *Agronomy Journal*, *81*(2), 303-305.

Sreeramulu S., Mostizky Y., Sunitha S., Shani E., Nahum H., Salomon D., Hayun L.B., Gruetter C., Rauh D., Ori N., Sessa G. (2013). BSKs are partially redundant positive regulators of brassinosteroid signaling in Arabidopsis. Plant J. **74**: 905–919.

Stanfield, R. C., & Bartlett, M. K. (2022). Coordination between phloem loading and structure maintains carbon transport under drought. *Frontiers in plant science*, *13*, 787837.

Stuttmann, J., Barthel, K., Martin, P., Ordon, J., Erickson, J. L., Herr, R., Ferik, F., Kretschmer, C., Berner, T., Keilwagen, J., Marillonnet, S., & Bonas, U. (2021). Highly efficient multiplex editing: one-shot generation of 8× Nicotiana and 12× Arabidopsis mutants. *The Plant Journal*, *106*(1), 8-22.

Sun, Y., Fan, X. Y., Cao, D. M., Tang, W., He, K., Zhu, J. Y., He, J. X., Bai, M. Y., Zhu, S., Oh, E., Patil, S., Kim, T. W., Ji, H., Wong, W. H., Rhee, S. Y. & Wang, Z. Y. (2010). Integration of brassinosteroid signal transduction with the transcription network for plant growth regulation in Arabidopsis. *Developmental cell*, *19*(5), 765-777.

Swinnen, G., Goossens, A., & Pauwels, L. (2016). Lessons from domestication: targeting cis-regulatory elements for crop improvement. *Trends in plant science*, *21*(6), 506-515.

Symanczik, S., Lehmann, M. F., Wiemken, A., Boller, T., & Courty, P. E. (2018). Effects of two contrasted arbuscular mycorrhizal fungal isolates on nutrient uptake by Sorghum bicolor under drought. *Mycorrhiza*, *28*(8), 779-785.

Szekeres, M., Németh, K., Koncz-Kálmán, Z., Mathur, J., Kauschmann, A., Altmann, T., Rédei, G.P., Nagy, F., Schell, J., & Koncz, C. (1996). Brassinosteroids rescue the deficiency of CYP90, a cytochrome P450, controlling cell elongation and de-etiolation in Arabidopsis. *Cell*, *85*(2), 171-182.

Tadesse, Y., Sagi, L., Swennen, R., & Jacobs, M. (2003). Optimisation of transformation conditions and production of transgenic Sorghum (Sorghum bicolor) via microparticle bombardment. *Plant Cell, Tissue and Organ Culture*, *75*, 1-18.

Takahashi, N., Goto, N., Okada, K., & Takahashi, H. (2002). Hydrotropism in abscisic acid, wavy, and gravitropic mutants of Arabidopsis thaliana. *Planta*, *216*, 203-211.

Takahashi, N., Suita, K., Koike, T., Ogita, N., Zhang, Y., & Umeda, M. (2024). DNA double-strand breaks enhance brassinosteroid signaling to activate quiescent center cell division in Arabidopsis. *Journal of Experimental Botany*, *75*(5), 1364-1375.

Tang W., et al. (2011). PP2A activates brassinosteroid-responsive gene expression and plant growth by dephosphorylating BZR1. Nat. Cell Biol. **13**: 124–131.

Tang W., Kim T.W., Oses-Prieto J.A., Sun Y., Deng Z., Zhu S., Wang R., Burlingame A.L., Wang Z.Y. (2008). BSKs mediate signal transduction from the receptor kinase BRI1 in Arabidopsis. Science **321**: 557–560.

Tapia-López, R., García-Ponce, B., Dubrovsky, J. G., Garay-Arroyo, A., Pérez-Ruíz, R. V., Kim, S. H., Acevedo, F., Pelaz, S., & Alvarez-Buylla, E. R. (2008). An AGAMOUS-related MADS-box gene, XAL1 (AGL12), regulates root meristem cell proliferation and flowering transition in Arabidopsis. *Plant physiology*, *146*(3), 1182-1192.

Taylor, J. R., Schober, T. J., & Bean, S. R. (2006). Novel food and non-food uses for Sorghum and millets. *Journal of cereal science*, *44*(3), 252-271.

Thijs, G., Lescot, M., Marchal, K., Rombauts, S., De Moor, B., Rouze, P., & Moreau, Y. (2001). A higher-order background model improves the detection of promoter regulatory elements by Gibbs sampling. Bioinformatics, 17(12), 1113-1122.

Thomas, M. R., Matsumoto, S., Cain, P., & Scott, N. S. (1993). Repetitive DNA of grapevine: classes present and sequences suitable for cultivar identification. *Theoretical and Applied Genetics*, *86*, 173-180.

Tian, Y., Fan, M., Qin, Z., Lv, H., Wang, M., Zhang, Z., Zhou, W., Zhao, N., Li, X., Han, C., Ding, Z., Wang, W., Wang, Z. Y. & Bai, M. Y. (2018). Hydrogen peroxide positively regulates brassinosteroid signaling through oxidation of the BRASSINAZOLE-RESISTANT1 transcription factor. *Nature Communications*, *9*(1), 1063.

Tong, H., Jin, Y., Liu, W., Li, F., Fang, J., Yin, Y., Qian, Q., Zhu, L., & Chu, C. (2009). DWARF AND LOW-TILLERING, a new member of the GRAS family, plays positive roles in brassinosteroid signaling in rice. *The Plant Journal*, *58*(5), 803-816.

Tong, H., Liu, L., Jin, Y., Du, L., Yin, Y., Qian, Q., Zhu, L., & Chu, C. (2012). DWARF AND LOW-TILLERING acts as a direct downstream target of a GSK3/SHAGGY-like kinase to mediate brassinosteroid responses in rice. *The Plant Cell*, *24*(6), 2562-2577.

Turatsinze, J. V., Thomas-Chollier, M., Defrance, M., & Van Helden, J. (2008). Using RSAT to scan genome sequences for transcription factor binding sites and cis-regulatory modules. *Nature protocols*, *3*(10), 1578.

Tuteja, N., & Mahajan, S. (2007). Calcium signaling network in plants: an overview. *Plant signaling & behavior*, *2*(2), 79-85.

Ullah, A., Nadeem, F., Nawaz, A., Siddique, K. H., & Farooq, M. (2022). Heat stress effects on the reproductive physiology and yield of wheat. *Journal of agronomy and crop science*, *208*(1), 1-17.

United Nations (2022). Department of Economic and Social Affairs, Population Division, "World population prospects 2022: Summary of Results;
https://www.un.org/development/desa/pd/sites/www.un.org.development.desa.pd/files/undesa_pd_2022_wpp_key-messages.pdf

Van Dijk, M., Morley, T., Rau, M. L., & Saghai, Y. (2021). A meta-analysis of projected global food demand and population at risk of hunger for the period 2010–2050. Nature Food, 2(7), 494-501.

Varoquaux, N., Cole, B., Gao, C., Pierroz, G., Baker, C. R., Patel, D., ... & Purdom, E. (2019). Transcriptomic analysis of field-droughted Sorghum from seedling to maturity reveals biotic and metabolic responses. *Proceedings of the National Academy of Sciences*, *116*(52), 27124-27132.

Venkateswaran, K., Elangovan, M., & Sivaraj, N. (2019). Origin, domestication and diffusion of Sorghum bicolor. In *Breeding Sorghum for diverse end uses* (pp. 15-31). Woodhead Publishing.

Vert G., Chory J. (2006). Downstream nuclear events in brassinosteroid signalling. Nature **441**: 96–100.

Vilarrasa-Blasi, J., González-García, M. P., Frigola, D., Fàbregas, N., Alexiou, K. G., Lopez-Bigas, N., Rivas, S., Jauneau, A., Lohmann, J.U., Benfey, P.N., Ibañes, M., & Cano-Delgado, A. I. (2014). Regulation of plant stem cell quiescence by a brassinosteroid signaling module. *Developmental cell*, *30*(1), 36-47.

Visarada, K. B. R. S., & Sai Kishore, N. (2015). Advances in genetic transformation. *Sorghum molecular breeding*, 199-215.

Vukašinović, N., Wang, Y., Vanhoutte, I., Fendrych, M., Guo, B., Kvasnica, M., Jiroutová, P., Oklestkova, J., & Russinova, E. (2021). Local brassinosteroid biosynthesis enables optimal root growth. *Nature plants*, *7*(5), 619-632.

Waite, J. M., & Dardick, C. (2018). TILLER ANGLE CONTROL 1 modulates plant architecture in response to photosynthetic signals. *Journal of Experimental Botany*, *69*(20), 4935-4944.

Wang, N., Ryan, L., Sardesai, N., Wu, E., Lenderts, B., Lowe, K., Che, P., Anand, A., Worden, A., van Dyk, D., Barone, P., Svitashev, S., Jones, T., & Gordon-Kamm, W. (2023). Leaf transformation for efficient random integration and targeted genome modification in maize and Sorghum. *Nature Plants*, *9*(2), 255-270.

Wang, Y. C., Yu, M., Shih, P. Y., Wu, H. Y., & Lai, E. M. (2018). Stable pH suppresses defense signaling and is the key to enhance Agrobacterium-mediated transient expression in Arabidopsis seedlings. *Scientific reports*, *8*(1), 17071.

Wang, D., Heckathorn, S. A., Barua, D., Joshi, P., Hamilton, E. W., & LaCroix, J. J. (2008). Effects of elevated CO2 on the tolerance of photosynthesis to acute heat stress in C3, C4, and CAM species. *American Journal of Botany*, *95*(2), 165-176.

Wang, G., Long, Y., Jin, X., Yang, Z., Dai, L., Yang, Y., Lu, G., & Sun, B. (2024). SbMYC2 mediates jasmonic acid signaling to improve drought tolerance via directly activating SbGR1 in Sorghum. *Theoretical and Applied Genetics*, *137*(3), 72.

Wang, H., Zhu, Y., Fujioka, S., Asami, T., Li, J., & Li, J. (2009). Regulation of Arabidopsis brassinosteroid signaling by atypical basic helix-loop-helix proteins. *The Plant Cell*, *21*(12), 3781-3791.

WANG, L. S., CHEN, Q. S., XIN, D. W., QI, Z. M., Zhang, C., LI, S. N., JIN, Y.M., LI, M., MEI, H.Y., SU, A.Y., & WU, X. X. (2018). Overexpression of GmBIN2, a soybean glycogen synthase kinase 3 gene, enhances tolerance to salt and drought in transgenic Arabidopsis and soybean hairy roots. *Journal of integrative agriculture*, *17*(9), 1959-1971.

Wang, S., Liu, D., Jin, T., Du, J., Tian, A., Huang, Q., Khan, M., Nie, S., Zhang, S., Deng, R., Zhang, M., & Wang, X. (2023). Manipulation of brassinosteroid signaling via overexpression of its major receptor SlBRI1 regulates salt tolerance in tomato. *Scientia Horticulturae*, *322*, 112457.

Wang, X., & Chory, J. (2006). Brassinosteroids regulate dissociation of BKI1, a negative regulator of BRI1 signaling, from the plasma membrane. *Science*, *313*(5790), 1118-1122.

Wang, X., Aguirre, L., Rodríguez-Leal, D., Hendelman, A., Benoit, M., & Lippman, Z. B. (2021). Dissecting cis-regulatory control of quantitative trait variation in a plant stem cell circuit. *Nature Plants*, *7*(4), 419-427.

Wang, X., Chen, J., Xie, Z., Liu, S., Nolan, T., Ye, H., Zhang, M., Guo, H., Schnable, P.S., Li, Z., & Yin, Y. (2014). Histone lysine methyltransferase SDG8 is involved in brassinosteroid-regulated gene expression in Arabidopsis thaliana. *Molecular plant*, *7*(8), 1303-1315.

Wang, X., Goshe, M. B., Soderblom, E. J., Phinney, B. S., Kuchar, J. A., Li, J., Asami, T., Yoshida, S., Huber, S.C., & Clouse, S. D. (2005). Identification and functional analysis of in vivo phosphorylation sites of the Arabidopsis BRASSINOSTEROID-INSENSITIVE1 receptor kinase. *The Plant Cell*, *17*(6), 1685-1703.

Wang, X., Li, X., Meisenhelder, J., Hunter, T., Yoshida, S., Asami, T., & Chory, J. (2005). Autoregulation and homodimerization are involved in the activation of the plant steroid receptor BRI1. *Developmental cell*, *8*(6), 855-865.

Wang, Y., Sun, S., Zhu, W., Jia, K., Yang, H., & Wang, X. (2013). Strigolactone/MAX2-induced degradation of brassinosteroid transcriptional effector BES1 regulates shoot branching. *Developmental cell*, *27*(6), 681-688.

Wang, Y., Zhang, L., Zhang, L., Xing, T., Peng, J., Sun, S., Chen, G., & Wang, X. (2013). A novel stress-associated protein SbSAP14 from Sorghum bicolor confers tolerance to salt stress in transgenic rice. *Molecular breeding*, *32*, 437-449.

Wang, Z. Y., Nakano, T., Gendron, J., He, J., Chen, M., Vafeados, D., Yang, Y., Fujioka, S., Yoshida, S., Asami, T. & Chory, J. (2002). Nuclear-localized BZR1 mediates brassinosteroid-induced growth and feedback suppression of brassinosteroid biosynthesis. *Developmental cell*, *2*(4), 505-513.

Wang, Z. Y., Seto, H., Fujioka, S., Yoshida, S., & Chory, J. (2001). BRI1 is a critical component of a plasma-membrane receptor for plant steroids. *Nature*, *410*(6826), 380-383.

Wehbi, H., Soulhat, C., Morin, H., Bendahmane, A., Hilson, P., & Bouchabké-Coussa, O. (2022). One-week scutellar somatic embryogenesis in the monocot Brachypodium distachyon. *Plants*, *11*(8), 1068.

Wei, H., Song, Z., Xie, Y., Cheng, H., Yan, H., Sun, F., Liu, H., Shen, J., Li, L., He, X., Wang, H., & Luo, K. (2023). High temperature inhibits vascular development via the PIF4-miR166-HB15 module in Arabidopsis. *Current Biology*, *33*(15), 3203-3214.

Weng, J., Gu, S., Wan, X., Gao, H., Guo, T., Su, N., Lei, C., Zhang, X., Cheng, Z., Guo, X., Wang, J., Jiang, L., Zhai, H., & Wan, J. (2008). Isolation and initial characterization of GW5, a major QTL associated with rice grain width and weight. *Cell research*, *18*(12), 1199-1209.

Wu, E., Lenderts, B., Glassman, K., Berezowska-Kaniewska, M., Christensen, H., Asmus, T.,Zhen, S., Chu, U., Cho, M.J., & Zhao, Z. Y. (2014). Optimized Agrobacterium-mediated Sorghum transformation protocol and molecular data of transgenic Sorghum plants. *In Vitro Cellular & Developmental Biology-Plant*, *50*, 9-18.

Wu, Q., Liu, Y., Xie, Z., Yu, B., Sun, Y., & Huang, J. (2022). OsNAC016 regulates plant architecture and drought tolerance by interacting with the kinases GSK2 and SAPK8. *Plant Physiology*, *189*(3), 1296-1313.

Xia, X. J., Gao, C. J., Song, L. X., Zhou, Y. H., Shi, K. A. I., & Yu, J. Q. (2014). Role of H2O2 dynamics in brassinosteroid-induced stomatal closure and opening in Solanum lycopersicum. *Plant, Cell & Environment*, *37*(9), 2036-2050.

Xiang, L., Nolan, T. M., Bao, Y., Elmore, M., Tuel, T., Gai, J., Shah, D., Wang, P., Huser, N. M., Hurd, A. M., McLaughlin, S. A., Howell, S. H., Walley, J. W., Yin, Y. & Tang, L. (2021). Robotic Assay for Drought (RoAD): An automated phenotyping system for brassinosteroid and drought responses. *The Plant Journal*, *107*(6), 1837-1853.

Xiao, Y., Liu, D., Zhang, G., Tong, H., & Chu, C. (2017). Brassinosteroids regulate OFP1, a DLT interacting protein, to modulate plant architecture and grain morphology in rice. *Frontiers in Plant Science*, *8*, 299021.

Xie, P., Tang, S., Chen, C., Zhang, H., Yu, F., Li, C., Wei, H., Sui, Y., Wu, C., Diao, X., Wu, Y., & Xie, Q. (2022). Natural variation in Glume Coverage 1 causes naked grains in Sorghum. *Nature Communications*, *13*(1), 1068.

Xie, Z., Nolan, T., Jiang, H., Tang, B., Zhang, M., Li, Z., & Yin, Y. (2019). The AP2/ERF transcription factor TINY modulates brassinosteroid-regulated plant growth and drought responses in Arabidopsis. *The Plant Cell*, *31*(8), 1788-1806.

Xing, D. H., Lai, Z. B., Zheng, Z. Y., Vinod, K. M., Fan, B. F., & Chen, Z. X. (2008). Stress-and pathogen-induced Arabidopsis WRKY48 is a transcriptional activator that represses plant basal defense. *Molecular plant*, *1*(3), 459-470.

Xiong, L., & Zhu, J. K. (2001). Abiotic stress signal transduction in plants: molecular and genetic perspectives. *Physiologia plantarum*, *112*(2), 152-166.

Xu, W., Huang, J., Li, B., Li, J., & Wang, Y. (2008). Is kinase activity essential for biological functions of BRI1?. *Cell research*, *18*(4), 472-478.

Xu, W., Rosenow, D. T., & Nguyen, H. T. (2000). Stay green trait in grain Sorghum: relationship between visual rating and leaf chlorophyll concentration. *Plant Breeding*, *119*(4), 365-367.

Xu, Z., Jiang, Y., & Zhou, G. (2015). Response and adaptation of photosynthesis, respiration, and antioxidant systems to elevated CO2 with environmental stress in plants. *Frontiers in plant science*, *6*, 701.

Yamamuro, C., Ihara, Y., Wu, X., Noguchi, T., Fujioka, S., Takatsuto, S., Ashikari, M., Kitano, H. & Matsuoka, M. (2000). Loss of function of a rice brassinosteroid insensitive1 homolog prevents internode elongation and bending of the lamina joint. *The Plant Cell*, *12*(9), 1591-1605.

Yang, Z., Chi, X., Guo, F., Jin, X., Luo, H., Hawar, A., Chen, Y., Feng, K., Wang, B., Qi, J., Yang, Y., & Sun, B. (2020). SbWRKY30 enhances the drought tolerance of plants and regulates a drought stress-responsive gene, SbRD19, in Sorghum. *Journal of plant physiology*, *246*, 153142.

Ye, H., Li, L., Guo, H., & Yin, Y. (2012). MYBL2 is a substrate of GSK3-like kinase BIN2 and acts as a corepressor of BES1 in brassinosteroid signaling pathway in Arabidopsis. *Proceedings of the National Academy of Sciences*, *109*(49), 20142-20147.

Ye, H., Liu, S., Tang, B., Chen, J., Xie, Z., Nolan, T. M., Jiang, H., Guo, H., Lin, H. Y., Li, L., Wang, Y., Tong, H., Zhang, M., Chu, C., Li, Z., Aluru, M., Aluru, S., Schnable, P. S. & Yin, Y. (2017). RD26 mediates

crosstalk between drought and brassinosteroid signalling pathways. *Nature Communications*, *8*(1), 14573.

Yin, Y., Vafeados, D., Tao, Y., Yoshida, S., Asami, T., & Chory, J. (2005). A new class of transcription factors mediates brassinosteroid-regulated gene expression in Arabidopsis. *Cell*, *120*(2), 249-259.

Yin, Y., Wang, Z. Y., Mora-Garcia, S., Li, J., Yoshida, S., Asami, T., & Chory, J. (2002). BES1 accumulates in the nucleus in response to brassinosteroids to regulate gene expression and promote stem elongation. *Cell*, *109*(2), 181-191.

Yokotani, N., Higuchi, M., Kondou, Y., Ichikawa, T., Iwabuchi, M., Hirochika, H., Matsui, M. & Oda, K. (2011). A novel chloroplast protein, CEST induces tolerance to multiple environmental stresses and reduces photooxidative damage in transgenic Arabidopsis. *Journal of experimental botany*, *62*(2), 557-569.

Yoshida, T., Fujita, Y., Maruyama, K., Mogami, J., Todaka, D., Shinozaki, K., & Yamaguchi-Shinozaki, K. (2015). Four A rabidopsis AREB/ABF transcription factors function predominantly in gene expression downstream of SnRK2 kinases in abscisic acid signalling in response to osmotic stress. *Plant, cell & environment*, *38*(1), 35-49.

Yu, J. Q., Wang, J. H., Sun, C. H., Zhang, Q. Y., Hu, D. G., & Hao, Y. J. (2018). Ectopic expression of the apple nucleus-encoded thylakoid protein MdY3IP1 triggers early-flowering and enhanced salt-tolerance in Arabidopsis thaliana. *BMC plant biology*, *18*, 1-13.

Yu, X., Li, L., Li, L., Guo, M., Chory, J., & Yin, Y. (2008). Modulation of brassinosteroid-regulated gene expression by Jumonji domain-

containing proteins ELF6 and REF6 in Arabidopsis. *Proceedings of the National Academy of Sciences*, *105*(21), 7618-7623.

Yu, X., Li, L., Zola, J., Aluru, M., Ye, H., Foudree, A., Guo, H., Anderson, S., Aluru, S., Liu, P., Rodermel, S. & Yin, Y. (2011). A brassinosteroid transcriptional network revealed by genome-wide identification of BESI target genes in Arabidopsis thaliana. *The Plant Journal*, *65*(4), 634-646.

Yuan, Z. C., Liu, P., Saenkham, P., Kerr, K., & Nester, E. W. (2008). Transcriptome profiling and functional analysis of Agrobacterium tumefaciens reveals a general conserved response to acidic conditions (pH 5.5) and a complex acid-mediated signaling involved in Agrobacterium-plant interactions. *Journal of Bacteriology*, *190*(2), 494-507.

Yuan, L., Yuan, Y., Du, J., Sun, J., & Guo, S. (2012). Effects of 24-epibrassinolide on nitrogen metabolism in cucumber seedlings under Ca (NO3) 2 stress. *Plant physiology and biochemistry*, *61*, 29-35.

Yue, J., You, Y., Zhang, L., Fu, Z., Wang, J., Zhang, J., & Guy, R. D. (2019). Exogenous 24-epibrassinolide alleviates effects of salt stress on chloroplasts and photosynthesis in Robinia pseudoacacia L. seedlings. *Journal of Plant Growth Regulation*, *38*, 669-682.

Zeng, H., Tang, Q., & Hua, X. (2010). Arabidopsis brassinosteroid mutants det2-1 and bin2-1 display altered salt tolerance. *Journal of Plant Growth Regulation*, *29*, 44-52.

Zhang, Q., Zhang, Y., Lu, M. H., Chai, Y. P., Jiang, Y. Y., Zhou, Y., Wang, X.C., & Chen, Q. J. (2019). A novel ternary vector system united

with morphogenic genes enhances CRISPR/Cas delivery in maize. *Plant Physiology*, *181*(4), 1441-1448.

ZHANG, D. F., ZENG, T. R., LIU, X. Y., GAO, C. X., LI, Y. X., LI, C. H., SONG, Y.C., SHI, Y.S., WANG, T.Y., & Yu, L. I. (2019). Transcriptomic profiling of Sorghum leaves and roots responsive to drought stress at the seedling stage. *Journal of integrative agriculture*, *18*(9), 1980-1995.

Zhang, D., Jing, Y., Jiang, Z., & Lin, R. (2014). The chromatin-remodeling factor PICKLE integrates brassinosteroid and gibberellin signaling during skotomorphogenic growth in Arabidopsis. *The Plant Cell*, *26*(6), 2472-2485.

Zhang, D., Ye, H., Guo, H., Johnson, A., Zhang, M., Lin, H., & Yin, Y. (2014). Transcription factor HAT 1 is phosphorylated by BIN 2 kinase and mediates brassinosteroid repressed gene expression in a rabidopsis. *The Plant Journal*, *77*(1), 59-70.

Zhang, H., Yu, F., Xie, P., Sun, S., Qiao, X., Tang, S., ... & Xie, Q. (2023). A Gγ protein regulates alkaline sensitivity in crops. *Science*, *379*(6638), eade8416.

Zhang, L. M., Leng, C. Y., Luo, H., Wu, X. Y., Liu, Z. Q., Zhang, Y. M., Zhang, H., Xia, Y., Shang, L., Liu, C.M., Hao, D.Y., Zhou, Y.H., Chu, C.C., Cai, H.W., & Jing, H. C. (2018). Sweet Sorghum originated through selection of Dry, a plant-specific NAC transcription factor gene. *The Plant Cell*, *30*(10), 2286-2307.

Zhang, L. Y., Bai, M. Y., Wu, J., Zhu, J. Y., Wang, H., Zhang, Z., ... & Wang, Z. Y. (2009). Antagonistic HLH/bHLH transcription factors mediate brassinosteroid regulation of cell elongation and plant

development in rice and Arabidopsis. *The Plant Cell*, *21*(12), 3767-3780.

Zhang, L., Xin, Z., Yu, X., Ma, C., Liang, W., Zhu, M., Cheng, Q., Li, Z., Niu, Y., Ren, Y., Wang, Z. & Lin, T. (2017). Osmotic stress induced cell death in wheat is alleviated by tauroursodeoxycholic acid and involves endoplasmic reticulum stress–related gene expression. *Frontiers in Plant Science*, *8*, 667.

Zhang, S., Cai, Z., & Wang, X. (2009). The primary signaling outputs of brassinosteroids are regulated by abscisic acid signaling. *Proceedings of the National Academy of Sciences*, *106*(11), 4543-4548.

Zhang, X., Wang, J., Huang, J., Lan, H., Wang, C., Yin, C., Wu, Y., Tang, H., Qian, Q., Li, J., & Zhang, H. (2012). Rare allele of OsPPKL1 associated with grain length causes extra-large grain and a significant yield increase in rice. *Proceedings of the National Academy of Sciences*, *109*(52), 21534-21539.

Zhang, Y., Mitsuda, N., Yoshizumi, T., Horii, Y., Oshima, Y., Ohme-Takagi, M., Matsui, M., & Kakimoto, T. (2021). Two types of bHLH transcription factor determine the competence of the pericycle for lateral root initiation. *Nature Plants*, *7*(5), 633-643.

Zhao J., Peng P., Schmitz R.J., Decker A.D., Tax F.E., Li J. (2002). Two putative BIN2 substrates are nuclear components of brassinosteroid signaling. Plant Physiol. **130**: 1221–1229

Zhao, Z. Y., Cai, T., Tagliani, L., Miller, M., Wang, N., Pang, H., Rudert, M., Schroeder, S., Hondred, D., Seltzer, J., & Pierce, D. (2000). Agrobacterium-mediated Sorghum transformation. *Plant Molecular Biology*, *44*, 789-798.

Zhao, P., Cui, R., Xu, P., Wu, J., Mao, J. L., Chen, Y., Zhou, C., Yu, L., & Xiang, C. B. (2017). ATHB17 enhances stress tolerance by coordinating photosynthesis associated nuclear gene and ATSIG5 expression in response to abiotic stress. *Scientific reports*, *7*(1), 45492.

Zhao, Z. Y., Cai, T., Tagliani, L., Miller, M., Wang, N., Pang, H., Rudert, M., Schroeder, S., Hondred, D., Seltzer, J., & Pierce, D. (2000). Agrobacterium-mediated Sorghum transformation. *Plant Molecular Biology*, *44*, 789-798.

Zhao, Z. Y., Gu, W., Cai, T., Tagliani, L., Hondred, D., Bond, D., Schroeder, S., Rudert, M., & Pierce, D. (2002). High throughput genetic transformation mediated by Agrobacterium tumefaciens in maize. *Molecular Breeding*, *8*, 323-333.

Zhao, Z., Tang, S., Li, W., Yang, X., Wang, R., Diao, X., & Tang, W. (2021). Overexpression of a BRASSINAZOLE RESISTANT 1 homolog attenuates drought tolerance by suppressing the expression of PLETHORA-LIKE 1 in Setaria italica. *The Crop Journal*, *9*(5), 1208-1213.

Zhao, Z., Wu, S., Gao, H., Tang, W., Wu, X., & Zhang, B. (2023). The BR signaling pathway regulates primary root development and drought stress response by suppressing the expression of PLT1 and PLT2 in Arabidopsis thaliana. *Frontiers in Plant Science*, *14*, 1187605.

Zhou, A., Wang, H., Walker, J. C., & Li, J. (2004). BRL1, a leucine-rich repeat receptor-like protein kinase, is functionally redundant with BRI1 in regulating Arabidopsis brassinosteroid signaling. *The Plant Journal*, *40*(3), 399-409.

Zhou, J., Liu, D., Wang, P., Ma, X., Lin, W., Chen, S., Mishev, K., Lu, D., Kumar, R., Vanhoutte, I., Meng, X., He, P., Russinova, E., & Shan, L. (2018). Regulation of Arabidopsis brassinosteroid receptor BRI1 endocytosis and degradation by plant U-box PUB12/PUB13-mediated ubiquitination. *Proceedings of the National Academy of Sciences*, *115*(8), E1906-E1915.

Zhou, J., Wang, J., Li, X., Xia, X. J., Zhou, Y. H., Shi, K., Chen, Z., & Yu, J. Q. (2014). H2O2 mediates the crosstalk of brassinosteroid and abscisic acid in tomato responses to heat and oxidative stresses. *Journal of Experimental Botany*, *65*(15), 4371-4383.

Zhu, T., Deng, X., Zhou, X., Zhu, L., Zou, L., Li, P., Zhang, D., & Lin, H. (2016). Ethylene and hydrogen peroxide are involved in brassinosteroid-induced salt tolerance in tomato. *Scientific reports*, *6*(1), 35392.

Zhu, Y., Zuo, M., Liang, Y., Jiang, M., Zhang, J., Scheller, H. V., Tan, M. & Zhang, A. (2013). MAP65-1a positively regulates H2O2 amplification and enhances brassinosteroid-induced antioxidant defence in maize. *Journal of experimental botany*, *64*(12), 3787-3802.

Zöllner, N. R., Bezrutczyk, M., Laureyns, R., Nelissen, H., Simon, R., & Frommer, W. B. (2021). An RNA in situ hybridization protocol optimized for monocot tissue. *STAR protocols*, *2*(2), 100398.

Zuo, J., Niu, Q. W., Frugis, G., & Chua, N. H. (2002). The WUSCHEL gene promotes vegetative-to-embryonic transition in Arabidopsis. *The Plant Journal*, *30*(3), 349-359.

LIST OF FIGURES

Figure 1.1 Working model of the brassinosteroid signal transduction. ...15

Figure 1.2 Brassinosteroids in plant adaptation to abiotic stress.....27

Figure 1.3 The impact of drought on Sorghum and its tolerance mechanisms 38

Figure 2.1 Regulatory sequence analysis output for *BRL3* promoter using Cis-BP dataset.....64

Figure 2.2 Regulatory sequence analysis output for *BRL3* promoter using JASPAR dataset. 65

Figure 2.3 Phylogenetic shadowing in *BRL3* promoter.....67

Figure 2.4 Refined promoter deletion analysis of *BRL3*. 69

Figure 2.5 *BRL3* expression under different promoter lengths. 70

Figure 2.6 *BRL3* is expressed in the stomata. 71

Figure 2.7 *BRL3* expression under different promoter lengths in the root apical meristem.....73

Figure 2.8 *BRL3* expression is induced in the hypocotyl and repressed in the root upon elevated temperature. 75

Figure 2.9 *BRL3* expression under different promoter lengths in the hypocotyl and root upon elevated temperatures. 77

Figure 2.10 *BRL3* expression is induced in the root meristem upon DNA damage. 79

Figure 2.11 *BRL3* expression under different promoter lengths in the root apical meristem upon DNA damage. 80

Figure 2.12 HB15 is a negative regulator of *BRL3* expression. 83

Figure 2.13 HAT9, together with HB15, is a negative regulator of *BRL3* expression.....85

Figure 2.14 Engineering *BRL3* promoter to enhance its vascular expression.....88

Figure 3.1 Thermomorphogenesis screening of TF T-DNA mutant lines. 97

Figure 3.2 TF overexpressing lines. 99

Figure 3.3 Overexpression of TF2 and TF8 confers drought tolerance. .101

Figure 3.4 Overexpression of TF10 confers drought tolerance. 102

Figure 3.5 *MYB96* is natively expressed in the root meristem, mature endodermis and in the cotyledon vasculature, epidermis and guard cells. 105

Figure 3.6 *MYB96* is expressed in the vascular initials and enriched in the epidermis initials. 106

Figure 3.7 Overexpression of *MYB96* results in drought tolerance in Arabidopsis. 107

Figure 3.8 Correlation of drought survival and rosette area. 108

Figure 3.9 MYB96 dephosphorylated form is stabilized by BR signaling via BIN2. 111

Figure 3.10 MYB96 interacts with BZR1 in the cytoplasm and in the nucleus. 113

Figure 3.11 MYB96, BZR1 and BRL3 coordinate transcriptionally responses to abiotic stress. 115

Figure 3.12 *MYB305* is natively expressed in mature root vasculature and in the guard cells. 117

Figure 3.13 *MYB305* is expressed in the pericycle. 119

Figure 3.14 Overexpression of *MYB305* results in drought tolerance in Arabidopsis. 121

Figure 3.15 Correlation of drought survival and rosette area. 122

Figure 3.16 MYB305 is stabilized by BR signaling via BIN2, inhibiting the proteasome-mediated degradation, but not by ABA signaling. 123

Figure 3.17 MYB305 interacts with BZR1 in the nucleus. 125

Figure 3.18 MYB305 transcriptionally regulates cellular responses to oxygen levels. 126

Figure 3.19 *HAT9* is natively expressed in mature root and cotyledon vasculature. 129

Figure 3.20 *HAT9* is expressed in the phloem pole pericycle, endodermis and lateral root primordia. 130

Figure 3.21 *HAT9* overexpression results in higher hydrotropic responses. 131

Figure 3.22 Overexpression of *HAT9* results in drought tolerance in Arabidopsis. 132

Figure 3.23 Correlation of drought survival and rosette area. 133

Figure 3.24 *HAT9* is transcriptionally induced by ABA. 135

Figure 3.25 HAT9 is stabilized by BR signaling via BIN2, inhibiting the proteasome-mediated degradation, but not by ABA signaling. 136

Figure 3.26 HAT9 interacts with BZR1 in the nucleus. 137

Figure 4.1 Sorghum BRI1 receptor is restoring Arabidopsis *bri1-301* insensitivity to osmotic stress. 147

Figure 4.2 Overexpression of *BRI1* results in drought susceptibility in Arabidopsis. 149

Figure 4.3 Sorghum *bri1* mutants are less sensitive to osmotic stress. 151

Figure 4.4 Sorghum NIL-*bri1*-87 mutants are less sensitive to osmotic stress. 152

Figure 4.5 Sorghum *bri1* mutants are tolerant to drought stress without growth penalization. 153

Figure 4.6 Sorghum NIL-*bri1*-87 mutants are tolerant to drought stress. 155

Figure 4.7 Consensus motif in TOP600 best scoring SbBES1 DAP-seq peaks. 157

Figure 4.8 Functional conservation of SbBES1 in terms of DNA binding to E-box motifs and regulating brassinosteroid biosynthesis. 159

Figure 4.9 Gene ontology enrichment analysis of Sorghum BES1 direct targets before peak positional filtering. 161

Figure 4.10 Gene ontology enrichment analysis of Sorghum BES1 direct targets after peak positional filtering. 162

Figure 4.11 Sorghum *bri1* mutants exhibit distinctive transcriptional regulation of photosynthesis and sugar biosynthesis to enhance stress resilience. 165

Figure 4.12 Differentially expressed genes in *bri1* mutants and SbBES1 target interaction. 167

Figure 4.13 Metabolite distribution. 169

Figure 4.14 Sorghum *bri1* mutants exhibit alterations in the phenylpropanoid pathway, leading to reduced levels of lignin precursors and accumulation of flavone. 171

Figure 5.1: Flow chart of excision-based TX430 Sorghum transformation protocol. 180

Figure 5.2: Immature Sorghum embryo isolation procedure..... 183

Figure 5.3 Schematic representation of the construct used in this work and tissue culture progression. 185

Figure 5.4 Gel electrophoresis of amplified DNA by PCR in transgenic and non-transgenic (WT) plants. 187

Figure 5.5 Confocal imaging pictures of transgenic roots with integrated membrane protein-GFP fusion and non-transgenic roots. 189

Figure 5.6 In situ hybridization of Zm*GIF1* and Zm*PLA1* RNA probes in Sorghum leaves and shoot apical meristem. 197

Figure 5.7 In situ hybridization of Sb*BRI1* shows *BRI1* ubiquitous expression. 198

Figure 5.8 In situ hybridization of Sb*BRI1* and Sb*BRL* shows *BRI1* expression in the shoot apical meristem. 198

Figure 5.9 In situ hybridization of Sb*BRL* shows *BRL* enriched expression in the vascular bundle. 200

Figure 5.10 GUS-stained calli and quantification for optimization of infection conditions. 202

Figure 5.11 Presence of non-excised morphogenic regulators and escapes. 207

Figure 5.12 Sb*BRL* overexpressor plants show leaf epinasty phenotypes. 208

Figure 5.13 SbBRL protein is internalizing upon BL treatment..... 209

Figure 6.1 Working model of the activation of MYB96, MYB305, and HAT9 by BRL3 in guard cells and root vasculature. 226

Figure 6.2 Working model of the Sorghum bicolor BRI1 receptor under control and drought stress conditions. 232

LIST OF TABLES

Table 1.1 Summary of currently available genetic tools in Sorghum. 41

Table 2.1 Transcription factors putatively binding to *BRL3* promoter. 63

Table 3.1 Selection of BRL3-dowsntream TFs.....95

Table 3.2 Selected TFs T-DNA mutants. 96

Table 5.1 Medium composition for Sorghum transformation.....179

Table 5.2 Primers and probes used for determining T-DNA integration and gene copy number by PCR and digital PCR, respectively.....188

Table 5.3 Primers used to generate RNA *in situ* hybridization probes for SbBRI1 and SbBRL. 191

Table 5.5 Transformation efficiency, escape frequency and excision efficiency in Sorghum transformation protocol. 205

ACKNOWLEDGMENTS

I would like to acknowledge all the people who have made this work and my personal enrichment possible, from the beginning of my Ph.D. thesis and from the beginning of my life. This work is not only a dissertation but an achievement I have been pursuing for a long time, and those I consider family have been supporting me from the very beginning.

Me gustaría agradecer a todas las personas que han hecho posible este trabajo y mi enriquecimiento personal, desde el comienzo de mi tesis doctoral y desde el inicio de mi vida. Este trabajo no es solo una disertación, sino un logro que he estado persiguiendo durante mucho tiempo y que aquellos a quienes considero familia han estado apoyando desde el principio.

Thanks especially to:

Gracias especialmente a:

Ana Caño, por darme la oportunidad de ver cómo es la ciencia, lo bonita y, a veces, difícil que puede ser. Por confiar en mis aptitudes desde el principio. Por enseñarme a ser un profesional científico, además de entrenarme en natación olímpica y la Champions League.

Laurens Pauwels, for helping me to develop my professional career.

Mar Marquès y Andrea Giordano, por escucharme y asesorarme en temas científicos y personales.

Aditi Gupta, Damiano Martignago, Fidel Lozano, Natalie Laibach and David Blasco, for being my scientific mentors and showing me the tricks that made my life easier. Especially to Fidel, Natalie, and David for doing it while having a beer.

Mar Ferreira, Andrés Rico y Ainoa Planas, por ser mis hermanos mayores durante la tesis doctoral. Gracias a vosotros he visto los peligros que me venían por delante y cómo los sorteabais (ventajas de ser el pequeño [dejadme al menos sentirme más joven en este aspecto])

Ivan Herrero, por ser mi compañero de escalada, mi compañero de laboratorio, mi amigo, por ser un pesado, porque con cada uno de tus discursos pedantes me sacabas una desesperación y una sonrisa.

Azahara Lopez, por hacer ver a la gente que todo se puede hacer con pasión y que, independientemente de tu situación, siempre se puede sonreír y hacer sonreír.

Veredas Coleto, por apoyarme siempre y ser original. No sabes lo mucho que me has ayudado.

Federico Jurado y Nicole Pradas, por uniros al clan "Sons of BRL3" y hacerme ver todo con perspectiva.

Marina Moreno, por darle un soplo de aire fresco al laboratorio y por ser una buena anfitriona cerdanyolenca.

Simone Pistillo, for helping me to understand Italians, even though I am still considering their nature.

Los "Valencianos", por hacerme desconectar de la tesis en los momentos que tocaba y traer las buenas costumbres valencianas a Barcelona, como la paellita de los domingos.

Los "Elegidos" y las "4 esquinas", por ser parte de mis fundamentos personales. Por estar ahí desde mis principios y por qué estaréis ahí también en mi futuro.

Mi madre, por apoyarme incondicionalmente. Por creer en mí de tal forma que piensa que soy el nuevo Einstein del siglo XXI. Por enseñarme a ser como soy.

Mi padre, por darme la fuerza para conseguir lo que me plantee. Por hacerme tener ambición de superarme en cada nueva aventura. Por ser la voz de la precaución, a veces tan necesaria.

Mi hermana Silvia, por enseñarme que hay que perseverar. Por sus innumerables consejos en los momentos más críticos.

Mi hermana Barbara, por hacerme reflexionar y enseñarme que la vida es cambio. Por su ayuda práctica y emocional. Por esta fantástica portada de tesis.

Mehdi, por ser un modelo a seguir. Por enseñarme que en el trabajo o en la vida diaria, hay que ser uno mismo.

Mis sobrinos Simón, Samuel, Guillaume y Emma por darme luz en los momentos oscuros. Por permitirme ser un niño y disfrutarlo a su lado.

Laura, mi esposa oficialmente, mi pareja en sociedad, mi chu en privado, por ser mi apoyo más valioso. Por estar a mi lado día a día e independientemente de mi humor. Por darme fuerzas y confiar en mí, incluso cuando yo mismo no lo hacía. Por ayudarme a construir la familia que tenemos hoy, que es lo más bonito que me ha pasado. Por que sin ti esta tesis no existiría.

Leonardo, mi hijo, por existir. Por dejarme acabar la tesis y entretener a la mamá para que pudiese escribir.

Esta tesis os la dedico a vosotros Laura y Leo, por que os quiero y por qué hacéis que quiera seguir creciendo a vuestro lado.